Evolutionary adaptations in developmental signaling pathways underlie regenerative scar-free wound repair in African Spiny Mouse (Genus *Acomys*)

Chris M. Brewer

A dissertation

submitted in partial fulfillment of the

requirements for the degree of

Doctor of Philosophy

University of Washington

2018

Reading Committee:

Mark W. Majesky, PhD, Chair

William M. Mahoney, Jr., PhD

Cyrus Ghajar, PhD

Program Authorized to Offer Degree:

Department of Pathology – Molecular Basis of Disease

University of Washington

Abstract

Evolutionary adaptations in developmental signaling pathways underlie regenerative scar-free wound repair in African Spiny Mouse (Genus *Acomys*)

Chris M. Brewer

Chair of Supervisory Committee:

Mark W. Majesky, PhD

Department of Pediatrics and Pathology

Vertebrate tissue regeneration is a property restricted to a small number of species within the teleost and urodele clades. Contrary to these assumptions, however, all mammalian species examined are also capable of regeneration *in utero*. However, this ability is lost at birth and repair is redirected to inflammation and scar tissue formation. This response, if left unchecked, will lead to organ failure. Evolutionary adaptations to avoid predation in the form of autotomy or self-amputation have allowed adult *Acomys cahirinus* (Egyptian Spiny Mouse) to escape this developmental transition to scar formation and instead repair external skin injuries in a scar free regenerative manner with complete restoration of hair follicles, cartilage, vasculature and peripheral neurons. Intriguingly, *A. cahirinus* have not dispensed altogether with injury activation of the myofibroblast (MF), the cellular contributor to scar tissue formation. Rather, *A. cahirinus* has evolved non-canonical MF functions that do not drive fibrosis. In identifying unique molecular signatures associated with this phenotype, RNA seq analysis identifies key

regulatory modifications of the Hippo-YAP pathway, a critical pathway in embryonic development. Specifically, the pathway effector protein YAP (Yes Associated protein) is reactivated in a biphasic manner, which is necessary for mediating *in vivo* regenerative repair. These phases include blastema formation, late stage reorganization and restoration of tissue architecture. The dynamic YAP activity observed is in part mediated by a PP2A-mediated surveillance phosphatase that rapidly and specifically dephosphorylates YAP regulatory residues. In addition to external skin repair, further investigation reveals *A. cahirinus* homeostatic adaptations to resist scar tissue formation are also found to extend to the kidney. Utilizing models of renal fibrosis that induce progressive kidney failure in muriod rodents, *A.cahirinus* restore kidney function with no apparent fibrotic scar tissue. Elucidating the genomic changes evolution has produced in *A.cahirinus* promises to provide new therapeutic approaches to treat fibropathologies currently affecting millions of individuals worldwide.

TABLE OF CONTENTS

LIST OF FIGURES

LIST OF TABLES

ACKNOWLEDGEMENTS

First and foremost, I would like to thank my doctoral advisor Dr. Mark Majesky for taking a chance on me and allowing me the opportunity to work in his lab. It has been a privilege to work with such a dedicated scientist and undergo such mentorship. Watching this project evolve from nothing but ideas to the level of "Big Science" is something I will always cherish and take great pride in.

I also want to thank members of The Majesky lab, Dr. Xiu Rong Dong and Dr. Robert Kao. They have been a constant source of support and a fountain of knowledge. Their expertise combined with their willingness to teach was no doubt paramount to my success.

I would also like to recognize the Millen lab particularly Dr. Kathleen Millen, Dr. Branden Nelson and Paul Wakenight. I truly appreciate the opportunity to work with each one of you. I would also like to extend my greatest thanks for allowing me to use equipment, lab space and resources. The *Acomys* research group was an excellent training environment.

My committee members Drs. Raymond Monnat, Cyrus Ghajar, Stanley McKnight and William Mahoney were valuable to both my development as a successful graduate student and scientist. The advice, recommendation letters and general support will not be forgotten. I personally would like to extend my humblest appreciation to Dr. Mahoney. Many times, you have gone out of your way to either share valuable insight be they scientific or professional.

I could not end this without the love and support of my mother Jeannette Brewer. I am eternally grateful for the compassion, care and wisdom she demonstrates.

Chapter 1. Introduction

1.1 Cellular decisions in wound repair outcomes

Wound healing in response to injury is required for homeostasis and survival of all species[1,2]. While evolution has produced an array of unique phenotypes, the evolution of wound repair mechanisms exhibit much less variation. The main methods of wound repair are complete restoration of tissue architecture and function (**regeneration**) or tissue replacement by extracellular matrix deposition (**scar tissue formation**)[3]. Irrespective of what mechanism is used, wound repair of complex tissue is undertaken by a limited number of cellular decisions. These cellular methods include four potential possibilities and can include a combination of the four. 1. Stem cell self-renewal and differentiation of daughter cells (**Fig1.1A**). 2. Dedifferentiation of specific cell types into a proliferating progenitor-like state (**Fig1.1B**). 3. Proliferation-free transdifferention of one cell type to another (**Fig1.1C**). 4. Differentiated cells that can re-enter cell cycle upon injury (ie. hepatocytes) (**Fig1.D**)[4-7]. To understand how a limited number of cellular decisions can result in two inherently different tissue repair outcomes, it is important to examine the evolutionary history that has shaped phylogenetic differences.

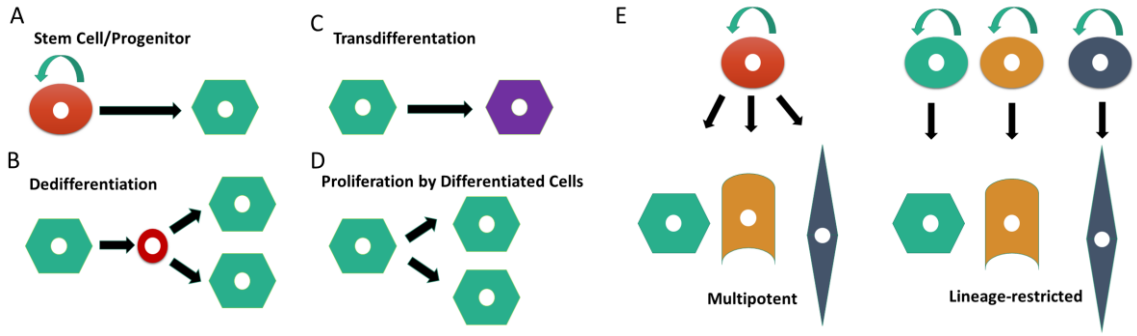

Figure 1.1 Cellular mechanisms of wound repair. (**A**) Schematic of outcomes from stem cell, (**B**) dedifferentiation, (**C**) transdifferention or (**D**) differentiated cell cycle re-entry based mechanisms. (**E**) Stem cell model showing pluripotent stem cell giving rise to all cell types (left). Tissue can also house different lineage restricted progenitor cells that individually cannot reconstitute the entire tissue (right)[8].

1.2 Regenerative repair as an evolutionary trait

Historically, there have been two schools of thought regarding the origins of regeneration in the animal kingdom. The first school of thought (the *inherent* hypothesis) supposes that our earliest multicellular ancestors all regenerated, but as certain clades diverged, the ability was lost. The second or *adaptive* hypothesis states regeneration is not an ancestral trait but rather an adaptive trait that has been independently gained or lost across phylogenetic history[9]. These two theories can be boiled down to one question: did regeneration occur once, or many times over evolutionary history?

This question has important ramifications for our hopes in the future of regenerative medicine. If the ability is *inherent* then one would only need to understand how it is blocked and then release it in non-regenerating tissues. However, if the capability is an *adaptive* feature unique to specific organisms, we have a slimmer chance in attempting to reactivate regenerative capacity. Due to the importance of the answer, scientific arguments for or against each theory have raged for the better part of a century[10]. If the inherent hypothesis is true and regeneration is an attribute of all early metazoans, one would expect the phenotype to be absent in some clades but the overall regenerative genomic blueprint to be maintained[9]. In assembling regenerative potential across metazoan phylogeny, one would see the ability to regenerate body segments, such as the limb, is a common phenomenon but not universal (**Fig. 1.2**)[11-13]. A common occurrence is the nonspecific distribution of regenerative properties both across and within broad numbers of phylogenies. Perhaps the best-known example of non-conservation is observed in the teleost (fish) class. Both the premier regeneration model zebrafish (Cyprinid family) and the scarring medaka (Adrianichthyid family)[14] exist within this phylogenic class.

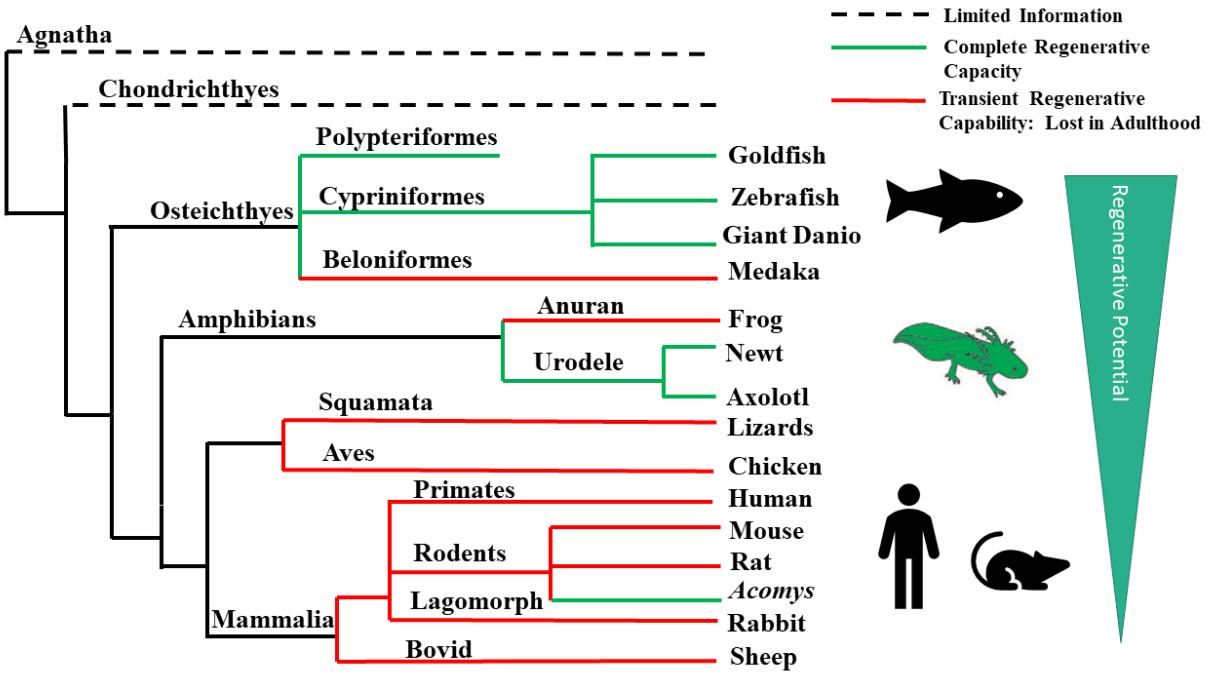

Figure 1.2 Evolutionary history of Chordate regenerative potential. Phylum Chordata includes numerous species that undergo regenerative repair. Numerous fish and amphibians exhibit robust regenerative capacity throughout the entirety of their lifespans. Higher ordered warm-blooded species instead exhibit transient embryonic and early post-natal regenerative potential. Phylogenetic tree was adapted from both *Jazwinska* and *Vivien et al*[12,15].

The argument for the *adaptive* hypothesis is made under the guise of independent natural selective pressures. Evolution has produced a variety of specific structures for specific functions in many organisms. Natural selective pressures could independently result in common phenotypes i.e. regeneration. Such events define convergent evolution. The best example is the evolution of the camera eye in cephalopods, vertebrates and cnidaria[16].

For every species that demonstrates the regenerative phenomenon, either theory could argue an evolutionary explanation as to why a closely related species does not. The accumulating evidence appears to be leaning towards the inherent model. Arguments for this position focus on the concept of regeneration as a trait that can be lost or gained. Natural selection drives evolutionary adaptions for a particular structure. However, natural selection would have to select

for regeneration as a process[10]. Regeneration is a complex process with multiple molecular and cellular events that must be coordinated within a discrete spatial-temporal window. If regeneration appeared by a *de novo* event, it must be assumed all the necessary mutations occurred simultaneously to activate all the required events within a narrow temporal window. Regeneration is an all or none event, so it is difficult to reconcile the phenomenon evolving piece by piece[10].

However, it is easier to envisage regeneration as a trait that can be lost, as opposed to gained, by single mutations accumulating over time as the *inherent* hypothesis would suggest. However, it is obvious how advantageous regeneration would be to any organism, so it's perplexing that this phenomenon is completely lost or restricted across many phylogenies. Perhaps, regeneration could be negatively selected for indirectly, as it may be incompatible with more useful adaptations. An argument for this theory comes from the observation that aquatic animals broadly have more limb regenerative potential then weight bearing limbed terrestrial organisms. An amputated terrestrial mammal that is dependent on movement for feeding or predator avoidance would likely not live long enough to positively select for the trait[17].

Homology in processes of regeneration is an important faucet of this discussion. If regeneration is an adaptive process, one can suppose that while the endpoint is the same, there would be a wide variety of independent mechanisms to achieve it. In contrast, an inherent trait would exhibit much fewer mechanisms that all display similarities across species. In agreement, metazoans routinely show conservation in the requirements of certain molecules and signaling pathways. The observation that many but not all aspects of regeneration mirror embryonic development also serves as a persuasive argument to support the *inherent* hypothesis[18].

The question regarding the evolutionary origin of the regenerative phenomenon remains an unanswered question. It will require a multifaceted approach with the true test being comparisons of organisms that have diverged long ago.

While regeneration as an endpoint is clearly defined, restoration of tissue structure and function, it is important to compare the cellular processes can be undertaken to achieve scar-free wound repair.

1.3 Mechanisms of regeneration

Morgan's landmark paper *Regeneration* in 1901 was the first to describe the process of regenerative repair as two discrete tissue reconstitution mechanisms. Each are identified by their distinguishable phenotypic differences[19]. He would name these processes morphallaxis and epimorphosis. Morphallaxis is tissue reconstitution by the reorganization of preexisting cells. The defining feature that separates morphallaxis from epimorphosis is that morphallaxis repair is initiated with little proliferation. Once remaining cells reorganize and pattern in a manner similar to the pre-injured tissue, cell proliferation is initiated to achieve normal body proportions[19].

The hydra is the guiding example of morphallaxis. Tremblay found that hydras can produce a complete individual from just $1/100^{th}$ of the remaining tissue[20]. Hydra regeneration is mechanistically accomplished by pre-existing cellular migration in the absence of cellular proliferation. When replacing lost structures, no cells are gained or lost. Once the tissue architectural plan has been restored, the size parameters are then achieved through secondary proliferative events[21]. Under homeostatic conditions however, hydras are constantly replacing dying cells by proliferation. Lineage tracing demonstrates different populations are actively being replaced by three distinct stem cell populations[22,23]. Why injury induced regeneration employs a

completely independent mechanism, distinct from homeostatic stem cell based tissue maintenance, remains an open question.

In contrast to morphallaxis, epimorphosis is described as repair through an initial injury site cell proliferation that gives rise to a mass of "undifferentiated cells". This population provides all the necessary cells for restoring absent tissue.

The classical model of epimorphosis is the planarian. Planarians, like hydras, can regenerate whole new individuals from limited tissue fragments[24]. In contrast to the hydra, the planarian amputation response involves formation of a unique structure named the blastema. The requirement of the blastema is supported by irradiation exposure experiments. Irradiation, which targets fast dividing cell populations, blocks blastema formation[25]. Identification of dividing cell types led to the discovery of a totipotent stem cell population named the neoblast [26]. High doses of irradiation, resulting in only one remaining neoblast, is sufficient to restore all germ layers in the regenerated tissue (**Fig.1.1E**). Furthermore, transplantation of a single labelled neoblast into lethally irradiated planarians is sufficient to restore regenerative potential[27]. Due to this phenomenon, the concept of the "undifferentiated pluripotent stem cell" persists as a defining feature of regeneration, even in teleost and amphibian models that display the contrary.

In contrast to the hydra and planaria, epimorphic regenerative capacity is differentially regulated in vertebrates. Newts, axolotls and zebrafish are well known for their ability to replace entire limbs, fins and other body parts following amputation, but they cannot undergo whole body reconstitution[28,29]. Due to their similarities in limb regeneration however, it has been asked if mechanisms like those of the planarian (multipotent stem cell, **Fig.1.1E**) are similar in vertebrates or has evolutionary pressures resulted in different cellular mechanisms.

Perhaps the most compelling evidence of evolutionary conservation is the requirement for blastema formation in both planarians and vertebrates [26,27,29]. Phenotypic similarities exist, such as sustained proliferation and tissue extension composed largely of mesenchymal cells surrounded by a thin epithelial cap. However, the advent of transgenics demonstrates vertebrate evolution has selected for mechanisms inconsistent with the classically held multipotent stem cell model.

Mesenchymal cells within the blastema are necessary for tissue reconstitution but determining their origins and fates have long been an unanswered question. A landmark paper addressing this question was reported by *Kragl et al* utilizing a transgenic approach[29]. Instead of applying dye based donor transplantation models, they transplanted transgenic GFP (Green fluorescent protein) donor cell populations from early embryonic structures. This strategy allows for tracing specific cell types such as fibroblasts, muscle and nerve cells based upon their developmental origins. Upon tissue regeneration, preexisting labelled cell types were found to contribute only to the same cell type and not to others. Lateral plate mesoderm derived dermal cells contributed to new connective tissue and cartilage but not to new muscle. Pre-existing Schwann cells contributed only to new Schwann cells. This study demonstrates cells within regenerating tissue maintain their previous cell identities and do not cross lineage boundaries[30]. Zebrafish use a similar mechanism. Cre-LoxP osteoblast tracing shows preexisting osteoblasts only contribute to new osteoblasts after tail fin amputation[31]. Similarities in cellular behavior across species would suggest lineage restriction is an evolutionary conserved regenerative wound repair feature (**Fig.1.1**).

These experiments disprove the commonly held myth that tissue regeneration is mediated by pluripotent stem cells (**Fig.1.1E)**. However, this study did not determine if tissue reconstitution is accomplished by lineage restricted stem cells or cellular dedifferentiation (**Fig1.1A,B**). To

address this question, *Xenopus* skeletal muscle injury models were used. Vertebrate skeletal muscle contains a well characterized progenitor population named satellite cells. Satellite cells, identified by Pax7 expression, reside within the mature muscle fibers, and when activated, serve as a source of new myocytes [32]. In Xenopus tail amputations, transplantation of embryonic labeled GFP^+ primitive muscle cells, from the early medial presomitic mesoderm, are not found within the regenerated tissue. Transplantation of late stage presomatic mesoderm, which now contains $Pax7^+$ satellite cells, are found to include labeled muscle fibers. This indicates $Pax7^+$ progenitor cells are the main contributor to muscle regeneration in *Xenopus*. However, this model has been questioned because *Xenopus* lose this capability after adult metamorphosis and instead resort to scar-like repair[33,34]. It has been argued this result is species specific and cannot be generalized as an all-encompassing mechanism, particularly to species that demonstrate lifelong regenerative capability[35,36]. The answer to these questions remained unaddressed until a landmark study fate mapped muscle fiber regeneration in two salamander species: *Notophtalmus viridescens* (newt) and *Ambystoma mexicanun* (axolotl)[32]. This study on two species that do retain regenerative capability throughout their lifespan elucidated an unexpected disparity in cellular behavior. While genetically similar, Cre-LoxP tracing revealed that pre-existing mature myofiber de-differentiation was responsible for mature myofibers in newts but not in axolotl (**Fig1.1B**). In contrast to newts, axolotl utilized a $Pax7^+$ progenitor to repopulate newly formed limbs with mature myofibers (**Fig 1.1A**)[37].

Regenerative repair in adult zebrafish, newt and axolotl is not restricted to just limbs, but also to cardiac tissue. Poss *et al* showed zebrafish cardiomyocytes can repopulate missing cardiac structures in a non-scarring manner after 20% ventricular resection[38,39]. Salamanders also undergo cardiac regeneration within 3-4 months post-resection[40]. Further characterization of cardiac

regeneration demonstrates this ability is not restricted to surgical ventricular resections but also to cryoinjury, mechanical crushing and genetic ablation injury models[41-43].

Understanding the cellular mechanisms teleost and amphibians have evolved for cardiac regeneration has clear therapeutic implications for human heart failure. To address the cellular mechanisms necessary for adult zebrafish cardiac regeneration, two independent groups employed Cre-LoxP lineage tracing to follow cardiomyocytes after cardiac injury. Labeling cardiomyocytes prior to ventricular resections gave similar results: newly formed cardiomyocytes are derived from previously labelled cardiomyocytes. This indicates that cells contributing to new cardiomyocytes are derived from proliferating pre-existing cardiomyocytes and not unlabeled progenitor cells that differentiated after injury[44]. Because cardiomyocyte specific promoters were used to drive GFP expression, it cannot be ruled out cardiomyocytes contributed to other cell types[45].

To investigate whether cardiomyocytes originated from other cardiac cell types, lineage tracing by the *tcf21* promoter yielded no epicardial cell contribution to regenerated cardiomyocytes. However, *tcf21*-derived perivascular cells were GFP labeled, suggesting epicardial cells do display limited cellular contributions to cardiac regeneration, but not directly to cardiomyocytes[39].

In contrast to amphibians and teleost, mammals have historically been viewed as being unable to undergo scar-free wound repair. These assumptions have been proven to be incorrect however, as recent evidence suggests regeneration exist but is temporally restricted. The earliest clinical evidence by Rowlatt *et al* detailed a limb amputation in a 20-week-old amniotic constricted human fetus. While the arm was unable to regenerate, histological examination revealed little necrotic activity or scarring at the amputation edge[46]. This observation led to the discovery that excisional injuries in embryonic mammalian skin can heal in a scar free manner (i.e. mice,

monkeys, sheep, rats and pig)[47,48]. Studies in rat and chicken embryos demonstrate this is not restricted to the skin, but also extends to the eye[49]. Interestingly, embryonic scar free healing is age dependent, with the response dissipating around the 3rd trimester of gestation[50]. The capacity for embryonic repair was thought to be dependent on the sterile, growth factor rich amniotic fluid within the womb or possibly the immaturity of embryonic immune system[51]. These theories have been disproven with elegant studies in embryonic marsupials, who develop in the pouch and not the uterus, heal incisional skin injuries in a scar free manner[52]. Subsequent experiments with grafting of fetal skin on adults and vice versa demonstrate this capacity is not due to external factors but intrinsic to fetal tissue itself[51].

The fetal capacity for regenerative repair also extends to complex organs, such as the heart. Genetic ablation of cardiomyocytes in embryonic day 12.5 *Mus musculus* results in a reduction of over 50% of resident cardiomyocytes. However, remaining cardiomyocytes proliferate to generate a fully functional heart[53]. The transient window of mammalian regenerative capability is further highlighted by a study undertaken by Porrello *et al*. As the developmental program for cardiomyocyte proliferation dissipates within days after birth, it was hypothesized regenerative potential may overlap with this temporal period[54]. Cardiac apical resection confirms the existence of this transient window with prenatal mice able to restore cardiac tissue and function up to the 7th day after birth. After this period, the regenerative repair processes is abolished and instead undergoes scar tissue formation[55]. This regenerative potential is not restricted to injury type as similar aged postnatal mice maintain this capability even after myocardial infarction[56]. Murine cardiomyocyte restoration exhibits similarities to teleost regeneration, as cardiomyocytes are derived from pre-existing cardiomyocytes that undergo proliferation. (**Fig 1.1**). These studies suggest that mammals do possess the all the molecular and cellular mechanisms necessary for

regenerative wound repair, if only transiently. Elucidating the genomic and proteomic mechanisms that mediate the mammalian temporal switch may one day provide clues in extending regenerative repair to adult humans.

1.4 Adult mammals repair injuries through scar tissue formation:

While most mammals employ regenerative repair during periods of embryonic and early post-natal development, wound repair in adults is accomplished by tissue replacement and remodeling[57,58]. Tissue replacement is characterized by the deposition of extracellular matrix (ECM) proteins that form a fibrous "scar". While several adult mammalian tissue systems maintain injury induced regenerative capabilities (epidermis, liver, gut epithelium, and hematopoietic system), injuries that severely perturb the connective stromal tissue will almost always result in scar tissue formation[12,59-63].

Since wound injuries in the skin are easily accessible, it is the most extensively studied scar mediated wound repair model. The adult mammalian repair response exhibits a well-defined sequence of events that are necessary for injury resolution across most organ systems. This sequence of events occurs in three overlapping but distinct stages: inflammation, new tissue formation and remodeling[64].

Inflammation: Inflammation is classically the first phase of wound repair, but it is subdivided into two separate events: 1) the vascular response; and 2) the inflammatory response. Immediately after tissue injury and vasculature disruption (bleeding), the coagulation cascade and immune system are activated to prevent ongoing blood loss and infection. Blood loss stoppage is achieved by circulating platelets. Platelets are activated by the newly exposed collagen matrix at the wound site. This activation results in their adherence and accumulation, also called the platelet plug[65]. A coordinated sequence of enzymatic reactions is then mediated by several tissue factors

that make up the clotting factor family[66]. These reactions result in the formation of a fibrin clot. The fibrin clot provides a provisional matrix for infiltrating cells[67]. As the scaffolding necessary for cellular migration is being assembled, both the activated complement system and degranulating platelets actively recruit neutrophil responders[68]. Monocytes arrive 1-2 days after injury and differentiate into macrophages. The macrophages phagocytose dead and dying cells, secreting several ECM degradative enzymes and releasing important growth factor instructions[69]. These critical growth factors include tumor necrosis factor-alpha (TNFα), transforming growth factor beta (TGFβ), the platelet derived growth factor (PDGF) family, and the vascular endothelial growth factors (VEGF family)[70]. These factors promote cellular migration and proliferation of both resident and infiltrating cell types[71].

Macrophage infiltration defines the beginning of the secondary stage of wound repair[72].

New Tissue Formation (Proliferation): The proliferative stage occurs 2-10 days after initial injury and is characterized by granulation tissue formation, angiogenesis, early neo-collagen deposition and re-epithelialization [55,56]. The aim of this phase is to close the injured area by contraction and proliferation. While there is considerable overlap in the timing of these events, re-epithelization is considered the first event. Epithelial cells in the periphery migrate into the wound site, forming a barrier prior to proliferation[73]. Local keratinocytes and epithelial stem cells, from nearby hair follicles and sweat glands, contribute to the migrating mass with the fibronectin- fibrin clot serving as a directional cue[74,69].

The wound area is simultaneously preparing to supply the cellular expansion with oxygen and nutrients through vascular remodeling. Expansion of blood vessels into the wound area occurs via angiogenesis[75]. This event is a coordinated process involving endothelial cell proliferation, rearrangement of the basement membrane, migration, tubular reorganization and recruitment of

perivascular cells[73]. The newly established endothelium is then wrapped by smooth muscle cells. The newly formed microvasculature transports oxygen, fluids, nutrients, and immune-competent cells to the wound stroma[75]. The arriving cells begin to form a structure named the granulation zone. The name is derived from the granular appearance of the transient tissue. The granulation tissue is formed through fibroplasia (increased fibroblasts proliferation) and increased synthesis of ECM components[76]. The predominant ECM component deposited at this stage is collagen type III, which serves as an anchor for the wound contraction process. At this stage, stromal cells will differentiate to form a unique contractionary cell type: the myofibroblast[77]. These cells accumulate at the wound borders and undergo contraction in order to close the wound [78].

Remodeling: Remodeling is the third phase of repair. It is initiated one-week post injury and may extend for years, depending on the severity of the initial insult [60]. The main aim of this stage is to achieve maximum tensile strength of the newly formed scar tissue. This is achieved by ECM reorganization, degradation and resynthesis. In the final stage of repair, the granulation zone is replaced by scar tissue that is both decellurized and devascularized[79]. The remodeling process is characterized by a progressive increase in both the complexity, concentration and type of collagen fibers. With the closure of the wound, collagen type III undergoes degradation and synthesis of collagen type I increases[61]. Collagen type I tensile strength is increased by crosslinking fibers into thickly bundled parallel sheets[80]. The regulation of the myofibroblast mediated collagen synthesis is regulated by several factors, such as TGF-β1 (Transforming growth factor beta) and FGF (Fibroblasts growth factor). The former has strong activation activity on the expression of collagen type 1 subunit proteins[81]. The cellular void in the scar is due to emigration and apoptosis of various cell populations that were previously involved in early repair[64].

It is important to note that scar formation as a mechanism of repair is imperfect. As opposed to regeneration, scar tissue will never again attain normal tensile strength as that of uninjured tissue[63]. Chronic scarring can result in structural and functional deterioration, which can be painful, unsightly, and ultimately deadly depending on the organ injured.

1.5 Fibrosis is a result of excessive scar tissue formation

Myofibroblast-mediated scar formation has evolved in adult mammals to be main mechanism of wound repair. Limited scarring is critical for survival, particularly in adult mammals that utilize high-pressure blood flow. An example is scar tissue formation in response to myocardial infarction. Collagen type I and III secretion is necessary for preventing catastrophic rupture[82]. However, prolonged inflammation or chronic injury can exacerbate the scar formation process, leading to pathological fibrosis. Fibrosis is defined as excessive accumulation of fibrillar extracellular matrix components, such as collagen type I/ III and fibronectin[83]. The prolonged remodeling disrupts the affected tissue architecture, leading to organ failure. Fibrosis affects almost all organ systems, such as lung, heart, liver, kidney and skin. Due to its role in many organ pathologies, fibrosis is a clear medical concern with economic loss being calculated to be in the billions[66]. Current therapies, such as small molecule drugs, are ineffective and unpredictable with most cases of end stage fibrosis requiring organ transplantation for survival. Understanding both the cellular and molecular regulators that mediate organ fibrosis is critical for designing new therapies.

1.6 Myofibroblasts are the main cellular contributor to fibrosis

While controversy exists regarding how severe a wound must be for the onset of fibrosis, what is clear is that the myofibroblast (MF) is the main contributor to fibrosis[61]. Myofibroblast formation can result from several injury activation signals, such as mechanical tension, chronic

inflammation and persistent cytokine signaling[84]. The most studied cytokine is TGFβ1[85]. Myofibroblasts are identified by *de novo* expression and stress fiber formation of ACTA2, also known as smooth muscle α-actin (αSMA), along with increased deposition of alternative splice variants extra domain A-fibronectin (EDA-Fibronectin) and collagen type I and III (**Table1.1**) [86-88]. In acute wounding, MFs are transiently present where they have critical roles of both restoring the ECM architecture and wound contraction[86]. It is unknown what becomes of the myofibroblast after injury resolution but current theories include apoptotic clearance or de-differentiation back to their original mesenchymal cell source[89-91]. Myofibroblast reprogramming has also been proposed as a potential myofibroblast clearance mechanism. This model stems from the observation, by Plikus *et al*, that dermal myofibroblasts directly contribute to the regeneration of adipocyte populations during periods of tissue injury resolution[92]. However, the pervasiveness of this phenomenon remains to be elucidated in other species and organ systems. In chronic injuries, myofibroblasts are not cleared but instead are maintained in a proliferative and activated state. Prolonged myofibroblast activation leads to organ failure. This persistent extracellular matrix deposition and ACTA2 stress fiber assembly allows the myofibroblast to disrupt the affected organ architecture[93].

Vimentin (VIM) positive	SM-MHC (MHC11) negative
De novo ACTA2 expression	Hypersecretion of collagen type 1
ACTA2 stress fiber assembly	*De novo* EDA-fibronectin (FN) expression
Super mature vinculin (VCL) focal adhesions	Increased contractionary activity

Table 1.1 Marker criteria for differentiated myofibroblasts. Myofibroblasts lack a specific identity marker so a dual positive/negative labeling strategy is typically used.

1.7 Cellular origins of myofibroblasts

Classical studies of wound repair first identified myofibroblasts by their morphology within the granulation tissue[94]. With the absence of specific markers to define the myofibroblast, it's been assumed the myofibroblasts are derived from modified fibroblasts within the resident stromal population (e.g., skin dermal fibroblasts and liver hepatic stellate cells)[95]. These assumptions have been challenged recently by studies suggesting that myofibroblasts can arise from several cellular sources, such as resident progenitor cells, infiltrating fibrocytes, pericytes, perivascular cells, endothelial cells and epithelial populations undergoing epithelial to mesenchymal transformation (EMT)[96] (**Fig 1.3**). These studies suggest there are independent populations of precursors cells that contribute to myofibroblast formation. The origin and percentage of cells that contribute to myofibroblast-mediated fibrotic remodeling may be organ-dependent.

Lineage tracing of bone marrow derived cells found fibrocytes contribute a substantial proportion of collagen type 1 secreting cells during bone marrow fibrosis[97]. In a similar manner, bone marrow derived fibrocytes, along with a small population of local Sca-1^+ progenitor cells, provide the bulk of collagen secretion in arterial fibrosis.[98]. However, this cellular mechanism appears to be restricted to specific organs. Genetic labeling techniques across a variety of other organ fibrosis models identify the tissue resident mesenchymal stromal cells as the myofibroblast precursor[99].

Bone marrow chimera lineage tracing studies demonstrate bone marrow derived cells are not the source of $ACTA2^+$ myofibroblasts in models of pulmonary or liver fibrosis[100,101]. Furthermore, both kidney tubular and lung alveolar epithelial cells do not contribute to myofibroblast formation. In contrast, myofibroblasts arise from both resident fibroblasts and

pericytes derived from a common *FoxD1*$^{+}$ embryonic mesenchymal progenitor cell in both the kidney and lung[100,102]. Lineage tracing studies in the heart find resident cardiac fibroblasts, derived from early embryonic *Tcf21*$^{+}$ proepicardial cells, are the primary contributors to the injury induced myofibroblast population.[103]. While dermal fibroblasts have been thought to be the sole contributors to myofibroblasts in the skin, only recently has this been confirmed. Lineage tracing of Engrailed1 (*En1*) during embryonic development shows this mesenchymal cell population migrates from the somites into the dorsal trunk, which later form the reticular dermis zone. This population produces the extracellular matrix during embryonic skin development[104,105]. Utilizing radiation-induced fibrosis and dorsal back skin excision models in adult mice, *En1*$^{+}$ GFP cells co-localize within scar bed. Flow sorting of excised dermal cells shows that the *En1*$^{+}$ fibroblasts are the most responsive to fibrokines, with robust increases in transcript levels of genes associated with fibrosis. Diphtheria toxin receptor mediated ablation or chemical inhibition of the cell-restricted receptor CD26 (Dipeptidyl peptidase-4) on *En1*$^{+}$ fibroblasts is sufficient to attenuate fibrotic scarring[104]. Future studies will be needed to identify the specific contribution of different mesenchymal stromal cells to various organ fibropathologies. Understanding the relative roles of resident fibroblasts, pericytes or mesenchymal stem cells populations in fibrotic repair may provide relevant therapeutic targets[102,106].

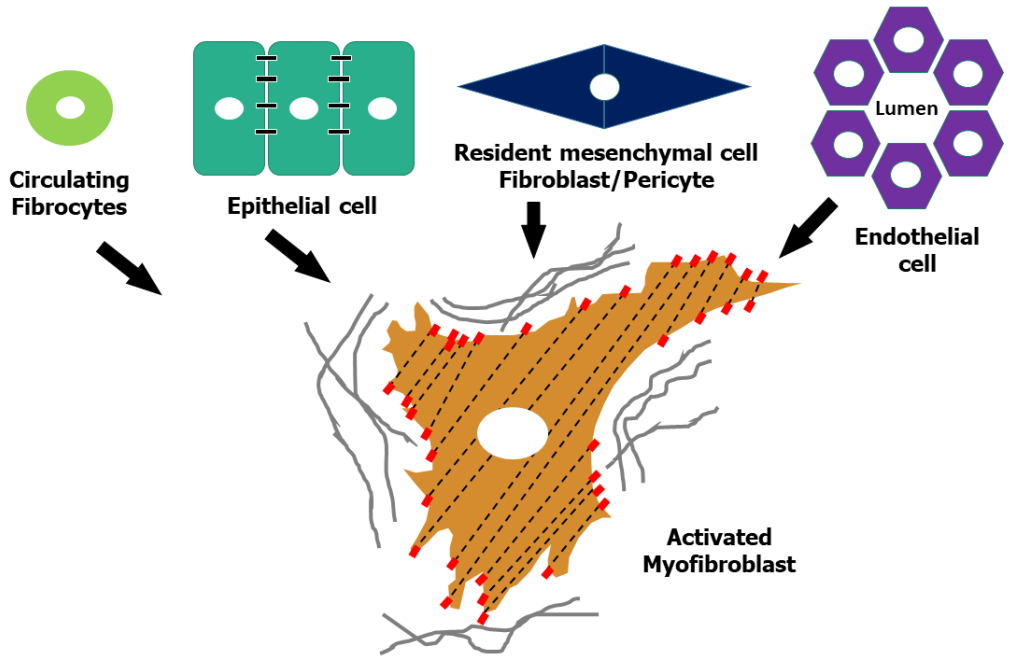

Figure 1.3: Cellular origins of the myofibroblasts. Tissue resident fibroblast/pericytes make up the bulk of the cellular contributors to injury induced myofibroblast. Other cell types have been proposed but their contribution appears to be limited and restricted to specific organ systems[98,102,107-109].

1.8 Signaling pathways that mediate myofibroblast activation

While controversy exists regarding the cellular sources of myofibroblasts *in vivo*, the same cannot be said about the molecular mechanisms that promote myofibroblast activation. The most well-studied is Transforming Growth Factor Beta 1 (TGFβ1), a polypeptide member of the Transforming Growth Factor Superfamily. Three separate isoforms of TGFβ exist (TGFβ1, 2 and 3) in vertebrates, which demonstrate 75-80% homology at the peptide level[110]. TGFβ1 is currently viewed as the master driver of fibrosis, as overexpression is sufficient for producing fibrosis in most organ systems[111]. TGFβ1 mediated myofibroblast activation can occur through two independent signaling mechanisms; canonical and non-canonical[112].

Canonical TGFβ Signaling Pathway

Canonical TGFβ1 signaling occurs through activation of the SMAD2/3 transcription factors[113]. Soluble TGFβ1 in the wound site can be derived from several sources. The most

immediate injury source of TGFβ1 are circulating platelets but other sources can include proteolytic cleavage from injury disrupted ECM, paracrine signaling from neighboring immune, parenchyma or mesenchymal cells along with autocrine signaling from wound activated fibroblasts[114]. Secreted TGFβ binds to the transmembrane TGFβ serine/threonine kinase receptor type II. This results in phosphorylation and activation of TGFβ receptor 1, which induces formation of a heteromeric receptor complex consisting of both receptors 1 and II. This complex forms docking sites for SMAD2/3 binding and phosphorylation (activation). [112]. The co-adapter SMAD4 will then bind to SMAD2/3 forming a transcription factor complex, which will then translocate into the cell nucleus and activate a myofibroblast gene profile (**Fig 1.4**)[85]. These targets genes include several inhibitors of matrix metalloproteases (MMPs), collagen types I/III and ACTA2[115]. The critical nature of canonical SMAD signaling in myofibroblast activation is illustrated by fibroblasts, isolated from *Smad3*$^{-/-}$ mice, resisting TGFβ1 mediated expression of profibrotic genes[116]. Furthermore, increased phosphorylation levels of SMAD2/3 are observed in most fibrotic tissues[117,118]. While SMAD-mediated signaling is an activator of myofibroblast formation, it alone may not be the dominant mechanism and may synergize with several other signaling pathways to promote fibrosis.

Non-Canonical TGFβ Signaling

TGFβ1 can also induce myofibroblast formation in a non-SMAD dependent manner. While TGFβ1 binds to TGFβ receptor II, TGFβ-activated kinase (TAK1) is instead phosphorylated leading to TAK binding protein (TAP) activation. This phosphorylation event will stimulate the mitogen activated protein kinases (MAPK) family. This kinase cascade will then activate the primary effector protein p38 (**Fig 1.4**)[112]. Inhibitors of p38, such as SB731445, have been shown to down-regulate TGFβ-induced myofibroblast markers (e.g., collagen type I, fibronectin, and

ACTA2) and reduce contractile activity across a variety of organ-specific fibroblasts *in vitro*[119]. These observations extend to several organ systems. p38 inhibitors attenuate various aspects of fibrosis *in vivo*[120-122]. Conversely, overexpression of the p38 activator (MAPK kinase 6; MKK6) is sufficient to induce interstitial fibrosis in numerous organ injury models (i.e. ischemia reperfusion, bleomycin, and unilateral ureter obstruction)[123]. It is not clear how extensive the cross talk is between these distinct pathways but current evidence suggests they share common transcription factors (e.g., SMADs 2/3) that encourage myofibroblast formation and maintenance. Regardless, TGFβ1 mediated non-canonical signaling is an important driver for fibrosis.

Angiotensin II (AngII)

AngII, a peptide hormone that increases blood pressure by vasoconstriction, has been well documented to be associated with various fibropathologies. Frequent infusion of AngII initiates and exacerbates fibrosis in various organ systems (e.g., heart, kidney and aorta)[124]. Similarly, AngII is a pharmacological target in end stage kidney failure and heart disease, as its inhibition delays fibrotic remodeling[125,126].

After being activated by the enzymatic activity of the angiotensin converting enzyme (ACE), AngII signals through the angiotensin type 1 (AT_1) G protein coupled receptor (GPCR) (**Fig.1.4**). AngII is an upstream activator of TGFβ signaling. In addition, AngII stimulation increases TGFβ1 transcript levels in several organ-specific fibroblasts (e.g., cardiac and skin fibroblasts) [127,128]. Furthermore, AngII-induced cardiac fibrosis is attenuated in TGFβ1-null mice. Synergy between these two signaling cascades activates core profibrotic gene targets (e.g., fibronectin, collagen type 1 and III, connective tissue growth actor (CTGF) and endothelin-1)[129]. Therefore, understanding how both these signaling pathways modulate each other's behavior during fibrotic progression will be an important facet in directing future therapeutics.

While AngII promotes myofibroblast activation, few studies have addressed its direct role. What is known is that AngII can induce ACTA2 stress fiber formation and increased contractile activity. However, this response occurs regardless of the presence or absence of TGFβR1[119]. This would indicate AngII can initiate myofibroblast activation through more than just one pathway.

Endothelin-1 (ET-1)

Endothelin is a class of secreted bioactive protein ligands with vasoconstriction and mitogenic properties[130]. Three isoforms exist with each resulting from independent genes (ET1/2/3). While endothelial cells were first discovered to secrete ET-1, macrophages, epithelial cells and fibroblasts also contribute to its production. Signal propagation of secreted endothelin is mediated by two GPCRs: Endothelial receptor subtype A and B (ET_A/ET_B)[131]. High levels of ET-1 is associated with various fibrogenic conditions, such as idiopathic pulmonary fibrosis, cirrhosis, and scleroderma[130,132]. Therefore, ET1 is an important regulator of fibrosis (**Fig.1.4**).

ET-1 is a downstream mediator of TGFβ signaling[84]. Stimulation of the ET-1 signal cascade results in increased ECM production and myofibroblast activation. Overexpression of ET-1 is sufficient to induce pulmonary and renal fibrosis[130,133]. ET-1-induced myofibroblast activation is mediated by SMAD-independent TAK1/JNK/p38 signaling (**Fig.1.4**)[134]. AngII and ET-1 also exhibit a close relationship in promoting cardiac fibrosis. Cardiac fibrosis is attenuated when endothelial cells are genetically deficient for ET-1 in AngII induced hypertension[135]. Cross-talk between ET-1 and AngII is also required for myofibroblast co-activation in CCl_4–induced chronic liver injury[136]. Taken together, ET-1 coordinates fibrosis synergistically with a broad number of signaling pathways to modulate fibrotic progression.

Platelet Derived Growth Factor Family (PDGF)

PDGFs are secreted peptides comprised of several homo- or heteromeric growth factors named PDGF-AA, -AB, -BB, -CC, -DD. These growth factors propagate signals through two structurally similar tyrosine kinase based receptors named PDGFR-α or β[137]. Upon stimulation, PDGF receptors dimerize either as a homo or heteromers[138]. Activation stimulates several downstream signaling pathway components, such as MAPK (Mitogen-activated protein kinase), PI3K(Phosphatidylinositol-4,5-bisphosphate-3-kinase), and PLCγ (Phosphoinositide phospholipase C)[139]. The PDGF peptides are growth factors with potent mitogenic, migratory and anti-apoptotic effects on mesenchymal cells (e.g., fibroblasts and smooth muscle cells)[140,141]. PDGF ligands play a critical role in promoting wound repair. Specific PDGF ligands, such as BB, are required for granulation tissue formation by recruiting and activating fibroblasts, smooth muscle cells and pericytes[142,143]. Chronic activation of the PDGF receptor family has been implicated in many pathological conditions, such as cancers, vascular disease and fibrosis[144,145]. Mesenchymal cells expressing the PDGF receptors (α and β) often co-localize with ACTA2 or collagen type 1 during fibrotic repair[108]. Reciprocally, conditional deletions of PDGF receptors or antibody directed antagonist treatments attenuate myofibroblast formation in several fibrotic organ models (e.g., skin and kidney)[146].

The molecular mechanism PDGF signaling utilizes to activate myofibroblast is unclear. While PDGF stimulates myofibroblast proliferation, migration and ECM production, its role in promoting ACTA2 transcription and assembly is less understood. While treatment with PDGF peptides is sufficient to cause collagen contraction across a broad range of organ specific fibroblasts, induction of ACTA2 expression occurs in only a subset of fibroblasts *in vitro* (e.g.,

corneal fibroblasts)[147]. Therefore, PDGF ligands and receptors are believed to synergize with TGFβ1 to produce the terminally differentiated myofibroblast phenotype[148].

Clinically, inhibitors of PDGFR tyrosine kinase signaling have been the most successful anti-fibrotic targets. GLEEVEC® (imatinib), first used for anti-cancer treatment, has had success in attenuating fibrosis in murine pulmonary, kidney and skin fibrosis models[149,150].

Mechanotransduction and Actin dynamics

Historically, soluble peptides (e.g., TGFβ1, ET-1 and PDGFs) have been the focus for therapeutic intervention during fibrosis. However, a paradigm shift has occurred with investigators now focusing on how cells transduce mechanical cues from the ECM into transcriptional responses via the cytoskeleton (mechanotransduction)[85]. Current theories suggest that because the cell cytoskeleton is pre-stiffened by its environment, it's in a unique position to sense mechanical signals, such as tension and stiffness, in a fashion independent of chemical transmission[151]. In agreement, fibroblasts and myofibroblasts are sensitive to both the organization and forces generated by the ECM. Three-dimensional collagen lattices and tunable gel substrate assays demonstrate fibroblasts up-regulate expression and assembly of ACTA2 in response to increasing matrix tension and rigidity[152]. In contrast, cell seeding of differentiated myofibroblasts on soft or elastic matrices can decrease ACTA2 protein levels[153,154]. Key regulators of mechanotranduction-mediated myofibroblast activation are SRF (Serum Response Factor) and MRTF-A (Myocardin Related Transcription Factor-A). SRF is a highly conserved and globally expressed transcription factor first identified by the Treisman lab[155]. A member of the MADS box family of transcription factors, SRF binds DNA at A/T rich regions flanked by double C/G regions called CArG boxes ($CC(AT_6)GG$). *In silico* approaches predict over 9000 conserved CArG elements, with targets ranging from genes involved with the immediate-early response, muscle contractility and actin-

based cytoskeletal movement[156]. Specificity for SRF target genes is achieved through signal responsive transcriptional co-regulators, the best known of these being myocardin and the ETS family proteins [157,158]. Promoter regions of contractile genes necessary for both smooth muscle and myofibroblast differentiation contain several SRF binding sites, with *Acta2* containing five boxes (**Fig.1.4**)[157]. While myocardin is a master co-transcriptional regulator for smooth muscle differentiation, the myocardin related transcriptional factor family (MRTF A/B) is more broadly expressed and are important promoters of myofibroblast differentiation[159]. Overexpression of MRTF-A activates ACTA2 stress fiber assembly in organ-specific fibroblasts populations *in-vitro*[160,161]. In a reciprocal manner, MRTF-A$^{-/-}$ mice display decreased fibrosis in various models of cardiac injury (e.g., AngII infusion and myocardial infarction)[160].

MRTFs have a specialized mechanism for nuclear accumulation and co-transactivation activity. MRTFs contain a N-terminal protein domain that directly binds to G-actin (globular). When G-actin is the dominant form of actin, G-actin sequesters MRTFs and inhibits exposure of the nuclear localization signal (NLS) within the N-terminal region. Upon G-actin polymerization into the F-actin (filamentous), this inhibition is released and the NLS is exposed, allowing for its nuclear trafficking in a α/β importin-dependent fashion[162,163]. Nuclear import allows for binding interaction with SRF and upregulation of profibrogenic gene expression.

Controversy existed regarding how signals at the ECM-cell surface interphase are interpreted that lead to MRTF activation and nuclear accumulation. Further investigation revealed Rho-GTPases, and their ability to modulate actin dynamics, are the primary culprits[164,165]. Focal adhesion complex modulations, either by receptor activation or EMC perturbation, activate RhoA and RhoC, the Rho signaling pathway mediators[166,167]. Downstream, Rho activity is mediated by the effector proteins ROCK (Rho-associated coiled-coil containing protein kinase) and mDia1

(mouse diaphanous-related formin-1)[168]. Activation of mDia1 induces nucleation and polymerization of F-actin while ROCK promotes F-actin stabilization[169]. The relationship between Rho-GTPase signaling and F-actin formation provides a link how extracellular matrix changes affect MRTF localization (**Fig.1.4**). This relationship is exemplified by addition of the ROCK inhibitor Y-27632, which results in the failure of MRTF-A nuclear translocation, being sufficient to stop activation of the profibrogenic gene program[160].

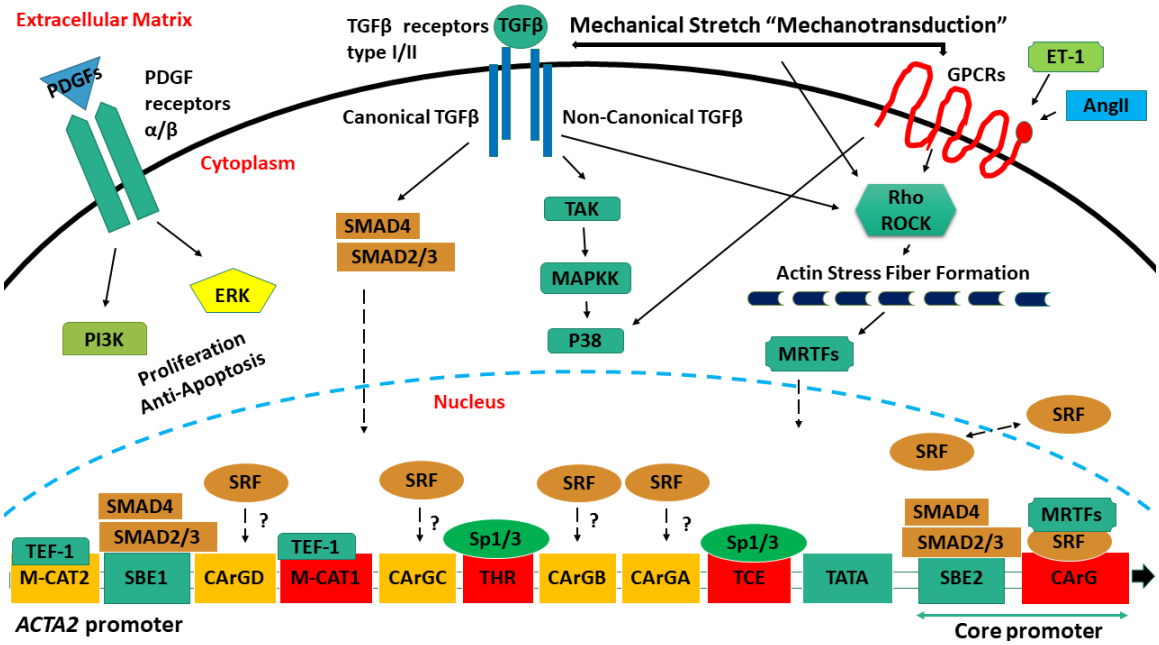

Figure 1.4: Multiple signaling pathways regulate myofibroblast *Acta2* transcriptional activity. Myofibroblast differentiation (i.e. expression of ACTA2) is mediated by several stimuli, singly or in a combinatorial fashion, activating a variety of downstream signaling pathway effector proteins. Question marks indicate it is unknown if promoter response element is necessary for driving myofibroblasts *Acta2* transcription.

1.9 Genus *Acomys* as a model for adult mammalian scar free wound repair

While myofibroblast-mediated scar formation is the most evolutionarily conserved mechanism for adult mammalian wound repair, a small number of mammals have evolved unique machinery for scar free healing. These include several species that make up the genus *Acomys*. *Acomys* ("Spiny Mouse") consists of 19 rodent species that inhabit portions of northern Africa, southwest Asia and the Middle East.[170] *Acomys* were believed to be closely related to *Mus*

musculus due to similarities in molar teeth morphology. However, genetic analysis by both nuclear and mitochondrial comparisons has demonstrated the *Acomys* are 25 million years removed from a common murine ancestor. Instead, *Acomys* show closer genetic similarity to *Gerbillus*[171] (**Fig 1.5**).

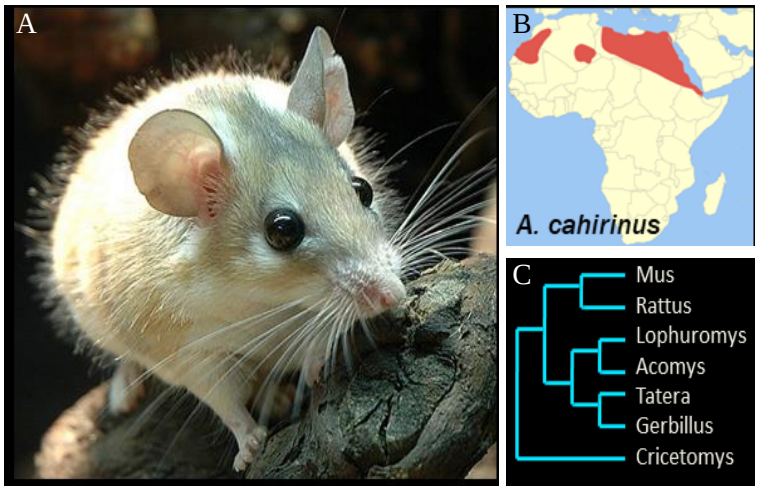

Figure 1.5: Genus *Acomys* as a model of mammalian scar free wound repair. (**A**) *Acomys* display stiff guard hairs as a deterrent to predation. (**B**) *Acomys cahirinus* or Egyptian Spiny Mouse is native to portions of northern Africa. (**C**) Phylogenic tree of the *Acomys* genus or "Spiny Mice" (19 species) with other members of the class Rodentia.

Due to their ecological niches, *Acomys* were once popular models for physiological studies, such as water retention and temperature regulation[172,173]. Several *Acomys* species were also models of mutation free nutritionally induced type 2 diabetes, due to their propensity for insulin resistance and hyperglycemia[174]. *Acomys* demonstrate precocial birth and exhibit full fur coats along with fully functional vision, smell and hearing within hours after birth. These unique features allow investigators to examine hippocampal and central nervous system development[175]. In addition, *Acomys* have developed unique adaptations to avoid predation. One adaptation, and the reason for the "Spiny Mouse" moniker, is the presence of stiff spine-like hairs along the dorsum. These spines make the animal painful for predators to swallow[176]. However, the most intriguing adaption, identified in several species of *Acomys*, is the ability of autotomy or "self-amputation"[177]. While

autotomy is commonly employed in several reptile species (e.g., skinks and geckos), *Acomys* skin autotomy is the first proof of its existence in mammals[177]. Furthermore, autotomy among the *Acomys* genus appears to be conserved, with the ability being demonstrated in three of the nineteen *Acomys* species (*A. kempi, A. percivali and A. cahirinus*). This unique mechanism allows the *Acomys* to shed up to 60% of its dorsal skin to avoid capture. What is most incredible about this property is that instead of undergoing exsanguination, desiccation or infection, *Acomys* exhibit complete restoration of the missing skin (hair follicles, sweat glands, dermis and cartilage) rather than scarring and fibrosis[177] (**Fig1.6**). This phenomenon was first reported in an ear punch injury, a common model for would repair, by Seifert *et al*[177]. Interestingly, as opposed to the dorsal incision model, the ear wound exhibits scar free wound repair in an epimorphic, blastemal-based fashion[178]. While rare, *Acomys* are not the only mammals to completely repair skin wounds in this manner, as the *Oryctolagus cuniculus* (common rabbit) and various mutant mouse strains (e.g. $p21^{-/-}$, nude mouse ($Foxn1^{nu}$) and Murphy's Roth Large (MRL/MpJ)) also exhibit these features[178].

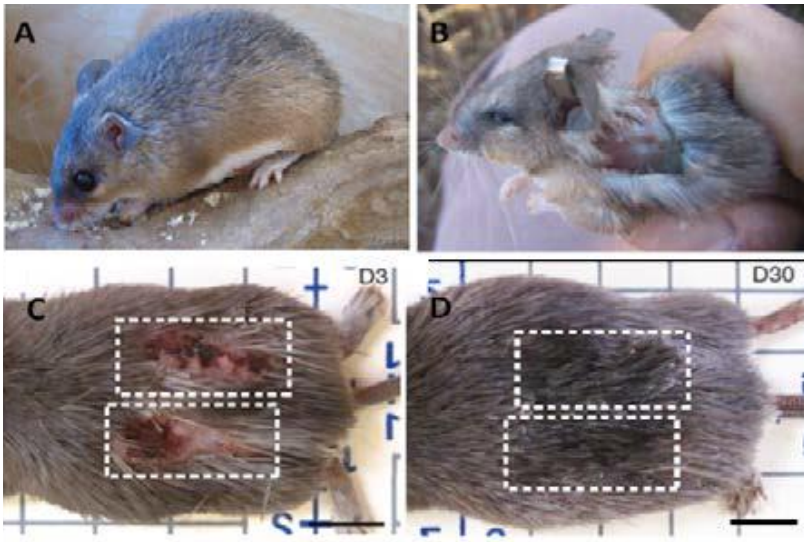

Figure 1.6 Skin Autonomy and rapid regeneration in adult African Spiny Mouse *A.kempi*. *(*B) Evasion response to predation in *Acomys* leads to degloving injury**. (C)** Normal scab formation at Day 3 post injury in full skin excisional model**. (D)** Same wound area now completely healed at Day *30*. Figure taken from *Seifert et al*[177].

A unifying theme between all the "super-healer" mammals is the ability to maintain proliferative potential in both mesenchymal and epidermal cell populations. While "non-healer" mammals, such as the *Mus musculus* demonstrate early cell cycle re-entry and proliferation, mid to late stage injuries undergo cell-cycle arrest and a decrease in proliferation. In contrast, animals with a "healer" phenotype maintain cell cycle progression, with a large percentage of cells continuously within the G2/M cell cycle phase[178]. Mechanistically, protein synthesis of G1 cell cycle inhibitors (p21 and p27) is deficient in "super-healer" mammals[179] They also exhibit decreased phosphorylation (activation) of retinoblastoma protein (Rb)[180]. These deficiencies maintain a skip of the G1-mediated cell cycling checkpoints[180]. In contrast, "non-healer" animals exhibit continual protein production and nuclear localization (active) of these cell cycle inhibitors[179,178,181].

It is important to distinguish that while wound closure is an important feature of epimorphic regenerative repair, it alone cannot be defined as true regeneration. Examples of this fallacy exist within both the MRL and $p21^{-/-}$ murine models. Both strains exhibit successful wound closure when compared to the Mus C57BL/6 and CD1 strains[178,180,182]. However, closer histological and cellular observations suggest these models display improper architectural and structural features when compared to uninjured tissue. These include failures in re-establishing mature cartilage, hair follicles, sebaceous glands and muscle. While rabbits and several *Acomys* species display epimorphic ear regeneration, there is an inverse relationship between injury size, with increasing hole diameters resulting in decreased wound closure and scar tissue formation in the MRL/MpJ and $p21^{-/-}$ murine strains[178,180,183].

Acomys regenerative repair is a natural survival response to predation. Understanding the cellular and molecular mechanisms underlying *Acomys* regeneration may translate more readily to

humans than current amphibian and teleost models. The *Acomys* also serves as a unique model to begin questioning the relationship between wound repair in embryonic and adult mammals. All mammals can undergo regenerative repair until early post-natal development. Unfortunately, regenerative repair is after this period is extinguished and instead redirected towards scar tissue formation. Therefore, the *Acomys* serves as a potential blueprint for extending the mammalian regenerative repair response into adulthood.

1.10 Hippo signaling pathway

During periods of development and regeneration, key cellular processes such as proliferation, migration, differentiation and size control must be appropriately regulated to establish homeostatic organ size parameters[66,69,184,185]. Regeneration, as a repair process, recapitulates elements of early embryonic development during periods of tissue reorganization and restoration of function. Therefore, signaling pathways that are critical for initiating the regenerative process are also intricately involved in organ formation and size control[186-193]. The Hippo signaling pathway is an ideal pathway candidate to begin investigating mechanisms of *Acomys* regenerative repair, as Hippo tightly coordinates both developmental processes. Hippo pathway was first identified in *Drosophila* forward genetic screens aimed at identifying genes that regulate organ size. Genetic deletions of *Drosophila wts* (Warts), *hpo* (Hippo) and *sav* (Salvador) all result in proliferation-based tissue overgrowth phenotypes [194,195]. Further studies show that these three elements interact both genetically and biochemically[195-197]. It was largely unknown how these components mediate their effect at the transcription level, until Huang *et al* discovered Yorkie (*yki*) is the key nuclear effector protein[198]. Deletion of *yki* suppresses the tissue overgrowth phenotype in both *hpo* and *wts* mutants[198].

The Hippo pathway is highly conserved in mammals with protein orthologs of Warts, Salvador and Yorkie being Large tumor suppressor homolog 1/2 (LATS1/2), Mammalian sterile 20-like 1/2 (MST1/2), Salvador (SAV1) and Yes-associated protein (YAP) respectively[199,200]. Their functions in mammals are highly conserved, with deletion of *Lats1/2* and *Mst1/2* resulting in overgrowth phenotypes in several organ systems (e.g., heart, liver, stomach and spleen)[201,202]. Deletion of murine *Yap* suppresses many of the overgrowth phenotypes. In mammals, the Hippo pathway contains a serine/threonine signaling kinase cascade (MST1/2 and LATS1/2) designed to regulate the phosphorylation, and ultimately, the activity of the transcriptional co-activator YAP (**Fig 1. 7**).

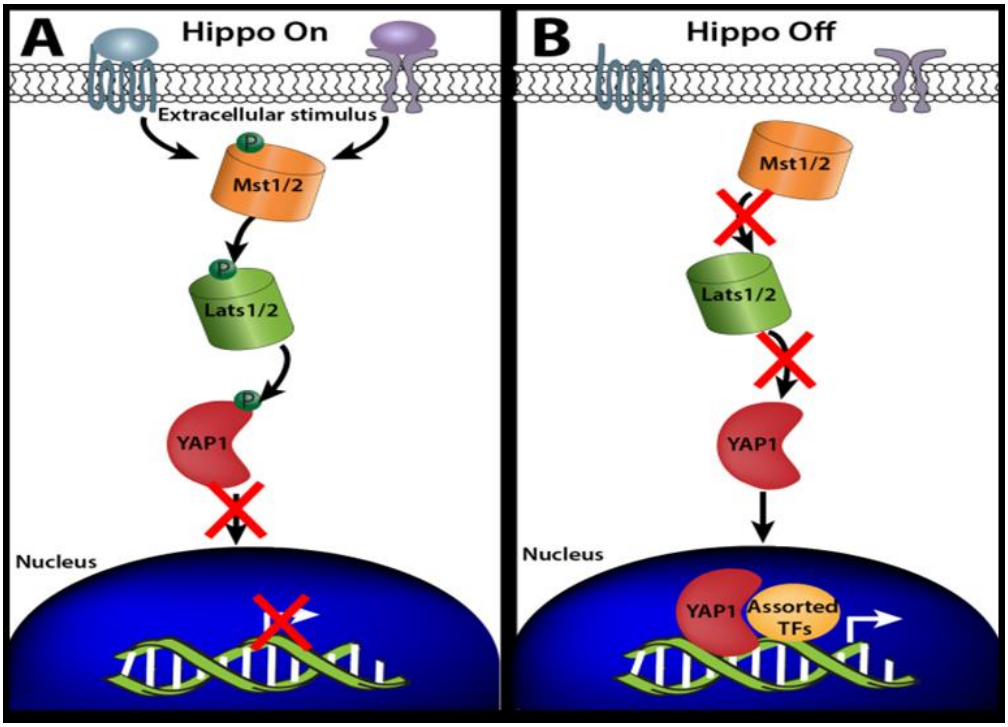

Figure 1.7 Canonical Mammalian Hippo Pathway (**A**) Activation of Hippo Pathway (Hippo On) results in the phosphorylation/activation of the upstream negative kinase regulators MST1/2 and LATS1/2. MST1/2 and LATS1/2 activation phosphorylates YAP leading to cytoplasmic accumulation and inactivation. (**B**) In the absence of stimulus (Hippo Off), YAP is dephosphorylated and localized to the nucleus where it is active. This enables YAP to interact with several transcription factors to drive gene transcription.

MST1/2 activation allows for phosphorylation and activation of SAV1. Active SAV1 serves as a binding domain for MST1/2, increasing its catalytic activity. Catalytically active MST1/2 will then proceed to phosphorylate and activate downstream kinases LATS1/2. Active LATS1/2 phosphorylates YAP, resulting in its transcriptional inactivation and cytoplasmic retention[203]. Hippo is considered "ON" when upstream kinase regulators MST1/2 and LATS1/2 are active and YAP is phosphorylated[204,205]. Phosphorylation of YAP inactivates its activity by several mechanisms. YAP has five consensus residues that can be phosphorylated by LATS1/2[206]. The two most important phosphorylation sites in humans are Serine127 (murine S118) and Serine397 (murine S381). Phosphorylation at S127 forms a docking site for the 14-3-3 protein family, which binds and sequesters YAP within the cytoplasm[205]. YAP S381 phosphorylation, the "phospho-degron" motif, recruits casein kinase 1 (CK1δ/ε), which in turn phosphorylates two more sites on YAP (S384 and S387). CK1δ/ε phosphorylation targets YAP for ubiquitin-mediated proteosomal degradation[207]. These two mechanisms allow LATS1/2 to regulate YAP in both a temporal and spatial manner by both mediating its subcellular localization and protein stability.

While human YAP sites S127 and S381 are the most well studied regulatory phosphosites, there are reports that other residues besides serine and threonine can regulate YAP activity. For example, Yap can be phosphorylated by cABL at Y357 and Y391 leading to p73-mediated apoptosis. [208].

In the absence of upstream kinase regulation (Hippo signaling "OFF"), YAP is un-phosphorylated and allowed to translocate into the cell nucleus. YAP is a transcription co-activator, so it lacks any native DNA binding elements and must interact with specific transcription factors. In *Drosophila*, Scalloped (*sd*) is the key transcriptional partner while the TEAD family of transcriptional factors (orthologs of Scalloped) are the primary binding partners in mammals[206,209].

While the TEADs (TEAD1-4) are the primary YAP binding partner, YAP can interact with other transcription factors, including RUNX1/2, p63/73, and SMAD2/3[198,210-215].

Transcriptional co-activator with PDZ binding motifs (TAZ), a YAP paralog, is also considered a final Hippo pathway effector protein. Originally identified to be a 14-3-3 binding partner in protein pulldown assays, TAZ shares 50% sequence homology with YAP suggesting shared regulation and function[216]. In agreement, LATS1/2 phosphorylation on S89 (equivalent to YAP S127) cytoplasmically localizes and inactivates TAZ[217]. Furthermore, YAP and TAZ share similar transcriptional binding partners, such as RUNX2, SMAD2/3, TEADs, and PPARγ[212,213,218,219].

Overexpression and knockout studies of *Yap* in both *Drosophil*a and mammalian systems shows little overlap in gene expression profiles[220]. These studies suggest Yap targets may be species, cell and tissue-specific. However, a small subset of genes exhibits similar functions when compared across species. Common *Drosophila yki* gene targets include *bantam, diap1,* and *cyclin E*, which regulate apoptosis inhibition and cellular proliferation[221]. In mammals, these genes are not identical but do exhibit functional overlap. Examples include *Birc2* and *Bric5*, homologs of *Drosophila diap1,* which also inhibit apoptotic programs[222]. Other mammalian targets include tissue patterning factors *Hoxa1* and *Hoxc13*[223]. However, most murine YAP targets are secreted factors such as amphiregulin (AREG), cysteine rich angiogenic inducer 61 (CYR61) and connective tissue growth factor (CTGF)[224,225].

YAP activity is also dependent on protein-protein binding interactions. YAP was first identified in yeast two-hybrid assays as an interacting partner of the Yes protein kinase, leading to the name **Y**es **a**ssociated **p**rotein of **65** kilodaltons (YAP65) [226].

Extensive structural characterization studies identified the existence of the WW domain, two tryptophan (W) residues separated by 20-25 amino acids, as a novel protein interaction domain. *YAP* encodes two isoforms, which result from alternative transcript splicing, conferring a protein with a single WW domain (YAP1) or two WW domains (YAP2)[227]. Elegant transcriptional and biochemical work by Sudol *et al* identified YAP2 to be the predominant isoform in vertebrates[228]. The WW domain on YAP mediates most of its protein interactions, as its reciprocal binding module PPxY is found on a substantial number of proteins (≥2000), including all upstream protein Hippo kinases[229]. YAP WW domains contain growth inhibitory sites, as mutations in either domain confer spontaneous transformation capabilities in many epithelial cell types (e.g., HEK293, MCF10A, and NMuMG)[230,231].

YAP contains a C-terminal PDZ binding pocket. The PDZ domain is named after the first three proteins discovered to share this homologous protein domain: **p**ost synaptic density protein (PSD95), **D**rosophila disc large tumor suppressor (Dlg1), and **z**onula occludens-1 protein (Zo-1)[232]. In YAP, the PDZ domain regulates cellular localization, as its deletion inhibits nuclear translocation and transactivation activity of CTGF expression, a YAP target gene[225].

The **T**EAD **I**nteracting **D**omain (TID) is located at the N-terminus of YAP. The TID domain confers binding specificity to the TEAD transcription factors. Mutations in the YAP TID abolish TEAD interaction, and subsequently, proliferation[233]. Therefore, TEADs are the primary transcription factor bound by YAP. Alanine substitutions at YAP S127, found within the TID, are sufficient to promote TEAD-mediated overgrowth phenotypes both *in vitro* and *in vivo*[205].

With core Hippo pathway components containing several protein-protein interaction modules, it is not a surprise that the pathway is not dependent on a single signaling input. Rather a broad range of upstream elements can influence Hippo-mediated YAP activity. In agreement,

the Hippo signaling cascade is now recognized as an important "integrator" of many signaling networks.

The upstream inputs that influence Hippo signaling have been pooled into different "modules", including extracellular growth factors, apical-basolateral polarity and tight junction proteins, adherin and cadherin-catenin complexes, morphogen gradients (Planar cell polarity) and actin mechanotransduction (**Fig 1.8**).

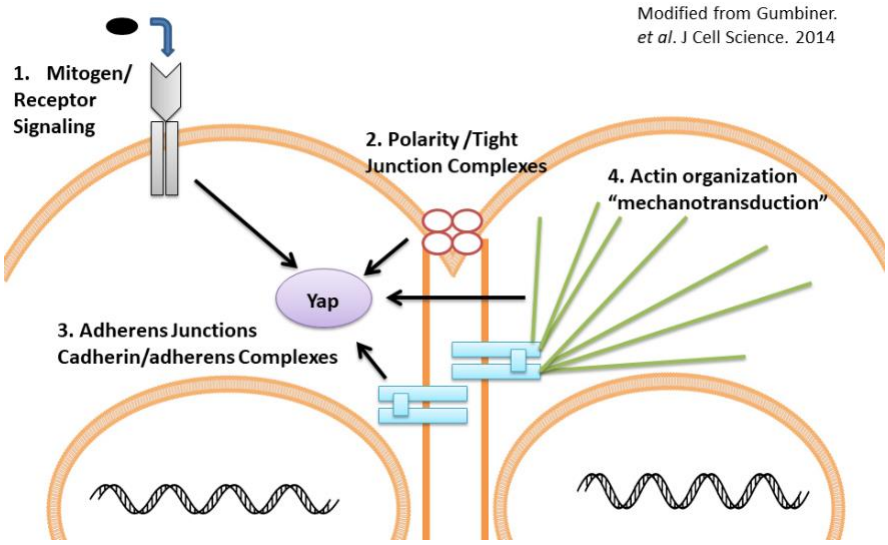

Figure 1.8 Multiple upstream inputs can regulate Hippo-Yap signaling. Due to the diversity of networks that can converge on YAP, it serves as an important signal integrator with broad influence in many cellular decisions. Modified from *Gumbiner et al*[234].

Extracellular growth factors: The best-characterized upstream regulatory module of Hippo signaling is the secreted small molecules that activate GPCRs (**Fig1.8**). Specific GPCR agonists (e.g., lysophosphatidic acid (LPA), sphingosine 1-phopsphate (S1P) and thrombin) activate downstream $G\alpha_{12/13}$ and $G\alpha_{q/11}$ signaling and inhibit phosphorylation of LATS1/2. LATS1/2 inactivation protects YAP from phosphorylation and allows for its nuclear accumulation. Conversely, specific hormones (e.g., epinephrine and glucagon) activate downstream $G\alpha_s$ signaling, leading to LATS1/2 activation and YAP inactivation[235]. Soluble EGF (epidermal growth factor) binding to its receptor (EGFR) activates PI3-kinase (PI3K) to repress LATS1/2 activity.[236].

Altered PI3K activity is an important regulator of many cancers, so inhibition of this signaling cascade has obvious clinical interest[237,238].

Most intriguing is the YAP signaling crosstalk with other known pathway activating factors. An example is the cross talk between YAP and the WNT signaling mediator β-catenin [239,240].Under conditions of WNT signaling inhibition ("Wnt off"), β-catenin is actively degraded in a destruction complex within the cytoplasm, thereby inhibiting β-catenin-mediated transcriptional activity (e.g., *Axin1*, *Myc* and *Hnf1a*). Interestingly, YAP is also cytoplasmic in the "Wnt off" condition. After stimulation with soluble WNT factors (WNT3a), YAP and β-catenin translocate to the nucleus and initiate downstream transcriptional activity[240]. Observations of YAP and β-catenin co-nuclear translocation led to the discovery that YAP is a scaffolding component of the WNT destruction complex. Destruction complex-YAP binding serves as a signaling cue to initiate β-TrCP-mediated ubiquitination of YAP and β-catenin. When WNT signaling is activate, YAP is dephosphorylated and decoupled from the destruction complex, leading to destruction complex instability and disassembly. Destruction complex decoupling allows β-catenin and YAP to both escape degradation and enter to the nucleus[240].

YAP cross-talk activity is not restricted to WNT signaling and is modulated by other ligand-activated signaling pathways, such as the TGFβ, BMP, NOTCH, and the JAK-STAT family[239,241-244]. The vast array of signaling pathways that intersect with Hippo highlights its importance as an integrator of multiple converging pathways, and as such, it is a critical modulator of cellular and tissue homeostasis[245].

Apical-basolateral polarity and tight junction proteins: Proteins that enable apical-basolateral cell positioning also regulate YAP activity (**Fig 1.8**). The first relationship was observed in *Drosophila* with mutations in polarity genes *scribble* and *dlg*. These mutations

phenocopy Hippo related tissue overgrowth phenotypes[246]. Loss of the human homolog *SCRIB* frequently leads to sustained nuclear YAP accumulation and is associated with various cancers[247]. The best characterized apical regulator of YAP is the *Drosophila* transmembrane protein Crumbs and its human ortholog CRUMBS3 (*CRB3*). siRNA knockdown in either species results in nuclear localization of Yap and hyperproliferation of contact inhibited epithelial cell cultures[248]. Mechanistic analysis reveals CRUMBS acts as a scaffolding protein that can interact with various Hippo pathway protein components. When CRUMBS extracellular domain contacts neighboring cells, MST1/2 and LATS1/2 are both sequestered to the CRUMBS intracellular domain and activated[248]. Other Hippo pathway scaffolding partners include the AMOT (Angiomotin) family, AMOT1,2 and 3. In contrast to canonical signaling, AMOT-YAP interactions are not dependent on phosphorylation but on WW binding domains[249]. AMOT proteins directly interact with YAP at tight junctions, thereby restricting Yap localization to the cytoplasm[250]. Other labs have described AMOT binding LATS1/2 and enhancing phosphorylation activity but this is still a subject of debate[250,251]. Interestingly, AMOT appears to be specific to mammals, as *Drosophila* homologs have yet to be identified[250,252].

Cadherin-catenin complexes: Proteins that enable cell-cell adherence influence Hippo signaling (**Fig 1.8**). An example is α-catenin, a linker protein that mediates interactions between membrane cadherins and the actin cytoskeleton[253]. In skin keratinocytes, α-catenin sequesters phosphorylated YAP and inhibits its dephosphorylation by PP2A (Protein phosphatase 2). Knockdown of α-catenin in skin basal cell progenitors causes hyperproliferation and failure in keratinocyte differentiation[254,255]. KIBRA (*WWC1*), an enhancer of cadherin stability, activates Hippo signaling[256]. Direct interaction between KIBRA, MST1/2 and LATS1/2 activate Hippo signaling, while preventing these kinases from ubiquitin mediated degradation[257].

Morphogen Gradient/Planar Cell Polarity: The first described upstream regulators of Hippo pathway were the planar cell polarity related proto-cadherins Fat and Dachsous[258,259]. Fat and Dachsous are both atypical cell surface receptors [260]. Fat signaling is genetically upstream of *yki*[258]. In *Drosophila,* deletion of *fat* results in imaginal disc overgrowth phenotypes, which are suppressed by *yki* deletion[261]. In contrast to direct 1-to-1 ligand binding interactions classically observed between cell membrane interacting proteins, Fat and Dachsous display a sharp gradient opposite of one another. When cells are freely able to move and proliferate, Fat-Dachsous binding is transient and downstream signaling is not activated. When space between cells becomes limited, Fat-Dachsous interactions increase and stabilize connections between adjacent cells[262]. Stabilization is reinforced by several other proteins, such as Dachs, an unconventional myosin protein. Dachs is a negative regulator of Warts (the *Drosophila* homologue of LATS1/2), but its exact mechanism of negative regulation is unknown[263].

Regardless of the exact mechanisms, regulation of Hippo signaling is an important focus of how organisms pattern complex tissue. However, much work is needed to elucidate how vertebrates have co-evolved this mechanism. The closest homolog to *Drosophila* Fat in mammals is FAT4 but there is currently minimal evidence that it functions in a similar manner[264].

Mechanotransduction/Actin networks: The physical environment and its influence on actin organization and assembly also affects YAP localization and activity (**Fig1.8**). Piccolo *et al* demonstrated YAP localization is regulated by substrate rigidity and tension[265]. When cells are grown on soft matrices (0.2-1kPA), YAP is exclusively localized in the cytoplasm. In contrast, YAP is localized within the nucleus when grown on hard matrixes (40-60kPA). Similarly, cell geometry affects YAP localization[265]. Mechanically induced YAP localization and activity extends to several *in vivo* models, such as blood vessel hemodynamics[266-268]. Endothelial cells are

exposed to continual unidirectional fluid sheer stresses. Under these conditions, YAP is cytoplasmically localized and inactivated. However, mice prone to atherosclerosis undergo periods of perturbed blood flow, stimulating Yap nuclear localization, transcriptional activation and cellular proliferation[269,267,270,271]. These studies highlight YAP's role in both vascular homeostasis and pathological remodeling.

Actin dynamics also modulate Hippo pathway activity. [272]. Inhibitors or activators of actin contractility, such as Rho-Rock inhibitors, perturb YAP activity and downstream target gene expression[265]. In addition, modulations of actin polymerization maintenance proteins, such as capping proteins, exhibit profound effects on Hippo signaling [273,274]. For example, knockdown of CAPZ, an inhibitor of F-actin polymerization, increases F-actin stress fiber formation, resulting in YAP nuclear localization. Overexpression of CAPZ results in F-actin disassembly and YAP cytoplasmic re-localization [275]. While the field of mechanotransduction is still in its infancy, it will be important to elucidate how these signals correspond to tissue patterning and homeostasis.

This overview highlights the concept that Hippo-YAP is in a unique position to act as a signaling integrator between various stimuli and can serve as a unique sensor of injury and homeostatic maintenance.

1.11 Hippo Pathway influences both regenerative and scar forming wound repair.

The role of Hippo signaling pathway, in organ development and tissue homeostasis, is conserved across a variety of species (e.g. axolotl, frogs, muriods and humans). However, YAP's direct role in injury resolution and healing is dependent on both organism model and injury context. For example, Yap is required in planarian (flatworm) regenerative repair. Planarian regeneration is mediated by a specific totipotent cell population, the neoblast (**Fig1.1B**). Following head amputation, expression of the planarian yki-related gene(*djyki*), the planarian homolog of *YAP*, is

restricted to neoblasts[200]. siRNA knockdown of *djyki* during head regeneration results in failed head reconstitution, due to failure of neoblast totipotency[276]. In agreement, neoblast exhaustion occurs when *djyki* is selectively depleted. Interestingly, siRNA knockdown of the planarian *lats1/2* homolog generates healed heads twice the size of the original tissue. This further exemplifies the conserved evolutionary role of Hippo-YAP in organ size control [276,277].

Yap activity is also vital in amphibian limb regeneration. *yap* is highly expressed and transcriptionally active in the mesenchymal cell populations during early periods of *Xenopus* blastema formation. Dominant negative expression of *yap* fails to properly regenerate functional limbs[277]. Intriguingly, *yap* inhibition does not stop proliferation in the blastema. Instead, mesenchymal blastema cells fail to differentiate, resulting in disrupted digit tip formation [278]. Gene expression arrays reveal Yap's role in body plan symmetry. Dominant negative Yap transgene disrupts expression of multiple Hox genes: *hoxa11* and *hoxa1*. Loss of Hox positional coordinates leads to blastema cell mis-localization and disrupted tissue patterning[277].

In zebrafish, Yap is absent within the uninjured tissue architecture. Upon tail amputation, Yap is up-regulated but differentially localized according to various cellular densities within a migrating proximal-distal gradient. Nuclear Yap in the proximal zone corresponds to areas of high cellular proliferation, while cytoplasmic Yap overlaps with areas of low distal proliferation [279]. The relationship between varying cellular densities and Yap localization during periods of fin regeneration is dependent on F-actin dynamics. Using the F-actin activator jasplakinolide, hyperconfluent distal cell populations induce Yap nuclear activity, leading to ectopic tail fin outgrowths. This would suggest Yap has separate spatial and temporal functions that must be tightly regulated to achieve proper tissue reconstitution[280].

While Yap generally functions in a pro-regenerative manner in lower order organisms, its role in adult mammalian wound repair is harder to dissect. As adult mammals exhibit diminished capacity for regenerative repair, limited models exist to determine YAP's specific role at the global level. Therefore, many studies focus on the role of YAP in organ-specific models of wound repair.

The liver is one of the few mammalian organs that demonstrates high regenerative capability. Amputation of 70% of the liver mass can be restored within 14-30 days in the rat or 3-6 months in humans[60,281-283]. In contrast to the various cell behaviors observed in limb regeneration (e.g., dedifferentiation and lineage restricted progenitor cells (**Fig1.1A,B**)), liver regeneration is achieved by hepatocyte compensatory growth (**Fig1.1D**)[5]. Terminally differentiated hepatocytes compensate for the loss of tissue mass by re-entering the cell cycle until normal liver size is restored[5,60].

Mammalian models of liver amputation (2/3 partial hepatectomy) demonstrate the Hippo pathway is required for regeneration[284]. Quiescent hepatocytes normally maintain active MST1/2, LATS1/2 and inactive YAP. Immediately upon injury (1hr), the upstream kinases are quickly inactivated and YAP is translocated to the hepatocyte nucleus. YAP nuclear translocation initiates and sustains hepatocyte proliferation. Upon restoration of normal liver size and tissue hemostasis (10-15 days post injury), hepatocytes quiesce and YAP is inactivated[284-286]. Paradoxically, YAP activation can also promote liver fibrosis. Utilizing the chronic CCL_4 –induced fibrosis model, YAP nuclear localization is enriched in the stromal myofibroblast populations[287,288]. Inhibition of YAP, either genetically or pharmacologically, attenuates fibrosis *in vivo* [289], with decreased myofibroblasts and collagen type 1 scar tissue[290,291]. It is unclear how YAP activity can initiate two seemingly opposite injury response outcomes. Current ideas focus on the differences in the cellular populations that require YAP activity for proliferation. In liver regeneration models,

hepatocytes are the primary proliferative cell type with no contribution from the myofibroblast population[292]. In fibrosis, myofibroblasts proliferate rather than hepatocytes[228]. Alternatively, YAP may promote the differentiation of hepatic stellate cells into myofibroblasts during fibrotic repair.[287,293]. However, this mechanism appears to be organ specific and not demonstrative for all fibrosis models.

The intestines also maintain regenerative potential in adulthood[294]. Like the skin, cells of the intestinal villus are constantly undergoing turnover. This self-renewal capability is due to a resident $LGR5^+$ stem cell population found at the base of the villus within the crypt pocket[295]. In models of both colitis (Dextran sodium sulfate/DSS) and radiation sickness (gamma irradiation), YAP orchestrates an ordered regeneration repair program, regulating both crypt cells proliferation and cell fate specification. In YAP conditional knockout mice, DSS-treated mice fail to expand the crypt $LRG5^+$ stem cell population, leading to villus architectural degradation[296,297].

In contrast to YAP generally promoting mammalian organ regeneration (e.g., skin, intestines, and liver), the kidney is the best specific organ example of its role in promoting fibrotic scar tissue formation. Ischemia reperfusion (IR) and unilateral ureter obstruction (UUO) models are severe kidney injury models that result in fibrosis-mediated organ failure [298,299]. YAP activity is generally beneficial for tubular epithelial survival in acute IR injuries[182]. However, chronic IR injury models promote maintained YAP activity, leading to aberrant tubular architecture and severe fibrotic remodeling[300]. The same is also seen in UUO injury models[300,301]. Yuen *et al* elucidated a potential mechanism by which Hippo and SMAD signaling both coordinate the fibrotic repair response. In kidney fibroblasts culture, YAP and SMAD form a transcriptional complex, which is sufficient to promote a myofibroblast-like gene expression pattern (e.g., collagen type I/III and ACTA2 stress fiber assembly)[302]. Interestingly, YAP-SMAD binding

potential is enhanced under conditions of increased substrate stiffness. Disruption of YAP-SMAD binding, by small molecule (e.g., YAP inhibitor Verteporfin), is sufficient to attenuate fibrotic remolding in UUO injury models. However, the antifibrotic effects of these drugs are only realized in pre-existing fibrotic conditions[303]. A possible interpretation could be that YAP does not initiate the fibrotic repair. Rather, YAP activity is sustained due to increasing tissue stiffness. The continuous stiffening may be promoting a systemic positive feedback loop, further exacerbating the ongoing fibrotic response[304]. Regardless, this result indicates matrix stiffness differences in regenerative and fibrotic responses may be a key factor in regulating the differential activity of YAP.

Adult mammalian cardiac tissue displays dismal proliferative potential, when compared to the liver, intestine and kidney. Injuries to the heart almost always result in maladaptive scar tissue repair, which reduces cardiac function[305,306]. Therefore, promoting adult cardiomyocyte proliferation is the goal for heart disease treatment. In this regard, YAP may be a potential target due to its role in cardiac development. YAP nuclear activity peaks during periods of active cardiomyocyte proliferation[307]. When reaching normal heart size, the Hippo pathway is stimulated with MST1/2, LATS1/2 activation and YAP inhibition.[308] Cardiomyocyte-specific YAP overexpression results in cardiac hyperplasia[307,309]. Correspondingly, *Yap* deletion causes lethal myocardial hypoplasia by impairing cardiomyocyte proliferation[310]. Because YAP promotes cardiomyocyte proliferation, inhibition of the Hippo pathway or YAP activation may be an important tool to stimulate adult mammalian cardiac regeneration [311]. In agreement, cardiomyocyte-specific deletion of SAV1, during and after myocardial infarction, is sufficient to stimulate proliferation in surviving cardiomyocytes and restore cardiac function while decreasing scar tissue formation[312-314]. Viral mediated YAP activation in cardiomyocytes display similar

results[315]. Taken together, these studies demonstrate the adult heart may have an unappreciated regenerative capability and YAP activity is key to unlocking this potential.

1.12 Summary and Research Aims

The overall goal of this study is to elucidate molecular mechanisms by which the African spiny mouse, a novel adult mammalian model of regeneration, achieves scar-free wound repair. As previously described, all mammals studied to date exhibit regenerative wound repair during fetal life. However, unlike species of fish and certain amphibians, most mammals lose this ability in early postnatal development and instead resort to scar tissue repair. While limited scar formation is an essential component in mammalian wound repair, excessive scarring from chronic injury and inflammation will ultimately result in fibrosis. Fibrotic conditions, such as chronic kidney disease, cirrhosis, dermal and pulmonary fibrosis, are enormous health burdens due to their direct role in organ failure. Unfortunately, no effective antifibrotic therapies exist, and advanced fibrosis requires organ transplantation for survival. To effectively develop therapies to inhibit fibrosis, new approaches are needed, particularly in the mammalian system.

Using *Acomys* as a model of adult mammalian regenerative potential**, the overall hypothesis is that in response to injury, adult *Acomys* can re-activate early developmental pathways necessary for organogenesis which are normally silenced in non-regenerative adult mammalian species**. While the cellular and molecular mechanisms directly responsible for this regeneration are unknown, an ideal candidate to begin probing how *Acomys* has genetically adapted the tools necessary for such a unique phenotype is the Hippo signaling effecter protein YAP. YAP, a transcriptional co-activator, is required for organ size control and tissue architecture, essential components of proper organogenesis. As elements of regeneration mirror certain aspects

of development, it is highly likely that these genetic adaptations would include alterations in YAP regulation.

Specific Aims1: Compare myofibroblast formation and resolution in regenerative (*Acomys*) and non-regenerative (adult Mus/Human) fibroblast populations in response to injury *in vivo* and fibrotic inducing agents *in vitro*

Specific Aim 2: Investigate the regulation of YAP activity to determine if adult regenerative potential is re-activation of developmentally regulated pathways.

Specific Aim 3: Characterize the cellular mechanisms *Acomys* utilize to undergo scar-free wound repair.

1.13 References

1 Wong, V. W., Gurtner, G. C. & Longaker, M. T. Wound healing: a paradigm for regeneration. *Mayo Clin Proc* **88**, 1022-1031, doi:10.1016/j.mayocp.2013.04.012 (2013).

2 Somorjai, I. M. L. Amphioxus regeneration: evolutionary and biomedical implications. *Int J Dev Biol* **61**, 689-696, doi:10.1387/ijdb.170219is (2017).

3 Gurtner, G. C., Werner, S., Barrandon, Y. & Longaker, M. T. Wound repair and regeneration. *Nature* **453**, 314-321, doi:10.1038/nature07039 (2008).

4 Weissman, I. L., Anderson, D. J. & Gage, F. Stem and progenitor cells: origins, phenotypes, lineage commitments, and transdifferentiations. *Annu Rev Cell Dev Biol* **17**, 387-403, doi:10.1146/annurev.cellbio.17.1.387 (2001).

5 Fausto, N. Liver regeneration and repair: hepatocytes, progenitor cells, and stem cells. *Hepatology* **39**, 1477-1487, doi:10.1002/hep.20214 (2004).

6 Jopling, C., Boue, S. & Izpisua Belmonte, J. C. Dedifferentiation, transdifferentiation and reprogramming: three routes to regeneration. *Nat Rev Mol Cell Biol* **12**, 79-89, doi:10.1038/nrm3043 (2011).

7 Selman, K. & Kafatos, F. C. Transdifferentiation in the labial gland of silk moths: is DNA required for cellular metamorphosis? *Cell Differ* **3**, 81-94 (1974).

8 Tanaka, E. M. & Reddien, P. W. The cellular basis for animal regeneration. *Dev Cell* **21**, 172-185, doi:10.1016/j.devcel.2011.06.016 (2011).

9 Ferretti, P. & Géraudie, J. *Cellular and molecular basis of regeneration : from invertebrates to humans*. (Wiley, 1997).

10 Goss, R. J. The evolution of regeneration: Adaptive or inherent? *Journal of Theoretical Biology* **159**, 241-260, doi:https://doi.org/10.1016/S0022-5193(05)80704-0 (1992).

11 Vivien, C., E Hudson, J. & Porrello, E. *Evolution, comparative biology and ontogeny of vertebrate heart regeneration*. Vol. 1 (2016).

12 Jazwinska, A. & Sallin, P. Regeneration versus scarring in vertebrate appendages and heart. *J Pathol* **238**, 233-246, doi:10.1002/path.4644 (2016).

13 Brockes, J. P., Kumar, A. & Velloso, C. P. Regeneration as an evolutionary variable. *J Anat* **199**, 3-11 (2001).

14 Ito, K. *et al*. Differential reparative phenotypes between zebrafish and medaka after cardiac injury. *Dev Dyn* **243**, 1106-1115, doi:10.1002/dvdy.24154 (2014).

15 Porrello, E. R. & Olson, E. N. A neonatal blueprint for cardiac regeneration. *Stem Cell Res* **13**, 556-570, doi:10.1016/j.scr.2014.06.003 (2014).

16 Kozmik, Z. *et al*. Assembly of the cnidarian camera-type eye from vertebrate-like components. *Proc Natl Acad Sci U S A* **105**, 8989-8993, doi:10.1073/pnas.0800388105 (2008).

17 Wagner, G. P. & Misof, B. Y. Evolutionary modification of regenerative capability in vertebrates: a comparative study on teleost pectoral fin regeneration. *J Exp Zool* **261**, 62-78, doi:10.1002/jez.1402610108 (1992).

18 Barr, H. J. Regeneration and Natural Selection. *The American Naturalist* **98**, 183-186, doi:10.1086/282317 (1964).

19 Morgan, T. H. *Regeneration*. (Macmillan, 1901).

20 Galliot, B. *Regeneration in Hydra*. (2006).

21 D. Park, H., B. Ortmeyer, A. & P. Blankenbaker, D. *Cell Division during Regeneration in Hydra*. Vol. 227 (1970).

22 Bosch, T. & N. David, C. *Stem Cells of Hydra magnipapillata can differentiate into somatic cells and germ line cells*. Vol. 121 (1987).

23 Bode, H. *The interstitial cell lineage of hydra: A stem cell system that arose early in evolution*. Vol. 109 (Pt 6) (1996).

24 M. Stevens, N. *Notes on regeneration in planaria lugubris*. Vol. 13 (1901).

25 Russell Bardeen M.D, C. & H. Baetjer M.D, F. *Inhibitive action of Roentgen rays on regeneration in plana-rians*. Vol. 1 (2005).

26 Baguna, J., Saló, E. & Auladell, C. *Regeneration and pattern formation in planarians III. Evidence that neoblasts are totipotent stem cells and the source of blastema cells*. Vol. 107 (1989).

27 Newmark, P. A. & Sanchez Alvarado, A. Bromodeoxyuridine specifically labels the regenerative stem cells of planarians. *Dev Biol* **220**, 142-153, doi:10.1006/dbio.2000.9645 (2000).

28 Rinkevich, Y., Paz, G., Rinkevich, B. & Reshef, R. Systemic bud induction and retinoic acid signaling underlie whole body regeneration in the urochordate Botrylloides leachi. *PLoS Biol* **5**, e71, doi:10.1371/journal.pbio.0050071 (2007).

29 Rinkevich, B., Shlemberg, Z. & Fishelson, L. Whole-body protochordate regeneration from totipotent blood cells. *Proc Natl Acad Sci U S A* **92**, 7695-7699 (1995).

30 Kragl, M. *et al*. Cells keep a memory of their tissue origin during axolotl limb regeneration. *Nature* **460**, 60-65, doi:10.1038/nature08152 (2009).

31 Tu, S. & Johnson, S. L. Fate restriction in the growing and regenerating zebrafish fin. *Dev Cell* **20**, 725-732, doi:10.1016/j.devcel.2011.04.013 (2011).

32 Relaix, F., Rocancourt, D., Mansouri, A. & Buckingham, M. A Pax3/Pax7-dependent population of skeletal muscle progenitor cells. *Nature* **435**, 948-953, doi:10.1038/nature03594 (2005).

33 Mescher, A. L. & Neff, A. W. Limb regeneration in amphibians: immunological considerations. *ScientificWorldJournal* **6 Suppl 1**, 1-11, doi:10.1100/tsw.2006.323 (2006).

34 Mescher, A. L. & Neff, A. W. Regenerative capacity and the developing immune system. *Adv Biochem Eng Biotechnol* **93**, 39-66 (2005).

35 Eguchi, G. *et al*. Regenerative capacity in newts is not altered by repeated regeneration and ageing. *Nat Commun* **2**, 384, doi:10.1038/ncomms1389 (2011).

36 Young, H. E., Bailey, C. F., Markwald, R. R. & Dalley, B. K. Histological analysis of limb regeneration in postmetamorphic adult Ambystoma. *Anat Rec* **212**, 183-194, doi:10.1002/ar.1092120213 (1985).

37 Sandoval-Guzman, T. *et al*. Fundamental differences in dedifferentiation and stem cell recruitment during skeletal muscle regeneration in two salamander species. *Cell Stem Cell* **14**, 174-187, doi:10.1016/j.stem.2013.11.007 (2014).

38 Poss, K. D., Wilson, L. G. & Keating, M. T. Heart regeneration in zebrafish. *Science* **298**, 2188-2190, doi:10.1126/science.1077857 (2002).

39 Itou, J. *et al*. Migration of cardiomyocytes is essential for heart regeneration in zebrafish. *Development* **139**, 4133-4142, doi:10.1242/dev.079756 (2012).

40 Witman, N., Murtuza, B., Davis, B., Arner, A. & Morrison, J. I. Recapitulation of developmental cardiogenesis governs the morphological and functional regeneration of adult newt hearts following injury. *Dev Biol* **354**, 67-76, doi:10.1016/j.ydbio.2011.03.021 (2011).

41 Gonzalez-Rosa, J. M., Martin, V., Peralta, M., Torres, M. & Mercader, N. Extensive scar formation and regression during heart regeneration after cryoinjury in zebrafish. *Development* **138**, 1663-1674, doi:10.1242/dev.060897 (2011).

42 Laube, F., Heister, M., Scholz, C., Borchardt, T. & Braun, T. Re-programming of newt cardiomyocytes is induced by tissue regeneration. *J Cell Sci* **119**, 4719-4729, doi:10.1242/jcs.03252 (2006).

43 Wang, J. *et al.* The regenerative capacity of zebrafish reverses cardiac failure caused by genetic cardiomyocyte depletion. *Development* **138**, 3421-3430, doi:10.1242/dev.068601 (2011).

44 Jopling, C. *et al.* Zebrafish heart regeneration occurs by cardiomyocyte dedifferentiation and proliferation. *Nature* **464**, 606-609, doi:10.1038/nature08899 (2010).

45 Kikuchi, K. *et al.* Primary contribution to zebrafish heart regeneration by gata4(+) cardiomyocytes. *Nature* **464**, 601-605, doi:10.1038/nature08804 (2010).

46 Rowlatt, U. Intrauterine wound healing in a 20 week human fetus. *Virchows Arch A Pathol Anat Histol* **381**, 353-361 (1979).

47 Takeo, M., Lee, W. & Ito, M. Wound healing and skin regeneration. *Cold Spring Harb Perspect Med* **5**, a023267, doi:10.1101/cshperspect.a023267 (2015).

48 Kishi, K., Okabe, K., Shimizu, R. & Kubota, Y. Fetal skin possesses the ability to regenerate completely: complete regeneration of skin. *Keio J Med* **61**, 101-108 (2012).

49 Spurlin, J. W., 3rd & Lwigale, P. Y. Wounded embryonic corneas exhibit nonfibrotic regeneration and complete innervation. *Invest Ophthalmol Vis Sci* **54**, 6334-6344, doi:10.1167/iovs.13-12504 (2013).

50 Cass, D. L. *et al.* Wound size and gestational age modulate scar formation in fetal wound repair. *J Pediatr Surg* **32**, 411-415 (1997).

51 Longaker, M. T. *et al.* Adult skin wounds in the fetal environment heal with scar formation. *Ann Surg* **219**, 65-72 (1994).

52 Armstrong, J. R. & Ferguson, M. W. Ontogeny of the skin and the transition from scar-free to scarring phenotype during wound healing in the pouch young of a marsupial, Monodelphis domestica. *Dev Biol* **169**, 242-260, doi:10.1006/dbio.1995.1141 (1995).

53 Drenckhahn, J. D. *et al.* Compensatory growth of healthy cardiac cells in the presence of diseased cells restores tissue homeostasis during heart development. *Dev Cell* **15**, 521-533, doi:10.1016/j.devcel.2008.09.005 (2008).

54 Porrello, E. R. *et al.* Heritable pathologic cardiac hypertrophy in adulthood is preceded by neonatal cardiac growth restriction. *Am J Physiol Regul Integr Comp Physiol* **296**, R672-680, doi:10.1152/ajpregu.90919.2008 (2009).

55 Porrello, E. R. *et al.* Transient regenerative potential of the neonatal mouse heart. *Science* **331**, 1078-1080, doi:10.1126/science.1200708 (2011).

56 Haubner, B. J. *et al.* Complete cardiac regeneration in a mouse model of myocardial infarction. *Aging (Albany NY)* **4**, 966-977, doi:10.18632/aging.100526 (2012).

57 Walmsley, G. G. *et al.* A mouse fetal skin model of scarless wound repair. *J Vis Exp*, 52297, doi:10.3791/52297 (2015).

58 Mackool, R. J., Gittes, G. K. & Longaker, M. T. Scarless healing. The fetal wound. *Clin Plast Surg* **25**, 357-365 (1998).

59 Bastakoty, D. *et al.* Inhibition of Wnt/beta-catenin pathway promotes regenerative repair of cutaneous and cartilage injury. *Faseb j* **29**, 4881-4892, doi:10.1096/fj.15-275941 (2015).

60 Fausto, N., Campbell, J. S. & Riehle, K. J. Liver regeneration. *J Hepatol* **57**, 692-694, doi:10.1016/j.jhep.2012.04.016 (2012).

61 Ho, Y. Y., Lagares, D., Tager, A. M. & Kapoor, M. Fibrosis--a lethal component of systemic sclerosis. *Nat Rev Rheumatol* **10**, 390-402, doi:10.1038/nrrheum.2014.53 (2014).

62 Beumer, J. & Clevers, H. Regulation and plasticity of intestinal stem cells during homeostasis and regeneration. *Development* **143**, 3639-3649, doi:10.1242/dev.133132 (2016).

63 Beerman, I., Luis, T. C., Singbrant, S., Lo Celso, C. & Mendez-Ferrer, S. The evolving view of the hematopoietic stem cell niche. *Exp Hematol* **50**, 22-26, doi:10.1016/j.exphem.2017.01.008 (2017).

64 Akaiwa, H. A Quantitative Study of Wound Healing in the Rat: II. Cell Growth during Wound Healing. *J Med Res* **40**, 371-413 (1919).

65 Menter, D. G. *et al*. Platelet "first responders" in wound response, cancer, and metastasis. *Cancer Metastasis Rev*, doi:10.1007/s10555-017-9682-0 (2017).

66 Rousselle, P., Montmasson, M. & Garnier, C. Extracellular matrix contribution to skin wound re-epithelialization. *Matrix Biol*, doi:10.1016/j.matbio.2018.01.002 (2018).

67 Davie, E. W. A brief historical review of the waterfall/cascade of blood coagulation. *J Biol Chem* **278**, 50819-50832, doi:10.1074/jbc.X300009200 (2003).

68 Simpson, D. M. & Ross, R. The neutrophilic leukocyte in wound repair a study with antineutrophil serum. *J Clin Invest* **51**, 2009-2023, doi:10.1172/jci107007 (1972).

69 Werner, S., Krieg, T. & Smola, H. Keratinocyte-fibroblast interactions in wound healing. *J Invest Dermatol* **127**, 998-1008, doi:10.1038/sj.jid.5700786 (2007).

70 O'Kane, S. & Ferguson, M. W. Transforming growth factor beta s and wound healing. *Int J Biochem Cell Biol* **29**, 63-78 (1997).

71 Qing, C. The molecular biology in wound healing & non-healing wound. *Chin J Traumatol* **20**, 189-193, doi:10.1016/j.cjtee.2017.06.001 (2017).

72 Daley, J. M. *et al*. Modulation of macrophage phenotype by soluble product(s) released from neutrophils. *J Immunol* **174**, 2265-2272 (2005).

73 Providence, K. M. & Higgins, P. J. PAI-1 expression is required for epithelial cell migration in two distinct phases of in vitro wound repair. *J Cell Physiol* **200**, 297-308, doi:10.1002/jcp.20016 (2004).

74 Ohyama, M. *et al*. Characterization and isolation of stem cell-enriched human hair follicle bulge cells. *J Clin Invest* **116**, 249-260, doi:10.1172/jci26043 (2006).

75 Eming, S. A., Brachvogel, B., Odorisio, T. & Koch, M. Regulation of angiogenesis: wound healing as a model. *Prog Histochem Cytochem* **42**, 115-170, doi:10.1016/j.proghi.2007.06.001 (2007).

76 Greaves, N. S., Ashcroft, K. J., Baguneid, M. & Bayat, A. Current understanding of molecular and cellular mechanisms in fibroplasia and angiogenesis during acute wound healing. *J Dermatol Sci* **72**, 206-217, doi:10.1016/j.jdermsci.2013.07.008 (2013).

77 Martin, P. & Nunan, R. Cellular and molecular mechanisms of repair in acute and chronic wound healing. *Br J Dermatol* **173**, 370-378, doi:10.1111/bjd.13954 (2015).

78 Darby, I., Skalli, O. & Gabbiani, G. Alpha-smooth muscle actin is transiently expressed by myofibroblasts during experimental wound healing. *Lab Invest* **63**, 21-29 (1990).

79 Wilgus, T. A., Ferreira, A. M., Oberyszyn, T. M., Bergdall, V. K. & Dipietro, L. A. Regulation of scar formation by vascular endothelial growth factor. *Lab Invest* **88**, 579-590, doi:10.1038/labinvest.2008.36 (2008).

80 Kurkinen, M., Vaheri, A., Roberts, P. J. & Stenman, S. Sequential appearance of fibronectin and collagen in experimental granulation tissue. *Lab Invest* **43**, 47-51 (1980).

81 Ignotz, R. A. & Massague, J. Transforming growth factor-beta stimulates the expression of fibronectin and collagen and their incorporation into the extracellular matrix. *J Biol Chem* **261**, 4337-4345 (1986).

82 Deb, A. & Ubil, E. Cardiac fibroblast in development and wound healing. *J Mol Cell Cardiol* **70**, 47-55, doi:10.1016/j.yjmcc.2014.02.017 (2014).

83 Zeisberg, M. & Kalluri, R. Cellular Mechanisms of Tissue Fibrosis. 1. Common and organ-specific mechanisms associated with tissue fibrosis. *American Journal of Physiology - Cell Physiology* **304**, C216-C225, doi:10.1152/ajpcell.00328.2012 (2013).

84 Davis, J. & Molkentin, J. D. Myofibroblasts: trust your heart and let fate decide. *J Mol Cell Cardiol* **70**, 9-18, doi:10.1016/j.yjmcc.2013.10.019 (2014).

85 Hinz, B. Tissue stiffness, latent TGF-beta1 activation, and mechanical signal transduction: implications for the pathogenesis and treatment of fibrosis. *Curr Rheumatol Rep* **11**, 120-126 (2009).

86 Desmouliere, A., Geinoz, A., Gabbiani, F. & Gabbiani, G. Transforming growth factor-beta 1 induces alpha-smooth muscle actin expression in granulation tissue myofibroblasts and in quiescent and growing cultured fibroblasts. *J Cell Biol* **122**, 103-111 (1993).

87 Serini, G. *et al*. The fibronectin domain ED-A is crucial for myofibroblastic phenotype induction by transforming growth factor-beta1. *J Cell Biol* **142**, 873-881 (1998).

88 Shinde, A. V. *et al*. The alpha4beta1 integrin and the EDA domain of fibronectin regulate a profibrotic phenotype in dermal fibroblasts. *Matrix Biol* **41**, 26-35, doi:10.1016/j.matbio.2014.11.004 (2015).

89 Driesen, R. B. *et al*. Reversible and irreversible differentiation of cardiac fibroblasts. *Cardiovasc Res*, doi:10.1093/cvr/cvt338 (2013).

90 Kisseleva, T. *et al*. Myofibroblasts revert to an inactive phenotype during regression of liver fibrosis. *Proc Natl Acad Sci U S A* **109**, 9448-9453, doi:10.1073/pnas.1201840109 (2012).

91 Desmouliere, A., Redard, M., Darby, I. & Gabbiani, G. Apoptosis mediates the decrease in cellularity during the transition between granulation tissue and scar. *Am J Pathol* **146**, 56-66 (1995).

92 Plikus, M. V. *et al*. Regeneration of fat cells from myofibroblasts during wound healing. *Science* **355**, 748-752, doi:10.1126/science.aai8792 (2017).

93 Desmouliere, A., Chaponnier, C. & Gabbiani, G. Tissue repair, contraction, and the myofibroblast. *Wound Repair Regen* **13**, 7-12, doi:10.1111/j.1067-1927.2005.130102.x (2005).

94 Gabbiani, G., Ryan, G. B. & Majne, G. Presence of modified fibroblasts in granulation tissue and their possible role in wound contraction. *Experientia* **27**, 549-550 (1971).

95 Darby, I. A., Zakuan, N., Billet, F. & Desmouliere, A. The myofibroblast, a key cell in normal and pathological tissue repair. *Cell Mol Life Sci* **73**, 1145-1157, doi:10.1007/s00018-015-2110-0 (2016).

96 Hinz, B. *et al*. The myofibroblast: one function, multiple origins. *Am J Pathol* **170**, 1807-1816, doi:10.2353/ajpath.2007.070112 (2007).

97 Verstovsek, S. *et al*. Role of neoplastic monocyte-derived fibrocytes in primary myelofibrosis. *J Exp Med* **213**, 1723-1740, doi:10.1084/jem.20160283 (2016).

98 Wu, J. *et al*. Origin of Matrix-Producing Cells That Contribute to Aortic Fibrosis in Hypertension. *Hypertension* **67**, 461-468, doi:10.1161/hypertensionaha.115.06123 (2016).

99 Schneider, R. K. *et al*. Gli1(+) Mesenchymal Stromal Cells Are a Key Driver of Bone Marrow Fibrosis and an Important Cellular Therapeutic Target. *Cell Stem Cell* **20**, 785-800.e788, doi:10.1016/j.stem.2017.03.008 (2017).

100 Hung, C. *et al*. Role of lung pericytes and resident fibroblasts in the pathogenesis of pulmonary fibrosis. *Am J Respir Crit Care Med* **188**, 820-830, doi:10.1164/rccm.201212-2297OC (2013).

101 Moore-Morris, T. *et al*. Infarct Fibroblasts Do Not Derive From Bone Marrow Lineages. *Circ Res* **122**, 583-590, doi:10.1161/circresaha.117.311490 (2018).

102 Humphreys, B. D. *et al*. Fate tracing reveals the pericyte and not epithelial origin of myofibroblasts in kidney fibrosis. *Am J Pathol* **176**, 85-97, doi:10.2353/ajpath.2010.090517 (2010).

103 Kanisicak, O. *et al*. Genetic lineage tracing defines myofibroblast origin and function in the injured heart. *Nat Commun* **7**, 12260, doi:10.1038/ncomms12260 (2016).

104 Rinkevich, Y. *et al*. Skin fibrosis. Identification and isolation of a dermal lineage with intrinsic fibrogenic potential. *Science* **348**, aaa2151, doi:10.1126/science.aaa2151 (2015).

105 Jiang, D. *et al*. Two succeeding fibroblastic lineages drive dermal development and the transition from regeneration to scarring. *Nat Cell Biol* **20**, 422-431, doi:10.1038/s41556-018-0073-8 (2018).

106 Kramann, R. *et al*. Perivascular Gli1+ progenitors are key contributors to injury-induced organ fibrosis. *Cell Stem Cell* **16**, 51-66, doi:10.1016/j.stem.2014.11.004 (2015).

107 Wang, S. *et al*. TGF-beta/Smad3 signalling regulates the transition of bone marrow-derived macrophages into myofibroblasts during tissue fibrosis. *Oncotarget* **7**, 8809-8822, doi:10.18632/oncotarget.6604 (2016).

108 Duffield, J. S. Cellular and molecular mechanisms in kidney fibrosis. *J Clin Invest* **124**, 2299-2306, doi:10.1172/jci72267 (2014).

109 Zeisberg, E. M. *et al*. Endothelial-to-mesenchymal transition contributes to cardiac fibrosis. *Nat Med* **13**, 952-961, doi:10.1038/nm1613 (2007).

110 Liu, W., Wang, D. R. & Cao, Y. L. TGF-beta: a fibrotic factor in wound scarring and a potential target for anti-scarring gene therapy. *Curr Gene Ther* **4**, 123-136 (2004).

111 Pohlers, D. *et al*. TGF-beta and fibrosis in different organs - molecular pathway imprints. *Biochim Biophys Acta* **1792**, 746-756, doi:10.1016/j.bbadis.2009.06.004 (2009).

112 Derynck, R. & Zhang, Y. E. Smad-dependent and Smad-independent pathways in TGF-beta family signalling. *Nature* **425**, 577-584, doi:10.1038/nature02006 (2003).

113 Budi, E. H., Duan, D. & Derynck, R. Transforming Growth Factor-beta Receptors and Smads: Regulatory Complexity and Functional Versatility. *Trends Cell Biol* **27**, 658-672, doi:10.1016/j.tcb.2017.04.005 (2017).

114 Beanes, S. R., Dang, C., Soo, C. & Ting, K. Skin repair and scar formation: the central role of TGF-beta. *Expert Rev Mol Med* **5**, 1-22, doi:doi:10.1017/S1462399403005817 (2003).

115 Verrecchia, F., Chu, M. L. & Mauviel, A. Identification of novel TGF-beta /Smad gene targets in dermal fibroblasts using a combined cDNA microarray/promoter transactivation approach. *J Biol Chem* **276**, 17058-17062, doi:10.1074/jbc.M100754200 (2001).

116 Hu, B., Wu, Z. & Phan, S. H. Smad3 mediates transforming growth factor-beta-induced alpha-smooth muscle actin expression. *Am J Respir Cell Mol Biol* **29**, 397-404, doi:10.1165/rcmb.2003-0063OC (2003).

117 Zhao, Y. & Geverd, D. A. Regulation of Smad3 expression in bleomycin-induced pulmonary fibrosis: a negative feedback loop of TGF-beta signaling. *Biochem Biophys Res Commun* **294**, 319-323, doi:10.1016/s0006-291x(02)00471-0 (2002).

118 Khalil, H. *et al*. Fibroblast-specific TGF-beta-Smad2/3 signaling underlies cardiac fibrosis. *J Clin Invest* **127**, 3770-3783, doi:10.1172/jci94753 (2017).

119 Davis, J., Burr, A. R., Davis, G. F., Birnbaumer, L. & Molkentin, J. D. A TRPC6-dependent pathway for myofibroblast transdifferentiation and wound healing in vivo. *Dev Cell* **23**, 705-715, doi:10.1016/j.devcel.2012.08.017 (2012).

120 Kompa, A. R. *et al*. Long-term but not short-term p38 mitogen-activated protein kinase inhibition improves cardiac function and reduces cardiac remodeling post-myocardial infarction. *J Pharmacol Exp Ther* **325**, 741-750, doi:10.1124/jpet.107.133546 (2008).

121 Stambe, C. *et al*. The role of p38alpha mitogen-activated protein kinase activation in renal fibrosis. *J Am Soc Nephrol* **15**, 370-379 (2004).

122 Matsuoka, H. *et al*. A p38 MAPK inhibitor, FR-167653, ameliorates murine bleomycin-induced pulmonary fibrosis. *Am J Physiol Lung Cell Mol Physiol* **283**, L103-112, doi:10.1152/ajplung.00187.2001 (2002).

123 Molkentin, J. D. *et al*. Fibroblast-Specific Genetic Manipulation of p38 Mitogen-Activated Protein Kinase In Vivo Reveals Its Central Regulatory Role in Fibrosis. *Circulation* **136**, 549-561, doi:10.1161/circulationaha.116.026238 (2017).

124 Lijnen, P. J. & Petrov, V. V. Role of intracardiac renin-angiotensin-aldosterone system in extracellular matrix remodeling. *Methods Find Exp Clin Pharmacol* **25**, 541-564 (2003).

125 Shibasaki, Y. *et al*. Impact of the angiotensin II receptor antagonist, losartan, on myocardial fibrosis in patients with end-stage renal disease: assessment by ultrasonic integrated backscatter and biochemical markers. *Hypertens Res* **28**, 787-795, doi:10.1291/hypres.28.787 (2005).

126 Diez, J. *et al*. Losartan-dependent regression of myocardial fibrosis is associated with reduction of left ventricular chamber stiffness in hypertensive patients. *Circulation* **105**, 2512-2517 (2002).

127 Campbell, S. E. & Katwa, L. C. Angiotensin II stimulated expression of transforming growth factor-beta1 in cardiac fibroblasts and myofibroblasts. *J Mol Cell Cardiol* **29**, 1947-1958, doi:10.1006/jmcc.1997.0435 (1997).

128 Lee, A. A., Dillmann, W. H., McCulloch, A. D. & Villarreal, F. J. Angiotensin II stimulates the autocrine production of transforming growth factor-beta 1 in adult rat cardiac fibroblasts. *J Mol Cell Cardiol* **27**, 2347-2357 (1995).

129 Rodriguez-Vita, J. *et al*. Angiotensin II activates the Smad pathway in vascular smooth muscle cells by a transforming growth factor-beta-independent mechanism. *Circulation* **111**, 2509-2517, doi:10.1161/01.cir.0000165133.84978.e2 (2005).

130 Rockey, D. C. & Chung, J. J. Endothelin antagonism in experimental hepatic fibrosis. Implications for endothelin in the pathogenesis of wound healing. *J Clin Invest* **98**, 1381-1388, doi:10.1172/jci118925 (1996).

131 Rosano, L., Spinella, F. & Bagnato, A. Endothelin 1 in cancer: biological implications and therapeutic opportunities. *Nat Rev Cancer* **13**, 637-651, doi:10.1038/nrc3546 (2013).

132 Abraham, D. *et al*. *Increased levels of endothelin-1 and differential endothelin type A and B receptor expression in scleroderma-associated fibrotic lung disease*. Vol. 151 (1997).

133 Shao, R. *et al*. Cell and molecular regulation of endothelin-1 production during hepatic wound healing. *Mol Biol Cell* **14**, 2327-2341, doi:10.1091/mbc.02-06-0093 (2003).

134 Shi-Wen, X. *et al*. Constitutive ALK5-independent c-Jun N-terminal kinase activation contributes to endothelin-1 overexpression in pulmonary fibrosis: evidence of an autocrine endothelin loop operating through the endothelin A and B receptors. *Mol Cell Biol* **26**, 5518-5527, doi:10.1128/mcb.00625-06 (2006).

135 Adiarto, S. *et al*. ET-1 from endothelial cells is required for complete angiotensin II-induced cardiac fibrosis and hypertrophy. *Life Sci* **91**, 651-657, doi:10.1016/j.lfs.2012.02.006 (2012).

136 Guidry, C. & Hook, M. Endothelins produced by endothelial cells promote collagen gel contraction by fibroblasts. *J Cell Biol* **115**, 873-880 (1991).

137 Seifert, R. A. *et al*. Two different subunits associate to create isoform-specific platelet-derived growth factor receptors. *J Biol Chem* **264**, 8771-8778 (1989).

138 Bowen-Pope, D. F., Hart, C. E. & Seifert, R. A. Sera and conditioned media contain different isoforms of platelet-derived growth factor (PDGF) which bind to different classes of PDGF receptor. *J Biol Chem* **264**, 2502-2508 (1989).

139 Gronwald, R. G. *et al*. Cloning and expression of a cDNA coding for the human platelet-derived growth factor receptor: evidence for more than one receptor class. *Proc Natl Acad Sci U S A* **85**, 3435-3439 (1988).

140 Mellgren, A. M. *et al*. Platelet-derived growth factor receptor beta signaling is required for efficient epicardial cell migration and development of two distinct coronary vascular smooth muscle cell populations. *Circ Res* **103**, 1393-1401, doi:10.1161/circresaha.108.176768 (2008).

141 Walker, L. N., Bowen-Pope, D. F., Ross, R. & Reidy, M. A. Production of platelet-derived growth factor-like molecules by cultured arterial smooth muscle cells accompanies proliferation after arterial injury. *Proc Natl Acad Sci U S A* **83**, 7311-7315 (1986).

142 Grotendorst, G. R., Chang, T., Seppa, H. E., Kleinman, H. K. & Martin, G. R. Platelet-derived growth factor is a chemoattractant for vascular smooth muscle cells. *J Cell Physiol* **113**, 261-266, doi:10.1002/jcp.1041130213 (1982).

143 Hellstrom, M., Kalen, M., Lindahl, P., Abramsson, A. & Betsholtz, C. Role of PDGF-B and PDGFR-beta in recruitment of vascular smooth muscle cells and pericytes during embryonic blood vessel formation in the mouse. *Development* **126**, 3047-3055 (1999).

144 Campbell, J. S. *et al*. Targeting stromal cells for the treatment of platelet-derived growth factor C-induced hepatocellular carcinogenesis. *Differentiation* **75**, 843-852, doi:10.1111/j.1432-0436.2007.00235.x (2007).

145 Leveen, P. *et al*. Mice deficient for PDGF B show renal, cardiovascular, and hematological abnormalities. *Genes Dev* **8**, 1875-1887 (1994).

146 Distler, J. H. *et al*. Imatinib mesylate reduces production of extracellular matrix and prevents development of experimental dermal fibrosis. *Arthritis Rheum* **56**, 311-322, doi:10.1002/art.22314 (2007).

147 Klinkhammer, B. M., Floege, J. & Boor, P. PDGF in organ fibrosis. *Mol Aspects Med*, doi:10.1016/j.mam.2017.11.008 (2017).

148 Jester, J. V., Huang, J., Petroll, W. M. & Cavanagh, H. D. TGFbeta induced myofibroblast differentiation of rabbit keratocytes requires synergistic TGFbeta, PDGF and integrin signaling. *Exp Eye Res* **75**, 645-657 (2002).

149 Horton, J. A. *et al*. Inhibition of radiation-induced skin fibrosis with imatinib. *Int J Radiat Biol* **89**, 162-170, doi:10.3109/09553002.2013.741281 (2013).

150 Jang, S. W. *et al*. Imatinib mesylate attenuates myocardial remodeling through inhibition of platelet-derived growth factor and transforming growth factor activation in a rat model of hypertension. *Hypertension* **63**, 1228-1234, doi:10.1161/hypertensionaha.113.01866 (2014).

151 Paluch, E. K. *et al*. Mechanotransduction: use the force(s). *BMC Biol* **13**, 47, doi:10.1186/s12915-015-0150-4 (2015).

152 Tomasek, J. J., Haaksma, C. J., Eddy, R. J. & Vaughan, M. B. Fibroblast contraction occurs on release of tension in attached collagen lattices: dependency on an organized actin cytoskeleton and serum. *Anat Rec* **232**, 359-368, doi:10.1002/ar.1092320305 (1992).

153 Brown, R. A., Prajapati, R., McGrouther, D. A., Yannas, I. V. & Eastwood, M. Tensional homeostasis in dermal fibroblasts: mechanical responses to mechanical loading in three-dimensional substrates. *J Cell Physiol* **175**, 323-332, doi:10.1002/(sici)1097-4652(199806)175:3<323::aid-jcp10>3.0.co;2-6 (1998).

154 Hyytiainen, M., Penttinen, C. & Keski-Oja, J. Latent TGF-beta binding proteins: extracellular matrix association and roles in TGF-beta activation. *Crit Rev Clin Lab Sci* **41**, 233-264, doi:10.1080/10408360490460933 (2004).

155 Norman, C., Runswick, M., Pollock, R. & Treisman, R. Isolation and properties of cDNA clones encoding SRF, a transcription factor that binds to the c-fos serum response element. *Cell* **55**, 989-1003 (1988).

156 Treisman, R. Identification of a protein-binding site that mediates transcriptional response of the c-fos gene to serum factors. *Cell* **46**, 567-574 (1986).

157 Kumar, M. S. & Owens, G. K. Combinatorial control of smooth muscle-specific gene expression. *Arterioscler Thromb Vasc Biol* **23**, 737-747, doi:10.1161/01.atv.0000065197.07635.ba (2003).

158 Wang, Z., Wang, D. Z., Pipes, G. C. & Olson, E. N. Myocardin is a master regulator of smooth muscle gene expression. *Proc Natl Acad Sci U S A* **100**, 7129-7134, doi:10.1073/pnas.1232341100 (2003).

159 Wang, D. Z. *et al*. Potentiation of serum response factor activity by a family of myocardin-related transcription factors. *Proc Natl Acad Sci U S A* **99**, 14855-14860, doi:10.1073/pnas.222561499 (2002).

160 Small, E. M. *et al*. Myocardin-related transcription factor-a controls myofibroblast activation and fibrosis in response to myocardial infarction. *Circ Res* **107**, 294-304, doi:10.1161/circresaha.110.223172 (2010).

161 Small, E. M. The actin-MRTF-SRF gene regulatory axis and myofibroblast differentiation. *J Cardiovasc Transl Res* **5**, 794-804, doi:10.1007/s12265-012-9397-0 (2012).

162 Vartiainen, M. K., Guettler, S., Larijani, B. & Treisman, R. Nuclear actin regulates dynamic subcellular localization and activity of the SRF cofactor MAL. *Science* **316**, 1749-1752, doi:10.1126/science.1141084 (2007).

163 Mouilleron, S., Langer, C. A., Guettler, S., McDonald, N. Q. & Treisman, R. Structure of a pentavalent G-actin*MRTF-A complex reveals how G-actin controls nucleocytoplasmic shuttling of a transcriptional coactivator. *Sci Signal* **4**, ra40, doi:10.1126/scisignal.2001750 (2011).

164 Rudrapatna, V. A., Bangi, E. & Cagan, R. L. A Jnk-Rho-Actin remodeling positive feedback network directs Src-driven invasion. *Oncogene* **33**, 2801-2806, doi:10.1038/onc.2013.232 (2014).

165 Schmitz, A. A., Govek, E. E., Bottner, B. & Van Aelst, L. Rho GTPases: signaling, migration, and invasion. *Exp Cell Res* **261**, 1-12, doi:10.1006/excr.2000.5049 (2000).
166 Katoh, K., Kano, Y. & Ookawara, S. Rho-kinase dependent organization of stress fibers and focal adhesions in cultured fibroblasts. *Genes Cells* **12**, 623-638, doi:10.1111/j.1365-2443.2007.01073.x (2007).
167 Katoh, K. Activation of Rho-kinase and focal adhesion kinase regulates the organization of stress fibers and focal adhesions in the central part of fibroblasts. *PeerJ* **5**, e4063, doi:10.7717/peerj.4063 (2017).
168 Schwartz, M. Rho signalling at a glance. *J Cell Sci* **117**, 5457-5458, doi:10.1242/jcs.01582 (2004).
169 Khasnis, M., Nakatomi, A., Gumpper, K. & Eto, M. Reconstituted human myosin light chain phosphatase reveals distinct roles of two inhibitory phosphorylation sites of the regulatory subunit, MYPT1. *Biochemistry* **53**, 2701-2709, doi:10.1021/bi5001728 (2014).
170 Hadid, Y. *et al*. Sympatric incipient speciation of spiny mice Acomys at "Evolution Canyon," Israel. *Proc Natl Acad Sci U S A* **111**, 1043-1048, doi:10.1073/pnas.1322301111 (2014).
171 Steppan, S., Adkins, R. & Anderson, J. Phylogeny and divergence-date estimates of rapid radiations in muroid rodents based on multiple nuclear genes. *Syst Biol* **53**, 533-553, doi:10.1080/10635150490468701 (2004).
172 Shanas, U., Afik, D., Scantlebury, M. & Haim, A. The effects of season and dietary salt content on body temperature daily rhythms of common spiny mice from different micro-habitats. *Comp Biochem Physiol A Mol Integr Physiol* **132**, 287-295 (2002).
173 Brunjes, P. C. The precocial mouse, Acomys cahirinus. *Psychobiology* **18**, 339-350, doi:10.3758/BF03327252 (1990).
174 Shafrir, E., Ziv, E. & Kalman, R. Nutritionally induced diabetes in desert rodents as models of type 2 diabetes: Acomys cahirinus (spiny mice) and Psammomys obesus (desert gerbil). *Ilar j* **47**, 212-224 (2006).
175 D'Udine, B. & Alleva, E. The Acomys cahirinus (spiny mouse) as a new model for biological and neurobehavioural studies. *Pol J Pharmacol Pharm* **40**, 525-534 (1988).
176 Jones, M. & Dayan, T. *Foraging Behavior and Microhabitat Use by Spiny Mice, Acomys cahirinus and A. russatus, in the Presence of Blanford's Fox (Vulpes cana) Odor*. Vol. 26 (2000).
177 Seifert, A. W. *et al*. Skin shedding and tissue regeneration in African spiny mice (Acomys). *Nature* **489**, 561-565, doi:10.1038/nature11499 (2012).
178 Gawriluk, T. R. *et al*. Comparative analysis of ear-hole closure identifies epimorphic regeneration as a discrete trait in mammals. *Nat Commun* **7**, 11164, doi:10.1038/ncomms11164 (2016).
179 Arthur, L. M. & Heber-Katz, E. The role of p21 in regulating mammalian regeneration. *Stem Cell Res Ther* **2**, 30, doi:10.1186/scrt71 (2011).
180 Bedelbaeva, K. *et al*. Lack of p21 expression links cell cycle control and appendage regeneration in mice. *Proc Natl Acad Sci U S A* **107**, 5845-5850, doi:10.1073/pnas.1000830107 (2010).
181 Arthur, L. M. *et al*. Epimorphic regeneration in mice is p53-independent. *Cell Cycle* **9**, 3667-3673, doi:10.4161/cc.9.18.13119 (2010).
182 Pepperberg, I. M. (Scribe Publications, New York, NY, 2009).

183 Zhang, Y. *et al*. Drug-induced regeneration in adult mice. *Science translational medicine* **7**, 290ra292-290ra292, doi:10.1126/scitranslmed.3010228 (2015).
184 Zhao, B., Li, L., Lei, Q. & Guan, K. L. The Hippo-YAP pathway in organ size control and tumorigenesis: an updated version. *Genes Dev* **24**, 862-874, doi:10.1101/gad.1909210 (2010).
185 Stanger, B. Z. Organ size determination and the limits of regulation. *Cell Cycle* **7**, 318-324, doi:10.4161/cc.7.3.5348 (2008).
186 Bielefeld, K. A., Amini-Nik, S. & Alman, B. A. Cutaneous wound healing: recruiting developmental pathways for regeneration. *Cell Mol Life Sci* **70**, 2059-2081, doi:10.1007/s00018-012-1152-9 (2013).
187 Liu, L. *et al*. Transcriptomic analysis of Portunus trituberculatus reveals a critical role for WNT4 and WNT signalling in limb regeneration. *Gene* **658**, 113-122, doi:10.1016/j.gene.2018.03.015 (2018).
188 Fraser, G. J., Bloomquist, R. F. & Streelman, J. T. Common developmental pathways link tooth shape to regeneration. *Dev Biol* **377**, 399-414, doi:10.1016/j.ydbio.2013.02.007 (2013).
189 Stabler, C. T. & Morrisey, E. E. Developmental pathways in lung regeneration. *Cell Tissue Res* **367**, 677-685, doi:10.1007/s00441-016-2537-0 (2017).
190 McGowan, S. Understanding the developmental pathways pulmonary fibroblasts may follow during alveolar regeneration. *Cell Tissue Res* **367**, 707-719, doi:10.1007/s00441-016-2542-3 (2017).
191 Ieda, M. Heart Development, Diseases, and Regeneration- New Approaches From Innervation, Fibroblasts, and Reprogramming. *Circ J* **80**, 2081-2088, doi:10.1253/circj.CJ-16-0815 (2016).
192 Xiao, Y., Leach, J., Wang, J. & Martin, J. F. Hippo/Yap Signaling in Cardiac Development and Regeneration. *Curr Treat Options Cardiovasc Med* **18**, 38, doi:10.1007/s11936-016-0461-y (2016).
193 Quaife-Ryan, G. A. *et al*. Multicellular Transcriptional Analysis of Mammalian Heart Regeneration. *Circulation* **136**, 1123-1139, doi:10.1161/circulationaha.117.028252 (2017).
194 Xu, T., Wang, W., Zhang, S., Stewart, R. A. & Yu, W. Identifying tumor suppressors in genetic mosaics: the Drosophila lats gene encodes a putative protein kinase. *Development* **121**, 1053-1063 (1995).
195 Wu, S., Huang, J., Dong, J. & Pan, D. hippo encodes a Ste-20 family protein kinase that restricts cell proliferation and promotes apoptosis in conjunction with salvador and warts. *Cell* **114**, 445-456 (2003).
196 Huang, H., Wu, W., Zhang, L. & Liu, X. Y. Drosophila ste-20 family protein kinase, hippo, modulates fat cell proliferation. *PLoS One* **8**, e61740, doi:10.1371/journal.pone.0061740 (2013).
197 Chan, E. H. *et al*. The Ste20-like kinase Mst2 activates the human large tumor suppressor kinase Lats1. *Oncogene* **24**, 2076-2086, doi:10.1038/sj.onc.1208445 (2005).
198 Huang, J., Wu, S., Barrera, J., Matthews, K. & Pan, D. The Hippo signaling pathway coordinately regulates cell proliferation and apoptosis by inactivating Yorkie, the Drosophila Homolog of YAP. *Cell* **122**, 421-434, doi:10.1016/j.cell.2005.06.007 (2005).
199 Hilman, D. & Gat, U. The evolutionary history of YAP and the hippo/YAP pathway. *Mol Biol Evol* **28**, 2403-2417, doi:10.1093/molbev/msr065 (2011).

200 Ikmi, A. *et al*. Molecular evolution of the Yap/Yorkie proto-oncogene and elucidation of its core transcriptional program. *Mol Biol Evol* **31**, 1375-1390, doi:10.1093/molbev/msu071 (2014).
201 Dong, J. *et al*. Elucidation of a universal size-control mechanism in Drosophila and mammals. *Cell* **130**, 1120-1133, doi:10.1016/j.cell.2007.07.019 (2007).
202 Zhao, B., Tumaneng, K. & Guan, K. L. The Hippo pathway in organ size control, tissue regeneration and stem cell self-renewal. *Nat Cell Biol* **13**, 877-883, doi:10.1038/ncb2303 (2011).
203 Hao, Y., Chun, A., Cheung, K., Rashidi, B. & Yang, X. Tumor suppressor LATS1 is a negative regulator of oncogene YAP. *J Biol Chem* **283**, 5496-5509, doi:10.1074/jbc.M709037200 (2008).
204 Yu, F. X., Zhao, B. & Guan, K. L. Hippo Pathway in Organ Size Control, Tissue Homeostasis, and Cancer. *Cell* **163**, 811-828, doi:10.1016/j.cell.2015.10.044 (2015).
205 Zhao, B. *et al*. Inactivation of YAP oncoprotein by the Hippo pathway is involved in cell contact inhibition and tissue growth control. *Genes Dev* **21**, 2747-2761, doi:10.1101/gad.1602907 (2007).
206 Zhao, B. *et al*. TEAD mediates YAP-dependent gene induction and growth control. *Genes Dev* **22**, 1962-1971, doi:10.1101/gad.1664408 (2008).
207 Zhao, B., Li, L., Tumaneng, K., Wang, C. Y. & Guan, K. L. A coordinated phosphorylation by Lats and CK1 regulates YAP stability through SCF(beta-TRCP). *Genes Dev* **24**, 72-85, doi:10.1101/gad.1843810 (2010).
208 Basu, S., Totty, N. F., Irwin, M. S., Sudol, M. & Downward, J. Akt phosphorylates the Yes-associated protein, YAP, to induce interaction with 14-3-3 and attenuation of p73-mediated apoptosis. *Mol Cell* **11**, 11-23 (2003).
209 Goulev, Y. *et al*. SCALLOPED interacts with YORKIE, the nuclear effector of the hippo tumor-suppressor pathway in Drosophila. *Curr Biol* **18**, 435-441, doi:10.1016/j.cub.2008.02.034 (2008).
210 Beyer, T. A. *et al*. Switch Enhancers Interpret TGF-beta and Hippo Signaling to Control Cell Fate in Human Embryonic Stem Cells. *Cell Rep* **5**, 1611-1624, doi:10.1016/j.celrep.2013.11.021 (2013).
211 Vassilev, A., Kaneko, K. J., Shu, H., Zhao, Y. & DePamphilis, M. L. TEAD/TEF transcription factors utilize the activation domain of YAP65, a Src/Yes-associated protein localized in the cytoplasm. *Genes Dev* **15**, 1229-1241, doi:10.1101/gad.888601 (2001).
212 Vitolo, M. I. *et al*. The RUNX2 transcription factor cooperates with the YES-associated protein, YAP65, to promote cell transformation. *Cancer Biol Ther* **6**, 856-863 (2007).
213 Mahoney, W. M., Jr., Hong, J. H., Yaffe, M. B. & Farrance, I. K. The transcriptional co-activator TAZ interacts differentially with transcriptional enhancer factor-1 (TEF-1) family members. *Biochem J* **388**, 217-225, doi:10.1042/bj20041434 (2005).
214 Kim, M. K., Jang, J. W. & Bae, S. C. in *BMB Rep* Vol. 51 126-133 (2018).
215 Lin, K. C., Park, H. W. & Guan, K. L. Regulation of the Hippo Pathway Transcription Factor TEAD. *Trends Biochem Sci* **42**, 862-872, doi:10.1016/j.tibs.2017.09.003 (2017).
216 Kanai, F. *et al*. TAZ: a novel transcriptional co-activator regulated by interactions with 14-3-3 and PDZ domain proteins. *Embo j* **19**, 6778-6791, doi:10.1093/emboj/19.24.6778 (2000).

217 Liu, C. Y. *et al*. The hippo tumor pathway promotes TAZ degradation by phosphorylating a phosphodegron and recruiting the SCF{beta}-TrCP E3 ligase. *J Biol Chem* **285**, 37159-37169, doi:10.1074/jbc.M110.152942 (2010).

218 Hong, J. H. *et al*. TAZ, a transcriptional modulator of mesenchymal stem cell differentiation. *Science* **309**, 1074-1078, doi:10.1126/science.1110955 (2005).

219 Brusgard, J. L. *et al*. RUNX2 and TAZ-dependent signaling pathways regulate soluble E-Cadherin levels and tumorsphere formation in breast cancer cells. *Oncotarget* **6**, 28132-28150, doi:10.18632/oncotarget.4654 (2015).

220 Bossuyt, W. *et al*. An evolutionary shift in the regulation of the Hippo pathway between mice and flies. *Oncogene* **33**, 1218-1228, doi:10.1038/onc.2013.82 (2014).

221 Nolo, R., Morrison, C. M., Tao, C., Zhang, X. & Halder, G. The bantam microRNA is a target of the hippo tumor-suppressor pathway. *Curr Biol* **16**, 1895-1904, doi:10.1016/j.cub.2006.08.057 (2006).

222 Rosenbluh, J. *et al*. beta-Catenin-driven cancers require a YAP1 transcriptional complex for survival and tumorigenesis. *Cell* **151**, 1457-1473, doi:10.1016/j.cell.2012.11.026 (2012).

223 Liu, M., Zhao, S., Lin, Q. & Wang, X. P. YAP regulates the expression of Hoxa1 and Hoxc13 in mouse and human oral and skin epithelial tissues. *Mol Cell Biol* **35**, 1449-1461, doi:10.1128/mcb.00765-14 (2015).

224 Lai, D., Ho, K. C., Hao, Y. & Yang, X. Taxol resistance in breast cancer cells is mediated by the hippo pathway component TAZ and its downstream transcriptional targets Cyr61 and CTGF. *Cancer Res* **71**, 2728-2738, doi:10.1158/0008-5472.can-10-2711 (2011).

225 Shimomura, T. *et al*. The PDZ-binding motif of Yes-associated protein is required for its co-activation of TEAD-mediated CTGF transcription and oncogenic cell transforming activity. *Biochem Biophys Res Commun*, doi:10.1016/j.bbrc.2013.12.100 (2013).

226 Sudol, M. Yes-associated protein (YAP65) is a proline-rich phosphoprotein that binds to the SH3 domain of the Yes proto-oncogene product. *Oncogene* **9**, 2145-2152 (1994).

227 Gaffney, C. J. *et al*. Identification, basic characterization and evolutionary analysis of differentially spliced mRNA isoforms of human YAP1 gene. *Gene* **509**, 215-222, doi:10.1016/j.gene.2012.08.025 (2012).

228 Fausther, M., Lavoie, E. G. & Dranoff, J. A. Contribution of Myofibroblasts of Different Origins to Liver Fibrosis. *Curr Pathobiol Rep* **1**, 225-230, doi:10.1007/s40139-013-0020-0 (2013).

229 Sudol, M. *et al*. Characterization of the mammalian YAP (Yes-associated protein) gene and its role in defining a novel protein module, the WW domain. *J Biol Chem* **270**, 14733-14741 (1995).

230 Zhao, B., Kim, J., Ye, X., Lai, Z. C. & Guan, K. L. Both TEAD-binding and WW domains are required for the growth stimulation and oncogenic transformation activity of yes-associated protein. *Cancer Res* **69**, 1089-1098, doi:10.1158/0008-5472.can-08-2997 (2009).

231 Rouleau, C. *et al*. Transformation by Polyomavirus Middle T Antigen Involves a Unique Bimodal Interaction with the Hippo Effector YAP. *Journal of Virology* **90**, 7032-7045, doi:10.1128/JVI.00417-16 (2016).

232 Holcomb, J. *et al*. PDZ Structure and Implication in Selective Drug Design against Cystic Fibrosis. *Curr Drug Targets* **16**, 945-950 (2015).

233 Lamar, J. M. *et al*. The Hippo pathway target, YAP, promotes metastasis through its TEAD-interaction domain. *Proc Natl Acad Sci U S A* **109**, E2441-2450, doi:10.1073/pnas.1212021109 (2012).
234 Gumbiner, B. M. & Kim, N. G. The Hippo-YAP signaling pathway and contact inhibition of growth. *J Cell Sci* **127**, 709-717, doi:10.1242/jcs.140103 (2014).
235 Yu, F. X. *et al*. Regulation of the Hippo-YAP pathway by G-protein-coupled receptor signaling. *Cell* **150**, 780-791, doi:10.1016/j.cell.2012.06.037 (2012).
236 Fan, R., Kim, N. G. & Gumbiner, B. M. Regulation of Hippo pathway by mitogenic growth factors via phosphoinositide 3-kinase and phosphoinositide-dependent kinase-1. *Proc Natl Acad Sci U S A* **110**, 2569-2574, doi:10.1073/pnas.1216462110 (2013).
237 Miller, E. *et al*. Identification of serum-derived sphingosine-1-phosphate as a small molecule regulator of YAP. *Chem Biol* **19**, 955-962, doi:10.1016/j.chembiol.2012.07.005 (2012).
238 Hao, F. *et al*. Insulin Receptor and GPCR Crosstalk Stimulates YAP via PI3K and PKD in Pancreatic Cancer Cells. *Mol Cancer Res* **15**, 929-941, doi:10.1158/1541-7786.mcr-17-0023 (2017).
239 Imajo, M., Miyatake, K., Iimura, A., Miyamoto, A. & Nishida, E. A molecular mechanism that links Hippo signalling to the inhibition of Wnt/beta-catenin signalling. *Embo j* **31**, 1109-1122, doi:10.1038/emboj.2011.487 (2012).
240 Azzolin, L. *et al*. YAP/TAZ incorporation in the beta-catenin destruction complex orchestrates the Wnt response. *Cell* **158**, 157-170, doi:10.1016/j.cell.2014.06.013 (2014).
241 Hubaud, A., Regev, I., Mahadevan, L. & Pourquie, O. Excitable Dynamics and Yap-Dependent Mechanical Cues Drive the Segmentation Clock. *Cell* **171**, 668-682.e611, doi:10.1016/j.cell.2017.08.043 (2017).
242 Slemmons, K. K. *et al*. A Novel Notch-YAP Circuit Drives Stemness and Tumorigenesis in Embryonal Rhabdomyosarcoma. *Mol Cancer Res*, doi:10.1158/1541-7786.mcr-17-0004 (2017).
243 Alarcon, C. *et al*. Nuclear CDKs drive Smad transcriptional activation and turnover in BMP and TGF-beta pathways. *Cell* **139**, 757-769, doi:10.1016/j.cell.2009.09.035 (2009).
244 Hiemer, S. E., Szymaniak, A. D. & Varelas, X. The transcriptional regulators TAZ and YAP direct transforming growth factor beta-induced tumorigenic phenotypes in breast cancer cells. *J Biol Chem* **289**, 13461-13474, doi:10.1074/jbc.M113.529115 (2014).
245 Barry, E. R. & Camargo, F. D. The Hippo superhighway: signaling crossroads converging on the Hippo/Yap pathway in stem cells and development. *Curr Opin Cell Biol* **25**, 247-253, doi:10.1016/j.ceb.2012.12.006 (2013).
246 Liu, J. *et al*. Loss of DLG5 promotes breast cancer malignancy by inhibiting the Hippo signaling pathway. *Sci Rep* **7**, 42125, doi:10.1038/srep42125 (2017).
247 Mohseni, M. *et al*. A genetic screen identifies an LKB1-MARK signalling axis controlling the Hippo-YAP pathway. *Nat Cell Biol* **16**, 108-117, doi:10.1038/ncb2884 (2014).
248 Varelas, X. *et al*. The Crumbs complex couples cell density sensing to Hippo-dependent control of the TGF-beta-SMAD pathway. *Dev Cell* **19**, 831-844, doi:10.1016/j.devcel.2010.11.012 (2010).
249 Adler, J. J. *et al*. Serum deprivation inhibits the transcriptional co-activator YAP and cell growth via phosphorylation of the 130-kDa isoform of Angiomotin by the LATS1/2 protein kinases. *Proc Natl Acad Sci U S A* **110**, 17368-17373, doi:10.1073/pnas.1308236110 (2013).

250 Zhao, B. *et al*. Angiomotin is a novel Hippo pathway component that inhibits YAP oncoprotein. *Genes Dev* **25**, 51-63, doi:10.1101/gad.2000111 (2011).
251 Wang, W., Huang, J. & Chen, J. Angiomotin-like proteins associate with and negatively regulate YAP1. *J Biol Chem* **286**, 4364-4370, doi:10.1074/jbc.C110.205401 (2011).
252 Chen, C. L., Schroeder, M. C., Kango-Singh, M., Tao, C. & Halder, G. Tumor suppression by cell competition through regulation of the Hippo pathway. *Proc Natl Acad Sci U S A* **109**, 484-489, doi:10.1073/pnas.1113882109 (2012).
253 Kobielak, A. & Fuchs, E. Alpha-catenin: at the junction of intercellular adhesion and actin dynamics. *Nat Rev Mol Cell Biol* **5**, 614-625, doi:10.1038/nrm1433 (2004).
254 Akladios, B. *et al*. Epidermal YAP2-5SA-DeltaC Drives beta-Catenin Activation to Promote Keratinocyte Proliferation in Mouse Skin In Vivo. *J Invest Dermatol* **137**, 716-726, doi:10.1016/j.jid.2016.10.029 (2017).
255 Schlegelmilch, K. *et al*. Yap1 acts downstream of alpha-catenin to control epidermal proliferation. *Cell* **144**, 782-795, doi:10.1016/j.cell.2011.02.031 (2011).
256 Wilson, K. E. *et al*. PTPN14 forms a complex with Kibra and LATS1 proteins and negatively regulates the YAP oncogenic function. *J Biol Chem* **289**, 23693-23700, doi:10.1074/jbc.M113.534701 (2014).
257 Genevet, A., Wehr, M. C., Brain, R., Thompson, B. J. & Tapon, N. Kibra is a regulator of the Salvador/Warts/Hippo signaling network. *Dev Cell* **18**, 300-308, doi:10.1016/j.devcel.2009.12.011 (2010).
258 Bennett, F. C. & Harvey, K. F. Fat cadherin modulates organ size in Drosophila via the Salvador/Warts/Hippo signaling pathway. *Curr Biol* **16**, 2101-2110, doi:10.1016/j.cub.2006.09.045 (2006).
259 Cho, E. *et al*. Delineation of a Fat tumor suppressor pathway. *Nat Genet* **38**, 1142-1150, doi:10.1038/ng1887 (2006).
260 Pan, G. *et al*. Signal transduction by the Fat cytoplasmic domain. *Development* **140**, 831-842, doi:10.1242/dev.088534 (2013).
261 Willecke, M. *et al*. The fat cadherin acts through the hippo tumor-suppressor pathway to regulate tissue size. *Curr Biol* **16**, 2090-2100, doi:10.1016/j.cub.2006.09.005 (2006).
262 Silva, E., Tsatskis, Y., Gardano, L., Tapon, N. & McNeill, H. The tumor-suppressor gene fat controls tissue growth upstream of expanded in the hippo signaling pathway. *Curr Biol* **16**, 2081-2089, doi:10.1016/j.cub.2006.09.004 (2006).
263 Mao, Y. *et al*. Dachs: an unconventional myosin that functions downstream of Fat to regulate growth, affinity and gene expression in Drosophila. *Development* **133**, 2539-2551, doi:10.1242/dev.02427 (2006).
264 Kuta, A. *et al*. Fat4-Dchs1 signalling controls cell proliferation in developing vertebrae. *Development* **143**, 2367-2375, doi:10.1242/dev.131037 (2016).
265 Dupont, S. *et al*. Role of YAP/TAZ in mechanotransduction. *Nature* **474**, 179-183, doi:10.1038/nature10137 (2011).
266 Nakajima, H. *et al*. Flow-Dependent Endothelial YAP Regulation Contributes to Vessel Maintenance. *Dev Cell* **40**, 523-536.e526, doi:10.1016/j.devcel.2017.02.019 (2017).
267 Xu, S., Koroleva, M., Yin, M. & Jin, Z. G. Atheroprotective laminar flow inhibits Hippo pathway effector YAP in endothelial cells. *Transl Res* **176**, 18-28.e12, doi:10.1016/j.trsl.2016.05.003 (2016).

268 Wang, K. C. *et al*. Flow-dependent YAP/TAZ activities regulate endothelial phenotypes and atherosclerosis. *Proc Natl Acad Sci U S A* **113**, 11525-11530, doi:10.1073/pnas.1613121113 (2016).

269 Nakajima, H. & Mochizuki, N. Flow pattern-dependent endothelial cell responses through transcriptional regulation. *Cell Cycle* **16**, 1893-1901, doi:10.1080/15384101.2017.1364324 (2017).

270 Sakabe, M. *et al*. YAP/TAZ-CDC42 signaling regulates vascular tip cell migration. *Proc Natl Acad Sci U S A* **114**, 10918-10923, doi:10.1073/pnas.1704030114 (2017).

271 He, J. *et al*. Yes-Associated Protein Promotes Angiogenesis via Signal Transducer and Activator of Transcription 3 in Endothelial Cells. *Circ Res* **122**, 591-605, doi:10.1161/circresaha.117.311950 (2018).

272 Mana-Capelli, S., Paramasivam, M., Dutta, S. & McCollum, D. Angiomotins link F-actin architecture to Hippo pathway signaling. *Mol Biol Cell* **25**, 1676-1685, doi:10.1091/mbc.E13-11-0701 (2014).

273 Seo, J. & Kim, J. in *BMB Rep* Vol. 51 151-156 (2018).

274 Panciera, T., Azzolin, L., Cordenonsi, M. & Piccolo, S. Mechanobiology of YAP and TAZ in physiology and disease. *Nat Rev Mol Cell Biol* **18**, 758-770, doi:10.1038/nrm.2017.87 (2017).

275 Aragona, M. *et al*. A mechanical checkpoint controls multicellular growth through YAP/TAZ regulation by actin-processing factors. *Cell* **154**, 1047-1059, doi:10.1016/j.cell.2013.07.042 (2013).

276 Lin, A. Y. & Pearson, B. J. Planarian yorkie/YAP functions to integrate adult stem cell proliferation, organ homeostasis and maintenance of axial patterning. *Development* **141**, 1197-1208, doi:10.1242/dev.101915 (2014).

277 Hayashi, S. *et al*. Transcriptional regulators in the Hippo signaling pathway control organ growth in Xenopus tadpole tail regeneration. *Dev Biol* **396**, 31-41, doi:10.1016/j.ydbio.2014.09.018 (2014).

278 Hayashi, S., Tamura, K. & Yokoyama, H. Yap1, transcription regulator in the Hippo signaling pathway, is required for Xenopus limb bud regeneration. *Dev Biol* **388**, 57-67, doi:10.1016/j.ydbio.2014.01.018 (2014).

279 Hu, J. *et al*. Yes-associated protein (yap) is required for early embryonic development in zebrafish (danio rerio). *Int J Biol Sci* **9**, 267-278, doi:10.7150/ijbs.4887 (2013).

280 Mateus, R. *et al*. Control of tissue growth by Yap relies on cell density and F-actin in zebrafish fin regeneration. *Development* **142**, 2752-2763, doi:10.1242/dev.119701 (2015).

281 Martins, P. N., Theruvath, T. P. & Neuhaus, P. Rodent models of partial hepatectomies. *Liver Int* **28**, 3-11, doi:10.1111/j.1478-3231.2007.01628.x (2008).

282 Madrahimov, N., Dirsch, O., Broelsch, C. & Dahmen, U. Marginal hepatectomy in the rat: from anatomy to surgery. *Ann Surg* **244**, 89-98, doi:10.1097/01.sla.0000218093.12408.0f (2006).

283 Mehendale, H. M. Tissue repair: an important determinant of final outcome of toxicant-induced injury. *Toxicol Pathol* **33**, 41-51, doi:10.1080/01926230590881808 (2005).

284 Grijalva, J. L. *et al*. Dynamic alterations in Hippo signaling pathway and YAP activation during liver regeneration. *Am J Physiol Gastrointest Liver Physiol* **307**, G196-204, doi:10.1152/ajpgi.00077.2014 (2014).

285 Lu, L. *et al*. Hippo signaling is a potent in vivo growth and tumor suppressor pathway in the mammalian liver. *Proc Natl Acad Sci U S A* **107**, 1437-1442, doi:10.1073/pnas.0911427107 (2010).
286 Miyamura, N. *et al*. YAP determines the cell fate of injured mouse hepatocytes in vivo. *Nat Commun* **8**, 16017, doi:10.1038/ncomms16017 (2017).
287 Martin, K. *et al*. PAK proteins and YAP-1 signalling downstream of integrin beta-1 in myofibroblasts promote liver fibrosis. *Nat Commun* **7**, 12502, doi:10.1038/ncomms12502 (2016).
288 Machado, M. V. *et al*. Accumulation of duct cells with activated YAP parallels fibrosis progression in non-alcoholic fatty liver disease. *J Hepatol* **63**, 962-970, doi:10.1016/j.jhep.2015.05.031 (2015).
289 Bertero, T. *et al*. A YAP/TAZ-miR-130/301 molecular circuit exerts systems-level control of fibrosis in a network of human diseases and physiologic conditions. *Sci Rep* **5**, 18277, doi:10.1038/srep18277 (2015).
290 Zhubanchaliyev, A., Temirbekuly, A., Kongrtay, K., Wanshura, L. C. & Kunz, J. Targeting Mechanotransduction at the Transcriptional Level: YAP and BRD4 Are Novel Therapeutic Targets for the Reversal of Liver Fibrosis. *Front Pharmacol* **7**, 462, doi:10.3389/fphar.2016.00462 (2016).
291 Mannaerts, I. *et al*. The Hippo pathway effector YAP controls mouse hepatic stellate cell activation. *J Hepatol* **63**, 679-688, doi:10.1016/j.jhep.2015.04.011 (2015).
292 Wang, Y. *et al*. Genetic tracing of hepatocytes in liver homeostasis, injury, and regeneration. *J Biol Chem* **292**, 8594-8604, doi:10.1074/jbc.M117.782029 (2017).
293 Liang, M. *et al*. Yap/Taz Deletion in Gli+ Cell-Derived Myofibroblasts Attenuates Fibrosis. *J Am Soc Nephrol*, doi:10.1681/asn.2015121354 (2017).
294 Saxena, S. K., Thompson, J. S. & Sharp, J. G. *Intestinal regeneration*. (R.G. Landes Co., 1993).
295 Barker, N. *et al*. Identification of stem cells in small intestine and colon by marker gene Lgr5. *Nature* **449**, 1003-1007, doi:10.1038/nature06196 (2007).
296 Gregorieff, A., Liu, Y., Inanlou, M. R., Khomchuk, Y. & Wrana, J. L. Yap-dependent reprogramming of Lgr5(+) stem cells drives intestinal regeneration and cancer. *Nature* **526**, 715-718, doi:10.1038/nature15382 (2015).
297 Barry, E. R. *et al*. Restriction of intestinal stem cell expansion and the regenerative response by YAP. *Nature* **493**, 106-110, doi:10.1038/nature11693 (2013).
298 Liu, J. *et al*. Molecular characterization of the transition from acute to chronic kidney injury following ischemia/reperfusion. *JCI Insight* **2**, doi:10.1172/jci.insight.94716 (2017).
299 Eddy, A. A. & Neilson, E. G. Chronic kidney disease progression. *J Am Soc Nephrol* **17**, 2964-2966, doi:10.1681/asn.2006070704 (2006).
300 Xu, J. *et al*. Involvement of the Hippo pathway in regeneration and fibrogenesis after ischaemic acute kidney injury: YAP is the key effector. *Clin Sci (Lond)* **130**, 349-363, doi:10.1042/cs20150385 (2016).
301 Zeng, F., Miyazawa, T., Kloepfer, L. A. & Harris, R. C. ErbB4 deletion accelerates renal fibrosis following renal injury. *Am J Physiol Renal Physiol*, ajprenal.00260.02017, doi:10.1152/ajprenal.00260.2017 (2017).
302 Szeto, S. G. *et al*. YAP/TAZ Are Mechanoregulators of TGF-beta-Smad Signaling and Renal Fibrogenesis. *J Am Soc Nephrol* **27**, 3117-3128, doi:10.1681/asn.2015050499 (2016).

303 Liang, M. *et al*. Yap/Taz Deletion in Gli+ Cell-Derived Myofibroblasts Attenuates Fibrosis. *J Am Soc Nephrol* **28**, 3278-3290, doi:10.1681/asn.2015121354 (2017).
304 Liu, F. *et al*. Mechanosignaling through YAP and TAZ drives fibroblast activation and fibrosis. *Am J Physiol Lung Cell Mol Physiol* **308**, L344-357, doi:10.1152/ajplung.00300.2014 (2015).
305 Chen, W. & Frangogiannis, N. G. Fibroblasts in post-infarction inflammation and cardiac repair. *Biochim Biophys Acta* **1833**, 945-953, doi:10.1016/j.bbamcr.2012.08.023 (2013).
306 Nguyen, T. P., Qu, Z. & Weiss, J. N. Cardiac fibrosis and arrhythmogenesis: The road to repair is paved with perils. *J Mol Cell Cardiol*, doi:10.1016/j.yjmcc.2013.10.018 (2013).
307 von Gise, A. *et al*. YAP1, the nuclear target of Hippo signaling, stimulates heart growth through cardiomyocyte proliferation but not hypertrophy. *Proc Natl Acad Sci U S A* **109**, 2394-2399, doi:10.1073/pnas.1116136109 (2012).
308 Lin, Z. *et al*. Acetylation of VGLL4 Regulates Hippo-YAP Signaling and Postnatal Cardiac Growth. *Dev Cell* **39**, 466-479, doi:10.1016/j.devcel.2016.09.005 (2016).
309 Xin, M. *et al*. Hippo pathway effector Yap promotes cardiac regeneration. *Proc Natl Acad Sci U S A* **110**, 13839-13844, doi:10.1073/pnas.1313192110 (2013).
310 Xin, M. *et al*. Regulation of insulin-like growth factor signaling by Yap governs cardiomyocyte proliferation and embryonic heart size. *Sci Signal* **4**, ra70, doi:10.1126/scisignal.2002278 (2011).
311 Heallen, T. *et al*. Hippo signaling impedes adult heart regeneration. *Development* **140**, 4683-4690, doi:10.1242/dev.102798 (2013).
312 Heallen, T. *et al*. Hippo pathway inhibits Wnt signaling to restrain cardiomyocyte proliferation and heart size. *Science* **332**, 458-461, doi:10.1126/science.1199010 (2011).
313 Morikawa, Y. *et al*. Actin cytoskeletal remodeling with protrusion formation is essential for heart regeneration in Hippo-deficient mice. *Sci Signal* **8**, ra41, doi:10.1126/scisignal.2005781 (2015).
314 Leach, J. P. *et al*. Hippo pathway deficiency reverses systolic heart failure after infarction. *Nature* **550**, 260-264, doi:10.1038/nature24045 (2017).
315 Lin, Z. *et al*. Cardiac-specific YAP activation improves cardiac function and survival in an experimental murine MI model. *Circ Res* **115**, 354-363, doi:10.1161/circresaha.115.303632 (2014).

Chapter 2. Evolutionary adaptations in developmental Hippo-YAP pathway underlies regenerative scar-free wound repair in African Spiny Mice

Chris Brewer [1,2,#] Branden Nelson[3,] Paul Wakenight[3], Aaron Mckenna[4], Jay Shendure[4], William M. Mahoney[1], Andrew Timms[2], Kathleen Millen[3,5], Mark W. Majesky[1,2,5]

1. Department of Pathology, University of Washington, Seattle, USA

2.Center for Developmental Biology & Regenerative Medicine, Seattle Children's Research Institute, Seattle, WA

3. Center for Integrative Brain Research, Seattle Children's Research Institute, Seattle, WA

4. Department of Genome Sciences, University of Washington, Seattle, WA

5. Department of Pediatrics, University of Washington, Seattle,WA

#Correspondence to:

Mark W. Majesky, Center for Developmental Biology & Regenerative Medicine, Seattle Children's Research Institute, University of Washington, Seattle, WA. mwm84@uw.edu

2.1 Abstract:

Adult mammals have evolved the capacity for restoring tissue hemostasis by utilizing fibrosis/inflammation. Unfortunately, unrestrained scar formation is a leading cause of organ failure. In contrast, adult *Acomys cahirinus* (African Spiny Mouse) has evolved the unique ability to resolve wound repair in a scar-free regenerative manner. Incredibly, *Acomys* have not dispensed altogether with the myofibroblast (MF), the cellular mediator of scarring. Instead, *Acomys* demonstrate evolutionary conserved induction of MFs during initial tissue injury, but evolved a non-conserved transient MF phenotype that does not drive scar tissue formation. De-novo transcriptome analysis reveals unique gene expression patterns of the organ size control pathway Hippo-YAP. In agreement, *Acomys* actively resist fibrokine mediated YAP inactivation/cytoplasmic sequestration in stark contrast to *Mus*/Human. Mechanistically, *Acomys* YAP nuclear activity is mediated by a novel high affinity PP2A-mediated surveillance protein complex that rapidly and specifically de-phosphorylates key amino acid regulatory residues. *In vivo*, the pathway effector protein YAP (Yes Associated protein) and its biphasic temporal activation are found to be necessary in mediating *Acomys* regeneration. These phases include blastema formation and later stage tissue architectural restoration. The therapeutic potential of *Acomys* is illustrated by phenocopying YAP activity attenuating *Mus*/Human myofibroblasts formation. Elucidating how *Acomys* have intrinsically manipulated the evolutionarily conserved Hippo pathway may one day provide avenues to abrogate fibrosis.

2.2 Introduction:

While vertebrate evolution has produced a spectacular range of phenotypic diversity, methods of vertebrate wound repair have been highly conserved with two clearly identifiable mechanisms mediating tissue repair after injury. These two distinct processes are regeneration, complete restoration of tissue architecture and function, and scar tissue formation identified by wound healing through increased extracellular matrix (ECM) deposition and remodeling. While regeneration is common in lower order vertebrates, higher order vertebrates such as adult mammals lose this ability during periods of late embryonic and early post-natal development[1-3]. Instead, scarring being the most commonly utilized mechanism of wound repair in terrestrial mammals. This myofibroblast mediated excessive ECM deposition and contraction are key feature in the development of scar tissue[4]. While limited scarring is an important feature in successful mammalian wound repair, chronic injury and/or inflammation can result in a pathogenic condition named fibrosis. Fibrotic diseases result in loss of organ function and subsequent mortality[5-7]. With most human organ systems susceptible to fibrosis and few therapies to combat its progression, identifying both cellular and molecular responses that are critical in mediating tissue repair decision between scar tissue formation or regeneration are paramount.

In contrast to adult mammalian scar mediated repair, several species within the genus *Acomys* have instead evolved the unique capability to undergo autotomy or skin shedding in order to escape predation. This adaption allows the *Acomys* to shed up to 60% of its dorsal skin. However, upon escape, the Acomys demonstrate complete restoration of skin components including hair follicles, dermis and cartilage in lieu of scarring and fibrosis[8]. Further characterization by *Seifert et al* has shown *Acomys* exhibit features of epimorphic regeneration during ear pinnae injury, a trait previously believed to be restricted to urodeles and teleost. Such a

phenomenon makes the *Acomys* one of few adult mammals to utilize this feature for scar free wound repair.

In response to injury, key cellular processes such as cell proliferation, differentiation and size control must be appropriately regulated to restore tissue function and organization. However, these processes must be properly orchestrated in order to restore tissue homeostasis. It is these processes that define the Hippo signaling pathway[9]. The evolutionarily conserved Hippo pathway first discovered in *Drosphilia* forward genetic screens, is a serine/threonine kinase cascade that regulates the activity of transcriptional co-activator proteins Yes-associated protein 1 (YAP) and transcriptional co-activator with PDZ motif (TAZ)[10]. Phosphorylation by upstream canonical Hippo pathway kinase components (MST1/2, LATS1/2) results in inactivation and cytoplasmic localization of YAP[11,12]. Dephosphorylated YAP is active and accumulates in the nucleus where it can interact with a number of transcription factors, most notably the transcriptional enhancer factors or TEADs[13, 14]. Biologically active YAP coactivates expression of numerous target genes that mediate cellular crowd control, mechanical tension, proliferation and differentiation at both the cellular and whole tissue level, all critical functions in tissue reconstitution. With such a wide span of upstream regulatory inputs and most core components of Hippo pathway found in nearly all cell types, YAP is in a unique position to coordinate regenerative wound healing responses in nearly all organ systems[15]. As such, we investigated whether the *Acomys cahirinus* has manipulated key features of the evolutionarily conserved Hippo-YAP signaling pathway to promote scar free wound repair.

2.3 Materials and Methods

2.3.1 Animal Maintenance and Manipulations:

The Seattle Children's Research Institute's Institutional Animal Care and Use Committee (IACUC) approved all animal procedures. Adult male and female *Mus musculus* (The Jackson Laboratory, CD1 Strain#) and *Acomys cahirinus* (Exotic Pet supply Company) were obtained, housed, and bred within the Seattle Children's Research Institute's onsite vivarium. CD1 mice were housed in a pathogen-free room maintained on 12:12 (Light:Dark) lighting schedule, *Acomys* were housed in a separate room maintained on 14:10 (Light:Dark) schedule, and all animals received food and water *ad libitum*. Acomys and Mus adult males and females were anaesthetized with 4% (v/v) vaporized isoflurane (Henry Schein Animal Health, Dublin, OH), and a 2mm thumb punch (Kent Scientific) was used to generate 2-3 punches across the medial ear pinna in the right and left ears, administered sequentially or concurrently as indicated: note, we did not detect overt sex differences at the current study level. For initial in vivo Yap inhibition experiments, adult Acomys received intraperitoneal injections of Verteporfin (VP, Tocris, 100mg/kg, 100mg/ml DMSO stock solution diluted 1:10 PBS prior to injection) every 3-4 days as described by Lui-Chittenden *et al* [16]: controls received equivalent volume of 10% DMSO in PBS. For subsequent experiments, adult Acomys received intraperitoneal injections of VP (100mg/kg, 20mg/ml mineral oil stock solution) every 3-4 days: controls received equivalent volume of mineral oil. All animals received post procedure monitoring, including body weight measurements, all of which were stable over the experimental timecourse. Some animals received intravenous tail vein injection of fluorescent Dextran-Rhodamine 1h prior to sacrifice. Upon study completion, animals were terminally euthanized under anesthesia by cardiac perfusion with cold PBS, ears were photographed (Olympus SZX16 Stereomicroscope), and tissue collected.

2.3.2 Cell Lines: Species-specific primary fibroblast cultures were established from adult male *Acomys cahirinus* and CD1 *Mus musculus* (3-4 month old) fresh ear tissue (2mm ear punches) using established procedures. The Human adult fibroblast cell line SK5 was a generous gift from Dr. Elaine Raines at the University of Washington. All cell lines were grown on collagen coated tissue culture plates (5ug/cm^2 BD Biosciences), maintained at the same culture conditions (DMEM 4.5g/L D-glucose, L-glutamine, 110mg/L sodium pyruvate supplemented with 10% FBS and 100 U/mL Pen-Strep, 37°C, 5.0% CO2) unless otherwise noted, and discarded after 15 passages in order to prevent gross genomic changes over long term *in vitro* culturing. For cell signaling experiments, ~80% confluent *Acomys*, Mus, and Human fibroblasts were serum starved for 12 hours (DMEM, .5% FBS and 100 U/ml Penicillin/Streptomycin; Serum Starvation Media/S.S.M) prior to addition of recombinant hTGFβ1 fibrokine (2ng/ml, unless stated otherwise, Cell Signaling Technologies) and/or other factors as indicated (Okadaic Acid [abcam], Tautomycetin [Tocris], etc). Stable lines of *Acomys* ear fibroblasts expressing pEGFP-C3-hYAP2 (Marius Sudol[17], Addgene plasmid #17844) were generated by transient transfection with FUGENE 6® (Promega). After 24 hours of plasmid uptake, stable cells were selected using G418 (Thermo Scientific) at a concentration of 500ug/ml for six days.

2.3.3 Tissue Preparation and Processing: For paraffin embedding, excised tissues were placed in 4% PFA (w/v) and stored overnight at 4°C with agitation, washed three times in PBS, stored in 70% (v/v) ethanol, processed using a Tissue-Tek VIP automatic processor (Sakura), and cut at 8-m per section. Histological staining including Masson's Trichrome, Alcian Blue, Saffron O and Verhoeff-Van Geisson's stain were done in collaboration with Benaroya Research Institute or the University of Washington South Lake Union Imaging and Histology Core. For cryosectioning,

tissue was embedded and frozen in O.C.T medium (TissueTech) using a dry-ice slurry/2-methybutanol mixture, and cut at 8-10µm per cryosection.

2.3.4 Immunofluorescence: Tissue cryosections were thawed, washed with PBS, post fixed with 4% (w/v) PFA for 10 minutes. Post fixation, slides were washed three times for five minutes with PBS followed by permeabilization using 0.2% Triton-X100 in PBS (PBT) for 10 minutes. Slides were blocked (5% BSA, 2% normal goat serum in PBT) at room temperature for 1 hour, tissue sections were incubated in primary antibody overnight at 4˚C in blocking solution (3% BSA, 0.2% Triton-X100 in PBS).. Primary antibodies used included anti-Cleaved Caspase 3 (1/200, rabbit; Cell Signaling # 9661), anti-EDA-Fibronectin (1/200, mouse; Abcam# ab6328), anti-Flag (1/500,mouse; Sigma # F1804), anti-Smooth Muscle Myosin Heavy Chain (1/500, rabbit; Biomedical Technologies # BT562), anti-ACTA2 (Smooth Muscle α-Actin) (1/2000, mouse; Sigma # A2547), anti-PCNA (1/100,mouse; Cell Signaling # 2586), anti-Vimentin (1/500,mouse; Sigma # V5255), anti-Vinculin (1/200,mouse; Sigma#V9131), and anti-Yap (1/500,rabbit; Santa Cruz # sc-15407) Slides were washed with PBS, and then incubated with ALEXA-Fluor 488- or 594-conjugated antibodies (Life Technologies) for 2 hours at room temperature in blocking solution. Cell nuclei were counterstained with Dapi (Molecular Probes) and mounted in 4% (w/v) propyl gallate anti-fade solution, or Fluoromount G (Fisher). For in immunolabeling adherent cell cultures, fibroblasts were plated into glass-bottom tissue culture multi-well plates (TissueTek) previously treated with ACID, washed 3X in PBS, and then coated in poly-d-lysine (10mg/ml) and collagen as described. Cell culture media was removed, cells were washed with PBS, fixed with 4% PFA for 10min, washed again with PBS, and blocked for 1h prior to addition of primary antibody solutions. Cells were incubated overnight at 4oC, washed with PBS, ALEXA-conjugated secondary antibodies applied for 1h, counterstained with Dapi, and mounted as described.

2.3.5 Immunoblotting: Cells were washed with ice-cold PBS (pH 7.4) and lysed at indicated time points using radioimmunoprecipitation assay buffer (50mM Tris, pH 7.4, 150mM NaCl, 1% TritonX-100, .5% Sodium deoxycholate, .1% SDS, 2mM EDTA, 2mM EGTA and 50mM NaF) supplemented with protease inhibitor cocktail (Sigma) and 10mM Na-Orthovanadate (Sigma). Normalization of protein concentrations was done using the Pierce™ BCA Protein Assay Kit (Thermo Scientific) and prepared in SDS sample buffer. Equal amounts of protein were resolved on SDS-Page and transferred to either a nitrocellulose (GE Healthcare) or PVDF (Thermo) depending on detection method. Membranes were incubated for 1 hour in LI-COR Biosciences block buffer. After washing, blots were incubated overnight at 4˚C with antibodies including anti-β-tubulin (1/5000,mouse; Sigma Aldrich # BT7R), anti-GAPDH (1/5000, rabbit; Cell Signaling #5174), anti-pLats-T1079 (1/1000,rabbit; Cell Signaling # 9159), anti-Acta2 (Smooth Muscle α-Actin) (1/2000,mouse; Sigma # A2547), ant-Smad2(1/2000, rabbit; Cell Signaling # 5339), anti-pSmad2-S465/467 (1/1000, rabbit; Cell Signaling # 3108), anti-Smad3(1/2000, rabbit; Cell Signaling #9593), anti-pSmad3-S423/425 (1/1000, rabbit; Cell Signaling # 9520), anti-phospho-p38MAPK-T180/W182 (1/1000, rabbit; Cell Signaling # 4511), anti-Taz (1/1000, rabbit #4883), anti-Yap (1/1000, mouse; Abcam # ab5670), anti-pYap-S127 (1/1000, rabbit; Cell Signaling # 4911), anti-pYapS381 (1/1000, rabbit Cell Signaling #13619), anti-Vinculin (1/5000, mouse; Sigma # V4505). After washing with TBST 0.1%, antigens were detected using either HRP-conjugated (Jackson Research Labs) or IRDye-labeled (LI-COR Biosciences) secondary antibodies. HRP reaction was performed using ECL Prime (GE Healthcare) and exposed to x-ray film. Band intensity was quantified using Image J (National Institute of Health). IRDye secondaries were detected with infrared imaging system Odyssey (LI-COR Biosciences) and band intensity quantified using Image Studio Version 5.2 (LI-COR Bioscience). Immunoblots shown

are presentative of experiments that were repeated a minimum of four independent times. Representative blots shown are those that demonstrate the least amount of nonspecific background and maintain lowest signal to noise ratio.

2.3.6 Transcriptomic Analysis: *Acomys* primary ear fibroblasts were grown to ~80% confluency in 10.0% FBS DMEM, and then switched to 0.1%FBS DMEM (serum starve) for 12h. Recombinant Tgfb1 (2ng/ml) or equivilant volume PBS was added to cells and cultured for 24h to induce a robust transcriptional response to fibrokine signaling (n=3 independent wells per treatment group). Afterwards, cells were washed with PBS and lysed in Trizol solution (Ambion). Total RNA was extracted, DNase treated, and purified (PureLink RNA Mini Kit, Thermo Fisher Scientific). RNA was processed with KAPA's Stranded mRNA-Seq kit (Illumina) following the manufacturer's protocol in duplicate for each sample. The resulting libraries were assessed for library quality using fragment length and number of cycles in real-time PCR. Passing samples were sequenced on a NextSeq 500 using a 300 cycle mid-output kit, with paired 150 basepair reads. The annotated de novo transcriptome of the Acomys cahirinus from Mamrot et al, (DOI:10.1038/s41598-017-09334-7) was downloaded from the Zenodo data sharing resource (https://zenodo.org/record/808870#.WdfH-hNSzdc), and indexed with Kallisto version v0.43.1 (doi:10.1038/nbt.3519). Expression of individual transcripts was performed using Kalisto's quant command with ten bootstraps per sample. The resulting expression profiles were analyzed using Sleuth to determine differentially expressed genes between cell exposed and control samples (doi.org/10.1038/nmeth.4324): ~1/2 of the DE transcripts have annotated gene names from other species (mouse, rat, human).

2.3.7 Identification of *Acomys* Yap Peptide Sequence: The exonic sequence of mouse YAP1 was compared to our *Acomys cahirinus* Genome (manuscript in preparation) using BLAT to

identify *Acomys* YAP genomic loci. Our previous RNAseq data from *Acomys* ear fibroblasts identified 8-9 homologous Yap1transcripts using CUFFLINKS, similar to the number of YAP isoforms identified in a variety of both mouse and human tissues (doi.org/10.1016/j.gene.2012.08.025). We compiled the transcript sequence information from those regions to identify their predicted *Acomy* YAP1 mRNA sequences. Open Reading Frame (ORF) analysis of the longest *Acomys* transcript revealed a potential start codon and contiguous ORF that generated a 490 amino acid peptide (ORFinder, NCBI) exhibiting high homology to human and mouse YAP1-2 isoform. Clustal Omega (www.ebi.ac.uk/Tools/msa/clustalo/) was used for multiple peptide alignments, and NetPhos 3.1 (http://www.cbs.dtu.dk/services/NetPhos/) to predict high probability Serine/Theonine/Tyrosine phosphorylation sites (see Supplemental Figure WW).

2.3.8 Lentiviral Transduction: Doxycycline-inducible human Flag-tagged YAP-S127A lentiviral plasmid (PIN20YAP1) was a generous gift of Drs. S. Song and R. Johnson, and previously described (Song et al., 2014 DOI: 10.1158/0008-5472.CAN-13-3569). Control lentiviral plasmid encoding CMV-based constitutive expression of GFP was purchased commercially (pLV[Exp]-Puro-CMV>EGFP, VectorBuilder). High-titer lentiviral particles for both constructs were generated (VectorBuilder), and Mus primary CD1 ear fibroblasts and human SK5 fibroblasts were transduced using polybrene as directed. Doxycycline (500 ug/ml) was added to media to induce Flag-Yap-S127A expression, which was confirmed by anti-Flag immunoblotting of cell lysates.

2.3.9 Quantitative Image Analysis:

Ear Wound Closure and Pigmentation: Calibrated digital images of whole mount ears were captured prior to embedding (Olympus SZX16 Stereomicroscope), converted to greyscale in FIJI,

and area of wound region interpolated using Surfaces function in Imaris 6.5 (Bitplane). Wound closure was calculated as the percent difference from starting area of a 2mm diameter punch to area size at time of sacrifice for timed injuries. Pigmentation levels were similarly determined by comparing percent difference from the average greyscale pixel intensity within the surrounding uninjured tissue, to the pixel intensity within the original 2mm diameter ear punch, using Surfaces function in Imaris (Bitplane). At least 4-6 animals were used per time point group. Snapshots were exported to Photoshop and panels assembled in Illustrator CS5-7 (Adobe).

Myofibroblast and New Blood Vessel Formation: High-resolution image volumes from fluorescently labeled sections were collected using the same imaging conditions across all samples (Leica TCS SP5 confocal microscope) (n = 3-6 sections across ear punch injury). Representative mid-injury sections were normalized to Z-depth of 5.4-5.9 m within the image volume (Imaris, Bitplane) (n = 1-2 sections per animal per injury, n = 4-6 animals per injury and time point). The subdermal wound volume was manually traced from the internal subdermal boundary at the distal edge of the blastema to the proximal wound edge cartilage cleavage plane, and converted to 3D volume using Surfaces (Imaris, Bitplane). The volume of ACTA2 immunolableling within this subdermal space was automatically rendered and segmented using Surfaces: channel = ACTA2, smooth surface grain size = 0.01, background subtraction = false, enable split = 5.68, manual threshold A = 38.12, auto-threshold B = true, voxels > 30.0 (Imaris, Bitplane). The rendered ACTA2 surface and subdermal wound volume were split into dorsal and ventral regions according to cartilage plane. Total ACTA2 surface volume (mm3) per total subdermal wound volume (mm3) was determined using Statistics (Imaris, Bitplane). Dorsal and ventral ACTA2 surface volumes (mm3) and subdermal wound volumes, respectively, as well as the ratio of dorsal to ventral ACTA2 surface volumes (mm3) and subdermal wound volumes, were similarly determined.

Myh11 immunolabeling was analyzed by further determining the intensity sum of Myh11 signal with the defined ACTA2 surface volume (Surfaces, Imaris, Bitplane). All quantative data was exported to Excel. Snapshots of maximum intensity projection or blended volume views of representative sections and isolated cells were exported to Photoshop and panels assembled in Illustrator CS5-7 (Adobe).

Nuclear Yap Localization: For in vitro studies, YAP immunolabeling within the nuclear and cytoplasmic compartments were determined from epifluorescent images by placing paired 300nm diameter circles within the Dapi-labeled nucleus and adjacent cytoplasm within individual cells using Spots (Imaris, Bitplane), and intensity sum of YAP nuclear and cytoplasmic signal exported to Excel. The ratio of nuclear to cytoplasmic YAP signal was calculated per cell (n= >50 cells per group). Snapshots exported to Photoshop and panels assembled in Illustrator (Adobe) (see Supplemental Figure SS). For in vivo studies, Dapi-labeled nuclei in the subdermal wound space were automatically rendered and segmented using Surfaces: channel = Dapi, smooth surface grain size = 0.4, background subtraction = 2.8, threshold = 21.85, enable split = 3.788, quality = 14.96, voxels > 10.0 (Statistics, Imaris, Bitplane) (see Supplemental Figure SS). Total nuclear YAP signal was determined by calculating the intensity sum of YAP immunolabeling within the total chromatin nuclear surface compartment (n = 1-2 sections per timepoint per animal, n = 4-6 animals per timepoint). All data was exported to Excel. Single nuclei surfaces within representative subdermal 3D volumes were plotted using Vantage (Imaris, Bitplane) with respect to dorsal-ventral (Y-axis) / proximal-distal (X-axis) position, intensity sum of YAP nuclear signal (Z-axis), and color coded for YAP levels to exemplify single nuclei differences within the total pattern of YAP activity in the subdermal wound compartment (see Supplemental Figure 1). Snapshots of

maximum intensity projection or blended volume views of representative sections and isolated cells / nuclei were exported to Photoshop and panels assembled in Illustrator CS5-7 (Adobe).

Cartilage Regeneration: Saffron O stained sections were scanned (Olympus VS120 Slide Scanner). The subdermal wound area and regions of new cartilage growth defined by Saffron O staining were traced, and the average area of regenerated cartilage per subdermal wound area was calculated (n = 6 sections per injury per time point; n = 4-6 animals per group; VS-Desktop Software). All data was exported to Excel. The difference between cartilage regeneration in control and Verteporfin treated animals was determined. Representative images were exported to Photoshop and panels assembled in Illustrator CS5-7 (Adobe).

2.3.10 Statistical Analysis: Unpaired Student's T-test was used to compare treatment groups to control groups in a species-specific manner. One-way ANOVA with a Bonferroni or Tukey post-hoc test used for multiple comparisons of three or more groups over time. Two-way ANOVA with a Bonferroni or Tukey post-hoc test used for multiple comparisons of three or more groups and between species and over time. $P < 0.05$ was considered to be significant. *P<0.05, **P<0.01, ***P<0.001, ****P<0.0001. Statistical analyses and graphic presentation were all done using Prism 6 (GraphPad) and Excel, and assembled using Illustrator CS5-7 (Adobe). Error bars on graphs ± standard deviation (SD) except when stated otherwise.

2.4 Results

2.4.1 *Acomys* exhibit transient myofibroblast formation prior to functional revascularization

A major focus in mammalian wound healing biology is the relationship between fibroblast homeostatic functions and injury induced transition to myofibroblasts (MFs), which are thought to mediate rapid wound healing but limit regenerative potential in most mammalian models[18-20]. However, an initial report indicated *Acomys* underwent epimorphic regenerative healing despite

the conserved presence of MFs within injured tissue[8]. We hypothesized that novel evolutionary adaptations underlying the fibroblast/myofibroblast relationship in *Acomys* might promote regenerative versus fibrotic wound healing. We tested this hypothesis using a 2mm ear pinnae punch injury model to investigate the cellular and molecular mechanisms underlying fibrotic wound healing in adult *Mus musculus* (outbred CD1 strain, referred to as CD1/*Mus*) compared to epimorphic regenerative wound repair in adult *Acomys cahirinus* (referred to as *Acomys*). As demonstrated previously , while CD1 *Mus* ear punch injuries healed, they failed to close, in contrast to *Acomys*, which exhibited rapid closure kinetics by 2-3 weeks post-injury and full restoration of pigmentation by 5 weeks post injury (**Fig 1 A, B**)[21].

While MFs are a well-known cell type, their identification is difficult as no one definitive marker is specific to MFs [22]. Hence, we utilized a panel of markers and double labeling strategies to identify MFs versus other cell types throughout periods of ear injury, including α-smooth muscle actin (ACTA2), smooth muscle myosin heavy chain (Myh11), and the alternative splice isoform of fibronectin Extracellular Domain A -Fibronectin (EDA-F). For example, in uninjured ear tissue from both *Mus* and *Acomys*, $ACTA2^{+}/Myh11^{+}$ mature vasculature associated smooth muscle cells are observed, without injury associated $ACTA2^{+}/Myh11^{-}$ or $ACTA2^{+}/EDA\text{-}F^{+}$ MFs (data not shown). However, ear punch injury induces a robust $ACTA2^{+}/Myh11^{-}$ MF response in both *Mus* and *Acomys* blastemas at early stages (weeks 1 and 2, **Fig 1C**).

However, we found that while *Mus* maintained a robust $ACTA2^{+}/Myh11^{-}$ MF response within the fibrotic tissue though at least week 4, *Acomys* initial $ACTA2^{+}/Myh11^{-}$ MF population resolved into $ACTA2^{+}/Myh11^{+}$ mature vascular smooth muscle cells evident by 2-3 weeks post injury (**Fig 1C**), in contrast to previous findings. Moreover, *Acomys* initial $ACTA2^{+}/Myh11^{-}$ MFs also upregulated EDA-F (**Fig 1D**), a fibronectin splice variant restricted to fibro-pathological

disorders in mammalian adults, which is required for MF differentiation and activation [23-26], indicating conserved MF induction pathways across species. By contrast, early injury induced *Acomys* ACTA2^{+}/EDA-F^{+} MFs also resolved into ACTA2^{+}/EDA-F^{-} cells by week 3 (**Fig 1D**), mirroring the appearance of new ACTA2^{+}/Myh11^{+} blood vessels (**Fig 1C**). Note that deposition of EDA-F into the extra-cellular matrix largely resolves, except in ventral regions of regenerated tissue and along the dermal/subdermal boundary at these post-injury time points (**Fig 1C**).

We developed a quantitative imaging approach to more extensively determine the spatial and temporal relationship between MF maintenance in *Mus*, compared to transient MF induction and subsequent generation of functional vasculature in *Acomys*. Surface rendering and isolation of ACTA2^{+} and Myh11^{+} immunolabeling within the subdermal blastema region clearly reveals the extent and persistence of ACTA2^{+}/Myh11^{-} MFs in both dorsal and ventral blastema compartments though week 4 in *Mus* (**Fig 1E**, top). By contrast, *Acomys* appear to have overall less ACTA2^{+}/Myh11^{-} MFs in general, and that ACTA2^{+}/Myh11^{+} new blood vessels originate in a dorsal to ventral manner during regenerative healing (**Fig 1E**, bottom). Quantification of total ACTA2^{+} immunolabeled volume within the subdermal wound space confirmed that *Mus* does in fact generate an increased and persistent MF response compared to *Acomys* (**Fig 1G**). Moreover, this abrupt loss of MFs (ACTA2^{+}/Myh11^{-}) proceeds an expansive revascularization event (ACTA2^{+}/Myh11^{+}) by week 3 (**Fig 1H**). Further, new ACTA2^{+}/Myh11^{+} blood vessels initially appear in dorsal to ventral manner evident by week 2 (**Fig 1I**), some of which have already restored functional blood flow evident by the presence of acute intracardiac injected high-molecular weight fluorescent dextran labeling in vessels within newly regenerated tissue at week 2 (**Fig 1F**). These novel data indicate *Acomys* maintain an evolutionary conserved induction of MFs during initial

tissue injury, but evolved a non-conserved transient MF phenotype that does not drive fibrosis, but rather may serve as cues for important functions during *Acomys* unique regenerative repair process.

2.4.2 Isolated *Acomys* fibroblasts maintain homeostasis in response to fibrokine signaling

We generated primary fibroblast cell lines from adult *Mus* and *Acomys* 2mm ear punches to further test the cell signaling and plasticity of this unique fibroblast versus myofibroblast relationship within *Acomys*. Classically, mammalian fibroblasts growing in low-serum conditions can be driven to induce MF differentiation (increased ACTA2 expression coupled with stress fiber formation) via fibrokine signaling, in particular TGFβ1 [27]. We grew *Acomys*, *Mus*, and human (SK5) primary fibroblasts to subconfluency, switched media to low serum (stress), and treated some wells with TGFβ1 to force MF differentiation (**Fig 2A**). Since TGFβ1-mediated MF induction occurs by both canonical SMAD and non-canonical Mitogen Activated Protein Kinase (MAPK) protein p38 mediated signaling [28], we first assayed whether *Acomys* cells can sense and respond to TGFβ1 signals similar to *Mus* and human. Western blots of *Acomys* and *Mus* cell lysates revealed that SMAD2, SMAD3, and p38 where all phosphorylated in response to TGFβ1, and both pathways necessary for MF differentiation were activated, similarly to *Mus* (**Fig 2B**). Surprisingly, quantitative immunoblotting for ACTA2 level changes in response to TGFβ1 treatment revealed *Acomys* fibroblasts normally express high levels of ACTA2 under control conditions compared to *Mus* and human cells (**Fig 2 C, D**). Furthermore, ACTA2 expression levels in *Acomys* cells remained constant upon exposure to TGFβ1 signaling, in contrast to *Mus* and human cells which revealed statistically significant increased ACTA2 induction (**Fig 2 C, D**). Immunolabeling cultured cells confirmed *Acomys* fibroblasts normally express higher levels of ACTA2 compared to *Mus* and human fibroblasts under control conditions, which did not increase in response to TGFβ1 treatment, by contrast to Mus and human MFs (**Fig 2E**). Moreover, TGFβ1 treated *Acomys*

fibroblasts did not reorganize their cytoskeleton into unidirectional mature stress fibers spanning the entire cell length unlike *Mus* MFs (**Fig 2F**) [29, 30]. These data demonstrate *Acomys* ear fibroblasts resist fibrokine mediated MF differentiation in a cell autonomous manner.

We used RNAseq to more broadly analyze cell intrinsic homeostatic transcriptional responses initiated by isolated Acomys fibroblasts to resist TGFβ1-mediated MF induction. We annotated our de novo transcriptome assembly against a recent *Acomys* transcriptomic resource, and identified differently expressed candidate transcripts[31]. Increased expression of *Serpine1 (Pia1)*, a well-known TGFβ1 signal transduction target, accompanied by no change in *Acta2* gene expression confirms our biochemical and cellular data demonstrating activated fibrokine signaling occurs without MF induction in isolated *Acomys* fibroblasts (**Fig 2G**). We also analyzed available transcriptomic datasets comparing *Mus* and *Acomys* ear tissue healing over time and confirmed that injury induced a similar *in vivo* fibrokine response (*Serpine1/Pia1*) in both species (**Fig 2H**)[21].

Further examination of our *in vitro* data revealed a unique anti-fibrotic like state with downregulation of known fibrotic signaling pathways (*Pdgfb, Tgfr2, Vegfd, Bmp4, Hgf)* and potentially new transcriptional regulators (*Klf15, Dlx3*), along with upregulation of genes and pathways considered more regenerative and potentially ant-inflammatory, especially secreted factors (*Lif, Wnt11, Il18, Ctgf*) (**Fig 2G**). Intriguingly, upregulation of *Ctgf* as well as *Cnn1, Lrg6,* and *Cyr61,* are all targets of Hippo-YAP signaling, strongly implicating concerted transcriptional activation of this well-known homeostatic pathway in response to fibrokine exposure in *Acomys* cells (**Fig 2G**)[32-35] . Indeed, *in vivo* analyses indicate decreased *Ctfg* expression during fibrotic healing in *Mus*, by contrast to increased *Ctgf* expression during regenerative healing in *Acomys* (**Fig 2H**). Altogether, these data indicate some mammals naturally evolved differential genomic solutions for responding to injury signals aimed to prevent fibrosis and promote regeneration,

including orchestrated systems-level responses and isolated cell autonomous responses. Importantly, these natural solutions in *Acomys* point to potential new therapeutic avenues aimed towards re-landscaping fibrotic genomic responses such as ours into more regenerative outcomes.

2.4.3 *Acomys* fibroblasts differentially regulate YAP activity when exposed to fibrokine signaling

We hypothesized differential Hippo-YAP signaling may contribute to *Acomys* increased homeostatic signaling and regenerative capacity upon fibrokine exposure and injury compared to *Mus*. Although input into Hippo-YAP signaling activity is highly contextual, signaling output can be more simply viewed by measuring the balance between YAP phosphorylation states that govern nuclear versus cytoplasmic location[36]. Activating inputs impinge on the upstream regulatory serine/theonine kinase Hippo (MST1), inducing auto-phosphylation and that of its substrate LATS1/2, a kinase that in turn phosphorylates YAP (S127 in humans). Phosphorylated YAP-S127 is sequestered in the cytoplasm and becomes a substrate for further phosphorylation and ultimately degradation. Since YAP is a transcriptional cofactor, cytoplasmic sequestration inhibits nuclear transcriptional activities, and YAP nuclear localization can be considered as a proxy for pathway activity: activating Hippo (MST) and LATS inhibits YAP[37].

We tested *Acomys* fibroblasts to determine if Hippo-YAP signaling underwent selective adaptations that contribute to their increased homeostatic capacity compared to *Mus* and human. Normally, in the context of cell-cell contact and fibrokine exposure, Hippo signaling is activated leading to increased YAP cytoplasmic sequestration an inhibition (**Fig 3A**)[36].We developed an imaging assay to measure nuclear versus cytoplasmic immunolabeled YAP in cultured fibroblasts (**Supp Fig 1A**). Quantification of YAP immunolabeling of subconfluent versus hyperconfluent *Acomys* and *Mus* fibroblasts under normal growth conditions exhibited high nuclear/cytoplasmic

(N/C) ratios, which became sequestered to the cytoplasm at hyperconfluency resulting in significantly low N/C ratios (**Fig 3 B, C**), confirming a conserved homeostatic response of Hippo signaling to cell-contact dependent growth inhibition.

Strikingly however, *Acomys* fibroblasts maintained nuclear YAP upon exposure to TGFβ1 treatment, by contrast to *Mus* and human fibroblasts that exhibit significantly increased cytoplasmic YAP shuttling during MF induction, resulting in low N/C ratios (**Fig 3D,E**). Quantitative immunoblotting of YAP-S127 phosphorylation state during TGFβ1-mediated MF induction revealed a small portion of the total pool of *Acomys* YAP protein is phosphorylated, by contrast to comparatively greater pYAP-S127 levels in *Mus* and Human cells and that whereas TGFβ1 treatment increased p-S127 levels over time in *Mus* and human MFs, *Acomys* p-S127 levels remained stable (**Fig 3F,G**). These data reveal that while pathways regulating cell-cell contact and organ size control are largely conserved, naturally selected genomic adaptations occurred within *Acomys* homeostatic control pathway responses to injury signals and fibrosis.

2.4.4 *Acomys* increased nuclear YAP is maintained by novel phosphatase activity

We compared YAP protein sequence and additional phosphorylation post-translational modifications regulating degradation status to further understand *Acomys* increased capacity for maintaining nuclear YAP. We identified the YAP locus in our *Acomys* genome (manuscript in preparation) using homologous *Mus* YAP exon sequence data, and used this template to compile all overlapping transcript reads from our *Acomys* RNAseq fibroblast dataset. This approach generated 8-9 potential YAP isoforms present in *Acomys* fibroblasts, the same number of isoforms present in multiple human and mouse tissues[38]. Open reading frame analysis of the longest *Acomys* transcripts revealed a predicted peptide (490 aa) that is 93% and 96% identical to human and mouse YAP1-2, respectively, with all key regulatory Serine/Theonine/Tyrosine phosphorylation sites

conserved (**Supp Fig 2**). Hence, regulation of YAP phosphorylation state, rather than sequence or isoform variation, likely contributes to increased YAP nuclear maintenance and activity in *Acomys* versus *Mus* and human.

YAP de-phosphorylation is mediated by PP1 and PP2A Serine/Threonine (S/T) class phosphatases[39, 40].We developed a pulse chase de-phosphorylation assay using okadaic acid (OA), a Serine/Threonine phosphatase inhibitor (**Fig 4A**) [41-43]: OA treatment allows MST/LATS-mediated phosphorylated YAP to accumulate, while wash-out allows PP1/PP2A-mediated YAP de-phosphorylation, which is evident by immunoblotting as a molecular weight gel shift. We established a stable *Acomys* fibroblast line expressing human YAP-GFP (hYAP-GFP), and observed both hYAP-GFP and endogenous *Acomys* YAP underwent hyper shift after OA pulsing (**Fig 4B**). *Acomys* YAP and hYAP-GFP de-phosphorylation in *Acomys* cells was specifically mediated by PP1/PP2A complex, since phosphorylated ERK levels did not shift in agreement with its role as a DUSP (dual specificity phosphatase) substrate (**Supp Fig 3A**) [44]. We compared the rate of endogenous PP1/PP2A-mediated YAP-S127 de-phosphorylation between *Acomys*, *Mus*, and human fibroblasts after OA washout (**Fig 4C**), and found that *Acomys* re-established PP1/PP2A-mediated YAP de-phosphorylation significantly faster than *Mus* and human cells (**Fig 4D**). We also found that de-phosphorylation of the Degron motif within the TAD domain (S381-*Mus*/S391-Human), which targets YAP to E3 dependent ubiquitination and proteasomal degradation [37] showed significantly rapid recovery to its normally low state in *Acomys* cells (**Fig 4E,F**).

We tested *Acomys* PP1/PP2A de-phosphorylation specificity further by analyzing endogenous TAZ and LATS1/2, since both are also substrates, and whether PP1, PP2A, or both phosphatase complexes conferred increased substrate targeting. We found that *Acomys* TAZ

paralog, a YAP partner/co-effector and LATS1/2 substrate, appeared degraded with lower levels overall in *Acomys* cells (**Fig 4G**), likely conserved due to the inverse relationship between TAZ stability and YAP abundance[45].We found that endogenous LATS1/2 de-phosphorylation rates were similar between *Acomys*, *Mus*, and human fibroblasts (**Fig 4H,I**), indicating conserved phosphatase regulation of the direct upstream regulator of YAP.

We refined our YAP de-phosphorylation assay by taking advantage of selective higher affinity Tautomycetin-mediated inhibition of PP1 versus higher affinity OA-mediated inhibition of PP2A [46, 47]. We quantified the change in endogenous levels of *Acomys* YAP phosphorylation (S-127) versus total YAP, compared to the changes in levels of phosphorylated Myosin Heavy Chain (S-20) versus total MLC, known preferential targets of PP1 and PP2A activity (**Supp Fig 3B,C**). Intriguingly, we saw specific increased phosphorylation of YAP at 200nM with OA and not Tautomycetin (**Fig 4J**), by contrast to MLC phosphorylation, which only increases at higher doses of both inhibitors. This indicated YAP de-phosphorylation was more sensitive to PP2A inhibition compared to MLC, a PP1 substrate (**Fig 4K, Supp Fig 3C**). These data indicate *Acomys* ear fibroblasts evolved a novel high affinity PP2A-mediated surveillance function that rapidly and specifically de-phosphorylates key regions regulating YAP protein location (S127, cytoplasm) and stability (S381, degradation) to maintain nuclear localization and activity. Altogether, our *in vitro* data reveal cell intrinsic beneficial adaptations in isolated *Acomys* fibroblasts in key homeostatic pathway responses to injury signals might contribute to *in vivo* functions underlying *Acomys* unique capacity to regenerate severely damaged skin and tissue as adult mammals.

2.4.5 Spatial and temporal YAP activity distinguishes ear tissue regeneration in *Acomys* versus fibrosis in *Mus*

We examined available *in vivo* ear tissue healing transcriptomic datasets to determine whether expression of Hippo-YAP signaling components where conserved between *Acomys* and *Mus* (**Supp Fig 4**). In *Mus*, upstream negative regulators *Mst1* and *Lats2* genes were maintained or upregulated and *Yap1* expression decreased, by contrast to *Acomys*, which downregulated *Mst1* and *Lats2* while upregulating *Yap1*, while both species upregulated and/or maintained expression of *Tead* co-factor genes, especially *Tead2* (**Supp Fig 4**), predicting overall decreased Yap signaling in *Mus* compared to *Acomys*. In support of this notion, *Birc5*, another well-known target of Yap activation, was also upregulated in *Acomys* compared to *Mus*. (**Supp Fig 4**),

We tested whether differences in YAP signaling were apparent by immunolabeling sections of *Mus* and *Acomys* ear punch injuries to validate YAP protein expression and determine YAP nuclear/cytoplasmic localization *in vivo*. Uninjured *Mus* and *Acomys* ear tissue indicated YAP was restricted to the cytoplasmic compartments of epidermal and hair follicle populations, excluded from subdermal mesenchyme (**Supp Fig 4**). We found by week 1 post-injury, YAP protein was present in ACTA2^{+} MFs in *Mus* (**Supp Fig 4**), and was largely localized to the perinuclear cytoplasm, which became restricted to a subpopulation of ACTA2^{+} MFs by week 2 (**Fig 5A**). By contrast, *Acomys* exhibited strong YAP nuclear localization in both transient ACTA2^{+} MFs and ACTA2^{-} cells within the early subdermal blastema at week 1 (**Supp Fig 4**) that was maintained through week 2, just prior to wound closure (**Fig 5A**). However, we noticed that by week 3, as *Acomys* MFs disappeared during ear tissue closure, *Acomys* YAP protein became relegated to the perinuclear cytoplasm in mesenchymal cells (**Fig 5A, Supp Fig 4**). Interestingly, by week 4, nuclear YAP localization was re-established in the majority of *Acomys* mesenchymal

cells, especially those residing in the ventral region of the regenerating tissue (**Fig 5A, Supp Fig 4**).

We co-opted our quantitative imaging approach to determine species and pattern differences in nuclear/cytoplasmic YAP localization in wounds during *in vivo* wound healing. We rendered, segmented, and isolated DAPI labeled nuclei within the subdermal wound region from high-resolution confocal image volumes of similarly stained and imaged immunolabeled sections (**Supp Fig 1**). This approach allowed 3D visualization of individual nuclei surfaces with respect to YAP and ACTA2 immunolabeling, and conferred unbiased quantification of YAP protein within nuclear volumes (**Supp Fig 1**). For example, during early week 1 blastema formation, high power 3D views of individual cells located near the leading blastema edge confirmed YAP is primarily localized in the $ACTA2^{+}$ cytoplasmic leading process in *Mus* MFs, by contrast to nuclear localized YAP in both transient $ACTA2^{+}$ MFs and $ACTA2^{-}$ *Acomys* cells (**Fig 5B**). Analysis of 3D plots comparing individual nuclei position within the subdermal blastema to overall YAP immunolabeling intensity within nuclei volumes, revealed that while some isolated *Mus* nuclei can exhibit increased nuclear YAP, many more *Acomys* nuclei exhibited much higher levels of nuclear YAP (**Fig 5C, Supp Fig 1**). Comparing *Acomys* 3D plots during later timepoints confirmed that YAP nuclear localization transiently decreases in most cells at week 3 upon wound closure, and then rapidly re-localizes to nuclear compartments by week 4, except for a small ventral subpopulation which maintains high relatively higher YAP during and after wound closure (**Fig 5C**). Quantifying total YAP intensity within the total subdermal wound nuclear compartment revealed significantly increased nuclear YAP levels overall in *Acomys* cells compared to *Mus*, particularly just before and after wound closure (**Fig 5D**). Moreover, we observed quantitatively significant spatial and temporal differences in *Acomys* nuclear YAP localization during early

proliferative (weeks 1-2) compared to later differentiating (weeks 3-4) periods (**Fig 5E**). *Acomys* unique spatial and temporal nuclear YAP patterning *in vivo* is highly consistent with our *in vitro* data revealing *Acomys* fibroblasts increased capacity for maintaining nuclear YAP. These data confirm that *Acomys* naturally evolved solutions for regenerative versus fibrotic wound healing *in vivo* include major alterations in YAP homeostatic signaling that might directly and reiteratively regulate early proliferative and later differentiation phases, including restoration of dorsal-ventral pattern information.

2.4.6 Blocking YAP signaling activity inhibits *Acomys* regenerative wound repair.

We tested whether YAP signaling was necessary for *Acomys* ear tissue regeneration by adopting a published strategy using verteporfin (VP) treatment, a pharmaceutic that inhibits YAP-TEAD interactions and induces cytoplasmic sequestration since genetic tools are not available[16, 48, 49].We pretreated adult *Acomys* (n = 5-6 per group) with VP [100mg/kg, DMSO] or equal volume DMSO every other day for a week to ensure delivery, which was maintained every 2-3 days thereafter and sequentially punched ears as depicted in **Fig 6A**. VP-treated animals exhibited attenuated wound closure of early week 1-2 injuries compared to controls, and although older wounds eventually closed in VP-treated animals, they appeared less pigmented (**Fig 6B**). Quantitation of wound area closure revealed a significant attenuation of early phase functions due to VP-treatment (**Fig 6C**), as did re-pigmentation in later injuries (**Fig 6D**). Indeed, YAP immunolabeling sections from 2 and 4 week old wounds from VP-treated animals appeared less nuclear and more cytoplasmic (**Fig 6E**). Moreover, in VP-treated animals $ACTA2^{+}/Myh11^{-}$ MFs appeared increased in early injuries, and maintained in older injuries, especially in dorsal regions and along tissue closure points, which although appeared closed macroscopically, failed to fuse properly upon microscopic inspection (**Fig 6F**). Quantitative image analyses of VP-treated early

stage injuries at week 2 revealed a statistically significant ~50% reduction in nuclear YAP localization in subdermal blastema nuclei, accompanied by increased MFs (total $ACTA2^+$ volume) and decreased vasculature maturation ($ACTA2^+/Myh11^+$ smooth muscle cells) (**Fig 6G**). A similarly significant effect was also observed in later stage VP-treated injury at week 4, whereby nuclear YAP was still reduced, MF were still present (total $ACTA2^+$ volume), and a trend of attenuated vasculature maturation apparent ($ACTA2^+/Myh11^+$ smooth muscle cells) (**Fig 6H**). These data reveal that even partial inhibition of *Acomys* naturally selected increased homeostatic YAP signaling severely attenuates *in vivo* regenerative ear tissue healing capacity, converting *Acomys* into a more *Mus*/human-like fibrotic response.

2.4.7 YAP signaling regulates early phase blastema formation and maintains later stage tissue differentiation during *Acomys* regenerative repair

We modified our VP-treatment to specifically test acute YAP signaling functions during initial blastema formation (weeks 2-3) and later differentiation events occurring after wound closure (weeks 4-5) (**Fig 7A**). We punched two 2mm holes simultaneously in one ear of adult *Acomys* (n = 4-6 per group), and allowed injuries to first undergo normal regenerative healing leading to closure by 3 weeks (**Fig 7A**): time point 2, weeks 3-5 (T2-week 5). Upon closure, two additional 2mm punches were applied simultaneously into the other ear of each animal, and some animals received immediate injections of VP ([100mg/kg; mineral oil, MO] or equal volume MO every other day for 2 weeks (**Fig 7A**): time point 1, weeks 0-2 (T1-week 2). This strategy allows validation of early phase results (T1-week2) without potentially mitigating DMSO effects and importantly, establishment of normal tissue polarity and patterning information prior to constant YAP inhibition (T2-week5) (**Fig 7A**).

VP-treatment in this manner resulted in clear and significant wound closure effects during early phase (T1-week 2), and impact on re-pigmentation at later phase (T2-week 5) (**Fig 7 B-D**). Histological examination confirmed pigment defects were due to lack of differentiated melanocytes near the dorsal dermal/subdermal region at later phases (T2-Week5) (**Fig 7E**). Consistent with our initial approach, VP-treatment using MO similarly increased $ACTA2^{+}$ labeling in the early subdermal blastema (T1-week 2) (**Fig 7F**), and as expected, did not exhibit increased $ACTA2^{+}/Myh11^{-}$ MFs at later phase (T2-week 5) (**Fig 7G**), since *Acomys* MFs normally disappear after wound closure (**Fig 5**). *In vivo* YAP nuclear staining was also reduced at each time point (not shown). Quantitative image analyses confirmed significantly increased ACTA2 levels and inhibition of vascular development in early phase VP-treated injuries compared to control (**Fig 7F**).

We noticed that while tissue remained intact in later phase (T2-week 5) VP-treated injuries, certain architectural features reminiscent of regenerated cartilage were less apparent (**Fig 7E**). We stained a series of histological sections of later phase (T2-week5) VP-treated and control injuries using Saffron O to identify regions of new cartilage growth. Control late phase (T2-week 5) injuries exhibit clear regions of newly regenerating cartilage extending from the original cartilage plate, as well as formation of de novo cartilage islands within injured tissue (**Fig 7G**). By contrast, VP-treated late phase (T2-week 5) injuries exhibit severely and significantly reduced cartilage regeneration (**Fig 7G,E**). Strikingly, in lieu of regenerated cartilage, VP-treated late phase (T2-week 5) injuries underwent a major cell fate change, whereby cartilage, adipose, and melanocyte progenitors were lost or fates reprogrammed towards hair follicle formation, which now autonomously appear in large numbers in ventrally located wound regions (**Fig 7G**). These data confirm an essential role for *in vivo* YAP signaling during early regenerative blastema formation,

including MF disappearance and re-vascularization. Furthermore, these data reveal additional key roles for YAP signaling in maintaining tissue patterning and cell fate lineage potential during later phases of *Acomys* tissue regeneration. Our studies into naturally selected solutions for mammalian tissue repair reveal provocative findings that directly question current notions concerning the relationship between fibroblasts-myofibroblasts-stem cells and fibrotic versus regenerative wound repair in adult mammals.

2.4.8 YAP activation prevents and rescues *Mus* and human in vitro myofibroblast formation

We tested whether *Acomys* unique adaptations in homeostatic responses to injury signals might be used to re-landscape normally fibrotic *Mus* and human genomic responses into a more beneficial regenerative phenotype. As a first step, we took advantage of our TGFβ-mediated MF induction assay combined with doxycycline (Dox)-inducible YAP-S127A-Flag lentiviral expression (referred to as LV-Dox-YAP), which limits MST/LATS-mediated phosphorylation and promotes YAP activity[50].We transduced *Mus* and human fibroblasts with either a constitutive CMV-mediated GFP control lentivirus (LV-GFP) or LV-Dox-YAP under growth conditions, and then analyzed transduced cellular responses to TGFβ1-mediated MF induction in the presence of Dox-mediated YAP-S127A expression at different time points (**Fig 8A**). Confocal imaging of ACTA2 and GFP/Flag immunolabeling in both *Mus* and human transduced fibroblasts that received concurrent TGFβ1 and Dox for 2 days revealed ACTA2 immunolabeling was decreased in YAP-S127A-Flag expressing fibroblasts, by contrast to neighboring uninfected cells and control GFP infected cells that exhibited clear $ACTA2^{+}$ stress fiber formation (**Fig 8B**). This could be due to YAP direct inhibition of *Acta2* gene expression [15, 51, 52].

Intriguingly, treating transduced fibroblasts with TGFβ1 for the first 24h to activate MF-induction pathways, and then treating with TGFβ1 and Dox during the second 24h appeared to

slow/reverse ACTA2^{+} stress fiber formation in YAP-S127-Flag expressing MFs, which appeared more cortically dispersed by contrast to neighboring uninfected cells and control GFP infected cells (**Fig 8C**). These initial data provide proof-of-principle that non-conserved naturally selected genomic adaptations in *Acomys* homeostatic responses to injury can be reciprocated in normally fibrotic mammalian genomes. Our novel approach provides a new strategy for accelerating translational treatments for fibrosis, a factor impacting virtually all human diseases and injuries.

2.5 Discussion:

While evidence of regenerative properties is numerous across a broad spectrum of lower order vertebrates, the potential for regeneration dwindles, particularly in the adult mammals. Instead, inflammation and myofibroblast mediated scar tissue formation are the predominant features of mammalian repair. In contrast, multiple members of the *Acomys* genus have evolved unique mechanisms that enable restoration of tissue homoeostasis. This novel mechanism consists of complete tissue reconstitution in an epimorphic like regenerative manner.

YAP is necessary during discrete phases of Acomys epimorphic wound repair.

In this study, we demonstrate *Acomys* regenerative capability being in part due to differential YAP activity. In particularly, *Acomy*s novel homeostatic control of nuclear YAP localization is necessary for scar free wound repair. While unrestrained YAP activity is a driver of numerous cancers throughout different tissues, *Acomys* regulate YAP activity in a temporal manner throughout periods of epimorphic repair. This dynamic YAP localization appears to control at least two independent phases of *Acomys* repair. These two dependent phases are 1. blastema formation/extension and 2. Tissue architectural reconstitution and patterning. Inhibition of YAP during these two phases ultimately results in failed regenerative wound repair. Interestingly, as compared to the *Mus* which inhibits YAP nuclear localization during early injury,

inhibition of *Acomys* YAP during these dynamic phases results in two unique and independent phenotypes. YAP inhibition during blastemal formation results in blunted tissue extension, myofibroblast accumulation and revascularization defects. YAP inhibition during secondary tissue closure/reconstitution phase results in several mesenchymal cell specification defects. This phenotype is demonstrated by melanocytes, adipocytes or cartilage found to be decreased or entirely absent in the newly formed tissue. YAP inhibition during 2nd phase also results in tissue patterning defects. The most striking being loss of ventral/distal tissue architecture

Hippo Pathway activity is altered both transcriptionally and post translationally in a species-specific manner.

Our data elucidates that *Acomys* have manipulated Hippo-YAP signaling during two levels of regenerative repair. The first being at the transcriptional level with downregulation of upstream negative regulators *Mst1/2* and *Lats1/2* while upregulating *Yap* in a converse manner. This unique transcriptional profile results in *Acomys* decreasing repressive upstream signals thereby allowing for YAP activity to be maintained during periods of epimorphic wound repair.

The second alteration is YAP post translational modifications in a cell autonomous fashion. While *Acomys* exhibit evolutionarily conserved features of Hippo signaling such as YAP inactivation under contact mediated hyper confluency, we show that *Acomys* YAP intrinsically resist fibrokine mediated phosphorylation and cytoplasmic accumulation/inactivation in contrast to both *Mus* and Human. This mechanism of YAP regulation is not due to species specific YAP peptide alteration but rather increased kinetics of Yap dephosphorylation. This unique *Acomys* YAP dephosphorylation potential appears to regulate both spatial and temporal activity as similar kinetics are observed on both S127 and S381 residues. Taken together, the removal of inhibitory signals promotes a freely available nuclear pool of active Yap ready to contribute to any number

of available transcriptional factors. Our VP analysis would suggest YAP-TEAD activity mediate a large proportion of the biological events observed during epimorphic regeneration but we cannot exclude other YAP transcriptional binding partners.

While excessive nuclear localization is known to contribute to excessive cell proliferation and loss of organ size parameters, *Acomys* corral unrestrained Hippo signaling not only by temporal/spatial control but also by differential regulation of YAP paralog TAZ. TAZ is actively degraded during periods of maintained YAP activity. We hypothesize this is a regulatory feature of *Acomys* to maintain Hippo homeostasis and restrain uncontrolled YAP/TAZ signaling in a context dependent manner. A critical aspect of the *Acomys* YAP dephosphorylation is its relationship to upstream negative regulator LATS1/2. Our assays demonstrate LATS1/2 activity is conserved across all mammalian species tested. This would confirm that no perturbations in the ability of *Acomys* LATS1/2 account for differential YAP regulation. Instead, we identify a species specific PP2A holoenzyme phosphatase interaction as the critical mediator of both YAP and LATS1/2 dephosphorylation. While PP2A has previously been shown to regulate YAP activity directly, the kinetics of dephosphorylation shared by both *Acomys* YAP and LATS1/2 suggest the possibility of a unique protein-protein complex assembly. While YAP-phosphatase interactions are well characterized to be required for homeostatic control in a number of tissue resident stem cells, it is unknown if this mechanism is deployed in *Acomys in vivo* [40, 53]. As PP2A/YAP/LATS1-2 signaling axis is necessary for maintained nuclear active YAP *in vitro,* it is entirely plausible this mechanism is employed *in vivo* as nuclear YAP is a defining feature of successful *Acomys* regenerative repair.

Yap activity modulates myofibroblast formation and accumulation.

Evidence pointing to altered *Acomys* YAP activity was first elucidated by Hippo target genes being highly expressed in a cell type commonly considered a "myofibroblast" in response to TGFβ. While YAP activity has been shown to be required in several epimorphic based limb regeneration models[54,55]. YAP's role in mammalian wound repair is increasingly more complicated to dissect and highly dependent on the context of injury. YAP is considered pro-regenerative in organs that can normally be repaired by stem cell turnover or resident cell proliferation, such as liver, intestinal crypts and cardiomyocytes[56-59]. In contrast, injury models that result in disruption of the interstitial population, such as the kidney, suggest YAP may also promote fibrosis. These mechanistic studies propose YAP acts as an inducer of myofibroblast differentiation and activation. [60-63]. On the contrary, our data demonstrate YAP is a potent inhibitor of myofibroblasts maturation and a mediator of their temporal retention. In non-regenerators, loss of YAP activity and cytoplasmic retention correlate with myofibroblasts activation and scar formation in both *in vivo* injuries and cell culture. However, nuclear retention of YAP appears to throttle *Acomys* myofibroblasts formation early in blastema formation, perhaps by preventing terminal differentiation or maintaining an immature labile state. Similarly, markers of mature myofibroblasts such as collagen deposition, increased ACTA2 protein expression and its assembly into mature stress fibers remain minimal in nuclear YAP^{+} *Acomys* myofibroblasts in culture. Confirming our *in vitro* data, pharmacological inhibition of YAP in *Acomys* injuries exacerbates myofibroblasts formation by inducing not only their expansion but also the length of their retention. This altered cellular response is correlated to multiple downstream perturbations such as failed revascularization and wound closure defects which ultimately contribute to failed regenerative repair. In agreement, phenotypically replicating YAP localization seen in *Acomys* cells by viral transduction is sufficient in blocking TGFβ1 mediated myofibroblasts differentiation

in both *Mus* and human dermal fibroblasts. In addition, forced YAP nuclear localization not only inhibits initial myofibroblast differentiation, but also induces myofibroblasts phenotypic regression in non-regenerators. To our knowledge, this result is the first described translational application of *Acomys* biology contributing to a potential therapeutic possibility. It is unknown if myofibroblasts manipulation will result in a regenerative phenotype, but the possibility of myofibroblast regression has clear clinical implications across a broad range of human chronic fibropathalogies. Regardless, these results demonstrate *Acomys* YAP activity contributes to regenerative repair, in part by mediating myofibroblast maturation and function.

In summary, this work provides a framework for further elucidating the relationship between conserved organ size control mechanisms and *Acomys* regenerative potential. Further elucidating how this adult mammal has intrinsically manipulated Hippo-YAP to achieve such a feat may one day provide therapeutic avenues to inhibit or possibly regress fibrotic conditions.

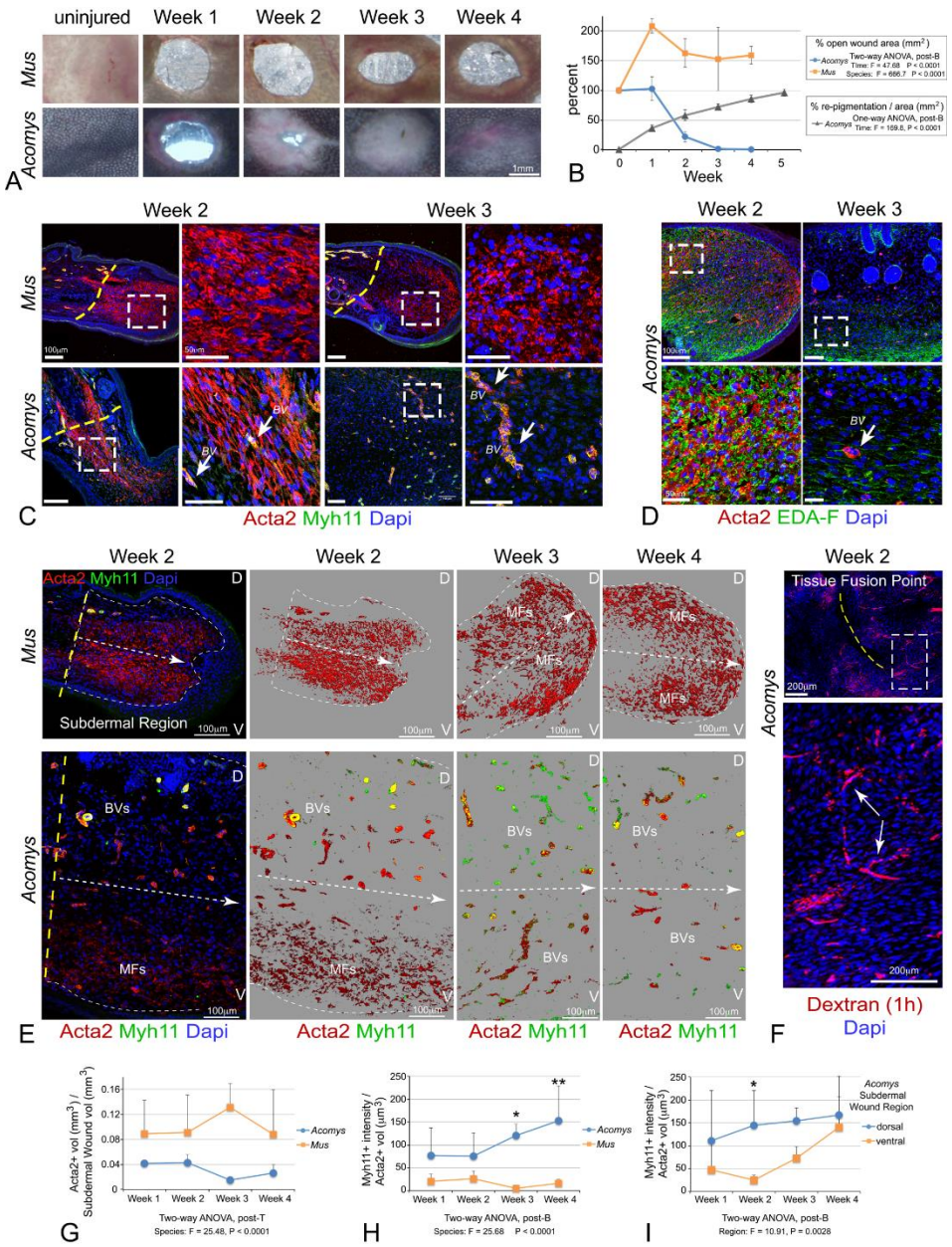

Figure 2.1 *Acomys* exhibit transient myofibroblast formation prior to functional revascularization. (**A**) Representative images of *Acomys* and *Mus* 2-mm ear hole injuries at indicated time points. (**B**) Summary data of *Acomys* and *Mus* ear closure and re-pigmentation kinetics (**C**) Immunostaining for ACTA2 and Myh11 localization at indicated time points. Arrows indicate blood vessels (BV). (**D**) Immunostaining for EDA-Fibronectin and Myh11 localization in weeks 2-3 *Acomys* ear wounds. (**E**)Spatial/temporal transitions of ACTA2^{+}/Myh11+ populations. (**F**) Dextran labeling for functional vasculature. (**G**) Quantification of *Acomys* and *Mus* ACTA2^{+} volume within the dermal wound zones. (**H**) Quantification of *Acomys* and *Mus* Myh11^{+} signal overlap within the ACTA2^{+} volume at indicated time points. (**I**) *Acomys* specific spatial and temporal pattern differences in ACTA2^{+}/Myh11^{-} to ACTA2^{+}/Myh11^{+} transition. Dashed lines indicate amputation plane. Dashed boxes indicate area of magnification. *p<0.05, **p<0.01, ***p<0.00

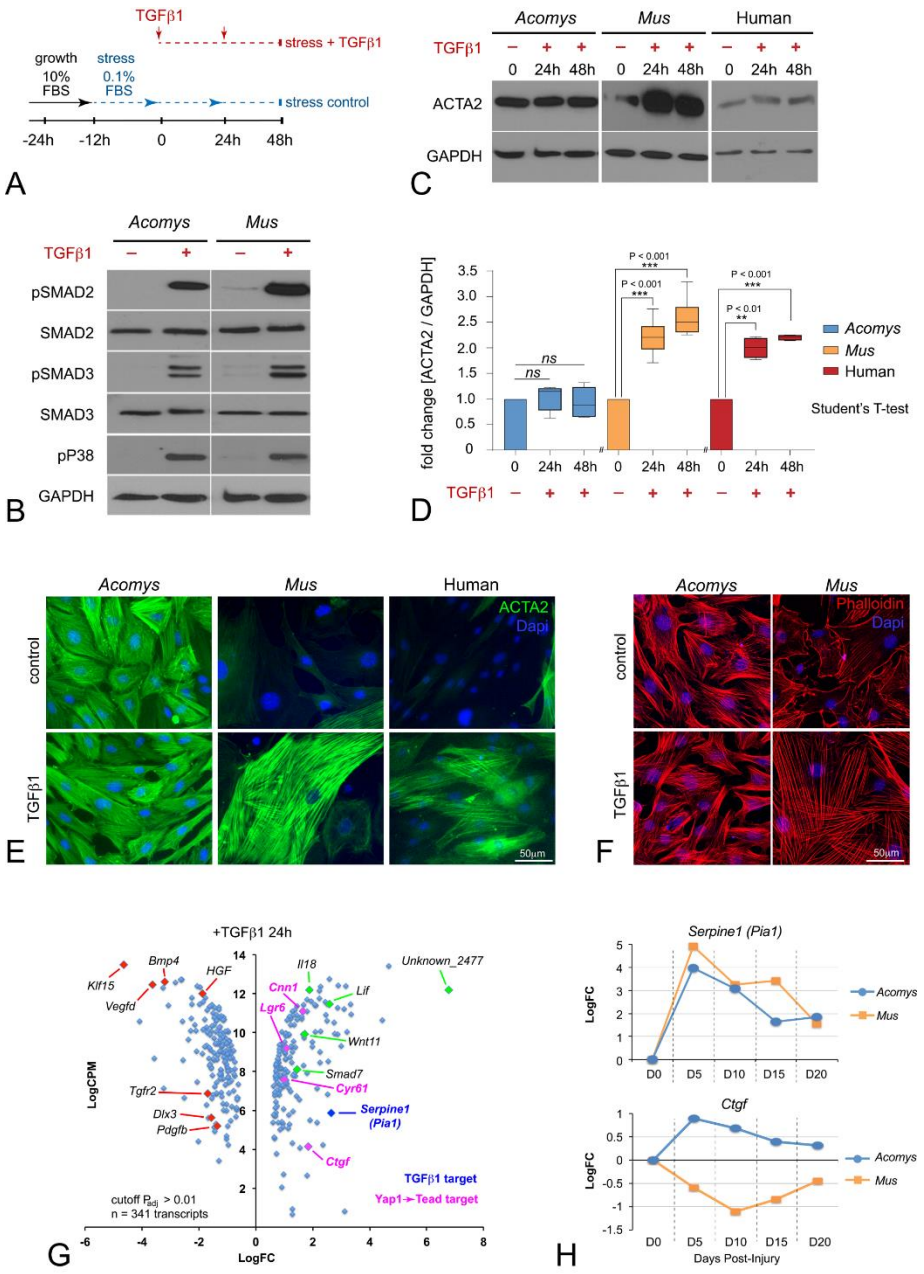

Figure 2.2 Isolated *Acomys* fibroblasts maintain homeostasis in response to fibrokine signals. (**A**) Diagram for myofibroblasts induction in response to fibrokines. (**B**) Western blot for *Acomys* and *Mus* SMAD2, SMAD3, and p38 phosphorylation in response to +/- 1hr TGFβ1. (**C**) Western blot of ACTA2 protein levels in response to +/- TGFβ1 at 0, 24 and 48hrs. (**D**)Quantification of species specific ACTA2 fold changes. Data are represented as mean centered box and whiskers. N ≥ 4 independent cultures. (**E**) Immunostaining staining for ACTA2 in 48hr +/- TGFβ1 treated Acomys, *Mus* and Human fibroblasts. (**F**) Immunostaining for F-actin stress fiber formation in 48hr +/- TGFβ1 treated *Acomys* and *Mus* fibroblasts. (**G**) RNA seq analysis of *Acomys* +/-24hr TGFβ1 reveals unique underlying homeostatic capability. All TGFβ1 treatments utilized 2ng/ml. (**H**) *In vivo* transcriptomic comparison of *Serpine1* (PAI-1) and *CTGF* expression in *Acomys* and *Mus* ear injury at indicated time points **p<0.01, ***p<0.001, ns=not significant.

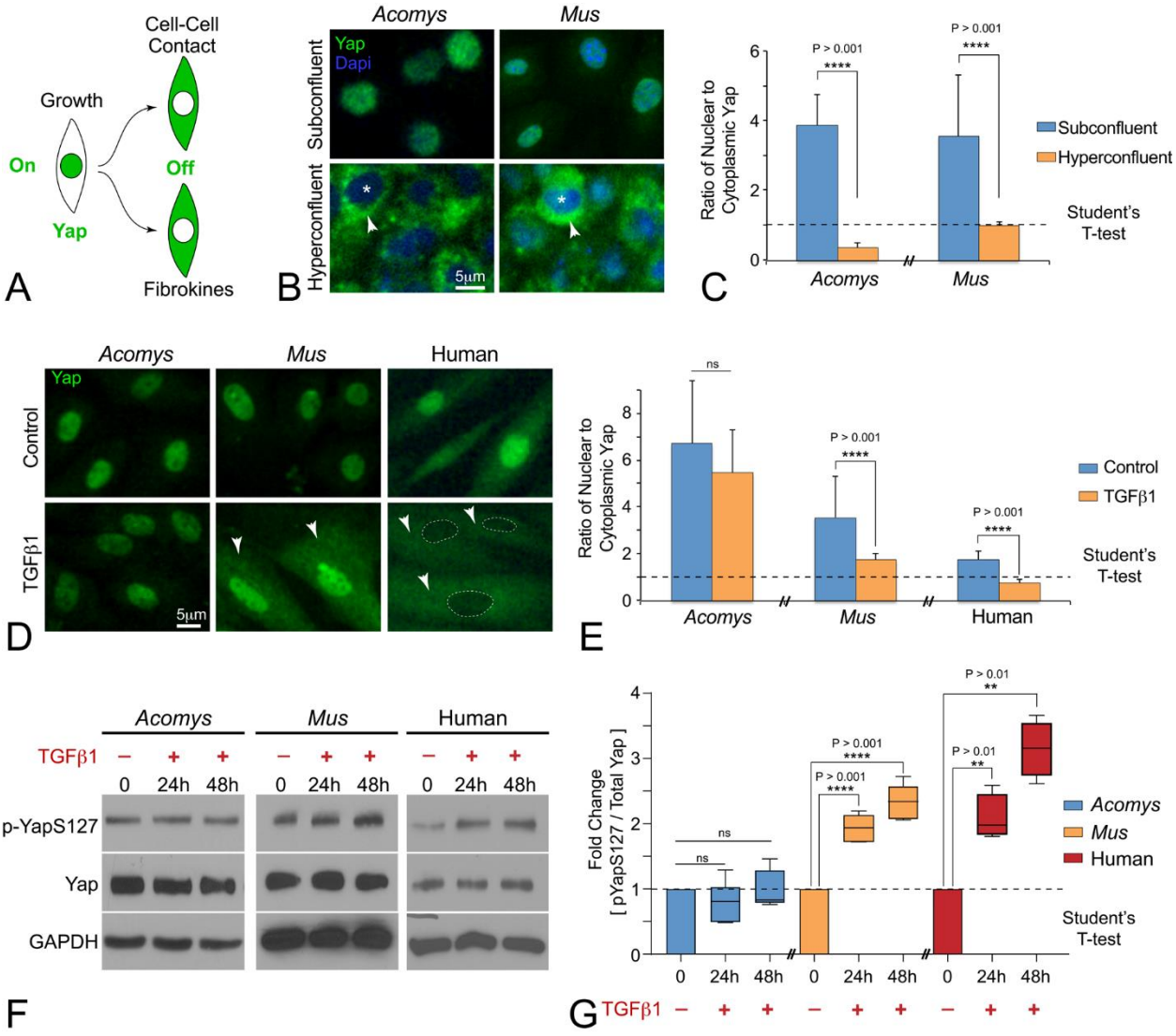

Figure 2.3 *Acomys* fibroblasts differentially regulate YAP activity when exposed to fibrokine signaling. (**A**) Diagram of YAP localization and activity in responses to differing stimuli. (**B**)Immunostaining for YAP localization in *Acomys* and *Mus* skin fibroblasts under subconfluent and hyperconfluent conditions. (**C**) Quantification of YAP localization ratio in *Acomys* and *Mus* subconfluent and hyperconfluent cultures. DAPI serves as a nuclear localization marker (**D**) Immunostaining for YAP localization in species specific fibroblasts +/- 48hr TGFβ1. (**E**) Quantification of YAP localization across species +/- 48hr TGFβ1. (**F**) Western blot for YAP phosphorylation across species in untreated, 24 and 48hr +/- TGFβ1 cultures. (**G**) Quantification of species specific YAP phosphorylation fold changes. Data represented as mean centered box and whiskers. N ≥ 4 independent cultures. All TGFβ1 treatments utilized 2ng/ml. **p<0.01, ***p<0.001, ****p<0.0001, ns = not significant.

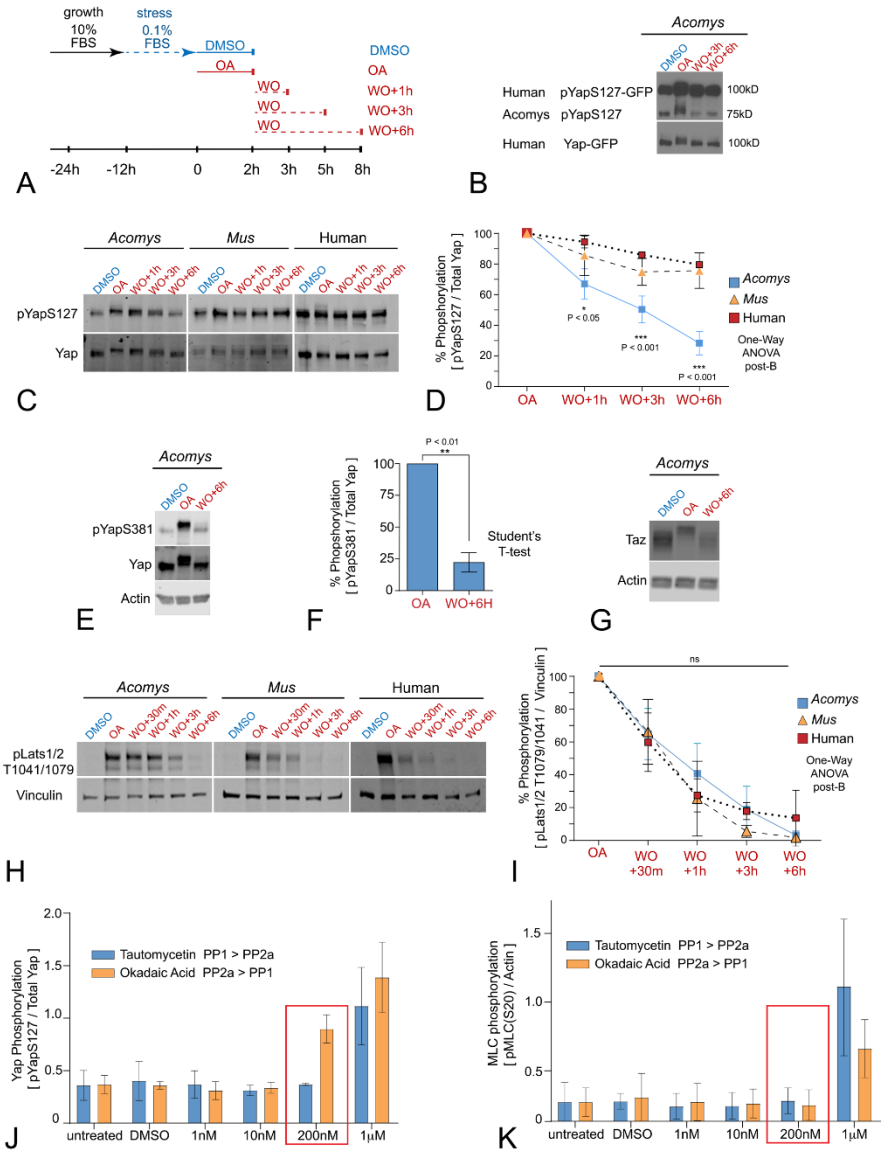

Figure 2.4 Increased PP2A dephosphorylation kinetics underlies *Acomys* species specific maintenance of nuclear YAP localization. (**A**) Diagram of okadaic acid (OA) pulse and withdrawal/ washout (WO) experiments. (**B**) Western blot for human YAP (hYAP-GFP) phosphorylation potential in *Acomys* transfected fibroblasts. (**C**)Western blot of *Acomys*, *Mus* and human YAP-S127 phosphorylation at indicated times during OA pulse and withdrawal. (**D**) Percent quantification of YAP-S127 phosphorylation. (**E**) Western blot of *Acomys* YAP-S381 phosphorylation during OA pulse and withdrawal. (**F**) Percent quantification of YAP-S381 phosphorylation. (**G**) Western blot for TAZ protein expression OA pulse and 6-hour wash-out.(**H**) Western blot of *Acomys*, *Mus* and human LATS1/2 phosphorylation at indicated times during OA pulse and withdrawal. (**I**) Percent quantification of LATS1/2 phosphorylation. (**J-K**) Quantification of YAP (**J**) and MLC (**K**) phosphorylation at varying concentrations of okadaic acid and tautomycetin. Red bars indicate inhibitor concentrations of interest. Data represented as mean ± S.D. N ≥ 4 independent cultures. OA was introduced at a concentration of 200nM unless indicated as otherwise. *p<.05, **p<0.01, ***p<0.001, ****p<0.0001, ns = not significant.

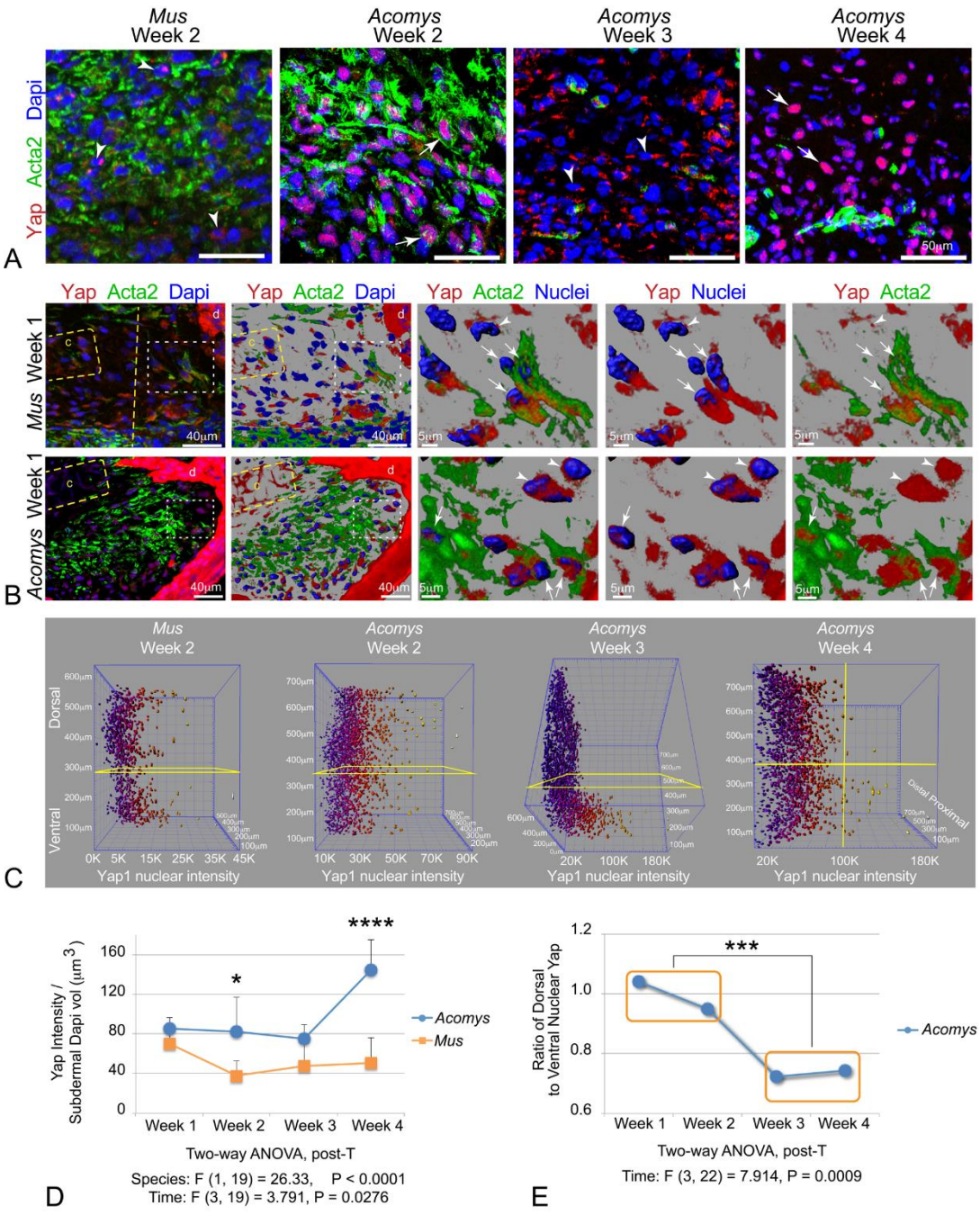

Figure 2.5 YAP localization and patterning distinguishes differences between fibrotic scarring in *Mus* and regenerative repair in *Acomys*. (**A**) Immunostaining for YAP and ACTA2 localization in *Acomys* and *Mus* at indicated time points. (**B**) High power rendering of YAP nuclear/cytoplasmic localization in ACTA2$^{+/-}$ populations in week 1 *Mus* (top) *Acomys* (bottom) ear injuries. (**C**) Single nuclei 3D plots reveal differences in levels and patterning between species. (**D**) Quantification illustrates *Acomys* exhibit increased YAP nuclear localization compared to *Mus* during indicated time points. (**E**) Quantification of *Acomys* YAP nuclear localization dorsal/ventral ratio reveals two distinct phases.

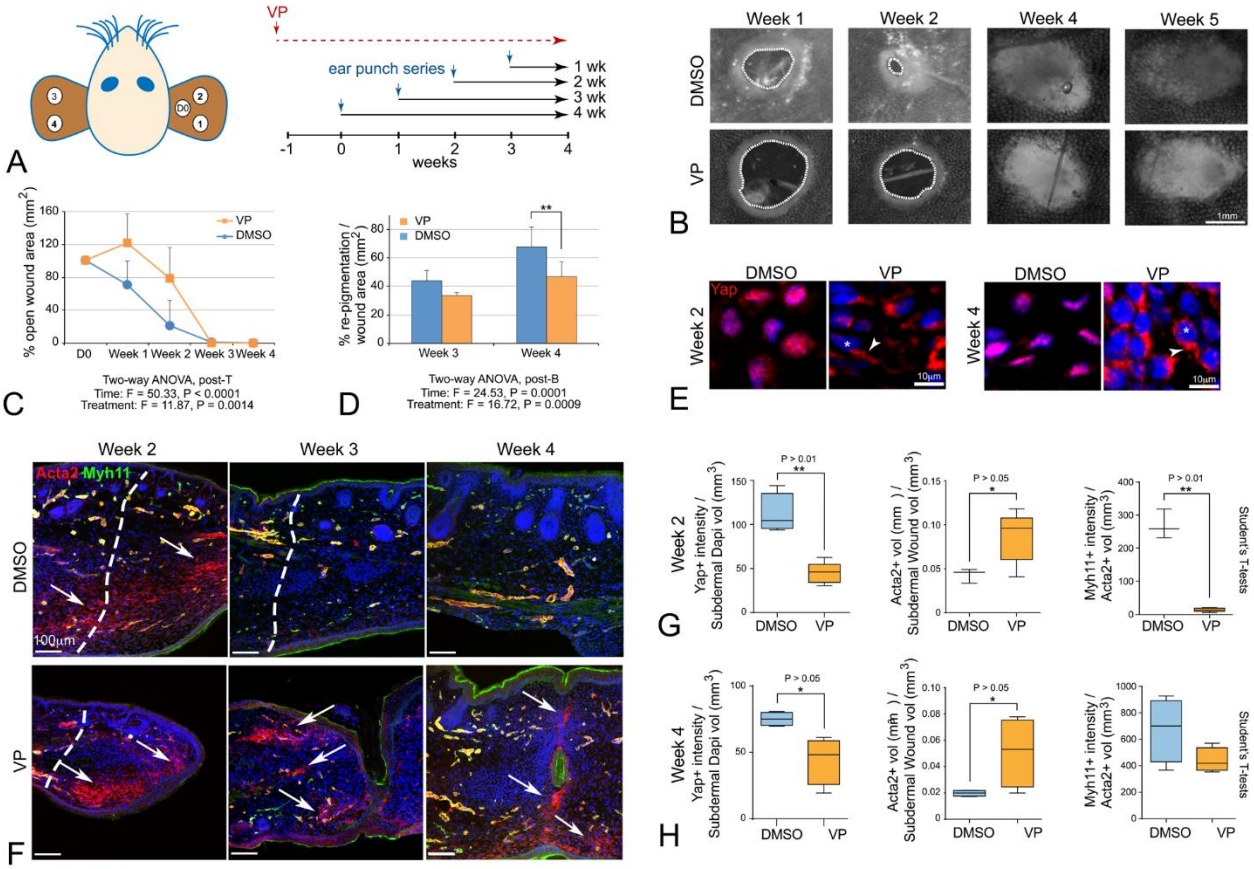

Figure 2.6 YAP signaling is necessary for *Acomy* epimorphic ear regeneration.
(**A**) Schematic of chronic VP (100mg/kg) injection model. (**B**) Representative images of *Acomys* VP and control ear hole closures. Dashed lines indicate border of open wound hole. (**C**) Percent quantification of open wound area in VP and control groups throughout injury time course. (**D**) Percent quantification of ear re-pigmentation in weeks 3 and 4 VP and control. (**E**) Immunostaining for YAP localization in weeks 2 and 4 VP and control. Areas of observation are within regenerating tissue. Stars indicate DAPI nuclear localization. Arrows correspond to YAP cytoplasmic distribution. (**F**) Immunostaining for ACTA2 and Myh11 in VP and control at indicated time points. Arrows indicate myofibroblast populations ($ACTA2^{+}/Myh11^{-}$). (**G**) Quantification of YAP nuclear localization, $ACTA2^{+}/Myh11^{+}$ and $ACTA2^{-}/Myh11^{+}$ levels in VP and control during week 2 (top) and week 4 (bottom). White dashed lines indicate plane of amputation. **p<0.01, ***p<0.001, ****p<0.0001, ns = not significant.

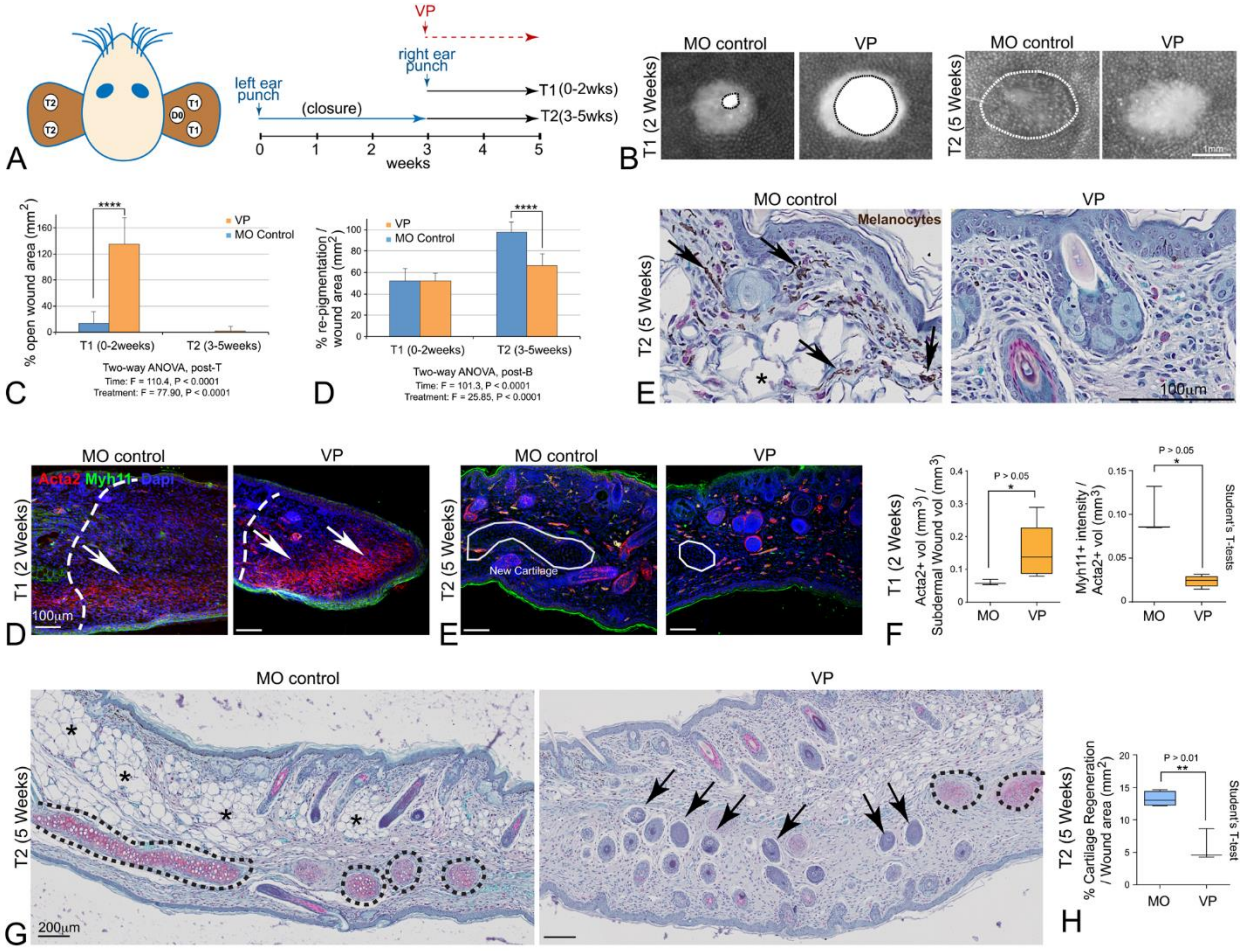

Figure 2.7 YAP regulates two distinct phases of Acomys epimorphic regeneration.
(A) Schematic of acute VP exposure (100mg/kg) injection model. (**B**) Representative images of VP and control (Mineral oil) ear injuries at indicated time points. (**C**) Percent quantification of open wound area in VP and control treatment groups at week3 (T1) and Week 5 (T2) time points. (**D**) Percent quantification of ear re-pigmentation in VP and control at T1 and T2 time points. (**E**) High Magnification of Saffron O stained VP and control wound areas at T2 time point. Arrows highlight melanocytes. Stars highlight adipocytes. (**F**) Immunostaining for ACTA2 and Myh11 in VP and MO treatment groups at T1 and T2 time points. Arrows highlight myofibroblast populations ($ACTA2^{+}/Mhy11^{-}$). White outlines indicated structures reminiscent of cartilage plate. (**G**) Quantification of $ACTA2^{+}$ levels and $ACTA2^{+}/Myh11^{+}$ levels in VP and control at T1 time point. (**H**) Saffron O histology of newly regenerated tissue in VP and control groups at T2 time point. Black dashed lines indicate new cartilage growth. (**I**) Quantification of new cartilage formation in VP and control at T2 time point. White dashed lines indicate plane of amputation. *p<.05, **p<0.01, ***p<0.001, ****p<0.0001, ns = not significant.

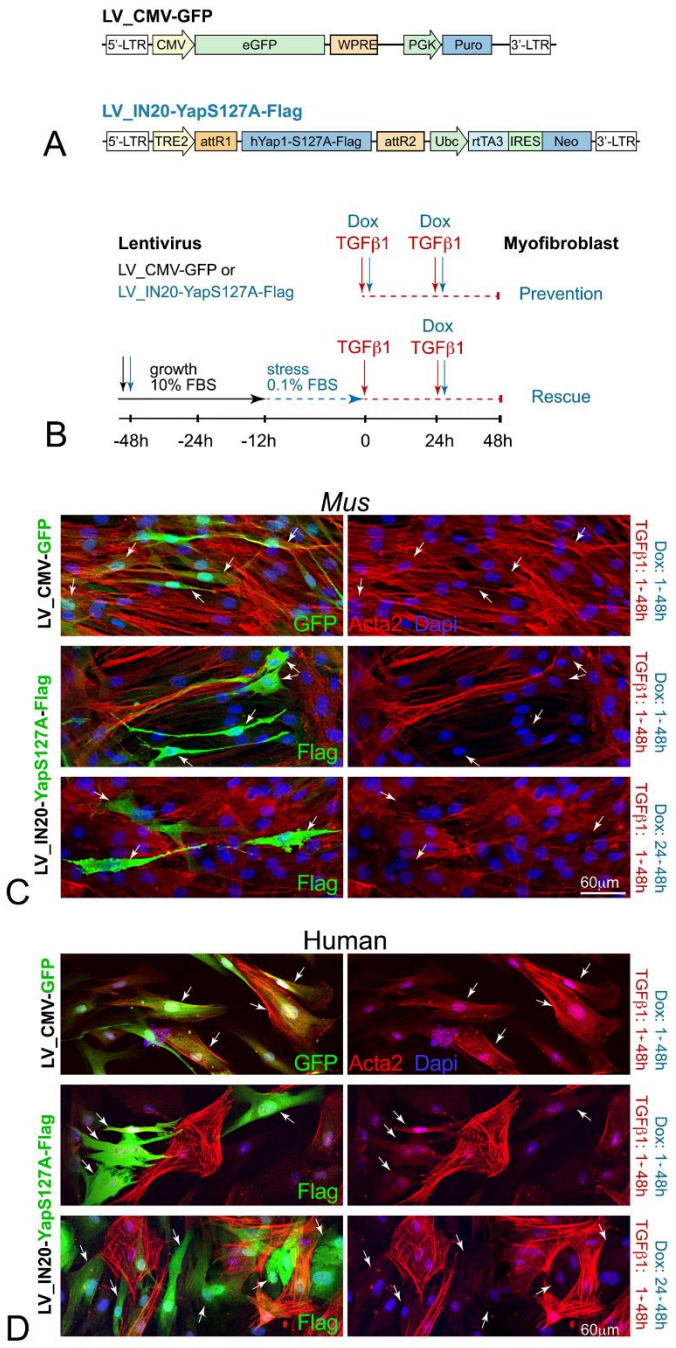

Figure 2.8 Reciprocating *Acomys* YAP activity attenuates non-regenerator myofibroblast activation (**A**) Lentiviral vector maps depicting CMV based constitutively active GFP control or doxycycline (Dox) inducible flag tagged human YAP^{S127A}. (**B**) Experimental diagram depicting introduction scheme of both TGFβ1 and Dox to assess MF inhibition (top) and regression (bottom). (**C**) Immunostaining for ACTA2, GFP control (top) and Flag tagged $hYAP^{S127A}$ (bottom) in *Mus* dermal fibroblasts after 48 hrs. indicated conditions (**D**) Immunostaining for ACTA2, GFP control (top) and Flag tagged $hYAP^{S127A}$ (bottom) in human dermal fibroblasts after 48hrs indicated conditions.

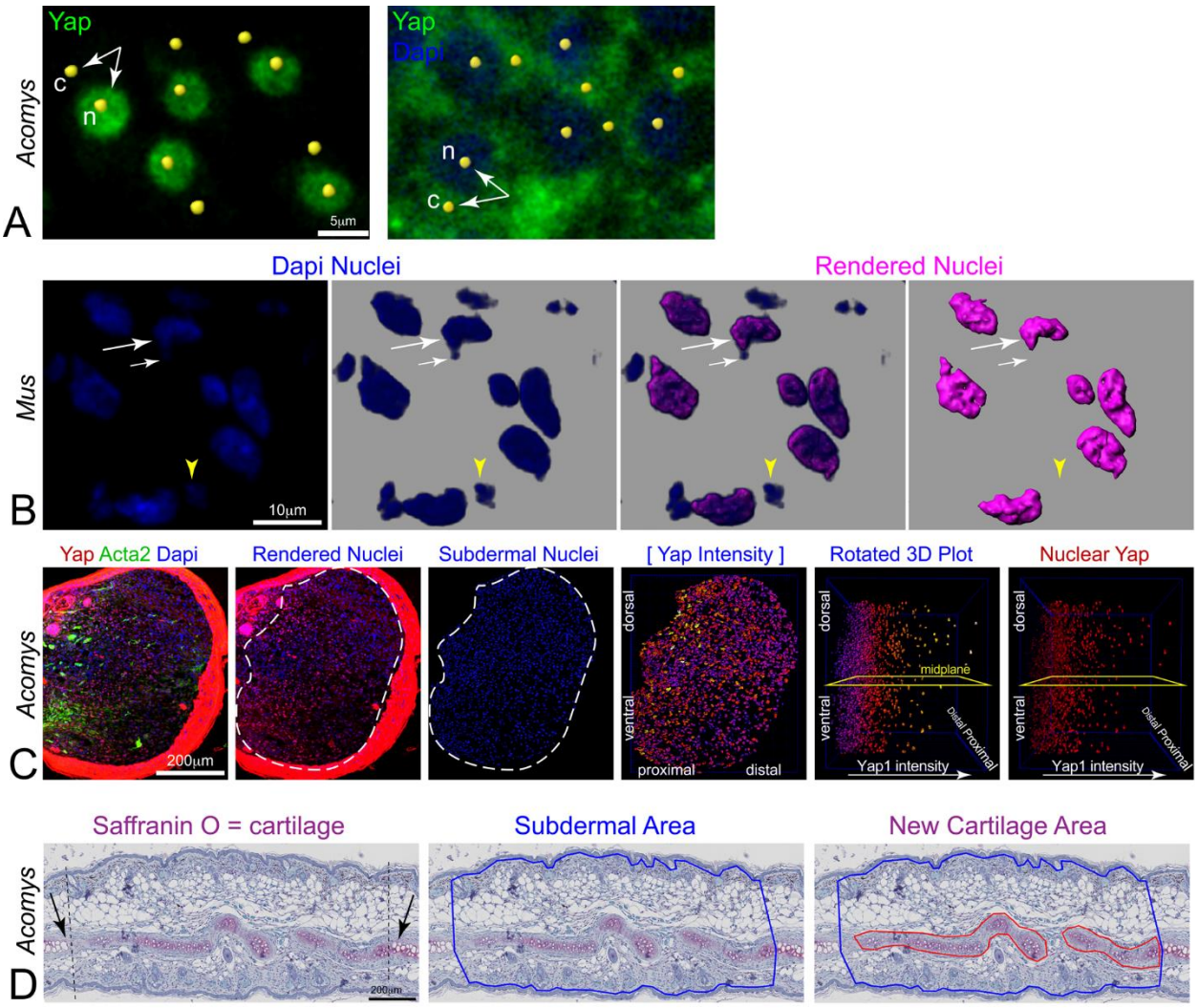

Figure 2.9 Supplemental 1: Visualization of image analysis and quantification. (**A**) YAP cytoplasmic/nuclear ratios is determined by 300nm diameter Amaris spot intensity sum function. DAPI serves as nuclear overlay intensity (50 cells per group). (**D**) Regenerated cartilage area is determined by quantifying the Saffron O stained new cartilage area adjacent to the amputation plane within subdermal injury.

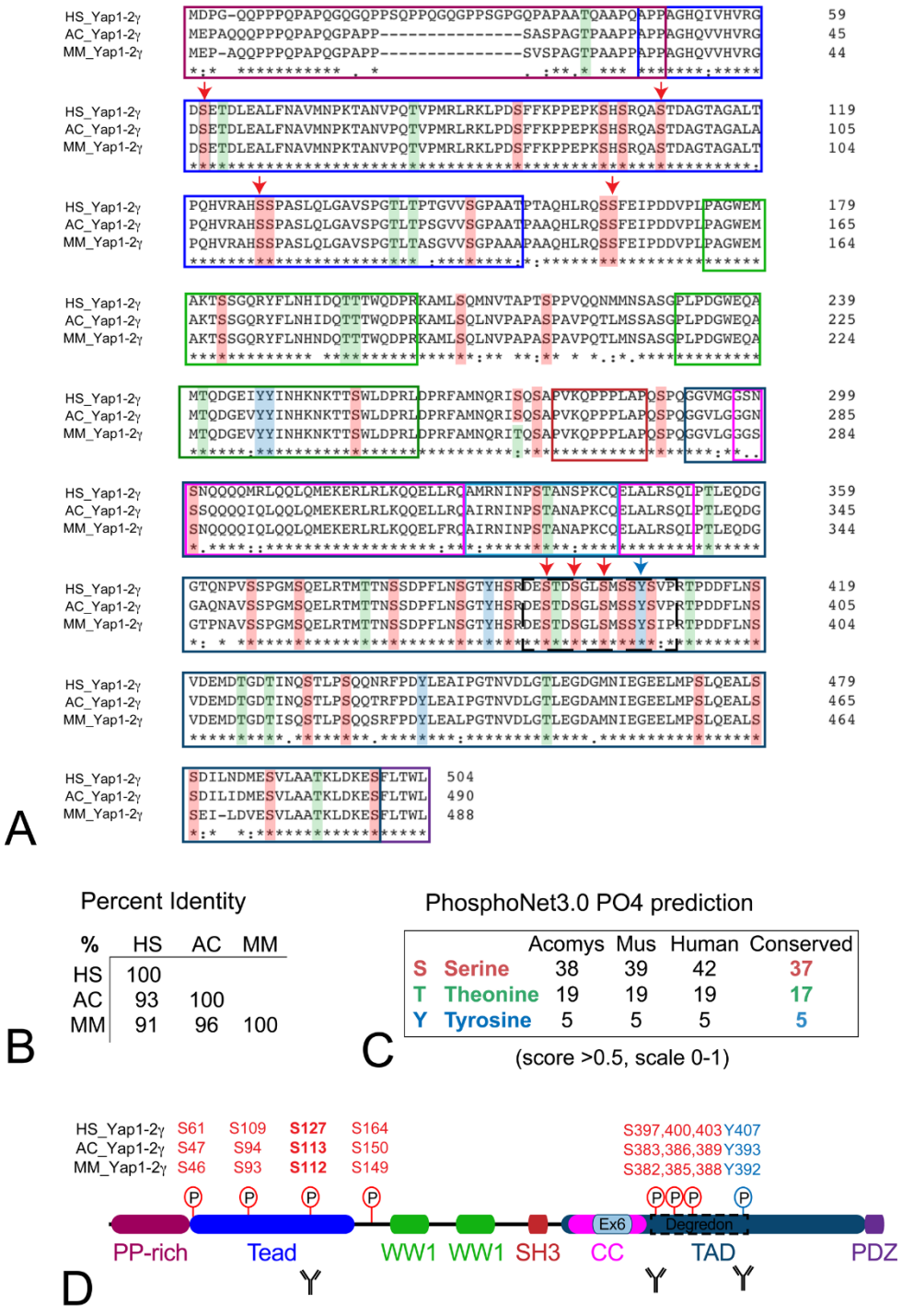

Figure 2.10 Supplemental 2: High conservation of YAP1-2 peptide sequence across *Acomys*, *Mus* and Human. (**A**) Peptide and domain sequence alignment of *Acomys Mus* and Human YAP1-2 isoform. (**B**) Comparison of percent amino acid sequence homology between *Acomys*, *Mus* and human YAP1-2. (**C**) Comparison of predicted amino acid within YAP capable of phosphorylation in *Acomys*, *Mus* and Human (**D**) Schematic of *Acomys* YAP protein domains with known residues targeted by phosphorylation.

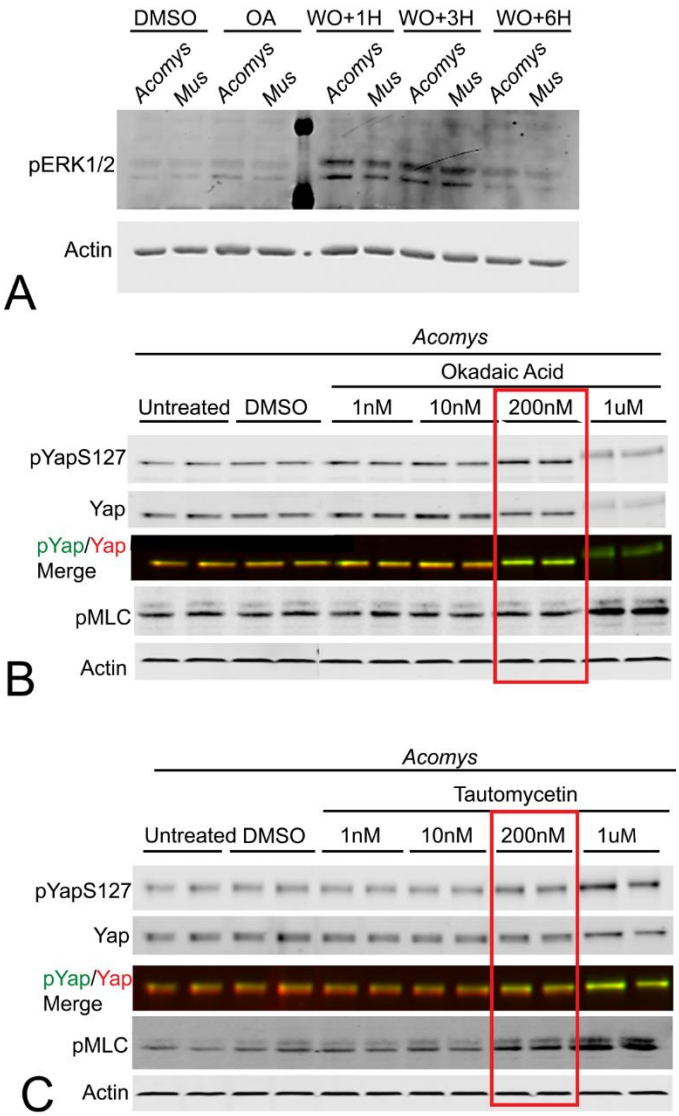

Figure 2.11 Supplemental 3: *Acomys* increased YAP/TAZ dephosphorylation kinetics is mediated by a Serine/Threonine class phosphatase. (**A**) Western blotting for ERK phosphorylation in *Acomys* and *Mus* fibroblasts during OA pulse and withdrawal. (**B**) Western blot for phosphorylation status of YAP-S127 and Myosin Light Chain-S20 in responses to various concentrations of OA(**C**) Western blot for phosphorylation status of YAP-S127 and Myosin Light Chain-S20 in responses to various concentrations of tautomycetin

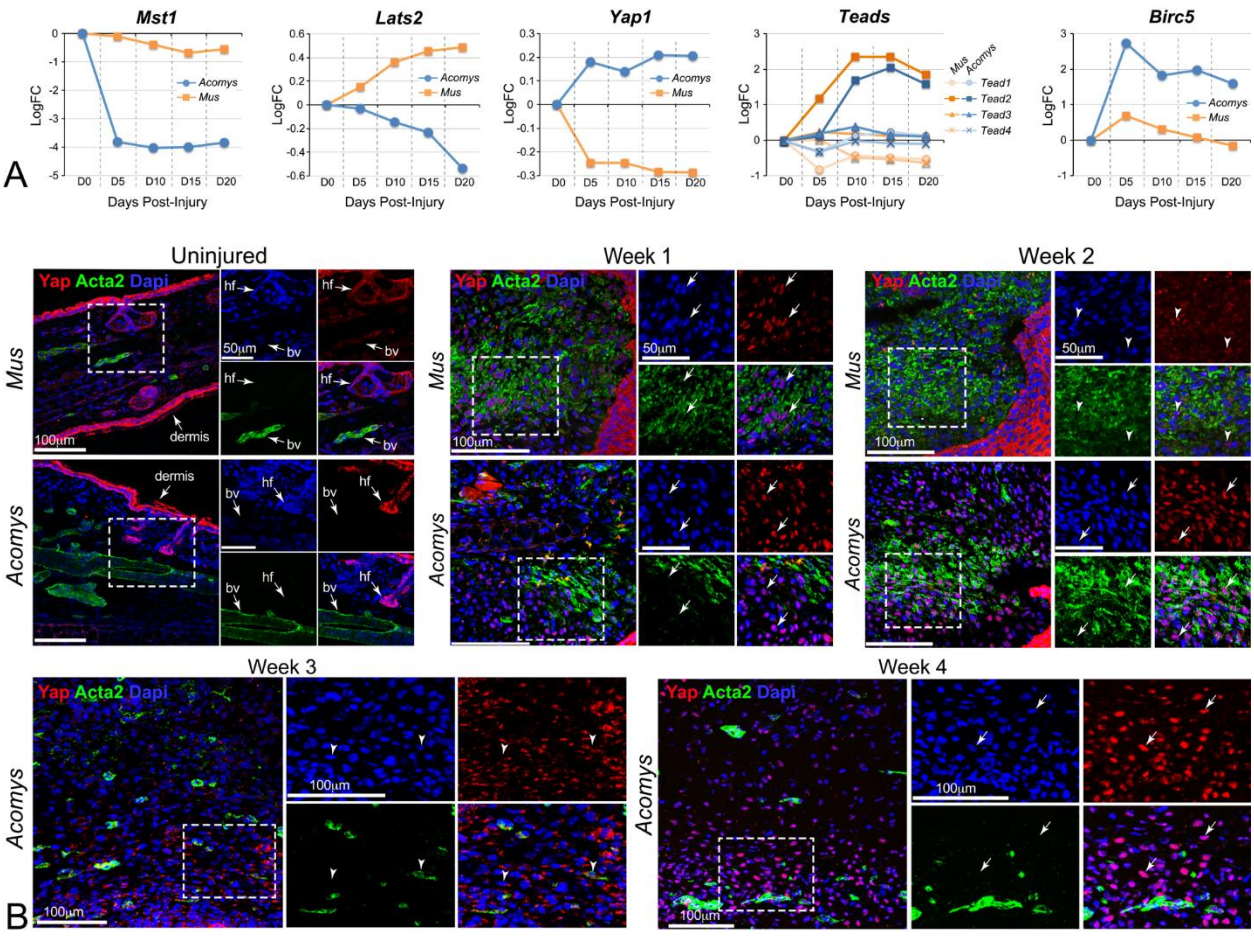

Figure 2.12 Supplemental 4: Comparative *in vivo* transcriptomic analysis during *Acomys* and *Mus* wound healing also reveals differential response in YAP signaling. (**A**) *In vivo* transcriptomic comparison of Hippo pathway components *Mst1*, *Lats2*, and *Yap1*, *TEAD1-4* and downstream YAP target genes *Ctgf* and *Birc5* in both *Acomys and Mus* ear injury at indicated time points(**B**) Immunostaining for YAP and ACTA2 localization in *Acomys* and *Mus* at indicated time points.

2.6 References

1. Porrello, E.R. *et al*. Transient regenerative potential of the neonatal mouse heart. *Science* **331**, 1078-1080 (2011).
2. Longaker, M.T. *et al*. Studies in fetal wound healing, VI. Second and early third trimester fetal wounds demonstrate rapid collagen deposition without scar formation. *J Pediatr Surg* **25**, 63-68; discussion 68-69 (1990).
3. Borgens, R.B. Mice regrow the tips of their foretoes. *Science* **217**, 747-750 (1982).
4. Gabbiani, G., Ryan, G.B. & Majne, G. Presence of modified fibroblasts in granulation tissue and their possible role in wound contraction. *Experientia* **27**, 549-550 (1971).
5. Gauglitz, G.G., Korting, H.C., Pavicic, T., Ruzicka, T. & Jeschke, M.G. Hypertrophic scarring and keloids: pathomechanisms and current and emerging treatment strategies. *Mol Med* **17**, 113-125 (2011).
6. Mallat, A. & Lotersztajn, S. Cellular mechanisms of tissue fibrosis. 5. Novel insights into liver fibrosis. *Am J Physiol Cell Physiol* **305**, C789-799 (2013).
7. Duffield, J.S. Cellular and molecular mechanisms in kidney fibrosis. *J Clin Invest* **124**, 2299-2306 (2014).
8. Seifert, A.W. *et al*. Skin shedding and tissue regeneration in African spiny mice (Acomys). *Nature* **489**, 561-565 (2012).
9. Dong, J. *et al*. Elucidation of a universal size-control mechanism in Drosophila and mammals. *Cell* **130**, 1120-1133 (2007).
10. Huang, J., Wu, S., Barrera, J., Matthews, K. & Pan, D. The Hippo signaling pathway coordinately regulates cell proliferation and apoptosis by inactivating Yorkie, the Drosophila Homolog of YAP. *Cell* **122**, 421-434 (2005).
11. Chan, E.H. *et al*. The Ste20-like kinase Mst2 activates the human large tumor suppressor kinase Lats1. *Oncogene* **24**, 2076-2086 (2005).
12. Hao, Y., Chun, A., Cheung, K., Rashidi, B. & Yang, X. Tumor suppressor LATS1 is a negative regulator of oncogene YAP. *J Biol Chem* **283**, 5496-5509 (2008).
13. Vassilev, A., Kaneko, K.J., Shu, H., Zhao, Y. & DePamphilis, M.L. TEAD/TEF transcription factors utilize the activation domain of YAP65, a Src/Yes-associated protein localized in the cytoplasm. *Genes Dev* **15**, 1229-1241 (2001).
14. Zhao, B. *et al*. TEAD mediates YAP-dependent gene induction and growth control. *Genes Dev* **22**, 1962-1971 (2008).
15. Zhao, B., Tumaneng, K. & Guan, K.L. The Hippo pathway in organ size control, tissue regeneration and stem cell self-renewal. *Nat Cell Biol* **13**, 877-883 (2011).
16. Liu-Chittenden, Y. *et al*. Genetic and pharmacological disruption of the TEAD-YAP complex suppresses the oncogenic activity of YAP. *Genes Dev* **26**, 1300-1305 (2012).
17. Sudol, M. *et al*. Characterization of the mammalian YAP (Yes-associated protein) gene and its role in defining a novel protein module, the WW domain. *J Biol Chem* **270**, 14733-14741 (1995).
18. Tomasek, J.J., Gabbiani, G., Hinz, B., Chaponnier, C. & Brown, R.A. Myofibroblasts and mechano-regulation of connective tissue remodelling. *Nat Rev Mol Cell Biol* **3**, 349-363 (2002).
19. Rockey, D.C., Weymouth, N. & Shi, Z. Smooth muscle alpha actin (Acta2) and myofibroblast function during hepatic wound healing. *PLoS One* **8**, e77166 (2013).

20. Darby, I., Skalli, O. & Gabbiani, G. Alpha-smooth muscle actin is transiently expressed by myofibroblasts during experimental wound healing. *Lab Invest* **63**, 21-29 (1990).
21. Gawriluk, T.R. *et al*. Comparative analysis of ear-hole closure identifies epimorphic regeneration as a discrete trait in mammals. *Nat Commun* **7**, 11164 (2016).
22. Eyden, B. The myofibroblast: a study of normal, reactive and neoplastic tissues, with an emphasis on ultrastructure. part 2 - tumours and tumour-like lesions. *J Submicrosc Cytol Pathol* **37**, 231-296 (2005).
23. Bhattacharyya, S. *et al*. FibronectinEDA promotes chronic cutaneous fibrosis through Toll-like receptor signaling. *Sci Transl Med* **6**, 232ra250 (2014).
24. Muro, A.F. *et al*. An essential role for fibronectin extra type III domain A in pulmonary fibrosis. *Am J Respir Crit Care Med* **177**, 638-645 (2008).
25. Serini, G. *et al*. The fibronectin domain ED-A is crucial for myofibroblastic phenotype induction by transforming growth factor-beta1. *J Cell Biol* **142**, 873-881 (1998).
26. Kohan, M., Muro, A.F., White, E.S. & Berkman, N. EDA-containing cellular fibronectin induces fibroblast differentiation through binding to alpha4beta7 integrin receptor and MAPK/Erk 1/2-dependent signaling. *Faseb j* **24**, 4503-4512 (2010).
27. Gronwald, R.G. *et al*. Cloning and expression of a cDNA coding for the human platelet-derived growth factor receptor: evidence for more than one receptor class. *Proc Natl Acad Sci U S A* **85**, 3435-3439 (1988).
28. Derynck, R. & Zhang, Y.E. Smad-dependent and Smad-independent pathways in TGF-beta family signalling. *Nature* **425**, 577-584 (2003).
29. Hinz, B., Celetta, G., Tomasek, J.J., Gabbiani, G. & Chaponnier, C. Alpha-smooth muscle actin expression upregulates fibroblast contractile activity. *Mol Biol Cell* **12**, 2730-2741 (2001).
30. Goffin, J.M. *et al*. Focal adhesion size controls tension-dependent recruitment of alpha-smooth muscle actin to stress fibers. *J Cell Biol* **172**, 259-268 (2006).
31. Mamrot, J. *et al*. De novo transcriptome assembly for the spiny mouse (Acomys cahirinus). *Sci Rep* **7**, 8996 (2017).
32. Shimomura, T. *et al*. The PDZ-binding motif of Yes-associated protein is required for its co-activation of TEAD-mediated CTGF transcription and oncogenic cell transforming activity. *Biochem Biophys Res Commun* (2013).
33. Zhang, H., Pasolli, H.A. & Fuchs, E. Yes-associated protein (YAP) transcriptional coactivator functions in balancing growth and differentiation in skin. *Proc Natl Acad Sci U S A* **108**, 2270-2275 (2011).
34. Lai, D., Ho, K.C., Hao, Y. & Yang, X. Taxol resistance in breast cancer cells is mediated by the hippo pathway component TAZ and its downstream transcriptional targets Cyr61 and CTGF. *Cancer Res* **71**, 2728-2738 (2011).
35. Mokalled, M.H. *et al*. Injury-induced ctgfa directs glial bridging and spinal cord regeneration in zebrafish. *Science* **354**, 630-634 (2016).
36. Zhao, B. *et al*. Inactivation of YAP oncoprotein by the Hippo pathway is involved in cell contact inhibition and tissue growth control. *Genes Dev* **21**, 2747-2761 (2007).
37. Zhao, B., Li, L., Tumaneng, K., Wang, C.Y. & Guan, K.L. A coordinated phosphorylation by Lats and CK1 regulates YAP stability through SCF(beta-TRCP). *Genes Dev* **24**, 72-85 (2010).
38. Gaffney, C.J. *et al*. Identification, basic characterization and evolutionary analysis of differentially spliced mRNA isoforms of human YAP1 gene. *Gene* **509**, 215-222 (2012).

39. Wang, P. *et al*. PP1A-Mediated Dephosphorylation Positively Regulates YAP2 Activity. *PLoS ONE* **6**, e24288 (2011).
40. Schlegelmilch, K. *et al*. Yap1 acts downstream of alpha-catenin to control epidermal proliferation. *Cell* **144**, 782-795 (2011).
41. Bialojan, C., Ruegg, J.C. & Takai, A. Effects of okadaic acid on isometric tension and myosin phosphorylation of chemically skinned guinea-pig taenia coli. *J Physiol* **398**, 81-95 (1988).
42. Zhang, L., da Costa, S.R., Yarber, F.A., Runnegar, M. & Hamm-Alvarez, S.F. Protein phosphatase inhibitors alter cellular microtubules and reduce carbachol-dependent protein secretion in lacrimal acini. *Curr Eye Res* **20**, 373-383 (2000).
43. Wang, G.L. & Semenza, G.L. Characterization of hypoxia-inducible factor 1 and regulation of DNA binding activity by hypoxia. *J Biol Chem* **268**, 21513-21518 (1993).
44. Sun, H., Charles, C.H., Lau, L.F. & Tonks, N.K. MKP-1 (3CH134), an immediate early gene product, is a dual specificity phosphatase that dephosphorylates MAP kinase in vivo. *Cell* **75**, 487-493 (1993).
45. Finch-Edmondson, M.L. *et al*. TAZ Protein Accumulation Is Negatively Regulated by YAP Abundance in Mammalian Cells. *J Biol Chem* **290**, 27928-27938 (2015).
46. Mitsuhashi, S. *et al*. Tautomycetin is a novel and specific inhibitor of serine/threonine protein phosphatase type 1, PP1. *Biochem Biophys Res Commun* **287**, 328-331 (2001).
47. Fernandez, J.J., Candenas, M.L., Souto, M.L., Trujillo, M.M. & Norte, M. Okadaic acid, useful tool for studying cellular processes. *Curr Med Chem* **9**, 229-262 (2002).
48. Liang, M. *et al*. Yap/Taz Deletion in Gli+ Cell-Derived Myofibroblasts Attenuates Fibrosis. *J Am Soc Nephrol* **28**, 3278-3290 (2017).
49. Feng, J. *et al*. Verteporfin, a suppressor of YAP-TEAD complex, presents promising antitumor properties on ovarian cancer. *Onco Targets Ther* **9**, 5371-5381 (2016).
50. Song, S. *et al*. Hippo coactivator YAP1 upregulates SOX9 and endows esophageal cancer cells with stem-like properties. *Cancer Res* **74**, 4170-4182 (2014).
51. Xie, C. *et al*. Yap1 protein regulates vascular smooth muscle cell phenotypic switch by interaction with myocardin. *J Biol Chem* **287**, 14598-14605 (2012).
52. Cao, X., Pfaff, S.L. & Gage, F.H. YAP regulates neural progenitor cell number via the TEA domain transcription factor. *Genes Dev* **22**, 3320-3334 (2008).
53. Hu, J.K. *et al*. An FAK-YAP-mTOR Signaling Axis Regulates Stem Cell-Based Tissue Renewal in Mice. *Cell Stem Cell* **21**, 91-106.e106 (2017).
54. Hayashi, S., Tamura, K. & Yokoyama, H. Yap1, transcription regulator in the Hippo signaling pathway, is required for Xenopus limb bud regeneration. *Dev Biol* **388**, 57-67 (2014).
55. Mateus, R. *et al*. Control of tissue growth by Yap relies on cell density and F-actin in zebrafish fin regeneration. *Development* **142**, 2752-2763 (2015).
56. Xin, M. *et al*. Hippo pathway effector Yap promotes cardiac regeneration. *Proc Natl Acad Sci U S A* **110**, 13839-13844 (2013).
57. Liu, Z. *et al*. MAPK-Mediated YAP Activation Controls Mechanical-Tension-Induced Pulmonary Alveolar Regeneration. *Cell Rep* **16**, 1810-1819 (2016).
58. Gregorieff, A., Liu, Y., Inanlou, M.R., Khomchuk, Y. & Wrana, J.L. Yap-dependent reprogramming of Lgr5(+) stem cells drives intestinal regeneration and cancer. *Nature* **526**, 715-718 (2015).

59. Heallen, T. *et al*. Hippo signaling impedes adult heart regeneration. *Development* **140**, 4683-4690 (2013).
60. Szeto, S.G. *et al*. YAP/TAZ Are Mechanoregulators of TGF-beta-Smad Signaling and Renal Fibrogenesis. *J Am Soc Nephrol* **27**, 3117-3128 (2016).
61. Liu, F. *et al*. Mechanosignaling through YAP and TAZ drives fibroblast activation and fibrosis. *Am J Physiol Lung Cell Mol Physiol* **308**, L344-357 (2015).
62. McNeill, H. & Reginensi, A. Lats1/2 Regulate Yap/Taz to Control Nephron Progenitor Epithelialization and Inhibit Myofibroblast Formation. *J Am Soc Nephrol* **28**, 852-861 (2017).
63. Liang, M. *et al*. Yap/Taz Deletion in Gli+ Cell-Derived Myofibroblasts Attenuates Fibrosis. *J Am Soc Nephrol* (2017).

Chapter 3. A heterogenous progenitor cell population, which includes ACTA2^{+} myofibroblasts, contributes to the *Acomys* blastema.

3.1 Abstract

Acomys cahirinus (African spiny mouse) employs epimorphic regeneration to restore skin tissue homeostasis after injury. Blastema based repair (epimorphosis) is commonly observed in both amphibian and fish limb amputation models, but far less is known regarding its adult mammalian counterpart. In assaying for progenitor markers that correlate to restored tissue types, we identify a heterogenous population of both resident and *de novo* progenitor cells that contribute to *A.cahirinus* blastema formation. Specifically, a SOX9^{+} population resides within a specific cartilage niche under normal tissue homeostatic conditions. This resident SOX9^{+} population migrates from the cartilage bud to contribute to the injury induced blastema. In contrast, expression of the myoblast specification marker MYF5 occurs *de-novo* after injury and is restricted to the blastema. These progenitor populations also contain subsets of cells that transiently co-label with the myofibroblast marker ACTA2 *or* smooth muscle α-actin. We further demonstrate YAP signaling is a crucial component for progenitor cell maintenance as YAP inhibition is sufficient to attenuate SOX9^{+} cells in the blastema, thereby contributing to failed cartilage restoration. Our results indicate *A.cahirinus* regenerative repair utilizes a heterogenous progenitor cell population that can include myofibroblast-like cell phenotypes for skin regeneration. The possibility of a myofibroblast with progenitor potential has important implications for redirecting mammalian scar tissue formation to a more regenerative repair response.

3.2 Introduction

Adult mammals exhibit limited regenerative repair capacity. Instead, the defining repair mechanisms for most mammals are scar tissue formation and inflammation. However, muriods from genus *Acomys* appear to be an evolutionary exception. Adult *A.cahirinus* (*Acomys*) restores skin tissue with all internal structures such as cartilage, muscle and peripheral neurons apparent within weeks of initial injury [1,2,Ch.2]. Therefore, these organisms have maintained regenerative repair capability into adulthood[3-5]. This mechanism is epimorphic in nature with formation of a blastema being required for successful tissue reconstitution[6]. The utilization of the blastema in *A.cahirinus* is peculiar as this repair process was previously believed to be restricted to urodeles and teleost appendage regeneration[7,8].

The blastema is an outgrowth of mesenchymal cells encased within a thin epithelial layer. This population contains all the necessary instructions and cell fates needed to faithfully reconstruct fully functioning tissue systems. The mesenchymal population of the blastema was initially believed to contain an undifferentiated mass of pluripotent cells[9,10]. However, this appears to be incorrect as further studies have demonstrated cells in the blastema maintain memory of their original tissue origin (e.g., new cartilage from cartilage and muscle from muscle)[11]. Thus, tissue reconstitution can employ a variety of cellular mechanisms that include both lineage restricted resident stem cells and dedifferentiated cells[12-17]. However, recent studies have suggested some cell types may exhibit more plasticity than previously believed.

In murine skin wounds, *Pikus et al* described populations of adipocytes derived from non-adipocyte origins. Cell fate tracing experiments determined these cells originated from the injury induced myofibroblast population within the wound bed. [18]. This conclusion has two important ramifications. The first is the myofibroblast can participate in regenerative repair. The second is

that myofibroblasts, previously believed to be terminally differentiated, can undergo cell fate decision and cross lineage boundaries. Myofibroblasts, characterized by their contractile behavior, excessive collagen deposition, and secretion of profibrotic cytokines, are identified as the primary contributor to pathogenic scarring in adult mammals[19-23]. Our previous work has demonstrated *A.cahirinus* also exhibit a phenotypic-like myofibroblast cell type during initial blastema formation. However, these cells do not engage in scar tissue formation. As opposed to scarring, they appear to have adopted a non-canonical role that promotes regenerative repair[Ch.2]. It is intriguing to speculate that *A.cahirinus* myofibroblasts may instead have evolved other roles, such as a progenitor cell reservoir that can contribute to tissue restoration.

Considering the similarities of cellular behaviors across a broad number of regenerative species, contributions of different progenitor and lineage restricted dedifferentiated cells most likely contribute to *A.cahirinus* regeneration. Therefore, our goal in this study was to identify progenitor cell populations that contribute to the formation of the *A.cahirinus* blastema. We also wished to understand the transient nature of the *A.cahirinus* myofibroblasts and their relationship to identified progenitor cell types. As *A.cahirinus* is a terrestrial adult mammal, understanding the cellular behaviors necessary for tissue regeneration is key to unlocking potential therapeutics in human fibrotic pathologies.

3.3 Materials and Methods

3.3.1 Animal Maintenance and Manipulations

The Seattle Children's Research Institute's Institutional Animal Care and Use Committee (IACUC) approved all animal procedures. Adult male and female *Mus musculus* (The Jackson Laboratory, Crl:CD1(ICR) and *Acomys cahirinus* (Exotic Pet supply Company) were obtained, housed, and bred within the Seattle Children's Research Institute's onsite vivarium. CD1 mice

were housed in a pathogen-free room maintained on 12:12 (Light:Dark) lighting schedule, *Acomys* were housed in a separate room maintained on 14:10 (Light:Dark) schedule, and all animals received food and water *ad libitum*. *Acomys* and *Mus* adult males and females were anaesthetized with 4% (v/v) vaporized isoflurane (Henry Schein Animal Health, Dublin, OH), and a 2mm thumb punch (Kent Scientific) was used to generate 2-3 punches across the medial ear pinna in the right and left ears, administered sequentially or concurrently as indicated: note, we did not detect overt sex differences at the current study level. For initial in vivo Yap inhibition experiments, adult Acomys received intraperitoneal injections of Verteporfin (VP, United States Pharmacopia, 100mg/kg, 100mg/ml DMSO stock solution diluted 1:10 PBS prior to injection) every 3-4 days as described by controls received equivalent volume of 10% DMSO in PBS. All animals received post procedure monitoring, including body weight measurements, all of which were stable over the experimental time course. Upon study completion, animals were terminally euthanized under anesthesia by cardiac perfusion with cold PBS, ears were photographed (Olympus SZX16 Stereomicroscope), and tissue collected.

3.3.2 Cell Lines

Species-specific primary fibroblast cultures were established from adult male *Acomys cahirinus* fresh ear tissue (2mm ear punches) using established procedures. All cell lines were grown on collagen coated tissue culture plates (5ug/cm^2 BD Biosciences), maintained at the same culture conditions (DMEM 4.5g/L D-glucose, L-glutamine, 110mg/L sodium pyruvate supplemented with 10% FBS and 100 U/mL Pen-Strep, 37^{o}C, 5.0% CO2) unless otherwise noted, and discarded after 15 passages to prevent gross genomic changes over long term *in vitro* culturing. For cell signaling experiments, ~90% confluent *Acomys* cells were serum starved for 12 hours (DMEM, .5% FBS and 100 U/ml Penicillin/Streptomycin; Serum Starvation Media/S.S.M) prior to addition of

recombinant hThrombin (1U/ml) or hTGFβ1 (2ng/ml) unless stated otherwise, (Cell Signaling Technologies).

3.3.3 Tissue Preparation and Processing

For paraffin embedding, excised tissues were placed in 4% PFA (w/v) and stored overnight at 4°C with agitation, washed three times in PBS, stored in 70% (v/v) ethanol, processed using a Tissue-Tek VIP automatic processor (Sakura), and cut at 8-m per section. Histological staining including Masson's Trichrome, Alcian Blue, Saffron O and Verhoeff-Van Geisson's stain were done in collaboration with Benaroya Research Institute or the University of Washington South Lake Union Imaging and Histology Core. For cryosectioning, tissue was embedded and frozen in O.C.T medium (TissueTech) using a dry-ice slurry/2-methybutanol mixture, and cut at 8-10µm per cryosection.

3.3.4 Immunofluorescence

Tissue cryosections were thawed, washed with PBS, post fixed with 4% (w/v) PFA for 10 minutes. Post fixation, slides were washed three times for five minutes with PBS followed by permeabilization using 0.2% Triton-X100 in PBS (PBT) for 10 minutes. Slides were blocked (5% BSA, 2% normal goat serum in PBT) at room temperature for 1 hour, tissue sections were incubated in primary antibody overnight at 4°C in blocking solution (3% BSA, 0.2% Triton-X100 in PBS). Primary antibodies used included anti-Acta2 (Smooth Muscle α-Actin) (1/2000, mouse; Sigma # A2547), anti-Myf5 (1/1000, rabbit; Santa Cruz # SC-302), anti-PPARγ (1/500, rabbit Cell Signaling Technology #2435), anti-Sox9 (1/1000,rabbit; Millipore # AB5535). Slides were washed with PBS, and then incubated with ALEXA-Fluor 488- or 594-conjugated antibodies (Life Technologies) for 2 hours at room temperature in blocking solution. Cell nuclei were counterstained with Dapi (Molecular Probes) and mounted in 4% (w/v) propyl gallate anti-fade

solution, or Fluoromount G (Fisher). For in immunolabeling adherent cell cultures, fibroblasts were plated into glass-bottom tissue culture multi-well plates (TissueTek) previously treated with 1mM magnesium acetate, washed 3X in PBS, and then coated in poly-d-lysine (10mg/ml) and collagen as described. Cell culture media was removed, cells were washed with PBS, fixed with 4% PFA for 10min, washed again with PBS, and blocked for 1h prior to addition of primary antibody solutions. Cells were incubated overnight at 4°C, washed with PBS, ALEXA-conjugated secondary antibodies applied for 1h, counterstained with Dapi, and mounted as described.

3.3.5 Immunoblotting

Cells were washed with ice-cold PBS (pH 7.4) and lysed at indicated time points using radioimmunoprecipitation assay buffer (50mM Tris, pH 7.4, 150mM NaCl, 1% TritonX-100, .5% Sodium deoxycholate, .1% SDS, 2mM EDTA, 2mM EGTA and 50mM NaF) supplemented with protease inhibitor cocktail (Sigma) and 10mM Na-Orthovanadate (Sigma). Normalization of protein concentrations was done using the Pierce™ BCA Protein Assay Kit (Thermo Scientific) and prepared in SDS sample buffer. Equal amounts of protein were resolved on SDS-Page and transferred to either a nitrocellulose (GE Healthcare) or PVDF (Thermo) depending on detection method. Membranes were incubated for 1 hour in LI-COR Biosciences block buffer. After washing, blots were incubated overnight at 4°C with antibodies including anti-β-tubulin (1/5000, mouse; Sigma Aldrich # BT7R), anti-GAPDH (1/5000, rabbit; Cell Signaling #5174), anti-Sox9 (1/1000,rabbit; Millipore # AB5535). After washing with TBST 0.1%, antigens were detected using either HRP-conjugated (Jackson Research Labs) or IRDye-labeled (LI-COR Biosciences) secondary antibodies. HRP reaction was performed using ECL Prime (GE Healthcare) and exposed to x-ray film. Band intensity was quantified using Image J (National Institute of Health). IRDye secondaries were detected with infrared imaging system Odyssey (LI-COR Biosciences)

and band intensity quantified using Image Studio Version 5.2 (LI-COR Bioscience). Immunoblots shown are presentative of experiments that were repeated a minimum of four independent times. Representative blots shown are those that demonstrate the least amount of nonspecific background and maintain lowest signal to noise ratio.

3.4 Results

3.4.1 Multiple resident skin cell progenitors contribute to wound repair

A.cahirinus has previously been shown to undergo epimorphic regenerative repair of the ear pinnae in contrast to the typical mammalian scar forming response[1]. The characteristic blastema contains all the necessary cells for tissue restoration. The skin is known to harbor several resident stem cell populations that occupy a variety of locations throughout the organ[24-28]. With *A.cahirinus* capable of regenerating skeletal muscle, smooth muscle, fat, and cartilage, we first identified several progenitor markers that direct these cell fate decisions in order to begin characterizing potential cellular mechanisms (**Figure 3.1**).

Cell specification:	**Transcription factors:**	**Location in skin:**
Adipogenesis	**PPARγ**, ZNF432	Fat cells, sebaceous glands
Myogenesis	PAX7, PAX3, **Myf5**	Throughout skeletal muscle
Chondrogenesis	**SOX9**, RUNX2	Dermal papilla, cartilage

Table 3.1 List of known transcription factors that mediate cell fate specification throughout the skin tissue.

We identified PPARγ, MYF5 and SOX9 to be good candidates for identifying resident stem cell populations as these markers have been well characterized to participate in both skin tissue development and repair[29-33]. Furthermore, antibody directed staining for these markers demonstrated broad cross species reactivity (e.g., *Acomys* and CD1 mice) when assaying for known positive control locations throughout several organ systems.

3.4.2 Both *Acomys* and *Mus* maintain subsets of resident progenitor populations under normal homeostatic conditions.

We immunostained uninjured *Acomys* and CD1 murine ear pinnae tissue to identify the existence of resident progenitor cell populations within the mesenchymal space. We previously identified dermal stromal cell populations as the most significant contributors to blastema [34,35,Ch.2]. Comparing both *A.cahirinus* and *Mus* CD1 skin tissue, we find both species contain a $SOX9^+$ (SRY related HMG-box) population within the cartilage plate. This observation is in agreement with previous reports of SOX9 expression in chondrocytes[36]. Confidence in successful staining is confirmed with SOX9 expression also apparent within the hair follicles and basal layer, well characterized $SOX9^+$ epidermal stem cell populations (**Figure 3.2A**). *A.cahirinus* and *Mus* both do not contain a $MYF5^+$ cell population within the tissue. (**Data not shown**). In contrast, the adipogenesis marker PPARγ (Peroxisome proliferator-activated receptor gamma) appears to be species tissue specific with *A.cahirinus* but not CD1 exhibiting a $PPAR\gamma^+$ population. However, $PPAR\gamma^+$ cells are not found within the dermal compartment. Instead, these cells are restricted to sebaceous glands within the epidermis compartment (**Figure 3.2B**). These findings show *A.cahirinus* skin contains at least two distinct resident progenitor populations ($SOX9^+$ and $PPAR\gamma^+$) that can potentially contribute to the injury induced blastema. The absence of the myogenic factor MYF5 indicates both species do not contain a resident satellite muscle progenitor under basal tissue conditions.

3.4.3 Heterogenous progenitor populations contribute to *Acomys* blastema formation.

With the identification of resident $SOX9^+$ and $PPAR\gamma^+$ progenitor populations within normal skin tissue structures, we next sought to characterize their relative contributions to the injury-induced *A.cahirinus* ear blastema. We previously identified that the blastema structure is

present during the first two weeks after 2mm ear punch injury[Ch.2]. Ear tissue closure is normally achieved by week 3, from which the tissue will then undergo repatterning and restoration of architecture during weeks 4-5 (**Fig 2.1**).

Comparing both *A.cahirinus* and murine CD1 at the two-week wound period, we observe clear differences in the presence of a $SOX9^+$ population. CD1 wound tissue is devoid of $SOX9^+$ cells with the limited tissue extension instead populated by $ACTA2^+$ myofibroblasts. This is in agreement with similarly timed murine CD1 ear injuries, which are composed entirely of scar tissue (**Ch.2, Fig 2.1**). In contrast, *A.cahirinus* displays a heterogenous mesenchymal $SOX9^+$ population contributing to the blastema at week 2 post injury. The $SOX9^+$ population includes both dermal fibroblasts ($SOX9^+/ACTA2^-$) and myofibroblasts ($SOX9^+/ACTA2^+$). Both mesenchymal populations appear to be migrating directly from the amputation plane of the remaining cartilage plate (**indicated by arrows**). Week 3 *A.cahirinus* ears display a noticeable shift between mesenchymal populations as the $SOX9^+/ACTA2^+$ myofibroblast cells are notably absent in the newly closed tissue. Instead, the remaining $SOX9^+/ACTA2^-$ dermal fibroblasts are now localized within the regenerating cartilage plane (**Fig 3.3A**). Observation of PPARγ within the *A.cahirinus* injury exhibited no contribution to the extending blastema. Instead, PPARγ reappearance was only observed during later stage tissue reconstitution when sebaceous glands have been restored (**Data not shown**). As such, we did not further pursue these cell types.

In contrast to the absence of a resident $MYF5^+$ cell population in both *A.cahirinus* and murine CD1 skin during normal homeostatic conditions, we observe a *de novo* $MYF5^+$ cell appearance within a specific temporal window of *A.cahirinus* repair. The $MYF5^+$ population is also heterogenous with both $ACTA2^{+/-}$ cells restricted to the newly expanding *Acomys* week 2 blastema. As opposed to SOX9, the $MYF5^+$ population does not appear to be originating from

pre-existing tissue structures. At week 3 post-injury, dermal MYF5^{+} populations are absent with most positive cells residing in the newly formed hair follicle bulge (**Fig 3.3B**). These studies suggest a heterogenous population of both resident and *de novo* progenitors that include myofibroblast-like phenotypes contribute to the *A.cahirinus* blastema.

3.4.4 YAP signaling is critical for mesenchymal blastema progenitor maintenance and later stage cartilage regeneration.

We have previously demonstrated YAP signaling is a critical component of at least two distinct phases of *A.cahirinus* epimorphic wound repair. These phases include blastema initiation (Weeks 1-2) and later stage tissue restoration (Weeks 4-5). Inhibition of YAP signaling during the tissue restoration phase results in several wound healing defects. The most striking are the absence of fat, muscle and cartilage. Furthermore, missing cartilage structures are instead replaced by ectopic hair follicles (**Fig 2.6 and 2.7**). As SOX9 is required for directing chondrocyte cell specification, we assayed for SOX9 expression to determine if cartilage loss is due to YAP signaling disruptions in the SOX9^{+} mesenchymal population[30].

To inhibit YAP signaling throughout the duration of regenerative wound repair, we treated *A.cahirinus* with verteporfin (VP)[37]. VP is a pharmaceutic agent that inhibits YAP-TEAD interactions[38,39]. We treated *Acomys* with VP [100mg/kg, DMSO] or equal volume control DMSO as depicted in **Fig 3.4A.** VP-mediated YAP-TEAD inhibition was confirmed by quantitative image analyses of VP-treated week 2 injuries exhibiting a statistically significant reduction in nuclear YAP localization in the dermal blastema (**Fig 2.6E**). We then stained *A.cahirinus* VP and DMSO weeks 2 and 3 injury sections with SOX9 and ACTA2 antibodies. DMSO control injuries show clear regions of heterogenous mesenchymal SOX9^{+} populations as previously observed. DMSO week 2 dermal SOX9^{+}/ACTA2^{+} and SOX9^{+}/ACTA2^{-} mesenchymal cells display similar migration

patterning from the original cartilage amputation plane. DMSO week 3 injuries show a sharp reduction of the $SOX9^{+}/ACTA2^{+}$ population with the remaining $SOX9^{+}/ACTA2^{-}$ subtype largely organized along the regenerating cartilage plane (**Fig3.4B**). In contrast, VP week 2 tissue exhibits perturbed blastema extension that is not yet resolved by week 3. Moreover, both weeks 2 and 3 VP tissue contain a noticeable reduction of $SOX9^{+}$ cells within the mesenchymal outgrowth with the majority of the $SOX9^{+}$ staining now restricted to the epithelium (**Fig 3.4C**). We therefore conclude that a subset of the mesenchymal $SOX9^{+}$ population are either lost or have undergone a cell fate change. This would confirm our previous hypothesis that YAP signaling in *A.cahirinus* is necessary for tissue regeneration.

3.4.5 Isolated *Acomys* fibroblasts express progenitor markers.

We previously have shown isolated *A.cahirinus* ear dermal fibroblasts have phenotypic markers of mammalian myofibroblasts ($ACTA2^{+}$), yet they fail to demonstrate many of the characteristic behaviors associated with this cell type both *in vitro* and *in vivo*[Ch.2]. For example, *A.cahirinus* resist upregulation of both *Acta2* and *Col1a1* when treated with Transforming growth factor beta-1 (TGFβ1). Therefore, we next asked if isolated *A.cahirinus* dermal fibroblasts instead display progenitor cell markers like those seen in response to injury. Surprisingly, we find isolated $ACTA2^{+}$ cells do exhibit nuclear localization of the SOX9 transcription factor under basal culturing conditions (**Fig 3.5A**). Because *A.cahirinus* fibroblasts are resistant to fibrokine-mediated myofibroblast activation, we assayed for SOX9 protein to determine if its expression is instead regulated by a variety of fibrokines. Indeed, 48-hour treatment with both TGFβ1 and thrombin reduced SOX9 protein expression in dermal fibroblasts when compared to untreated control (**Figure 3.5B,C**). Our data would confirm *A.cahirinus* myofibroblasts have adopted a modified progenitor-like cell profile.

3.5 Discussion

The genus *Acomys* has evolved the unique capacity for blastema – mediated regenerative repair, a trait previously believed to be restricted to urodeles and teleost[1]. The blastema is required for restoration of tissue structures such as cartilage, muscle, fat and hair follicles However, the cellular contributors to the *A.cahirinus* blastema remained unclear. In this study, we find the *A.cahirinus* ear blastema contains several heterogenous progenitor populations. These contributing precursor cells express both the chondrocyte specification marker, SOX9, and the myogenic specification marker, MYF5.

The $SOX9^+$ cells reside within the uninjured cartilage plate and then migrate into the blastema upon injury. We suspect these cells are resident progenitors, poised to engage in regenerative repair[40] as we identify one cell fate to include chondrocytes (**Fig 3.4**). Furthermore, YAP is a critical mediator of $SOX9^+$ progenitor maintenance and chondrocyte cell fate decisions. Disruption of YAP signaling leads to a decreased $SOX9^+$ cells and later stage cartilage restoration failure. Because *de-novo* hair follicle structures, also regulated by SOX9, instead occupy the missing cartilage space, we cannot conclude if the $SOX9^+$ population was instead redirected to a separate cell fate. Identifying if these progenitor cells exhibit multipotential or lineage restrictions will be an important future direction.

In contrast, a $MYF5^+$ population is absent in *A.cahirinus* uninjured skin. This provides evidence that a resident myogenic progenitor most likely does not exist in the *A.cahirinus* ear tissue. However, $MYF5^+$ cells do contribute to the blastema formation. As opposed to the resident $SOX9^+$ population, we observe $MYF5^+$ cells appear *de novo* during injury but are restricted to the blastema (**Fig 3.3**). We can only speculate the source of these temporally restricted $MYF5^+$ cells. Previous studies in lower order vertebrates have shown regenerative repair to include cell type

specific de-differentiation mechanisms[41,42]. For examples, new cardiomyocytes are restored by remaining cardiomyocytes regressing into a more primitive proliferative state during zebrafish cardiac resection injuries[43]. These regressed cells will then re-differentiate into mature cardiomyocytes. The de-differentiation event is dependent on re-expression of Gata4, an embryonic cardiomyocyte specification marker[44,45]. The similarities between the temporal reactivation of Gata4 and MYF5 during regeneration are striking. It is enticing to speculate the re-expression of MYF5 in *A.cahirinus* to be indicative of a de-differentiation event, as MYF5 downregulation is proceeded by newly restored striated muscle tissue. However, we cannot conclusively determine if these cells do contribute to new muscle without genetic lineage tracing tools.

Intriguingly, within the *A.cahirinus* heterogenous progenitor population, there are cell subsets that express myofibroblast-like markers ($ACTA2^{+}$) (**Fig 3.5,6**). This may indicate *A.cahirinus* myofibroblasts, while phenotypically similar to *Mus*, are not true myofibroblasts. In contrast to active scar tissue formation, *A.cahirinus* myofibroblasts may be acting as a stem cell reservoir that can participate in tissue restoration [18]. Expression of *ACTA2* in human mesenchymal stem cells can influence downstream cell lineage decisions [46,46,47]. The mesenchymal progenitor properties in isolated *A.cahirinus* myofibroblasts can be confirmed *in-vitro*. Defined growth factor supplements, specific for adipocytes, chondrocytes, and myoblast induction, can be used in culture and differentiation identified by cell type specific transcription factor expression[48].

Myofibroblast-mediated scar formation is the main mechanism driving the development of organ fibropathologies in both human and muriods. However, our data indicate *Acomys* myofibroblasts are necessary for scar-free tissue repair. These findings suggest that manipulating human myofibroblast activation, mirroring those seen in *Acomys* wounding, may offer an

important therapeutic opportunity to induce regenerative repair. Therefore, identifying the mechanisms controlling *Acomys* myofibroblast plasticity has important ramifications in manipulating scar formation outcomes in human diseases.

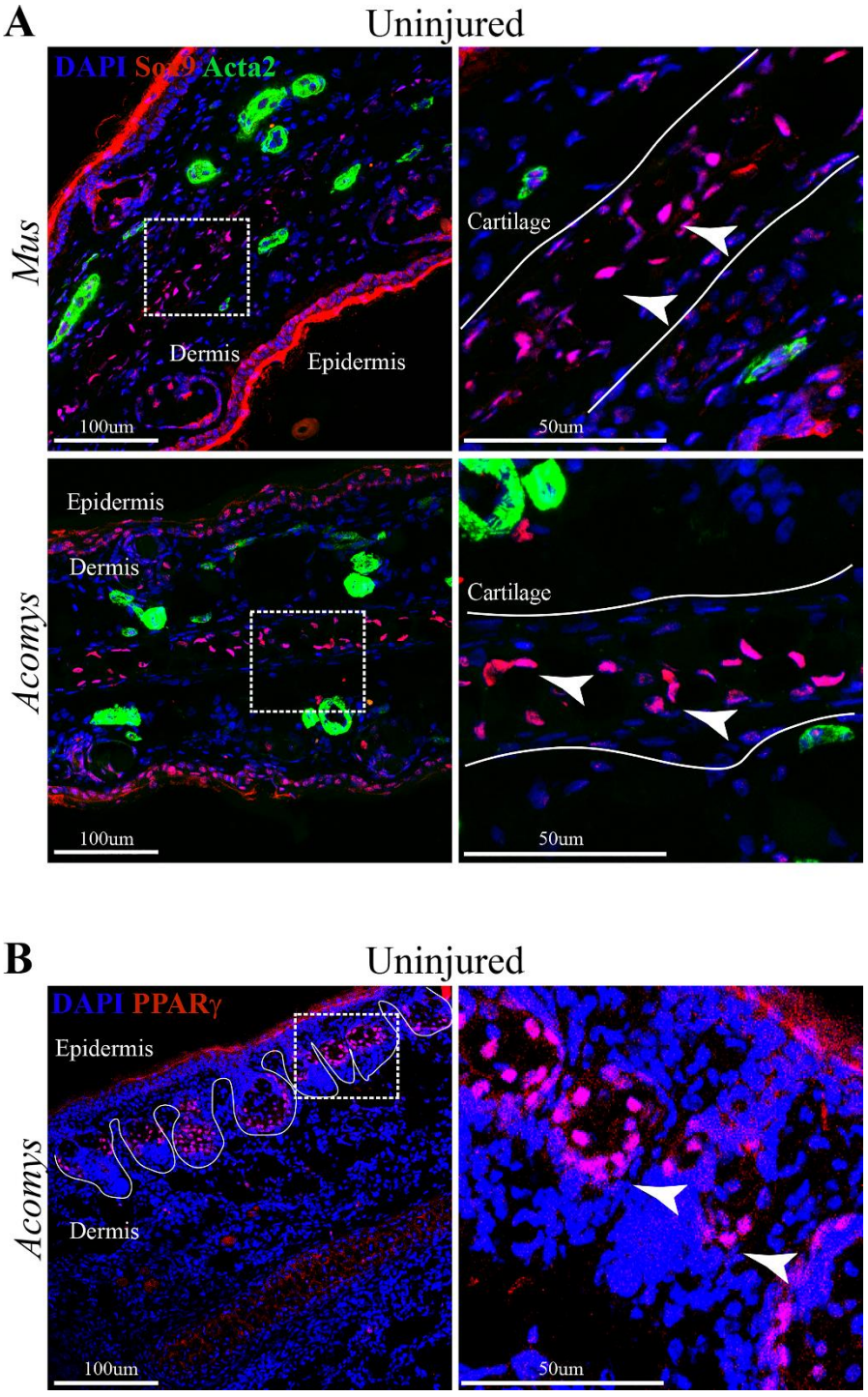

Figure 3.1 Tissue resident progenitor cells are found in both *Acomys* and CD1 *Mus* during normal homeostatic conditions. (**A**) Both species contain a resident $SOX9^{+}$ mesenchymal population within the cartilage plate. (**B**) *Acomys* but not CD1 *Mus* exhibit an epidermal $PPAR\gamma^{+}$ population residing within the sebaceous glands. Solid lines indicate structures of interest. Dashed boxes indicate area of magnification. Arrows indicate cells of interest.

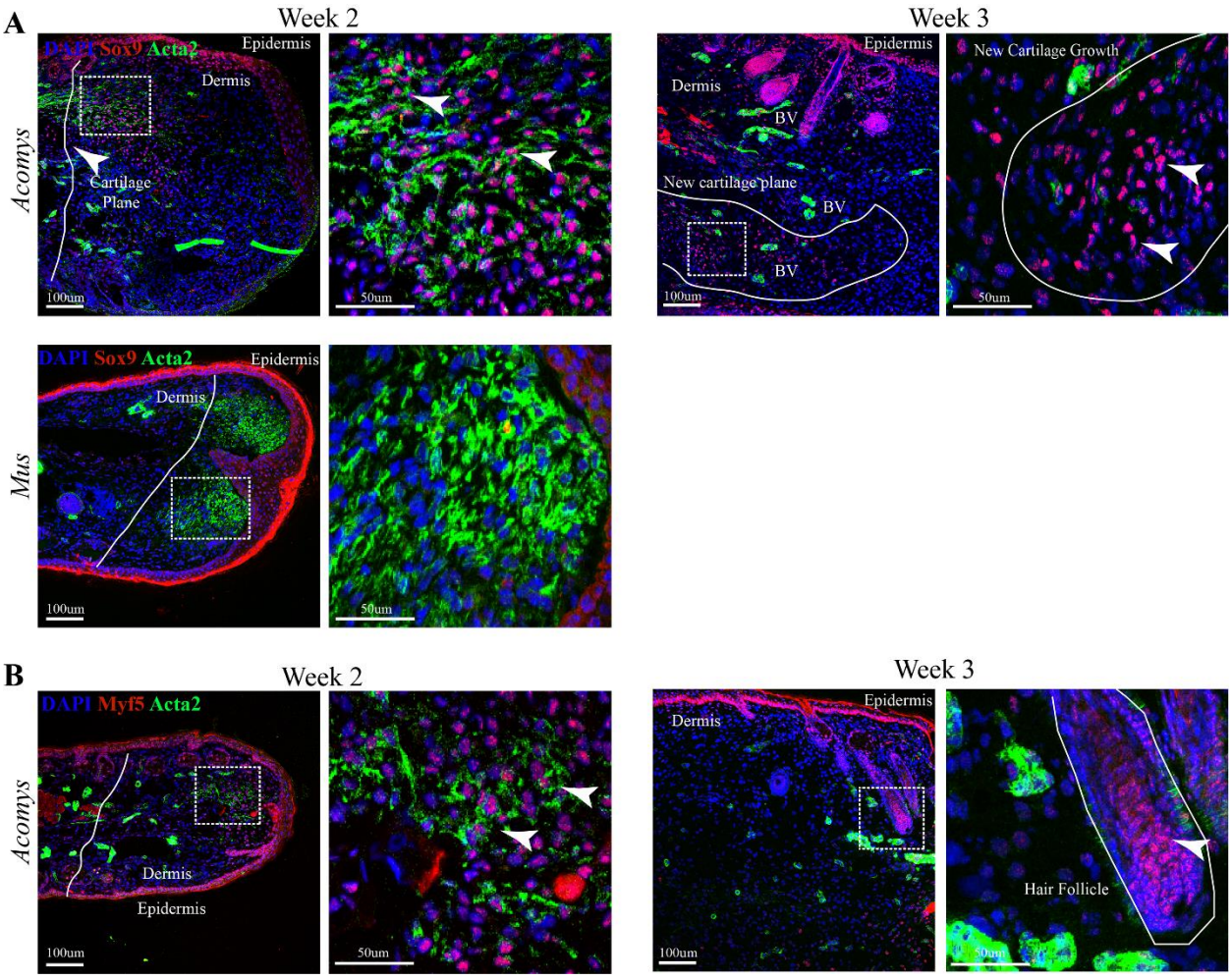

Figure 3.2 Heterogenous progenitor populations acquire myofibroblast phenotypes when contributing to *Acomys* blastema. (**A**) *Acomys* mesenchymal SOX9^{+}/ACTA2^{+} cells migrate into the blastema from the cartilage amputation plane at week 2 (Left). Mesenchymal SOX9^{+}/ACTA2^{-} cells have assembled within the regenerating cartilage plate at week 3 (Right). CD1 *Mus* have no mesenchymal SOX9^{+} cells in the injured tissue at either time point (Bottom) (**B**) *Acomys* blastema exhibits *de-novo* expression of MYF5 in both ACTA2$^{+/-}$ populations at week 2 (Left). MYF5 expression is reduced in the dermis with staining restricted to epidermal structures (Right-Arrows). White lines indicate amputation plane. Dashed boxes indicated areas of magnification. Arrows indicate cells of interest.

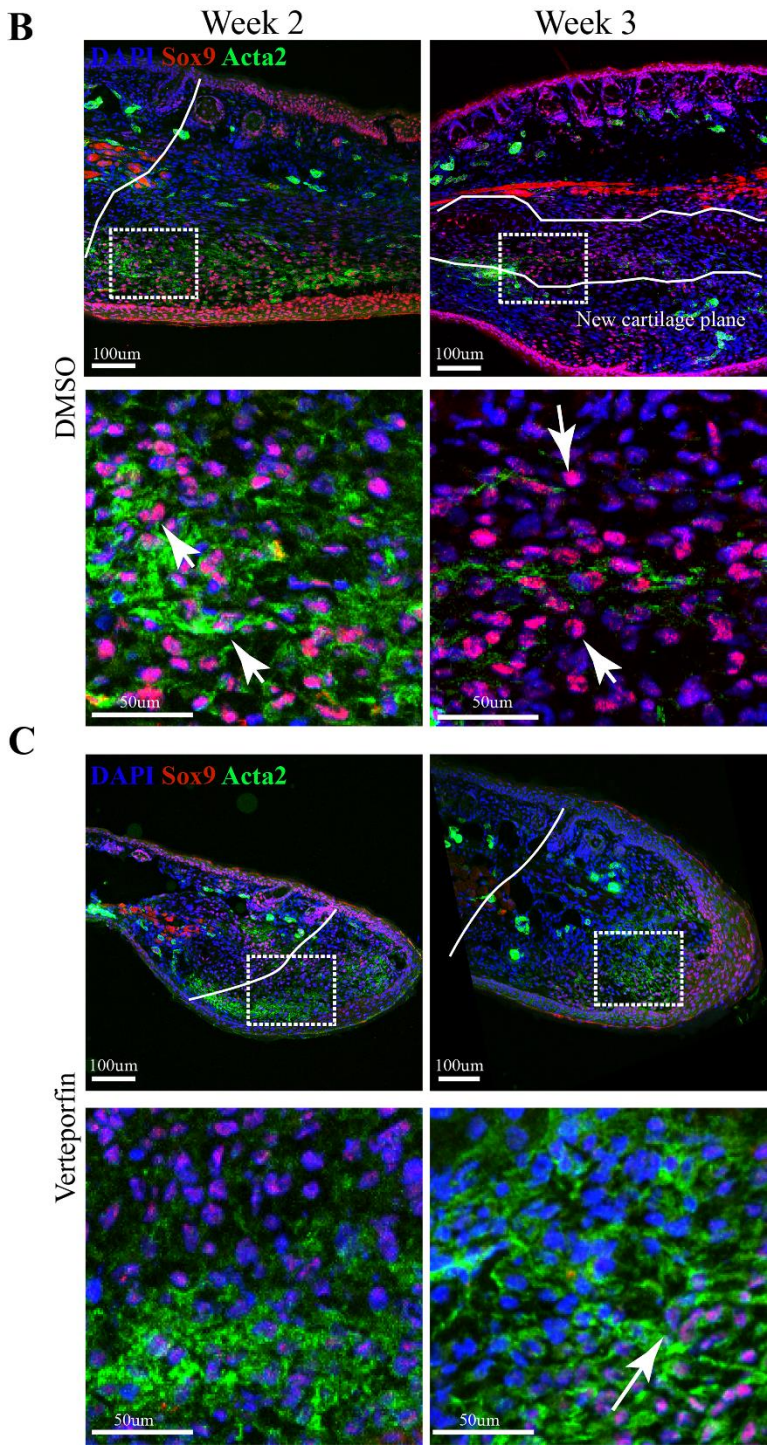

Figure 3.3 Yap signaling is necessary for SOX9 progenitor maintenance. (**A**) Schematic of *Acomys* chronic verteporfin injection model. (**B**) Mesenchymal SOX9^{+} cells infiltrate the blastema and pattern within the extending cartilage plate in DMSO control (Weeks 2-3). (**C**) VP treated *Acomys* exhibit perturbed blastema extension and closure (Weeks 2-3). A reduction of SOX9^{+} mesenchymal cells are observed throughout the entirety of injury time course. White lines indicate amputation plane. Dashed boxes indicated areas of magnification. Arrows indicate cells of interest.

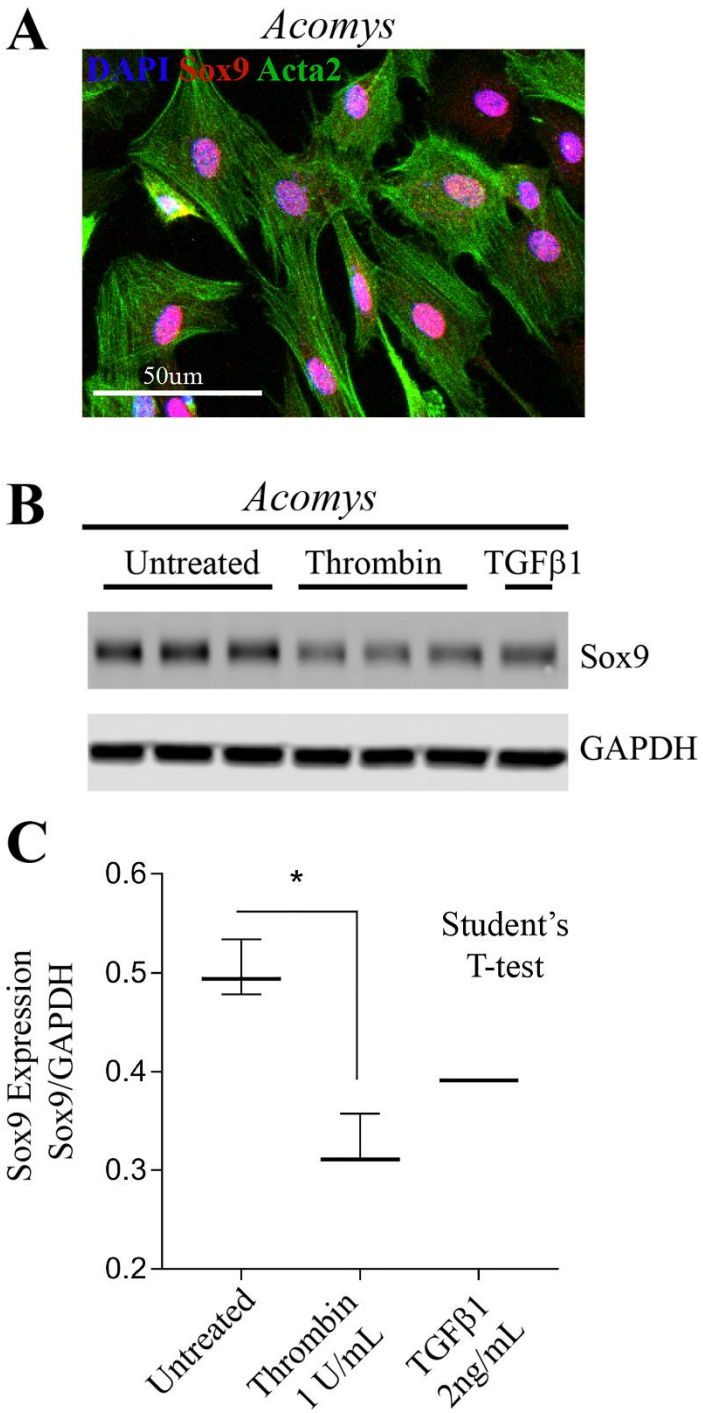

Figure 3.4 Isolated *Acomys* myofibroblasts downregulate progenitor cell markers in response to fibrokines. (**A**) Isolated *Acomys* dermal myofibroblasts ($ACTA2^{+}$) exhibit nuclear localization of SOX9.(**B**) Western blot of SOX9 protein levels after 48 hour thrombin and TGFβ1 introduction.(**C**) Quantification of Acomys fibroblast SOX9 expression. Data are represented as mean centered box and whiskers. $N \geq 3$ independent cultures. *$p<.05$.

3.6 References

1 Gawriluk, T. R. *et al*. Comparative analysis of ear-hole closure identifies epimorphic regeneration as a discrete trait in mammals. *Nat Commun* **7**, 11164, doi:10.1038/ncomms11164 (2016).

2 Seifert, A. W. *et al*. Skin shedding and tissue regeneration in African spiny mice (Acomys). *Nature* **489**, 561-565, doi:10.1038/nature11499 (2012).

3 Longaker, M. T. *et al*. Adult skin wounds in the fetal environment heal with scar formation. *Ann Surg* **219**, 65-72 (1994).

4 Mackool, R. J., Gittes, G. K. & Longaker, M. T. Scarless healing. The fetal wound. *Clin Plast Surg* **25**, 357-365 (1998).

5 Porrello, E. R. *et al*. Transient regenerative potential of the neonatal mouse heart. *Science* **331**, 1078-1080, doi:10.1126/science.1200708 (2011).

6 Simkin, J., Gawriluk, T. R., Gensel, J. C. & Seifert, A. W. Macrophages are necessary for epimorphic regeneration in African spiny mice. *Elife* **6**, doi:10.7554/eLife.24623 (2017).

7 Satoh, A., Bryant, S. V. & Gardiner, D. M. Regulation of dermal fibroblast dedifferentiation and redifferentiation during wound healing and limb regeneration in the Axolotl. *Dev Growth Differ* **50**, 743-754, doi:10.1111/j.1440-169X.2008.01072.x (2008).

8 Tanaka, E. M. & Reddien, P. W. The cellular basis for animal regeneration. *Dev Cell* **21**, 172-185, doi:10.1016/j.devcel.2011.06.016 (2011).

9 Morgan, T. H. *Regeneration*. (Macmillan, 1901).

10 Baguna, J., Sal, E. & Auladell, C. *Regeneration and pattern formation in planarians. III. Evidence that neoblasts are totipotent stem cells and the source of blastema cells*. Vol. 107 (1989).

11 Kragl, M. *et al*. Cells keep a memory of their tissue origin during axolotl limb regeneration. *Nature* **460**, 60-65, doi:10.1038/nature08152 (2009).

12 Gargioli, C. & Slack, J. M. Cell lineage tracing during Xenopus tail regeneration. *Development* **131**, 2669-2679, doi:10.1242/dev.01155 (2004).

13 Wagner, G. P. & Misof, B. Y. Evolutionary modification of regenerative capability in vertebrates: a comparative study on teleost pectoral fin regeneration. *J Exp Zool* **261**, 62-78, doi:10.1002/jez.1402610108 (1992).

14 Steen, T. P. Origin and differentiative capacities of cells in the blastema of the regenerating salamander limb. *Am Zool* **10**, 119-132 (1970).

15 Tu, S. & Johnson, S. L. Fate restriction in the growing and regenerating zebrafish fin. *Dev Cell* **20**, 725-732, doi:10.1016/j.devcel.2011.04.013 (2011).

16 Singh, S. P., Holdway, J. E. & Poss, K. D. Regeneration of amputated zebrafish fin rays from de novo osteoblasts. *Dev Cell* **22**, 879-886, doi:10.1016/j.devcel.2012.03.006 (2012).

17 Knopf, F. *et al*. Bone regenerates via dedifferentiation of osteoblasts in the zebrafish fin. *Dev Cell* **20**, 713-724, doi:10.1016/j.devcel.2011.04.014 (2011).

18 Plikus, M. V. *et al*. Regeneration of fat cells from myofibroblasts during wound healing. *Science* **355**, 748-752, doi:10.1126/science.aai8792 (2017).

19 Muro, A. F. *et al*. An essential role for fibronectin extra type III domain A in pulmonary fibrosis. *Am J Respir Crit Care Med* **177**, 638-645, doi:10.1164/rccm.200708-1291OC (2008).

20 Hinz, B. Tissue stiffness, latent TGF-beta1 activation, and mechanical signal transduction: implications for the pathogenesis and treatment of fibrosis. *Curr Rheumatol Rep* **11**, 120-126 (2009).

21 Hinz, B. *et al*. The myofibroblast: one function, multiple origins. *Am J Pathol* **170**, 1807-1816, doi:10.2353/ajpath.2007.070112 (2007).

22 Campanholle, G., Ligresti, G., Gharib, S. A. & Duffield, J. S. Cellular mechanisms of tissue fibrosis. 3. Novel mechanisms of kidney fibrosis. *Am J Physiol Cell Physiol* **304**, C591-603, doi:10.1152/ajpcell.00414.2012 (2013).

23 Tomasek, J. J., Gabbiani, G., Hinz, B., Chaponnier, C. & Brown, R. A. Myofibroblasts and mechano-regulation of connective tissue remodelling. *Nat Rev Mol Cell Biol* **3**, 349-363, doi:10.1038/nrm809 (2002).

24 Beverdam, A. *et al*. Yap controls stem/progenitor cell proliferation in the mouse postnatal epidermis. *J Invest Dermatol* **133**, 1497-1505, doi:10.1038/jid.2012.430 (2013).

25 Tucker, A. S. *et al*. Mapping the distribution of stem/progenitor cells across the middle ear during homeostasis and inflammation. *Development*, doi:10.1242/dev.154393 (2017).

26 Lay, K., Kume, T. & Fuchs, E. FOXC1 maintains the hair follicle stem cell niche and governs stem cell quiescence to preserve long-term tissue-regenerating potential. *Proc Natl Acad Sci U S A* **113**, E1506-1515, doi:10.1073/pnas.1601569113 (2016).

27 Adam, R. C. *et al*. Pioneer factors govern super-enhancer dynamics in stem cell plasticity and lineage choice. *Nature* **521**, 366-370, doi:10.1038/nature14289 (2015).

28 Hsu, Y. C., Li, L. & Fuchs, E. Transit-amplifying cells orchestrate stem cell activity and tissue regeneration. *Cell* **157**, 935-949, doi:10.1016/j.cell.2014.02.057 (2014).

29 Yan, Y. L. *et al*. A zebrafish sox9 gene required for cartilage morphogenesis. *Development* **129**, 5065-5079 (2002).

30 Liu, C. F., Samsa, W. E., Zhou, G. & Lefebvre, V. Transcriptional control of chondrocyte specification and differentiation. *Semin Cell Dev Biol* **62**, 34-49, doi:10.1016/j.semcdb.2016.10.004 (2017).

31 Relaix, F., Rocancourt, D., Mansouri, A. & Buckingham, M. A Pax3/Pax7-dependent population of skeletal muscle progenitor cells. *Nature* **435**, 948-953, doi:10.1038/nature03594 (2005).

32 Relaix, F. *et al*. Six Homeoproteins Directly Activate Myod Expression in the Gene Regulatory Networks That Control Early Myogenesis. *PLoS Genetics* **9**, e1003425, doi:10.1371/journal.pgen.1003425 (2013).

33 Rosen, E. D. *et al*. PPAR gamma is required for the differentiation of adipose tissue in vivo and in vitro. *Mol Cell* **4**, 611-617 (1999).

34 Hirata, A., Gardiner, D. M. & Satoh, A. Dermal fibroblasts contribute to multiple tissues in the accessory limb model. *Dev Growth Differ* **52**, 343-350, doi:10.1111/j.1440-169X.2009.01165.x (2010).

35 Cook, A. B. & Seifert, A. W. Beryllium nitrate inhibits fibroblast migration to disrupt epimorphic regeneration. *Development* **143**, 3491-3505, doi:10.1242/dev.134882 (2016).

36 de Crombrugghe, B. *et al*. Transcriptional mechanisms of chondrocyte differentiation. *Matrix Biol* **19**, 389-394 (2000).

37 Liu-Chittenden, Y. *et al*. Genetic and pharmacological disruption of the TEAD-YAP complex suppresses the oncogenic activity of YAP. *Genes Dev* **26**, 1300-1305, doi:10.1101/gad.192856.112 (2012).

38 Michels, S. & Schmidt-Erfurth, U. Photodynamic therapy with verteporfin: a new treatment in ophthalmology. *Semin Ophthalmol* **16**, 201-206, doi:10.1076/soph.16.4.201.10298 (2001).
39 Feng, J. *et al*. Verteporfin, a suppressor of YAP-TEAD complex, presents promising antitumor properties on ovarian cancer. *Onco Targets Ther* **9**, 5371-5381, doi:10.2147/ott.s109979 (2016).
40 Bastakoty, D. *et al*. Inhibition of Wnt/beta-catenin pathway promotes regenerative repair of cutaneous and cartilage injury. *Faseb j* **29**, 4881-4892, doi:10.1096/fj.15-275941 (2015).
41 McHedlishvili, L., Epperlein, H. H., Telzerow, A. & Tanaka, E. M. A clonal analysis of neural progenitors during axolotl spinal cord regeneration reveals evidence for both spatially restricted and multipotent progenitors. *Development* **134**, 2083-2093, doi:10.1242/dev.02852 (2007).
42 Sandoval-Guzman, T. *et al*. Fundamental differences in dedifferentiation and stem cell recruitment during skeletal muscle regeneration in two salamander species. *Cell Stem Cell* **14**, 174-187, doi:10.1016/j.stem.2013.11.007 (2014).
43 Poss, K. D., Wilson, L. G. & Keating, M. T. Heart regeneration in zebrafish. *Science* **298**, 2188-2190, doi:10.1126/science.1077857 (2002).
44 Kikuchi, K. *et al*. Primary contribution to zebrafish heart regeneration by gata4(+) cardiomyocytes. *Nature* **464**, 601-605, doi:10.1038/nature08804 (2010).
45 Kikuchi, K. *et al*. tcf21+ epicardial cells adopt non-myocardial fates during zebrafish heart development and regeneration. *Development* **138**, 2895-2902, doi:10.1242/dev.067041 (2011).
46 Hinz, B., Celetta, G., Tomasek, J. J., Gabbiani, G. & Chaponnier, C. Alpha-smooth muscle actin expression upregulates fibroblast contractile activity. *Mol Biol Cell* **12**, 2730-2741 (2001).
47 Rockey, D. C., Weymouth, N. & Shi, Z. Smooth muscle alpha actin (Acta2) and myofibroblast function during hepatic wound healing. *PLoS One* **8**, e77166, doi:10.1371/journal.pone.0077166 (2013).
48 Tong, L. *et al*. Fibroblast Growth Factor-10 (FGF-10) Mobilizes Lung-resident Mesenchymal Stem Cells and Protects Against Acute Lung Injury. *Sci Rep* **6**, 21642, doi:10.1038/srep21642 (2016).

Chapter 4. Scarless repair of acute and chronic kidney injury in African Spiny mice (*Acomys cahirinus*)

Daryl M. Okamura[1,3,*,#], Chris M. Brewer[2,3,*], Paul Wakenight[4,*], Nadia Bahrami[3], Kristina Bernardi[3], Amy Tran[3], Jill Olson[3], Kay Shi[3], Adrian Piliponsky[1,2,5], Branden Nelson[4], David R. Beier[1,3,] Kathleen J. Millen[1,4,#], Mark W. Majesky[1,2,3,6,#]

1 Department of Pediatrics, University of Washington, Seattle, WA, USA

2 Department of Pathology, University of Washington, Seattle, WA, USA

3 Center for Developmental Biology & Regenerative Medicine, Seattle Children's Research Institute, Seattle, WA

4 Center for Integrative Brain Research, Seattle Children's Research Institute, Seattle, WA

5 Center for Immunity & Immunotherapies, Seattle Children's Research Institute, Seattle, WA

6 Institute for Stem Cell & Regenerative Medicine, University of Washington, Seattle, WA

*Authors contributed equally to this work.

#Correspondence to:

Daryl M. Okamura, Center for Developmental Biology & Regenerative Medicine, Seattle Children's Research Institute, University of Washington, Seattle, WA. daryl.okamura@seattlechildrens.org

Kathleen J. Millen, Center for Integrative Brain Research, Seattle Children's Research Institute, University of Washington, Seattle, WA. kathleen.millen@seattlechildrens.org

Mark W. Majesky, Center for Developmental Biology & Regenerative Medicine, Seattle Children's Research Institute, University of Washington, Seattle, WA. mwm84@uw.edu

4.1 Summary

Solid organ fibrosis is a major burden on global health and medical care costs. Muroid rodents of the genus *Acomys* (African Spiny mice) are terrestrial mammals that evolved remarkable abilities to regenerate severe skin wounds without scar formation. However, whether scar-free wound repair in *Acomys* extends beyond skin to vital internal organs is not known. Here, we used two aggressive kidney injury models known to produce severe renal fibrosis and show that despite equivalent acute kidney injury, there was rapid restoration of nephron structure and function without fibrosis in *Acomys* compared to extensive fibrosis leading to renal failure in *Mus musculus*. These results suggest *Acomys* species have evolved genomic adaptations for wound healing that activate regenerative repair pathways not only in skin, but also in vital internal organs. Our findings have important implications for discovering a long-sought evolutionary solution to internal organ injury and regeneration.

4.2 Introduction

Solid organ fibrosis is the result of chronic inflammatory processes and dysregulated wound healing that leads to progressive loss of tissue function and eventual organ failure.[1] The global health care burden for cumulative loss of vital organ function due to progressive fibrosis is enormous.[2] There are currently very few treatment options for patients with end stage renal disease or similar degenerative fibrotic conditions in the heart, lung, liver, or other critical internal organs.[3] Looking to nature for a possible solution, it was reported that adult rodents of the genus *Acomys* (African spiny mice) can shed their dorsal skin as a deterrent to avoid predators and fully regenerate the lost tissue without fibrosis or tissue overgrowth.[4] The restored skin is complete with hair follicles, sebaceous glands, cartilage, adipose tissue, nerves, and blood vessels in the correct architectural organization.[5,6] While this remarkable wound healing response in the skin has been examined in some detail, the important question of whether or not scarless regenerative wound repair in *Acomys* species extends beyond skin to vital internal organs remains unanswered.

In the experiments reported here, our objective was to produce injuries to *Acomys* kidney that are known to promote severe fibrotic responses leading to organ failure in murine kidney. Our goal was to determine whether or not scarless, regenerative wound healing observed in *Acomys* skin extends to critical internal organs. We now provide the first reported evidence that scarless wound repair first observed in the skin does indeed extend to a major internal organ in the African spiny mouse. We demonstrate that in two aggressive models of kidney disease, unilateral ureteral obstruction (UUO) and ischemia reperfusion injury (IRI), there was a near complete absence of fibrosis and a rapid regeneration of nephron function in *A. cahirinus*. By contrast, paired groups of *M. musculus* (outbred CD-1 or inbred C57BL/6J) developed severe kidney fibrosis that rapidly progressed to complete renal failure. These studies represent the first step in an evolutionary

approach to understand how mammalian wound healing can be uncoupled from the fibrotic response to injury and redirected toward regeneration of complex organ function in mammals.

4.3 Materials and Methods

4.3.1 Experimental Design

We utilized two models of kidney injury to investigate the differences in wound healing and fibrosis: Unilateral ureteral obstruction (UUO) and ischemia reperfusion injury (IRI). C57BL/6J (B6) and CD-1 mice were used as inbred and outbred strains of *M. musculus*, respectively. Surgery was performed on male animals between 3 and 6 months of age. UUO surgeries were performed as previously described[25,26] (n =6-8/group), and animals were sacrificed at 3, 7, 14, and 21 days after surgery. Mice received isoflurane anesthesia (5% induction; 1-3% maintenance) in oxygen through a precision vaporizer (Portable Anesthesia Machine, PAM; Molecular Imaging Products, Bend, OR, USA).

Unilateral IRI (uni-IRI) surgeries were performed as previously described[25,26] except that the vascular pedicle was clamped for 40 minutes (n=5-6/group), and animals were sacrificed at 24h, 72h, 7 days, and 14 days after surgery. In order to assess initial injury, the contralateral kidney was removed at the time of uni-IRI surgery and sacrificed at 24h after surgery. In order to quantify kidney function in the uni-IRI kidney after initial injury, a contralateral nephrectomy was performed 14 days post-surgery as previously described.[25] Blood was drawn daily until sacrifice at 2 days post-nephrectomy. All procedures were performed in accordance with the guidelines established by National Research Council Guide for the Care and Use of Laboratory Animals and approval of our Institute Animal Care and Use Committee (IACUC). Contralateral, UUO, and IRI kidneys were harvested and processed for RNA and protein extraction and histological studies as previously described.[25-27] Frozen tissue samples were stored at-80°C.

4.3.2 Collagen Content

Hydroxyproline content of kidney tissue (□g of hydroxyproline per mg of wet weight kidney section) was measured by acid hydrolysis of the tissue section using procedures established in our laboratory.[25-27]

4.3.3 Histological Examination

Immunohistochemical staining was performed on sections of paraffin-embedded tissue or cryosections of snap-frozen tissue using procedures established in our laboratory with VECTASTAIN *Elite* ABC Kits (Vector Laboratories, Inc.) and AEC Substrate Chromogen K3464 (Dako Corp.). Sections were blocked with Avidin/Biotin blocking kit (Vector Laboratories, Inc.). Computer-assisted image analysis was performed on 6 randomly selected 400x magnified images of slides from individual animals with Image-Pro Plus software (Mediatech). The investigator was blinded to the experimental groups at the time of analysis. Picrosirius red staining was performed as previously described.[25,27] In brief, quantification of interstitial staining of picrosirius red (SR) staining was performed in a blinded manner using Image-Pro software with randomly selected cortical fields. SR glomerular staining was subtracted and net SR area was normalized to net tubulointerstitial area of 400x field (Net area = Total – glomerular area - empty space). Masson Trichrome and hematoxylin eosin stains were performed on paraffin sections by standard protocols. Interstitial fibrosis and tubular atrophy (IFTA) scores was analyzed on 6 randomly selected 400x Masson Trichrome stained images. The following IFTA scores were assigned, in a blinded manner, based on the estimated percent area affected with tubular atrophy, loss of tubular structure, interstitial inflammation, and interstitial fibrosis in the field: 1 (normal); 2 (<10%), 3 (10-25%); 4 (26-50%); or 5 (>50%). Dilated tubular area was measured using Image-Pro software on 400x Masson trichrome stained images. Tubular casts and intraluminal debris area was

measured using Image-Pro software on 200x PAS-stained images and normalized to net tubulointerstitial area for 6 randomly selected cortical fields. Secondary antibodies were shown to be non-reactive with tissue sections stained without the primary antibody.

4.3.4 F4/80 Macrophage Quantification

Mice were perfused with cold normal saline and contralateral and UUO kidneys were placed on ice, digested with Liberase TL (Roche) with 1% DNase (Sigma-Aldrich), then placed at 37°C for 10 minutes, as previously described. Glomeruli were removed by passing cell suspension through a 40□m Nylon filter. Cells were stained per protocol with DAPI, PE-Cy7-anti-CD45, PE-anti-CD11b, APC-eFluor780-F4/80 from BD Sciences. Cells were blocked with mouse Fc Block (BD Biosciences). Leukocytes were identified and gated based on their positive F4/80 expression. Data was acquired on the LSR II flow cytometer (BD Biosciences) and analyzed using FlowJo software (Tree Star, Inc).

4.3.5 Kidney Function

Serum was analyzed for blood urea nitrogen (BUN) using the Urea Nitrogen (BUN) Reagent Set kit (Teco Diagnostics). Samples were processed according to manufacturer's protocol. All samples were performed in triplicate.

4.3.6 Immunofluorescence

For cryosectioning, excised tissue was embedded and flash-frozen in O.C.T medium (Tissue Tech) using a dry-ice slurry/2-methylbutanol mixture and cryosectioned between 8-10um. Tissue cryosections were washied with PBS and fixed with 4% PFA for 10 min. Post fixation, slides were washed three times for 5 min each with PBS followed by permeabilization using 0.2% Triton-X100 in PBS (PBT) for 10 min. Slides were then blocked (5% BSA, 2% normal goat serum in PBT) at room temperature for 1hr. Post block, tissue sections were then incubated in primary

antibody overnight at 4C in blocking solution (3% BSA, 0.2% Triton-X100 in PBS). Primary antibodies used include pan-Laminin (Abcam, #ab11575), *Acta2* (Sigma, #A2547), F4/80 (Invitrogen, #MF48020), and *Cdh1* (BD Bioscience, #610181). After overnight incubation, slides were washed with PBS, and then incubated with goat ALEXA-Fluor 594- or ALEXA-Fluor 488-conjugated antibodies (Thermo Fisher Scientific) for 2h at room temperature in blocking solution. Cell nuclei were counterstained with DAPI (Molecular Probes) and mounted in 4% (w/v) propyl gallate anti-fade solution. Immunofluorescent images were obtained using an SP5 confocal microscope (Leica). *Acta2* and *Cdh1* confocal image analysis was performed as previously described.[25,27]

4.3.7 Statistical analysis

All data are presented as the mean and standard error. All statistical analyses were performed using GraphPad PRISM 7.0 (GraphPad Software) and STATA 14 (StataCorp LP) software. Two-way analysis of variance (ANOVA) was performed for all parametric data including computer-assisted image analysis data for time and species. For image analysis data, the arithmetic mean of six randomly selected images of slides for each animal was used for the two-way ANOVA. Sidak's and Tukey's multiple comparison post-tests were utilized for time and species, respectively. Nonparametric data (IFTA and tubular injury scores) was analyzed using the Mann-Whitney U test. A P value <0.05 was considered statistically significant. UUO kidney weights were analyzed by linear regression.

4.4 Results

4.4.1 *A. cahirinus* fails to develop fibrosis after UUO injury

Tubulointerstitial fibrosis is the final common pathway of many forms of kidney disease.[1,3,7] Unilateral ureteral obstruction (UUO) is a reliable and aggressive model of chronic

kidney injury and robust interstitial fibrosis. In previously reported studies where the contralateral kidney was removed after 7d of obstruction in *M. musculus*, UUO kidneys were found to have about 50% function. After 14d they become nonfunctional resulting in 100% mortality from kidney failure.[8] We performed UUO surgeries on *A. cahirinus* and *M. musculus* (outbred CD-1 and inbred C57BL/6J (B6) strains were used) and retrieved injured kidneys (UUO) and contralateral kidneys (NK) at the times indicated in **Fig 1**. We found that even after 14d of obstruction with obvious signs of hydronephrosis (**Fig 1A,B**), the gross anatomic structure and parenchymal thickness (between arrows, **Fig 1C**) were remarkably preserved in *A. cahirinus* compared to *M. musculus* (B6). This preservation of tissue structure was confirmed by the maintenance of relatively normal kidney weights (UUO/NK) in obstructed *A. cahirinus* kidneys compared to rapid declines in kidney weight in *M. musculus* as a a result of progressive fibrosis (*ratio of slopes:* m_{Mus}/m_{Acomys}*=-7.5; p=0.03,* **Fig 1C**). There were no significant differences in uninjured contralateral kidney weights between *A. cahirinus* and *M. musculus* (data not shown).

Progression of fibrosis was monitored by three different assays. Total collagen levels were measured as hydroxyproline content per wet kidney weight. Kidney collagen levels increased rapidly in *M. musculus* while *A. cahirinus* exhibited no significant change from the uninjured contralateral kidney (NK) (n=6-8, **Fig 1D**). Remarkably, even out to 21d of obstruction, there were no significant differences in total collagen levels between UUO kidney and uninjured contralateral kidney (NK) in *A. cahirinus* (**Fig 1D;** *Acomys:NK vs D3-21, NS*). Computer-assisted image analysis of picrosirius red-stained kidney tissue sections demonstrated a nearly complete absence of interstitital matrix fibrosis at each time point after UUO injury in *A. cahirinus* even out to 21d of obstruction (*Acomys*: *NK vs D3-21, NS*), compared to extensive fibrosis in *M. musculus* kidneys (**Fig 1E, Supp Fig 1**). Interstitial fibrosis, inflammation, and tubular atrophy (IFTA) were blindly

scored on Masson's trichrome stained sections. We found that IFTA scores were markedly reduced in *A.cahirinus* compared to *M. musculus* (B6) despite chronic obstructive injury in both species (**Fig 1F, Supp Fig 2**). In order to test our findings in an outbred strain of *M. musculus*, we performed UUO surgeries on CD-1 mice and measured fibrosis severity by picrosirius red staining. Of interest, we found even more dramatic increases in interstitial fibrosis in CD-1 mice producing even greater differences in fibrotic tissue areas when compared to *A. cahirinus* (**Fig G,H**; *p<0.0001*). All together, these results demonstrate that, in contrast to either inbred or outbred *M. musculus* strains, *A. cahirinus* does not develop fibrotic tissue in response to severe chronic obstructive kidney injury.

4.4.2 *A.cahirinus* maintains tubular integrity and fails to accumulate myofibroblasts after UUO injury

In order to quantify the degree of obstructive tubular injury, we measured the dilated tubular area in *A. cahirinus* and *M. musculus* (B6) at 3d through 14d after UUO. As expected from the obvious hydronephrosis seen in **Fig 1A,B**, we found that tubular dilation increased significantly in both species following UUO compared to the contralateral uninjured kidney, and peaked at 7d (**Fig 1I**; *p<0.05*). Importantly, there were no significant differences in the extent of tubular dilation between *A. cahirinus* and *M. musculus* at any of the time points examined (**Fig 1I**). Activated myofibroblasts (positive for smooth muscle α-actin, *Acta2*) are a significant source of collagen-rich extracellular matrix produced during kidney fibrosis. Chronic tubular injury is known to promote the production of intrarenal profibrotic cytokines that activate myofibroblasts.[9] While *Acta2* immunolabeling increased after UUO in both species, *M. musculus* exhibited higher levels of *Acta2*+ myofibroblasts compared to *A. cahirinus* (**Fig 2A,B;** *p<0.01*). In contrast to the lack of significant fibrosis in *A. cahirinus* after UUO (**Fig 1D,E**), there was a significant increase in

Acta2+ myofibroblasts at D14 after UUO compared to both NK and D3 time points (**Fig 2B**, $p<0.05$). These results suggest that the absence of interstitial matrix deposition in *A. cahirinus* after UUO injury is not due to the absence of myofibroblasts.

Chronic inflammation with a predominance of macrophages is a characteristic finding in organ injury and is strongly correlated with tissue fibrosis.[10] In order to quantify macrophage infiltration, whole kidneys were enzymatically digested into single cell suspensions and analyzed for F4/80 expression by flow cytometry (**Fig 2C,D).** As expected, the number of F4/80 macrophages increased in *M. musculus* UUO kidneys with advancing obstruction (7d and 14d) compared to contralateral normal kidneys ($p<0.001$). In *A. cahirinus,* increases in macrophage content were both delayed and diminished over the same time course (**Fig 2D**). Similar to *Acta2* data from *A. cahirinus* kidneys, there was a significant increase in F4/80+ macrophages at D14 compared to NK and D3 time points (**Fig 2D,** $p<0.001$). In comparing *A. cahirinus* with *M. musculus* kidneys, significant reductions in F4/80+ macrophage content were found at each time point examined ($p<0.05$) but less dramatic than the fibrosis (**Fig 1D,E**) and myofibroblast (**Fig 2B**) data. These results suggest that the unique absence of fibrosis in *A. cahirinus* is not due to a complete absence of a chronic inflammatory response or an absence of myofibroblasts in injured kidney tissues but suggests an evolutionary adaptation in wound repair.

Tubular integrity is strongly correlated with nephron function and can serve as a histological surrogate of whole kidney function.[11,12] *Cdh1* (E-cadherin) is an indicator of tubular cell integrity and polarity whose expression is lost with ongoing obstructive injury leading to loss of tubular architecture.[13] As expected for *M. musculus* there was progressive loss of *Cdh1* expression with each time point after UUO compared to the contralateral normal kidney (**Fig 2E,F**). However, in *A. cahirinus*, there were no significant changes in *Cdh1* protein levels with

advancing obstructive injury until D14 compared to the contralateral uninjured kidney. There were no differences in *Cdh1* expression levels in uninjured contralateral kidneys between *A. cahirinus* and *M. musculus* (**Fig 2F**). Thus, despite severe chronic obstruction, *Cdh1* protein levels were maintained in *A. cahirinus* while becoming significantly decreased in *M. musculus* injured kidneys with each time point (**Fig 2F**). All together, these results demonstrate that despite equivalent tubular dilation with obstruction (**Fig 1K**), we found significant attenuations in myofibroblast activation, macrophage infiltration, and loss of *Cdh1* in *A. cahirinus* kidneys that were correlated with preservation of tubular integrity and lack of interstitial fibrosis compared to *M. musculus*.

4.4.3 Renal fibrosis is reduced in *A. cahirinus* despite equivalent ischemic injury

Although the UUO model is useful in the study of renal fibrosis, it is not directly translatable to human kidney disease. By contrast, ischemic kidney injury is one of the most common causes of acute kidney injury in humans. We sought to test our findings in a second model of severe kidney injury with unilateral ischemia-reperfusion injury (uni-IRI) following prolonged 40 min of ischemia. One of the questions arising from our results with the UUO model was whether *A. cahirinus* was able to resist acute kidney damage rather than alter the subsequent fibrogenic cascade. Therefore, we performed uni-IRI with a simultaneous contralateral nephrectomy (uni-IRI+Nx) on *A. cahirinus* and *M. musculus* and sacrificed them at 24h after surgery in order to correlate kidney function with histology after severe acute injury. We found a significant elevation in blood urea nitrogen (BUN) levels 24h after uni-IRI+Nx in both *A. cahirinus* and *M. musculus* (**Fig 3A**). Importantly, these acutely elevated BUN levels were not significantly different between species (**Fig 3A**). In fact, there was a trend towards higher BUN levels in *A. cahirinus* (BUN: *Acomys* vs *Mus*, 129±24 vs 102±16 mg/dL). H&E sections on the Uni-IRI-Nx kidneys from *A. cahirinus* and *M. musculus* at 24h were analyzed for tubular cell necrosis, casts,

and dilation and assigned cumulative tubular injury scores. Consistent with our kidney function data, we found no differences in tubular injury scores at 24h between *A. cahirinus* and *M. musculus* (**Fig 3B,C**) and therefore conclude that both species experience equivalent levels of acute ischemic injury and tissue damage after prolonged renal ischemia as assessed both histologically and functionally.

In order to investigate the ability of *A. cahirinus* to repair acute kidney injury, we performed uni-IRI without contralateral nephrectomy to allow long term survival in both species and then sacrificed animals at 14d to assess kidney structure by histology. Remarkably, despite severe acute ischemic injury, we found a near complete absence of fibrosis by picrosirius red staining, and a robust preservation of renal mass, in *A. cahirinus* compared to *M. musculus* (either outbred CD-1 or inbred B6) (**Fig 3D-F**). For example, IRI/contralateral kidney weight ratios at 14d were maintained in *A. cahirinus* (0.92±0.02) compared to almost 40% loss of renal parenchymal mass to fibrosis in *M. musculus* (**Fig 3D**). Likewise, fibrosis severity measured by picrosirius red staining indicated a near total absence of fibrosis in *A. cahirinus* compared to either CD-1 or B6 strains of *M. musculus* (**Fig 3E,F**).

To assess the degree of functional restoration in the uni-IRI damaged kidney, we performed uni-IRI followed by a contralateral nephrectomy at day 14 and then measured kidney function over the next 2 days. Importantly, we found striking and reproducible differences in 16d BUN levels between *A. cahirinus* and *M. musculus* (**Fig 3G**). Consistent with a near complete absence of tubular damage and interstitial fibrosis at 14d, we found that BUN levels were nearly normal in *A. cahirinus* indicative of almost complete restoration of kidney function by 16d after IRI (compare **Fig 3A** to **Fig 3G**)**.** By contrast, *M. musculus* BUN levels were substantially increased indicative of progressive renal failure (**Fig 3G**). Likewise, staining for the tubular epithelial cell basement

membrane protein laminin showed progressive disruption and thickening by 14d in *M. musculus* kidney (B6) consistent with tubular atrophy while basement membrane structures at 14d in *A. cahirinus* kidney strongly resembled normal uninjured kidney (Ctrl) (**Fig 3H**) consistent with our Sirius red results (**Fig 3E**). The removal of necrotic and cellular debris is an important precursor in wound repair and tissue regeneration.[2] Intraluminal casts and debris were quantitated from kidney sections and showed that both species exhibited abundant casts/debris at equivalent levels by 24h after IRI (**Fig 4A,B,C,** arrows). At later time points, *M. musculus* retained these intraluminal debris while *A. cahirinus* efficiently cleared them from the tubular network (**Fig 4A, D-G).** Histologic examination by periodic acid Schiff (PAS) stains demonstrated that there were similar levels of tubular necrosis and tubular casts seen in the corticomedullary junction at 24h after severe IRI in both *A. cahirinus* and *M. musculus* (**Supp Fig 3A-C).** However, what was strikingly different in *A. cahirinus* was the abundance of polymorphonuclear cells and other nucleated cells within intraluminal tubular casts (**Supp Fig 3D,E**, arrows) that was seen much less frequently in *M. musculus* (**Supp Fig 3B**, arrow). By 72h after IRI, tubular casts, dilation, and interstitial inflammation progressed in *M. musculus* (**Supp Fig 3F,G**) while in *A. cahirinus* the intraluminal cellular debris had been removed and replaced by highly nuclear, somewhat disorganized tubular structures (**Supp Fig 3H**) with flattened epithelial cells suggesting progression toward a more dedifferentiated state (**Supp Fig 3I,J**, arrows). By 7d, monocytic infiltrates, tubular damage and interstitial fibrosis continue to progress in *M. musculus* compared to the appearance of defined tubular structures with open lumens in *A. cahirinus* (**Supp Fig 3M,N**) and PAS-positive brush border structures signifying mature differentiated tubular epithelial cells (**Supp Fig 3O**). These findings confirm that the response to severe acute kidney injury in *A. cahirinus* does not lead to the progressive, degenerative fibrotic response characteristic of *M.*

musculus and human kidneys, but instead results in near complete restoration of nephron structure and function.

4.5 Discussion

Using two different and highly aggressive forms of experimental kidney injury, we show that there was a near complete absence of interstitial renal fibrosis and a remarkable restoration of kidney function in *A. cahirinus* compared to either inbred (B6) or outbred (CD-1) strains of *M. musculus*. These remarkable differences in wound healing responses were not due to the failure of our injury models to produce acute tissue damage in *A. cahirinus* kidneys since histological and functional assays showed equivalent tissue injuries in the first 24-72h after UUO or IRI surgeries in both species. Particularly striking was the almost complete restoration of normal kidney function, assessed by blood urea nitrogen levels, by 14d after severe ischemia-reperfusion injury in *A. cahirinus* (**Fig 3G**). By contrast, in parallel experiments with *M. musculus*, injured kidneys were severely fibrotic and progressing rapidly towards complete kidney failure (**Fig 3G**).

Muroid rodents of the genus *Acomys* (Spiny mice) have evolved the ability to shed their dorsal skin to avoid predation and then to completely regenerate the lost skin tissues without fibrosis or scar formation (4-6). Mechanical and histological assays showed that *Acomys* skin is specialized to be structurally fragile and prone to tear under low tensile forces.[4] Therefore it cannot be assumed that the regenerative response to tissue injury in the skin, the first target of predatory attacks in the wild, necessarily extends to internal organs in *Acomys* species. A similar ear skin regenerative response was previously reported for the MRL/MpJ strain of mice.[14] However, multiple attempts to determine if regenerative wound healing extended to internal organs, including kidneys, of these mice were generally negative.[15-17] Thus, our results on the striking absence of fibrotic tissue formation in *A. cahirinus* kidney suggest that the regenerative wound

healing response previously described in the skin[4-6] may indeed be a systemic property that extends to critical internal organs in this species.

Acute kidney injury (AKI) initiates a fibrogenic cascade that leaves patients at high risk for developing chronic kidney disease and progressive loss of renal function.[18-20] Although elegant studies in *M. musculus* have produced substantial insights into the pathogenesis of renal fibrosis, translating these findings into therapeutic solutions has been poor. Wound healing in most adult mammals, including humans, is a process of repair that ultimately replaces functional tissue with a collagen-rich extracellular matrix resulting in a corresponding loss of organ function. By contrast, some fish and amphibian species can fully regenerate tissue damage and restore organ function after amputation or severe tissue injuries.[21] In the zebrafish kidney, for example, there is evidence of formation of new nephrons after gentamicin nephrotoxicity.[22] However, in adult mammals there are no reports of nephron formation *de novo* after kidney injury. We now provide evidence for a potentially transformative new mammalian model for kidney disease that has evolved a distinctly different wound healing response to kidney injury than the currently studied mouse, rat, or human, models. If confirmed for other organs, an in-depth analysis of the molecular basis for scar-free wound healing in Acomys species could be a gateway for novel anti-fibrotic therapies.

While our results demonstrating nearly complete restoration of kidney function after severe IRI injury (**Fig 3G**) are consistent with the likelihood there is nephron regeneration in *A. cahirinus*, they are not currently sufficient to prove this. In models of true vertebrate regeneration, such as axolotl limb,[23] zebrafish heart,[24] or *Acomys* skin,[5] tissue mass is removed by surgical resection and the lost tissue is fully restored both structurally and functionally. Although tissue damage produced by 40 minutes of renal ischemia/reperfusion is extensive (**Fig 3A-C, Fig 4)** and

restoration of kidney function is remarkably robust (**Fig 3G**), further work is required to definitively establish whether new nephrons are being formed in this model. The most robust phenotypic difference between *A. cahirinus* and *M. musculus* in our study is the near complete absence of fibrotic tissue formed in injured *A. cahirinus* kidneys after either UUO or IRI procedures. The extent to which lack of fibrosis is sufficient to explain the differences in wound healing outcomes reported here, or whether other changes in the *A. cahirinus* genome are essential for regenerative wound repair, are important questions for future work.

Acknowledgments

This work was supported by a grant from the W.M. Keck Foundation, the US National Institutes of Health grant 1R21OD-023838, the Loie Power Robinson Stem Cell & Regenerative Medicine Fund, and the Seattle Children's Research Institute.

Author Contributions

DMO, CMB, PW, NB, KB, AT, KS, JO, BN performed the experiments. DMO, DRB, MWM designed the experiments. DMO, CMB, MWM wrote the manuscript. DMO, KJM, MWM obtained funding for the project. All authors made critical input into editing the manuscript.

Author Information

Correspondence and requests for materials should be addressed to one of the following: DO (daryl.okamura@seattlechildrens.org); KJM (kathleen.millen@seattlechildrens.org); or MWM (mwm84@uw.edu).

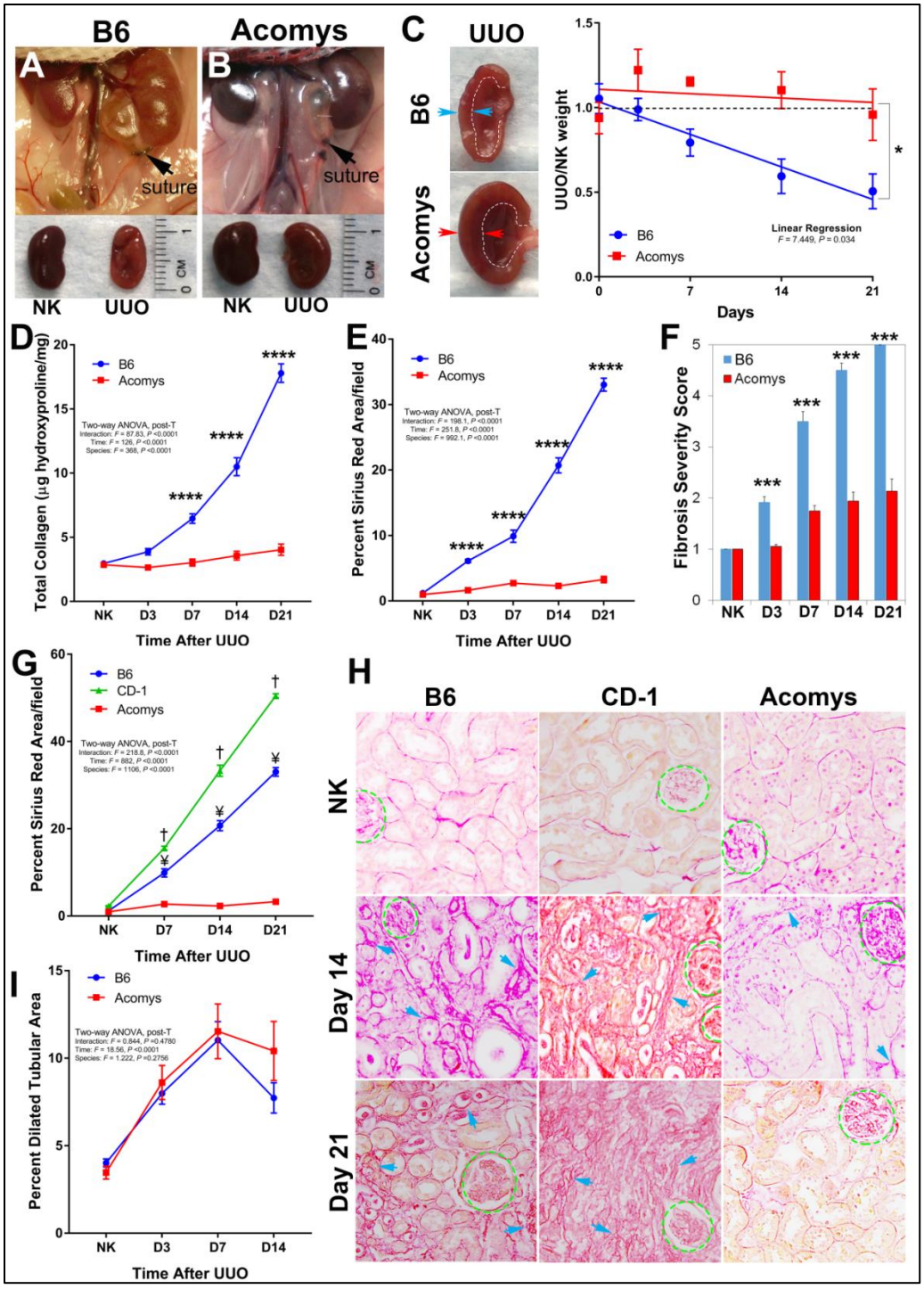

Figure 4. 1 Absence of fibrosis after severe obstructive injury in *A. cahirinus*. (A,B) (Upper) The ureter from the left kidney was ligated (arrow) to produce obstructive injury in both *A. cahirinus* and C57BL/6J (B6) mice. (Lower) Upon gross inspection, contralateral kidneys (NK) from the two species are similar in length but *A. cahirinus* UUO kidneys appear less damaged than B6 UUO kidneys after 14d of obstruction; **(C)** Left panel demonstrates preservation of parenchymal thickness (greater distance between arrows) in *A. cahirinus* kidney with renal pelvis noted by dotted white line. The graph demonstrates the best fit line of the ratio of UUO:NK kidneys

for each time point and the slopes were analyzed by linear regression (n=6-10/time point); **(D)** Total collagen content was measured by micrograms hydroxyproline per mg wet kidney weight. Graph summarizes total collagen measurement for B6 and *A. cahirinus* NK and UUO kidneys, (n=6-8/time point for each group); **(E)** Graph summarizes image analysis of picrosirius red staining for each UUO time point (n=6/time point for each group); **(F)** Masson trichrome sections were blindly scored for IFTA and inflammation (*see Methods*, n=6/time point for each group); Graph summarizes IFTA scores (fibrosis severity score) for each time point; **(G)** UUO was performed on outbred CD-1 mice (green)(n=3-4/time point) and the development of fibrosis was compared to B6 (blue) and *A. cahirinus* (red). Graph summarizes image analysis of picrosirius red staining with **(H)** representative digital images (400x). Glomeruli are outlined (dotted green). Arrows demonstrate Sirius red staining of interstitial matrix. **(I)** Dilated tubular area was measured in Masson trichrome sections; Graph summarizes image analysis of tubular dilation area in B6 and *A. cahirinus* after UUO (n=6-7/time point for each group): *B6 vs A. cahirinus*: * $p<0.05$, ** $p<0.01$, *** $p<0.001$, **** $p<0.0001$; *CD-1 vs A. cahirinus*: † $p<0.0001$; *B6 vs CD-1*: ¥ $p<0.0001$).

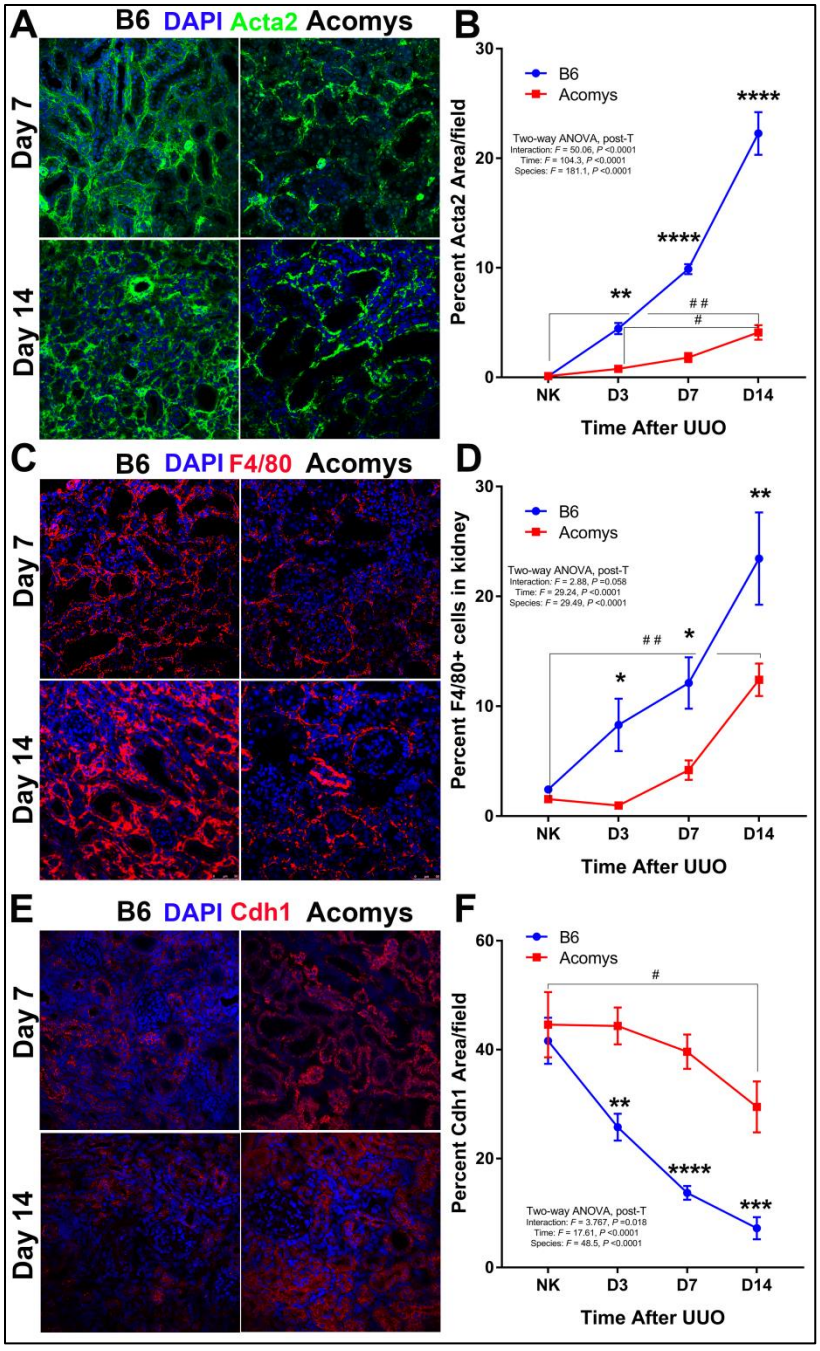

Figure 4. 2. Myofibroblast formation and macrophage infiltration do not generate a fibrotic response in *A. cahirinus*. (A) Smooth muscle alpha actin (*Acta2*) expression was investigated by immune-confocal microscopy at days 3, 7, and 14 after UUO. Representative digital images (400x) *Acta2* expression (green) for B6 and *A. cahirinus* at days 7 and 14 after UUO; **(B)** Graph summarizes image analysis for *Acta2* at each time point (n=6/time point for each group). **(C)** F4/80 macrophage infiltration was examined by confocal microscopy and quantified by flow cytometry. Representative digital images (400x) of F4/80 (red) expression at days 7 and 14 after UUO. **(D)** Flow cytometry was performed on single cell suspensions from whole kidney and analyzed for F4/80 expression. Graph summarizes percent F4/80+ cells at days 3, 7, and 14 after UUO analyzed

by FACS (n=3-4/time point per group). **(E)** Tubular integrity was examined by confocal microscopy for *Cdh1* (E cadherin). Representative digital images (400x) of *Cdh1* (red) expression for B6 and *A. cahirinus*. **(F)** Graph summarizes image analysis results for *Cdh1* levels at each time point (n=6/time point for each group). (B6 (blue) vs. *A. cahirinus* (red): *p<0.05, **p<0.01, ***p<0.001, ****p<0.0001; between time points # p<0.05, ## p<0.01)

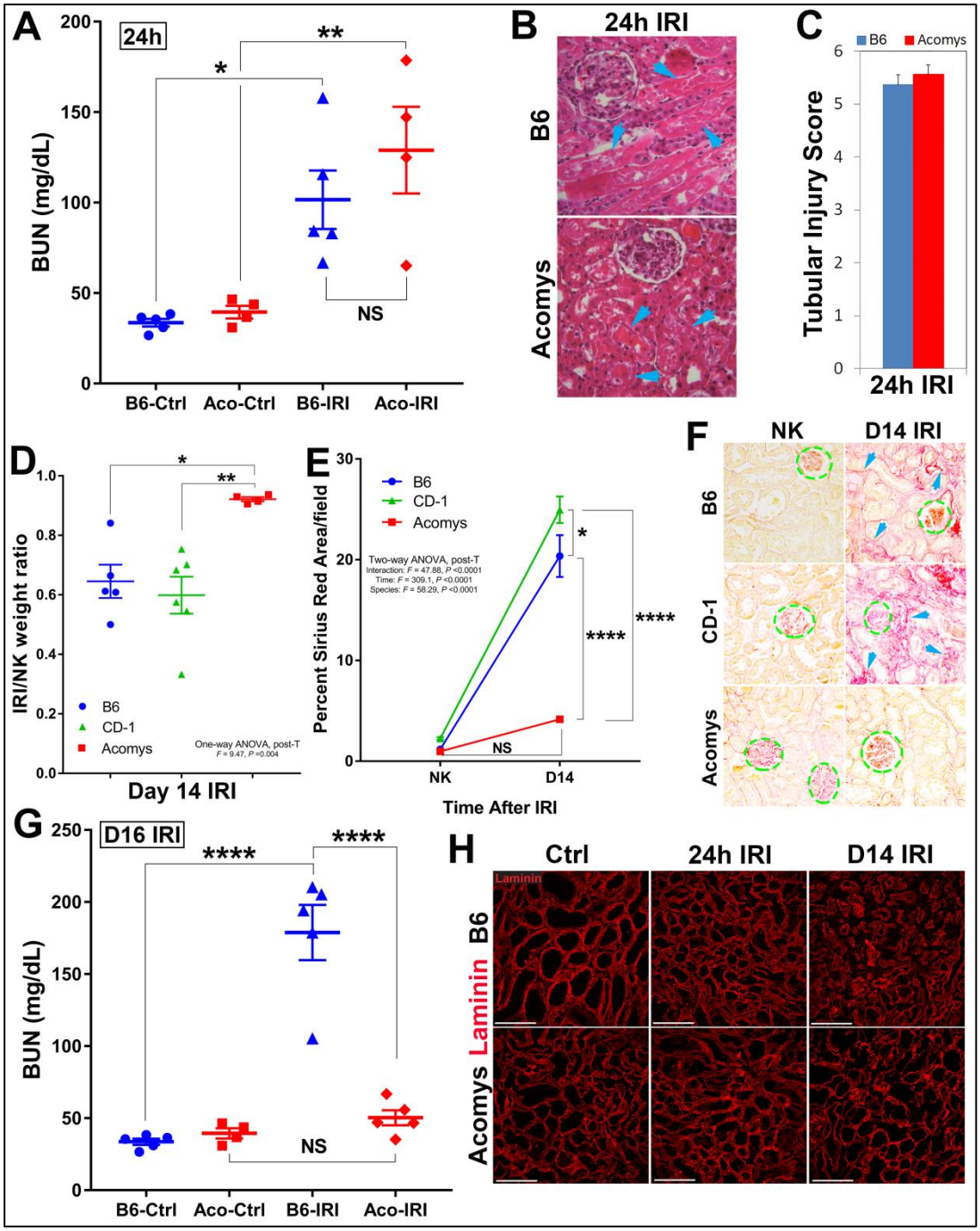

Figure 4. 3. Near complete recovery of nephron function after severe ischemic injury in *A. cahirinus*. **(A)** B6 and *A. cahirinus* underwent unilateral IRI (uni-IRI) with contralateral nephrectomy and sacrificed at 24h. BUN levels were assessed in uninjured animals (Ctrl) and those sacrificed at 24h (n=4-5/time point per group):): NS–not significant, * p<0.05, **p<0.01. Note that both species exhibited equivalent severe acute kidney damage in response to ischemic injury. **(B)** H&E stained sections were blindly scored for tubular injury (*see Methods*, n=4-5/group); Representative H&E digital images (400x) at 24h from IRI kidneys. Arrows indicate tubular casts and necrotic cell debris. **(C)** Graph summarizes tubular injury scores at 24h after IRI. **(D)** In order to determine effect of acute injury on repair, uni-IRI was performed without

nephrectomy on B6, CD-1, and *A.cahirinus*. Graph summarizes data on IRI/contralateral (NK) kidney weight ratio at time of sacrifice at 14d (n=4-6/group): * $p<0.05$, **$p<0.01$. **(E)** Graph summarizes image analysis of picrosirius red staining for each UUO time point (n=5-6/time point for each group); (B6 (blue), CD-1 (green), *A.cahirinus* (red): * $p<0.05$, ****$p<0.0001$. **(F)** Representative picrosirius red digital images (400x). Glomeruli are outlined (dotted green). Arrows demonstrate Sirius red staining of interstitial matrix. **(G)** In order to determine functional recovery, uni-IRI was performed, the contralateral kidney was removed at day 14 and kidney function was monitored until sacrifice at day 16. BUN levels were determined in uninjured animals (Ctrl) and those sacrificed at day 16, 2 days after contralateral nephrectomy (IRI). Note the nearly complete recovery of nephron function in the injured *A. cahirinus* kidneys at 16d compared to the high BUN levels indicative of kidney failure in B6 injured kidneys: NS-not significant, ****$p<0.0001$. **(H)** Laminin (red) immunostaining of tubular epithelial basement membrane architecture at days 0, 1, and 14 after IRI injury (400x; scale bars 100um). Note *A. cahirinus* kidney at day 14 (D14 IRI) strongly resembles uninjured kidney (Ctrl) in tubular basement membrane architecture, while B6 basement membranes demonstrate collapse and thickening with advancing fibrosis. Scale bars; 100μm.

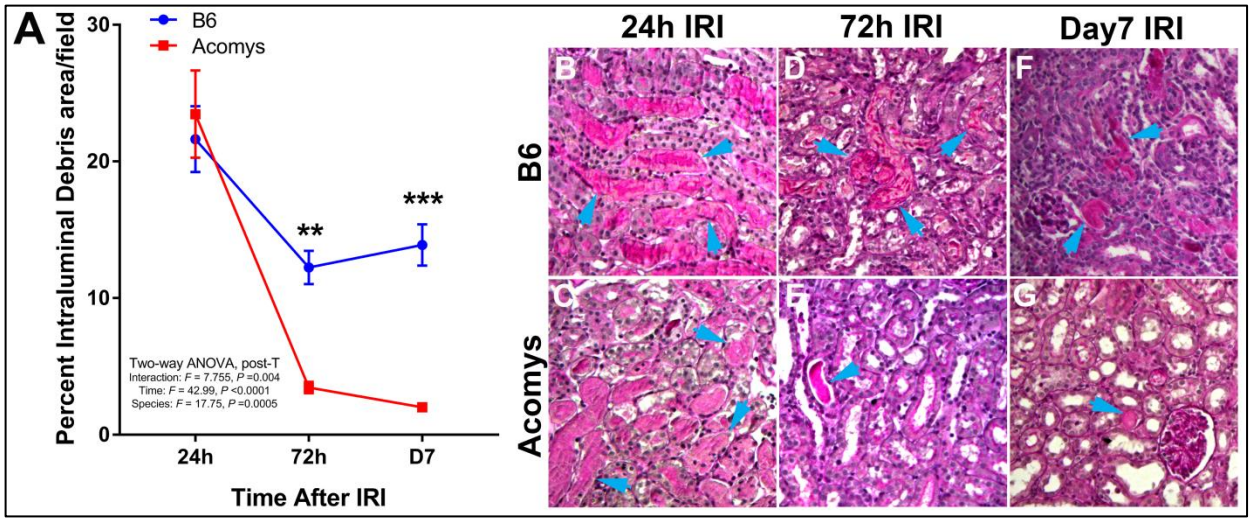

Figure 4.4 Rapid clearance of tubular debris after severe ischemic injury in *A. cahirinus*. Tubular casts and debris were identified on Periodic acid Schiff (PAS) stain in unilateral IRI kidneys at 24h, 72h, and 7 days in B6 and *A. cahirinus*.. **(A)** Graph summarizes image analysis results for tubular casts and intraluminal debris after IRI. (B6-blue, *A. cahirinus*-red; *B6 vs A. cahirinus*: **p<0.01, ***p<0.001). Representative fields from 200x images demonstrate representative tubular casts and intraluminal debris (arrow) in IRI kidneys at 24h **(B,C)**, 72h **(D,E)**, and 7 days **(F,G)** in B6 and *A. cahirinus* kidneys. Arrows demonstrate areas of intraluminal debris/casts.

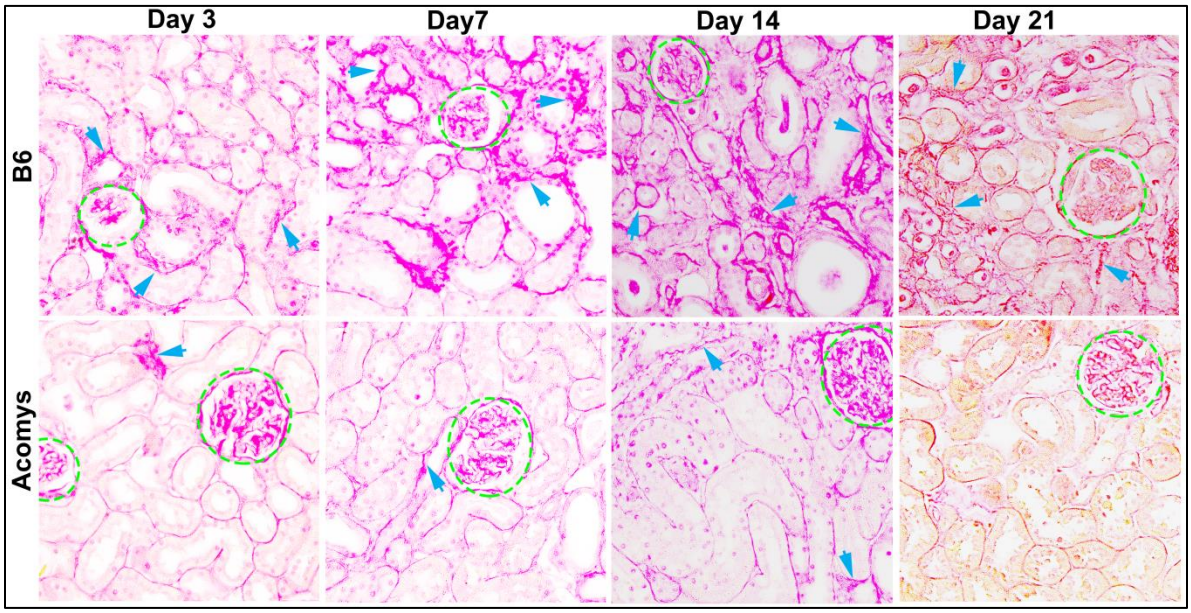

Figure 4.5 Supplemental 1. Picrosirius red staining in B6 and *A. cahirinus*. Representative picrosirius red digital images (400x) in B6 and *A. cahirinus* after UUO. Glomeruli are outlined (dotted green). Arrows demonstrate Sirius red staining of interstitial matrix.

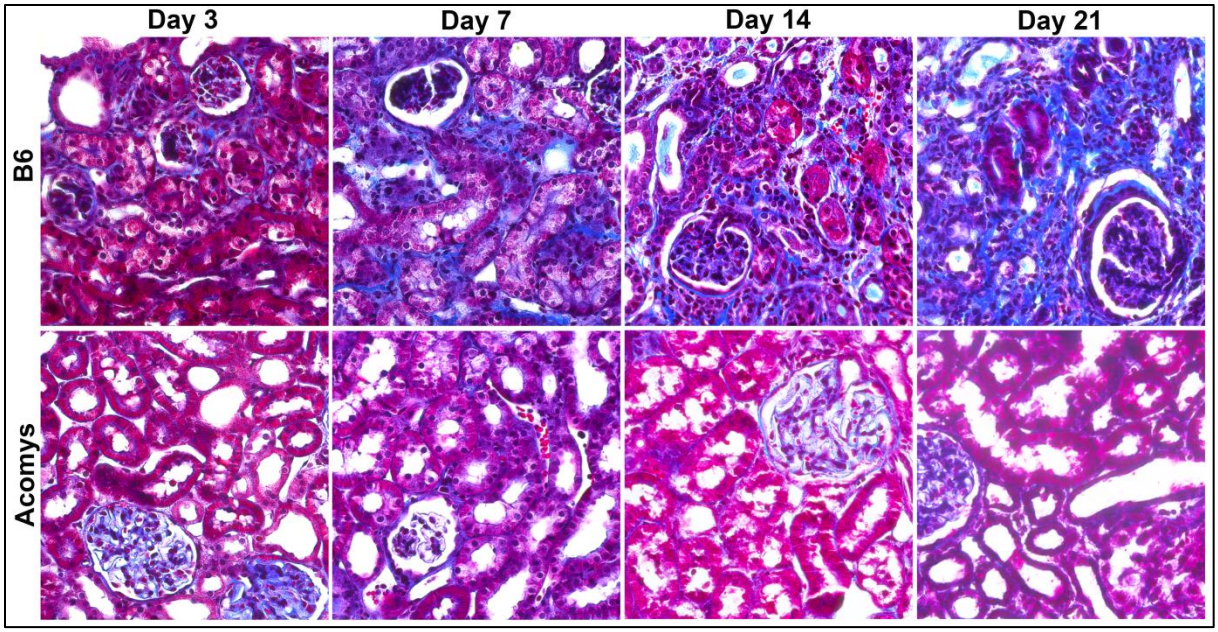

Figure 4.6 Supplemental Figure 2. Fibrosis severity score in B6 and *A. cahirinus*. Masson trichrome sections from were blindly scored for IFTA and inflammation (*see Methods*, n=6/time point for each group). Representative Masson trichrome digital images (400x) after UUO.

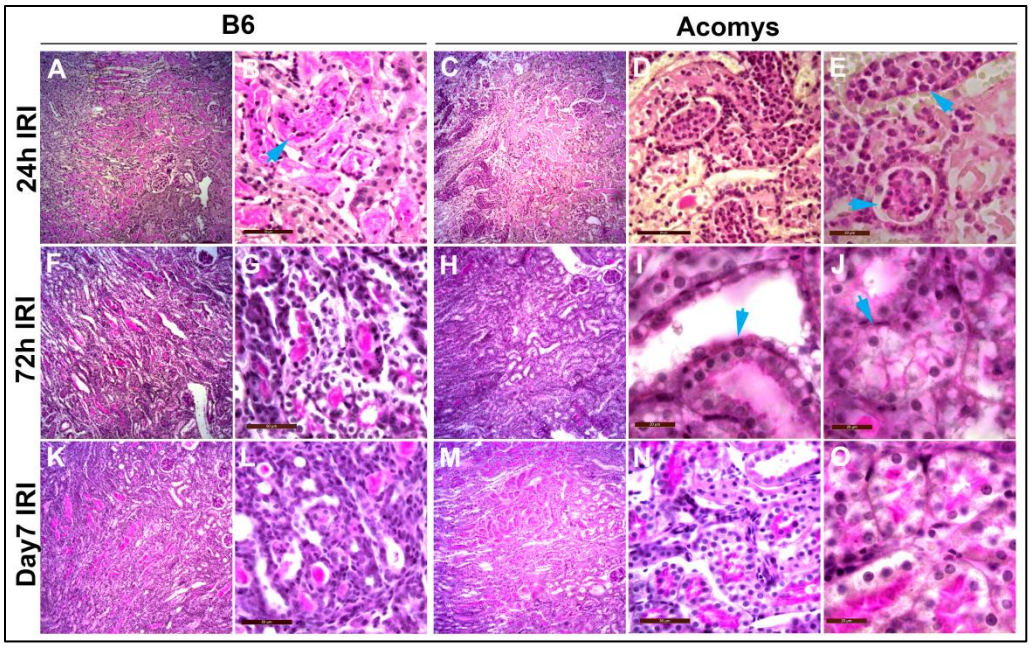

Figure 4.7 Supplemental Figure 3. Restoration of nephron structure after severe ischemic injury in *A. cahirinus*. Periodic acid Schiff (PAS) stain was performed on unilateral IRI kidneys at **(A-E)** 24h, **(F-J)** 72h, and **(K-O)** 7 days in B6 and *A. cahirinus*. Low power images (100x) in B6 demonstrate progression of **(A)** necrotic kidney injury to **(F,K)** tubular casts and loss of tubular structure with interstitial inflammation. In comparison, low power images in *A. cahirinus* show similar necrotic injury **(C),** with accelerated repair and restoration of nephron structure (**H,M)**. At 24h, polymorphonuclear cells can be seen in tubular lumens and casts in B6 (arrow **B**), and to an

even greater extent in *A. cahirinus* (arrows **E**). At 72h, tubular casts are nearly resolved (arrow, I), and flattened, dedifferentiated tubular epithelial cells **(I)** and tubular lumens in repair (arrow **J**) can be seen in *A. cahirinus*. At 7 days, tubular casts and interstitial inflammation remain in B6 **(L)**, compared to PAS positive brush border cells in *A. cahirinus* **(N,O)**.

4.6 References

1. Duffield, J.S. *et al*. Host responses in tissue repair and fibrosis. *Annu. Rev. Pathol.* **8,** 241-276 (2013).
2. Gurtner, G.C. *et al*. Wound repair and regeneration. *Nature* **453,** 314-321 (2008).
3. Humphreys, B.D. Mechanisms of renal fibrosis. *Annu. Rev. Physiol.* **80,** (2018).
4. Seifert, A.W. *et al*. Skin shedding and tissue regeneration in African spiny mice *(Acomys)*. *Nature* **489,** 561-565 (2012).
5. Gawriluk, T.R. *et al*. Comparative analysis of ear-hole closure identifies epimorphic regeneration as a discrete trait in mammals. *Nat. Commun.* **7,** 11164 (2016).
6. Matias Santos, D. *et al*. Ear wound regeneration in the African spiny mouse Acomys cahirinus. *Regeneration (Oxf)* **3,** 52-61 (2016).
7. Duffield, J.S. Cellular and molecular mechanisms in kidney fibrosis. *J. Clin. Invest.* **124,** 2299-2306 (2014).
8. Tapmeier, T.T. *et al*. Reimplantation of the ureter after unilateral ureteral obstruction provides a model that allows functional evaluation. *Kidney Int.* **73,** 885-889 (2008).
9. Liu, J. *et al*. Cell-specific translational profiling in acute kidney injury. *J. Clin. Invest.* **124,** 1242-1254 (2014).
10. Lin, S.L. *et al*. Bone marrow Ly6Chigh monocytes are selectively recruited to injured kidney and differentiate into functionally distinct populations. *J. Immunol.* **183,** 6733-6743 (2009).
11. Liu, W. *et al*. Dragon (repulsive guidance moledule GGMb) inhibits E-cadherin expression and induces apoptosis in renal tubular epithelial cells. *J. Biol. Chem.* **288,** 31528-31539 (2013).
12. Chaabane, W. *et al*. Renal functional decline and glomerulotubular injury are arrested but not restored by release of unilateral ureteral obstruction (UUO). *Am. J. Physiol. Renal Physiol.* **304,** F432-F439 (2013).
13. Zheng, G. *et al*. Alpha3 integrin of cell-cell contact mediates kidney fibrosis by integrin-linked kinase in proximal tubular E-cadherin-deficient mice. *Am. J. Pathol.* **186,**1847-1860 (2016).
14. Leferovich, J.M. *et al*. Heart regeneration in adult MRL mice. *Proc. Natl. Acad. Sci. USA* **98,** 9830-9835 (2001).
15. Robey, T.E., Murry, C.E. Absence of regeneration in the MRL/MpJ mouse heart following infarction or cryoinjury. *Cardiovasc. Pathol.* **17,** 6-13 (2008).
16. Oh, Y.S. *et al*. Scar formation after ischemic myocardial injury in MRL mice. *Cardiovasc. Pathol.* **13,** 203-206 (2004).
17. Iwata, T. *et al*. Aberrant macrophages mediate defective kidney repair that triggers nephritis in lupus-susceptible mice. *J. Immunol.* **188,** 4568-4580 (2012).
18. Chawla, L.S., *et al*. Acute kidney injury and chronic kidney disease as interconnected syndromes. *New Engl. J. Med.* **371,** 58-66 (2014).
19. Ferenbach DA, Bonventre JV. Mechanisms of maladaptive repair after AKI leading to accelerated kidney ageing and CKD. *Nat. Rev. Nephrol.* **11,** 264-276 (2015).
20. Liu, J. *et al*. Molecular characterization of the transition from acute to chronic kidney injury following ischemia/reperfusion. *JCI Insight* **2,** e94716 (2017).
21. Poss, K.D. Advances in understanding tissue regenerative capacity and mechanisms in animals. *Nat. Rev. Genet.* **11,** 710-722 (2010).

22. McCampbell, K.K., Wingert, R.A. New tides: using zebrafish to study renal regeneration. *Transl. Res.* **163,** 109-122 (2014).
23. Kragl, M. *et al*. Cells keep a memory of their tissue origin during axolotl limb regeneration. *Nature* **460,** 60-65 (2009).
24. Kikuchi, K. *et al*. Primary contribution to zebrafish heart regeneration by gata4(+) cardiomyocytes. *Nature* **464,** 601-605 (2010).
25. Pennathur, S. *et al*. The macrophage phagocytic receptor CD36 fibrogenic pathways on removal of apoptotic cells during chronic kidney injury. *Am J Pathol* **185**, 2232-2245 (2015).
26. Okamura, DM. *et al*. Cysteamine modulates oxidative stress and blocks myofibroblast activity in CKD. *J Am Soc Nephrol* **25**, 43-54 (2014).
27. Okamura, DM. *et al*. CD36 regulates oxidative stress and inflammation in hypercholesterolemic CKD. *J Am Soc Nephrol* **20**, 495-505 (2009).

Chapter 5 Discussion

5.1 Summary of Results

Terrestrial muriods of the genus *Acomys* (Spiny mice) have evolved the ability to undergo autotomy (self-amputation) to avoid predation. When undergoing tissue repair after injury, *Acomys* have been reported to restore tissue architecture in a scar free manner[1]. While scar-free wound repair is common in mammalian embryonic and post-natal development, the *Acomys* repair phenotype is the first to be described in adults[2]. Adult mammals, such as murine rodents and humans, normally repair injury by inflammation and scar tissue formation. Unfortunately, chronic scarring results in a pathological condition named fibrosis, which can lead to organ failure. The adult *Acomys* repair phenotype represents the first opportunity to develop evolutionary approaches to attenuate and/or inhibit the fibrotic repair response. Therefore, the goal of this thesis was to identify the cellular and molecular mechanisms that underlie *Acomys cahirinus* (Egyptian Spiny mice) scar-free wound repair. In accordance with this goal, I present the following discoveries:

1. *Acomys cahirinus* (genus *Acomys*) is a bonafide adult mammalian model of skin regeneration. In 2mm ear tissue biopsies, the adult *A. cahirinus* will undergo complete tissue restoration of hair follicles, muscle, peripheral nerves, cartilage, vasculature and pigmentation. This contrasts with the scar tissue repair response utilized by most adult terrestrial mammals.

2. *A. cahirinus* exhibits epimorphic based blastema formation during 2mm ear hole closure. The blastema is composed of a heterogenous population of at least two mesenchymal progenitor cell types. The two populations identified contain either the chondrogenic transcription factor SOX9 or the myogenic determination factor MYF5. These cell types together constitute the bulk of the blastema. However, these two populations display significant diversity in their behavior during both basal and injured states. $SOX9^{+}$ positive cells normally reside within the cartilage plate

in uninjured skin tissue. Upon injury, the $SOX9^{+}$ population migrates from the amputated cartilage bud and into the blastema. One potential SOX9 cell fate appears to be mature chondrocytes. In contrast, $MYF5^{+}$ cells appear *de novo* only during early (Weeks 1-2) periods of blastema formation.

3. *A. cahirinus* displays a conserved induction of myofibroblast-like cells during the initial ear punch injury response (Weeks 1-2). However, in contrast to CD1 *Mus musculus*, the myofibroblast population is transient with complete absence upon tissue closure. *A. cahirinus* myofibroblasts (MF) exhibit similar phenotypic markers as their *M. musculus* counterparts, such as ACTA2 (smooth muscle α-actin), EDA-Fibronectin (*Fn*), vimentin (*Vim*) and are negative for smooth muscle-myosin heavy chain (*Myh11*). In contrast to non-regenerating mammals, *A. cahirinus* displays non-canonical myofibroblast properties, such as not driving fibrosis. Instead, the transient *A. cahirinus* MF population provides important cues for re-vascularization and tissue patterning. In agreement, disrupting MF resolution with YAP-TEAD inhibitor verteporfin results in attenuated angiogenesis and delayed hole closure. MFs within the blastema contain several lineage restricted progenitor markers such as SOX9 and MYF5. This may indicate *A. cahirinus* MFs have evolved precursor cell properties.

4. Comparative analysis of isolated non-regenerative and regenerative dermal fibroblasts, both *in vivo* and i*n vitro*, indicates increased homeostatic capacity in *A. cahirinus* is cell autonomous. While *A. cahirinus* dermal fibroblasts contain the necessary signaling components to propagate TGFβ1 signaling, they resist upregulation of activated myofibroblast markers *Acta2* and *Col1a1* in contrast to their non-regenerator counterparts (**Fig 5.1.B,C**).

5. *A. cahirinus* demonstrates genome wide adaptations, in response to injury, that may be exploited to prevent fibrosis and promote scar-free wound repair. RNA-seq of both *in vivo* and *in*

vitro systems reveal a unique anti-fibrotic state with downregulation of known fibrotic signaling pathways (*Pdgfb, Tgfr2, Vegfd, Bmp4, Hgf)*. Instead, a transcriptional profile of genes and pathways (*Lif, Wnt11, Il18, Ctgf*) considered more embryogenesis-like and anti-inflammatory are observed.

6. An *A. cahirinus* specific adaptation includes altered regulatory control of the evolutionarily conserved organ size control pathway, Hippo-YAP. The pathway effector protein YAP (Yes Associated protein) and its biphasic reactivation are necessary in mediating *in vivo* regenerative skin repair (**Fig 5.1.B,C**). The first phase of YAP activation occurs during blastema formation (Weeks 1-2) where its roles include MF resolution, re-vascularization and wound closure. The secondary phase of YAP activity occurs during late stage tissue reconstitution (Weeks 4-5). YAP signaling during phase two is necessary for proper tissue reorganization by both proximal-distal patterning and cell fate decisions. At least three cell fates appear to be regulated by YAP activity. These cell types include chondrocytes, adipocytes and melanocytes. Limited inhibition of YAP signaling during these two phases is sufficient in converting *A. cahirinus* regenerative repair into a more *Mus*/human-like fibrotic response. These findings suggest *A. cahirinus* perceives injury as a loss of organ mass and polarity, which then stimulates healing by reactivating developmental organogenesis pathways. This behavior differs from scar-forming species, where YAP activity is inhibited, resulting in prolonged inflammation and scar tissue formation.

7. YAP localization dynamics in *A. cahirinus* are due to a novel high affinity PP2A-mediated surveillance protein complex that rapidly and specifically de-phosphorylates key amino acid regulatory residues. These targeted residues control YAP protein location (S127, cytoplasm) and stability (S381, degradation). This mechanism is context dependent because both *A.cahirinus*

and *M.musculus* inactivate YAP under conditions of cell-contact inhibition. The PP2A regulatory mechanism contributes to *in vivo* YAP activity during scar free healing (**Fig.5.1. B,C**).

8. Deciphering genomic adaptations that promote *A. cahirinus* scar free repair provides a potential blueprint for reducing human skin fibrosis. As a proof of concept, mimicking *Acomys* YAP nuclear retention in both murine and human fibroblasts is sufficient to attenuate TGFβ1-mediated myofibroblast activation *in vitro* (**Fig.5.1. B,C**).

9. In addition to external scar free wound repair, *A. cahirinus* resistance to scarring also extends to the kidney, an internal organ. Employing two aggressive models of murine kidney fibrosis, unilateral ureter obstruction (UUO) and ischemia reperfusion (IRI), both *A. cahirinus* and *M.musculus* exhibit similar early injury responses. These responses include tubular architectural disruption and perturbed filter function (increased BUN levels, Blood Urea Nitrogen). However, in contrast to the progressive kidney deterioration in *M.musculus*, *A. cahirinus* exhibits restoration of both kidney structure and function with no discernible fibrotic tissue. This result suggests *A. cahirinus* genomic adaptations may be systemic in nature.

10. The absence of fibrotic tissue and restored nephron function after both acute (IRI) and chronic (UUO) *A. cahirinus* kidney injury are not due to the lack of inflammation and myofibroblast activation. In agreement, macrophage and myofibroblast infiltration and activation both occur during injury. Rather, *A. cahirinus* displays homeostatic adaptations that attenuate their accumulation and fibrotic behavior.

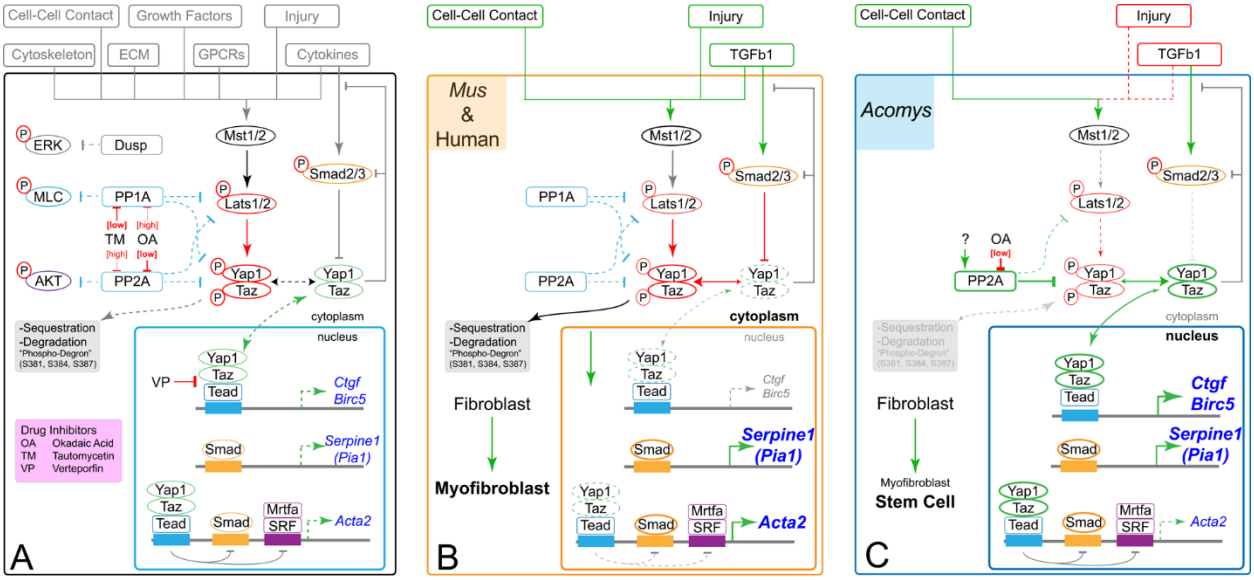

Figure 5.1 Diagram of *A. cahirinus* differential signaling pathways activity. (**A**) Diagram depicts cell signaling pathways tested across species *in vivo* and *in vitro*. (**B**) Schematic illustrates human and mouse dermal fibroblast signaling pathway outcomes in response to various stimuli. (C) Schematic illustrates *A. cahirinus* dermal fibroblast signaling pathway outcomes in response to various stimuli.

5.2 Future Directions:

These experiments have elucidated several *A. cahirinus*-specific cellular and molecular adaptations that are necessary to promote regenerative repair. However, many questions remain unanswered.

Determine if *Acomys* adult regenerative potential is an extension of developmentally regulated processes observed in early mammalian embryogenesis. The adult *Acomys* ability to regenerate all components of the skin organ after injury is stunning. Intriguingly, the observed behavior mirrors dermal injury repair demonstrated in most mammalian fetuses[3-6].

While the similarities are striking, it remains an open question if *Acomys* regeneration is truly redeployment of embryonic developmental pathways. To test this, one would have to identity both cellular identity and signaling pathway differences-similarities at the single cell level. This can be done by molecular profiling both regenerative and non-regenerative tissues. While it is

technically challenging to obtain enough tissue from the embryo at the desired injury time points, the advent of single cell RNA sequence analysis now allows profiling with relatively few cells. Theoretically, the hypothesis can be tested by isolating tissue from both homeostatic and timed injury tissue from embryonic/adult *Acomys*, *Mus*, Human and axotyl limbs. Single cell RNA-seq profiling would allow one to build an organ specific "cellulome" across species, developmental age and time. One would anticipate the analysis to reveal significant overlap in both cellular composition and intercellular communication between regenerative adult *Acomys*, adult axolotyl, and embryonic *Mus* and Human when compared to non-regenerative *Mus* and Human cells. Regenerator species may display an immature myofibroblasts transcriptome profile (decreased actin organizational components, ECM, fibrokine production) compared to terminally differentiated adult myofibroblasts[7-9]. Playing devil's advocate, it could also be observed regenerator species display no similarity to one another with each species demonstrating disparate molecular profiles. Regardless, this type of analysis would provide new insights into the behavior and potential function of each cell type across a wide range of regenerative and scar forming conditions.

Identify Yap-transcriptional factor interactions and downstream transcriptional targets. Pharmacological inhibition of YAP reveals transcription factor binding specificity is an important element in *Acomys* regenerative repair. However, it remains unresolved what transcriptional factors YAP is physical interacting with in the *Acomys* genomic landscape. Considering the evolutionary history of Hippo-YAP, it would not be surprising to find YAP is interacting with several transcription factors during *Acomys* repair. TEAD family (TEAD1-4), SMAD2/3, AP-1, KLF4, CREB and RUNX family are just a small number of YAP transcriptional

binding partners[10-15]. The verteporfin study suggest one if not all TEAD factors are necessary during *Acomys* wound repair[16].

Clarifying the YAP-transcription factor (TF) interaction differences in both *Mus* and *Acomys* will be necessary, as these interactions determine cis-gene target specificity and trans-regulatory activity. While many genes are considered canonical YAP targets, such as *Cyr61*, *Ctgf* and *Areg*, an important aspect that deserves attention will be to identify cell type specific YAP targets[17,18]. The importance of identifying novel cell specific targets is illustrated from a recent paper by Zhao *et al*[19]. Their studies elucidated *Ccl2* and *Csf1* are hepatocyte specific YAP transcriptional targets. These genes are involved in macrophage recruitment and polarization. This study is intriguing because it demonstrates nuclear YAP^+ tumor hepatocytes actively recruit polarized macrophages to protect themselves from adaptive immune clearance. This is the first report of YAP oncogenic activity conferring selective pressure not only within the cell itself but also by modulating its surrounding microenvironment (non-cell autonomous)[19]. This has clear implication in regenerative biology as *Acomys* myofibroblasts and mesenchymal fibroblasts are the main YAP^+ cell types within the *Acomys* blastema. Nuclear YAP^+ mesenchymal cells may exhibit specific YAP target genes that act not only cell autonomously but also in a non-cell autonomous manner. YAP dependent paracrine activity could be an important component of initializing resident and recruited neighboring cells to begin the regenerative response. YAP ChiP-seq can be used to identify both YAP novel and canonical gene targets in a cell specific manner. TEAD factors ChiP-seq could also be done concurrently to compare genomic YAP-TEAD binding sites. This could function as a preliminary study to begin dissecting TEAD dependent or independent YAP target genes within the *Acomys* system. In the age of CRISPR/Cas9, gene editing techniques can be employed to identify novel YAP transcriptional partners and targets in cell

culture systems. Manipulating *Yap* gain or loss of function by Cas9, followed by comparative RNA-seq, may offer insight to several stimuli specific targets. Co-IP of YAP followed by mass spec in both *Acomys in vivo* and *in vitro* systems will be important in identifying YAP-TF complexes that are critical in mediating nuclear activity[20].

Determine Yap protein-protein complexes formed in *Acomys* cells and their association with PP2A phosphatase complex. The data presented establish both *Acomys* dermal fibroblasts and tubular epithelia in-*vitro* maintain dephosphorylated, nuclear active YAP in a context dependent manner. This contrasts with their scar forming mammalian counterparts (*Mus*/human), which accumulate inactive phospho-YAP. Nuclear retention of *Acomys* YAP is due to robust dephosphorylation activity of a PP2A holoenzyme, a serine/threonine phosphatase. Intriguingly, upstream negative regulator LATS1/2 also exhibits similar kinetics of PP2A mediated dephosphorylation. The relationship between *Acomys* PP2A/YAP/LATS1/2 suggest there may be a unique species-specific protein complex designed to regulate Hippo activity. While PP2A is known to interact with both YAP and LATS1/2 independently[20-22], no study has shown a complex interaction with both simultaneously.

PP2A is a heteromeric protein complex with three distinct modules that must first be assembled for functional biochemical activity. These three subunits consist of the catalytic core (PP2AC) which contains the hydrolysis enzymatic activity, the scaffold domain that serves as the protein backbone (PP2AA) and the regulatory beta subunit domain (PP2AB) which determines substrate specificity[23]. To make matters more complicated, PP2A heterotrimeric phosphatases can also associate with several super-complex structures, such as the STRIPAK family (striatin-interacting phosphatase and kinase)[22,24,25].

Western blot analysis indicates no differences in the protein level nor localization of the catalytic domain (PP2AC) in *Mus* and *Acomys* (**Data not shown**). No overt species differences in YAP amino acid sequence and phosphorylation capabilities are observed. Therefore, increased dephosphorylation kinetics may be due to difference in combinatorial swapping of subunits that alter substrate specificity. These could also include factors, such as the beta domain or supra-complexing partners themselves. *Mus* alone contains four families of the beta subunit with 16 regulatory domains available for combinatorial activity[26,27]. To begin elucidating partners of the *Acomys* YAP-LATS1/2-PP2A phosphatase complex, an unbiased mass spectrometry proteomic approach would be needed. With serine/threonine inhibitor studies identifying the PP2A phosphatase culprit, a co-immunoprecipitation approach can help identify key interactors[28,29]. Employing the okadaic acid (OA) pulse chase assay, reciprocal Co-IP mass spec of YAP and PP2A, in both *Acomys* and *Mus,* may allow one to build a species-specific proteome interaction map that might offer insights into YAP-PP2A interactions[24,30]. Comparative proteomics can be used to investigate if *Acomys* evolved novel species-specific "healing" proteins that are absent in *Mus* and Human. While highly unlikely, this possibility is not without merit. A good example is the cleavable cell surface glycoprotein Prod1. In screening assays for secreted molecules required for salamander limb bud regeneration, the Brockes lab identified the three-finger protein superfamily member that remains salamander restricted[31,32].

With YAP activity intricately linked to *Acomys* regeneration, elucidating how *Acomys* have manipulated PP2A mediated dephosphorylation of YAP may provide therapeutic avenues to inhibit fibrosis and promote scar-free wound repair.

Identifying novel genomic regulators of *Acomys* myofibroblast formation: This study, comparing *Acomys* and *Mus* skin tissue injuries, demonstrates *Acomys* display altered functional

properties in the myofibroblast population. Myofibroblast function in adult mammalian wounding includes excessive collagen deposition, fibrokine secretion, and contractile activity that is conferred by *de novo Acta2* expression. In contrast, *Acomys* MFs are phenotypically similar but display disparate functions both *in vitro* and *in vivo*. These disparities result in an immature myofibroblast-like state that does not contribute to scar tissue formation. Rather, their function appears to promote successful tissue reconstitution. The key question then becomes how do *Acomys* alternatively regulate the myofibroblasts to promote regenerative repair? To answer this question, a comparative analysis of myofibroblast cell populations at the genomic level would be appropriate. It is reasonable to hypothesize that differences in myofibroblast functions are due to differential regulation at both the transcriptional and epigenetic level. The greatest evidence for this speculation is that *Acomys* do not upregulate ACTA2 protein in response to TGFβ1.

Because *Acta2* expression is a common element in discriminating for myofibroblast populations, this phenomenon can serve as a lynchpin to begin dissecting molecular mechanisms[9,33,34]. An expansive knowledge base is already available regarding transcriptional regulatory mechanisms in the *Acta2* promoter region.

To identify differential regulation of *Acta2* expression, *Acomys* and murine myofibroblasts can be isolated from injured tissue. Isolated species specific myofibroblasts can then be utilized for chromatin immunoprecipitation (ChIP) analysis. With the *Acta2* promoter highly characterized, it would be interesting to compare transcription factor occupancy of known myofibroblasts mediators such as SRF, SMAD2/3, TEADS and MRTF-A/B[35-38].

It is important to remember myofibroblast differentiation and activation is also dependent on repressive transcriptional mechanisms. Factors such as Kruppel like factor 4 (KLF4), NKX2.5, peroxisome proliferator–activated receptor (PPAR), and Y-box binding protein either directly or

indirectly compete for binding occupancy within promoter control elements (**See Fig 1.4**)[39-42]. Characterizing enhancer and repressor sites present in stretches within or near myofibroblast specific gene promoters could offer some regulatory insight.

Chromatin modifications near critical myofibroblast genes markers could limit TF interactions or repress transcriptional accessibility. Therefore, investigating the epigenetic landscape of the *Acomys* myofibroblast populations may also be an important direction. Histone medications, such as acetylation or methylation, modulate chromatin structure. Structure and accessibility can be assessed by ChiP techniques. Focusing on post translational modifications such as acetylated histones H3 and H4, one could identify epigenetic modifications associated with *Acta2* regulatory region[43-45]. **A**ssay for **T**ransposase-**A**ccessible **C**hromatin using **seq**uencing (ATAC-seq) to elucidate global genomic accessibility could also be used.

Identify cellular mechanisms of *Acomys* wound repair: An important goal for the *Acomys* model will be determine the cellular mechanisms that are necessary for tissue reconstitution. A variety of cellular strategies can be used either singly or in combination to achieve regeneration. These strategies include pluripotent stem cells, lineage restricted progenitor cells, de-differentation and or transdifferentation (**Fig.1.1**)[46-48]. In respect to the *Acomys* model, it will be important to investigate the fate of the fibroblast-myofibroblast phenotype. The mesenchymal population demonstrate unforseen heterogenity with a number of cells showing expression of progenitor TFs, such as SOX9 chondrocyte and MYF5 myogenic specification factors[49,50]. It becomes enticing to speculate that the *Acomys* myofibroblasts are not being eliminated but rather actively contributing to new tissue formation. Unfortunately, we cannot conclude this because the *Acomys* is a non-model system, thus lacking the proper lineage tracing tools.

While lacking an *Acomys* transgenic model, it is theoretically possible to begin asking these questions using viral based delivery systems. A strategy to examine myofibroblast tissue contributions can be determined by employing a cell specific CRE based tracing system. This would employ an $MCAT^{CREER}$/ROSAConfetti reporter construct virally delivered into an uninjured *Acomys* ear[51]. MCAT elements are promoter-enhancer regions of many cardiac, smooth, and skeletal muscle-specific genes. The *Acta2* promoter contains several of these elements, which are critical for driving gene expression. What makes this element attractive is that expression in smooth muscle cells during embryogenesis is MCAT dependent but independent at adulthood. However, MCAT elements are required for *Acta2* expression in activated adult dermal myofibroblasts[37]. Therefore, MCAT elements driving CRE mediated recombination of the confetti reporter should selectively label myofibroblasts in a clonal fashion. After injecting tamoxifen to activate the reporter in early injuries, one could observe if fluorescently labelled myofibroblast clones are incorporated into newly regenerated structures such as the cartilage, muscle, vasculature and interstitial mesenchyme.

One could also ask if progenitor marker positive cells constitute a distinct lineage-restricted population or if these single cell types have the potential to form all the necessary cell types. A promoter based CRE/LoxP system delivered with a ROSAmT/mG allows a cell population to be permanently labelled if expressing a gene of interest[52]. Identifying the cellular strategies necessary for adult *Acomys* scar free healing will be an important next step and may prevent or attenuate human imperfect scar healing.

Identify if *Acomys* genomic adaptations to resist scarring extend to other organ systems: With the discovery that attenuated scar formation in skin also extends to the kidney, the most obvious question now becomes how many other organ systems are included. This question

has clear clinical implications with fibrosis occuring in almost all internal organs[53,54]. Perhaps the most clinically relevant are fibropathologies that occur in both the heart and lungs. Luckily many of these injury models already exist and can readily be utilized in the *Acomys*. Injuries, such as myocardial infarction and bleomycin inhalation, could be employed to measure both loss of function and fibrotic scarring in the heart and lung respectively. Any model of organ damage would be sufficient but the questions remain the same. How systemic is the anti-scarring phenotype in *Acomys* and do theses injuries heal in a fundamentally different way from *Mus*? Understanding the extent of *Acomys* scar free wound healing is one of the first steps in making strides for anti-fibrotic treatments. It should be stated that these models only test if *Acomys* resist scar tissue formation. Therefore, the true test to identify regenerative potential in individual organs would be to dissect out functional tissue. *Acomys* cardiac apex, nephron or lung lobe resection would be excellent models to test if genomic adaptations that promote skin regenerative repair extend to other organs

In conclusion, the findings presented in this thesis have important rammifications for the discovery of long sought anti-fibrotic treatments. Since *Acomys* are mammals, molecular adaptations that promote regeneration are likely to be directly translatable to human biology. When comparing adult mammals that undergo scar tissue formation to those that utilize regeneration, Hippo-YAP nuclear reactivation, mediated by a PP2A phosphatase underlies many aspects of successful *Acomys* regenerative repair. Determining specific mechanisms, and ultimately theurapuetic drugs, that can reactivate YAP activity during human wounding, where YAP in inhibited, may provide avenues to attenuate scar tissue accumulation in major organs. With current therapies to treat human fibrotic diseases inadaquate, understanding the *Acomys* regenerative repair process provides the first step for the development of long-sought anti-fibrotic remedies for patients currently afflicted with pathological fibrotic diseases.

5.3 References

1 Seifert, A. W. *et al*. Skin shedding and tissue regeneration in African spiny mice (Acomys). *Nature* **489**, 561-565, doi:10.1038/nature11499 (2012).

2 Gawriluk, T. R. *et al*. Comparative analysis of ear-hole closure identifies epimorphic regeneration as a discrete trait in mammals. *Nat Commun* **7**, 11164, doi:10.1038/ncomms11164 (2016).

3 Spurlin, J. W., 3rd & Lwigale, P. Y. Wounded embryonic corneas exhibit nonfibrotic regeneration and complete innervation. *Invest Ophthalmol Vis Sci* **54**, 6334-6344, doi:10.1167/iovs.13-12504 (2013).

4 Rowlatt, U. Intrauterine wound healing in a 20 week human fetus. *Virchows Arch A Pathol Anat Histol* **381**, 353-361 (1979).

5 Longaker, M. T. *et al*. Adult skin wounds in the fetal environment heal with scar formation. *Ann Surg* **219**, 65-72 (1994).

6 Porrello, E. R. *et al*. Transient regenerative potential of the neonatal mouse heart. *Science* **331**, 1078-1080, doi:10.1126/science.1200708 (2011).

7 Bhattacharyya, S. *et al*. FibronectinEDA promotes chronic cutaneous fibrosis through Toll-like receptor signaling. *Sci Transl Med* **6**, 232ra250, doi:10.1126/scitranslmed.3008264 (2014).

8 Hinz, B., Celetta, G., Tomasek, J. J., Gabbiani, G. & Chaponnier, C. Alpha-smooth muscle actin expression upregulates fibroblast contractile activity. *Mol Biol Cell* **12**, 2730-2741 (2001).

9 Hinz, B., Dugina, V., Ballestrem, C., Wehrle-Haller, B. & Chaponnier, C. Alpha-smooth muscle actin is crucial for focal adhesion maturation in myofibroblasts. *Mol Biol Cell* **14**, 2508-2519, doi:10.1091/mbc.E02-11-0729 (2003).

10 Azzolin, L. *et al*. YAP/TAZ incorporation in the beta-catenin destruction complex orchestrates the Wnt response. *Cell* **158**, 157-170, doi:10.1016/j.cell.2014.06.013 (2014).

11 Zhao, B. *et al*. TEAD mediates YAP-dependent gene induction and growth control. *Genes Dev* **22**, 1962-1971, doi:10.1101/gad.1664408 (2008).

12 Basu, S., Totty, N. F., Irwin, M. S., Sudol, M. & Downward, J. Akt phosphorylates the Yes-associated protein, YAP, to induce interaction with 14-3-3 and attenuation of p73-mediated apoptosis. *Mol Cell* **11**, 11-23 (2003).

13 Beyer, T. A. *et al*. Switch Enhancers Interpret TGF-beta and Hippo Signaling to Control Cell Fate in Human Embryonic Stem Cells. *Cell Rep* **5**, 1611-1624, doi:10.1016/j.celrep.2013.11.021 (2013).

14 Mahoney, W. M., Jr., Hong, J. H., Yaffe, M. B. & Farrance, I. K. The transcriptional co-activator TAZ interacts differentially with transcriptional enhancer factor-1 (TEF-1) family members. *Biochem J* **388**, 217-225, doi:10.1042/bj20041434 (2005).

15 Vitolo, M. I. *et al*. The RUNX2 transcription factor cooperates with the YES-associated protein, YAP65, to promote cell transformation. *Cancer Biol Ther* **6**, 856-863 (2007).

16 Liu-Chittenden, Y. *et al*. Genetic and pharmacological disruption of the TEAD-YAP complex suppresses the oncogenic activity of YAP. *Genes Dev* **26**, 1300-1305, doi:10.1101/gad.192856.112 (2012).

17 Shimomura, T. *et al*. The PDZ-binding motif of Yes-associated protein is required for its co-activation of TEAD-mediated CTGF transcription and oncogenic cell transforming activity. *Biochem Biophys Res Commun*, doi:10.1016/j.bbrc.2013.12.100 (2013).

18 Lai, D., Ho, K. C., Hao, Y. & Yang, X. Taxol resistance in breast cancer cells is mediated by the hippo pathway component TAZ and its downstream transcriptional targets Cyr61 and CTGF. *Cancer Res* **71**, 2728-2738, doi:10.1158/0008-5472.can-10-2711 (2011).
19 Guo, X. *et al*. Single tumor-initiating cells evade immune clearance by recruiting type II macrophages. *Genes Dev* **31**, 247-259, doi:10.1101/gad.294348.116 (2017).
20 Kohli, P. *et al*. Label-free quantitative proteomic analysis of the YAP/TAZ interactome. *Am J Physiol Cell Physiol* **306**, C805-818, doi:10.1152/ajpcell.00339.2013 (2014).
21 Schlegelmilch, K. *et al*. Yap1 acts downstream of alpha-catenin to control epidermal proliferation. *Cell* **144**, 782-795, doi:10.1016/j.cell.2011.02.031 (2011).
22 Bae, S. J. *et al*. SAV1 promotes Hippo kinase activation through antagonizing the PP2A phosphatase STRIPAK. *Elife* **6**, doi:10.7554/eLife.30278 (2017).
23 Lambrecht, C., Haesen, D., Sents, W., Ivanova, E. & Janssens, V. Structure, regulation, and pharmacological modulation of PP2A phosphatases. *Methods Mol Biol* **1053**, 283-305, doi:10.1007/978-1-62703-562-0_17 (2013).
24 Couzens, A. L. *et al*. Protein interaction network of the mammalian Hippo pathway reveals mechanisms of kinase-phosphatase interactions. *Sci Signal* **6**, rs15, doi:10.1126/scisignal.2004712 (2013).
25 Hauri, S. *et al*. Interaction proteome of human Hippo signaling: modular control of the co-activator YAP1. *Mol Syst Biol* **9**, 713, doi:10.1002/msb.201304750 (2013).
26 Kamibayashi, C. *et al*. Comparison of heterotrimeric protein phosphatase 2A containing different B subunits. *J Biol Chem* **269**, 20139-20148 (1994).
27 McCright, B. & Virshup, D. M. Identification of a new family of protein phosphatase 2A regulatory subunits. *J Biol Chem* **270**, 26123-26128 (1995).
28 Mitsuhashi, S. *et al*. Tautomycetin is a novel and specific inhibitor of serine/threonine protein phosphatase type 1, PP1. *Biochem Biophys Res Commun* **287**, 328-331, doi:10.1006/bbrc.2001.5596 (2001).
29 Runnegar, M., Berndt, N., Kong, S. M., Lee, E. Y. & Zhang, L. In vivo and in vitro binding of microcystin to protein phosphatases 1 and 2A. *Biochem Biophys Res Commun* **216**, 162-169 (1995).
30 Fernandez, J. J., Candenas, M. L., Souto, M. L., Trujillo, M. M. & Norte, M. Okadaic acid, useful tool for studying cellular processes. *Curr Med Chem* **9**, 229-262 (2002).
31 Garza-Garcia, A., Harris, R., Esposito, D., Gates, P. B. & Driscoll, P. C. Solution structure and phylogenetics of Prod1, a member of the three-finger protein superfamily implicated in salamander limb regeneration. *PLoS One* **4**, e7123, doi:10.1371/journal.pone.0007123 (2009).
32 da Silva, S. M., Gates, P. B. & Brockes, J. P. The newt ortholog of CD59 is implicated in proximodistal identity during amphibian limb regeneration. *Dev Cell* **3**, 547-555 (2002).
33 Darby, I., Skalli, O. & Gabbiani, G. Alpha-smooth muscle actin is transiently expressed by myofibroblasts during experimental wound healing. *Lab Invest* **63**, 21-29 (1990).
34 Goffin, J. M. *et al*. Focal adhesion size controls tension-dependent recruitment of alpha-smooth muscle actin to stress fibers. *J Cell Biol* **172**, 259-268, doi:10.1083/jcb.200506179 (2006).
35 Small, E. M. *et al*. Myocardin-related transcription factor-a controls myofibroblast activation and fibrosis in response to myocardial infarction. *Circ Res* **107**, 294-304, doi:10.1161/circresaha.110.223172 (2010).

36 Johnson, L. A. *et al*. Novel Rho/MRTF/SRF inhibitors block matrix-stiffness and TGF-beta-induced fibrogenesis in human colonic myofibroblasts. *Inflamm Bowel Dis* **20**, 154-165, doi:10.1097/01.mib.0000437615.98881.31 (2014).

37 Gan, Q., Yoshida, T., Li, J. & Owens, G. K. Smooth muscle cells and myofibroblasts use distinct transcriptional mechanisms for smooth muscle alpha-actin expression. *Circ Res* **101**, 883-892, doi:10.1161/circresaha.107.154831 (2007).

38 Hu, B., Wu, Z. & Phan, S. H. Smad3 mediates transforming growth factor-beta-induced alpha-smooth muscle actin expression. *Am J Respir Cell Mol Biol* **29**, 397-404, doi:10.1165/rcmb.2003-0063OC (2003).

39 Subramanian, S. V. *et al*. Induction of vascular smooth muscle alpha-actin gene transcription in transforming growth factor beta1-activated myofibroblasts mediated by dynamic interplay between the Pur repressor proteins and Sp1/Smad coactivators. *Mol Biol Cell* **15**, 4532-4543, doi:10.1091/mbc.E04-04-0348 (2004).

40 Hu, B. *et al*. Gut-enriched Kruppel-like factor interaction with Smad3 inhibits myofibroblast differentiation. *Am J Respir Cell Mol Biol* **36**, 78-84, doi:10.1165/rcmb.2006-0043OC (2007).

41 Hu, B., Wu, Y. M., Wu, Z. & Phan, S. H. Nkx2.5/Csx represses myofibroblast differentiation. *Am J Respir Cell Mol Biol* **42**, 218-226, doi:10.1165/rcmb.2008-0404OC (2010).

42 Burgess, H. A. *et al*. PPARgamma agonists inhibit TGF-beta induced pulmonary myofibroblast differentiation and collagen production: implications for therapy of lung fibrosis. *Am J Physiol Lung Cell Mol Physiol* **288**, L1146-1153, doi:10.1152/ajplung.00383.2004 (2005).

43 Zhang, X., Liu, H., Hock, T., Thannickal, V. J. & Sanders, Y. Y. Histone deacetylase inhibition downregulates collagen 3A1 in fibrotic lung fibroblasts. *Int J Mol Sci* **14**, 19605-19617, doi:10.3390/ijms141019605 (2013).

44 Perugorria, M. J. *et al*. Histone methyltransferase ASH1 orchestrates fibrogenic gene transcription during myofibroblast transdifferentiation. *Hepatology* **56**, 1129-1139, doi:10.1002/hep.25754 (2012).

45 Hu, B., Gharaee-Kermani, M., Wu, Z. & Phan, S. H. Essential role of MeCP2 in the regulation of myofibroblast differentiation during pulmonary fibrosis. *Am J Pathol* **178**, 1500-1508, doi:10.1016/j.ajpath.2011.01.002 (2011).

46 Jopling, C. *et al*. Zebrafish heart regeneration occurs by cardiomyocyte dedifferentiation and proliferation. *Nature* **464**, 606-609, doi:10.1038/nature08899 (2010).

47 Sandoval-Guzman, T. *et al*. Fundamental differences in dedifferentiation and stem cell recruitment during skeletal muscle regeneration in two salamander species. *Cell Stem Cell* **14**, 174-187, doi:10.1016/j.stem.2013.11.007 (2014).

48 Kragl, M. *et al*. Cells keep a memory of their tissue origin during axolotl limb regeneration. *Nature* **460**, 60-65, doi:10.1038/nature08152 (2009).

49 Liu, C. F., Samsa, W. E., Zhou, G. & Lefebvre, V. Transcriptional control of chondrocyte specification and differentiation. *Semin Cell Dev Biol* **62**, 34-49, doi:10.1016/j.semcdb.2016.10.004 (2017).

50 Braun, T. & Gautel, M. Transcriptional mechanisms regulating skeletal muscle differentiation, growth and homeostasis. *Nat Rev Mol Cell Biol* **12**, 349-361, doi:10.1038/nrm3118 (2011).

51 Cai, D., Cohen, K. B., Luo, T., Lichtman, J. W. & Sanes, J. R. Improved tools for the Brainbow toolbox. *Nat Methods* **10**, 540-547, doi:10.1038/nmeth.2450 (2013).

52 Muzumdar, M. D., Tasic, B., Miyamichi, K., Li, L. & Luo, L. A global double-fluorescent Cre reporter mouse. *Genesis* **45**, 593-605, doi:10.1002/dvg.20335 (2007).

53 Duffield, J. S. Cellular and molecular mechanisms in kidney fibrosis. *J Clin Invest* **124**, 2299-2306, doi:10.1172/jci72267 (2014).

54 Hung, C. *et al*. Role of lung pericytes and resident fibroblasts in the pathogenesis of pulmonary fibrosis. *Am J Respir Crit Care Med* **188**, 820-830, doi:10.1164/rccm.201212-2297OC (2013).

Appendix A: Supplemental Figures

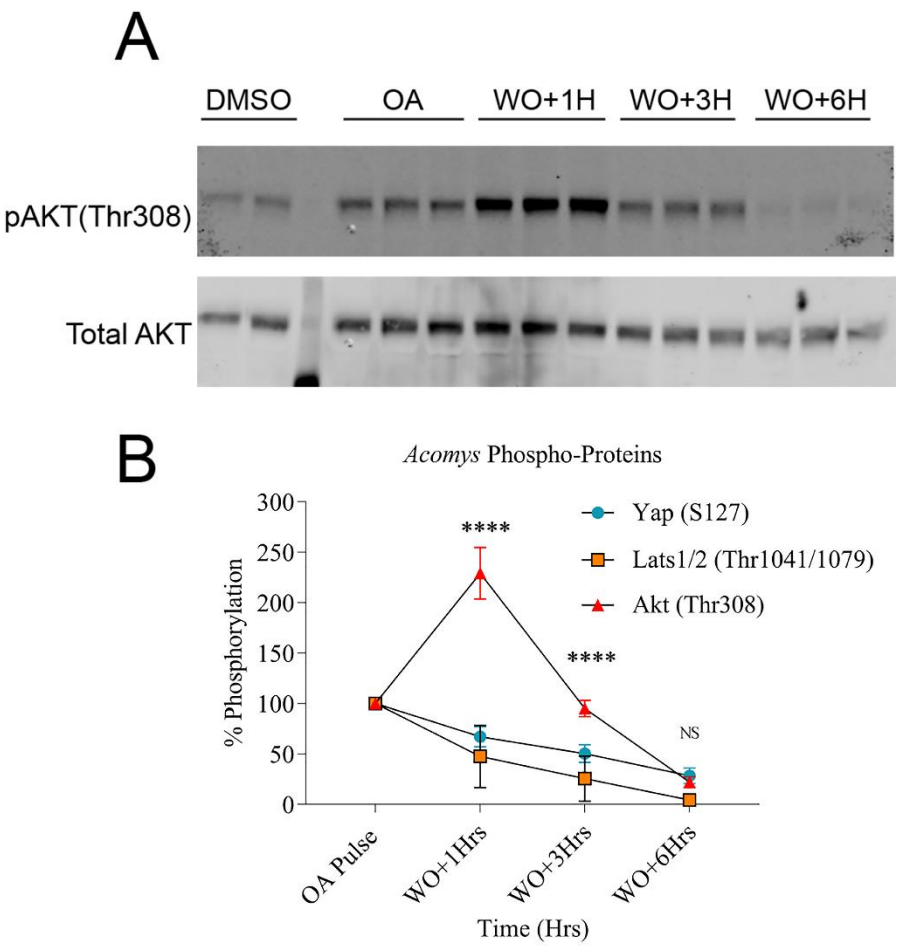

Supplemental Figure 1 *Acomys* Hippo pathway components YAP and LATS1/2 display similar dephosphorylation kinetics. (**A**) Western blot of okadaic acid pulsed (2hrs) *Acomys* dermal fibroblasts exhibit increased pAKT (Thr308) phosphorylation compared to DMSO control. This confirms AKT is a PP2A phosphatase substrate. Upon OA withdrawal or washout (WO), pAKT shows dynamic dephosphorylation. (**B**) Serine/Threonine residues of YAP, LATS1/2 and AKT are PP2A phosphatase targets. However, overlap of protein phosphorylation percentages after OA pulse indicate YAP and LATS1/2 display similar dephosphorylation kinetics when compared to AKT. This would indicate the *Acomys* PP2A rapidly and specifically de-phosphorylates key Hippo pathway components simultaneously.

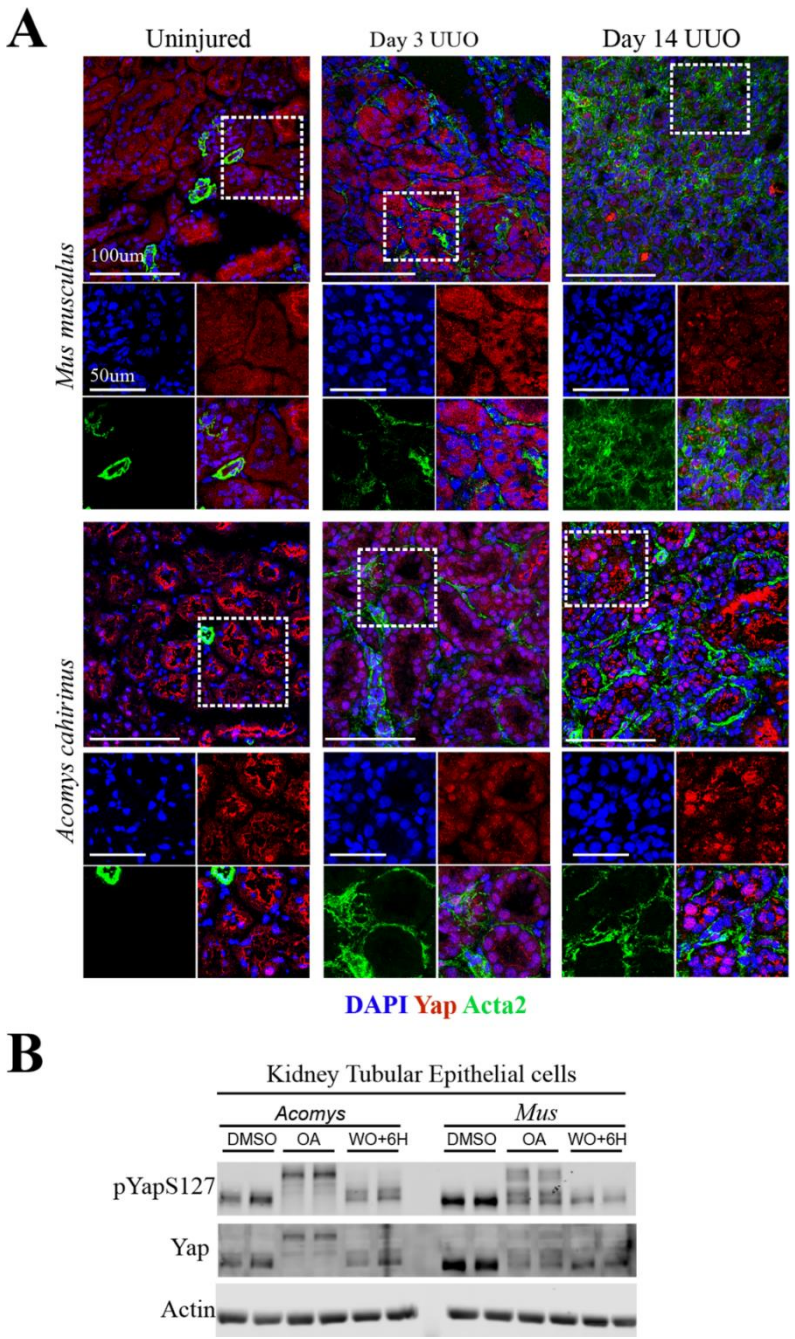

Supplemental Figure 2 *Acomys* resistance to fibrotic inducing UUO kidney injury is correlated to maintained YAP activity. (**A**) Both *Acomys* and *Mus* tubular epithelial cells display low nuclear YAP localization under homeostatic conditions. Day 3 of Unilateral Ureter Obstruction (UUO), *Acomys* and *Mus* exhibit disparate YAP activity. Observation of *Mus* tubular structures display clear Yap cytoplasmic localization, corresponding to inactivation. Furthermore, myofibroblasts ($ACTA2^{+}$) begin expanding within the interstitial space. *Acomys* also contain activated myofibroblasts ($ACTA2^{+}$) indicating response to UUO insult. In contrast to Mus however, *Acomys* display YAP nuclear compartmentalization in a substantial number of renal tubular cells. At Day 14, *Mus* myofibroblast accumulation has resulted in disrupted tubular

structure and subsequent kidney failure. Furthermore, YAP staining is not apparent. *Acomys* display little expansion of the myofibroblast population while nuclear YAP localization is still observed in tubular cells. This data may indicate that *Acomys* altered YAP regulatory potential is associated with abrogated kidney fibrosis. (**B**) Comparison of isolated *Mus* and *Acomys* kidney tubular epithelial cells to OA pulse and washout demonstrates both species display cell autonomous PP2A mediated YAP dephosphorylation. In contrast to *Acomys*, *Mus* YAP is degraded after OA phosphorylation.

Appendix B: List of Antibodies and Reagents

Key Resources Table

	SOURCE	IDENTIFIER
Antibodies		
Mouse monoclonal anti-Actin (C4)	Millipore	Cat# MAB1501, RRID: AB_2223041
Mouse monoclonal anti-Actin, alpha Smooth Muscle (clone 1A4) (Acta2)	Sigma-Aldrich	Cat# A2547, RRID: AB_476701
Mouse monoclonal anti-EDA-Fibronectin (IST-9)	Abcam	Cat# ab6328, RRID: AB_305428
Rabbit monoclonal anti-GAPDH (D16H11)	Cell Signaling Technology	Cat# 5174, RRID: AB_10622025
Mouse monoclonal anti-GFP	Abcam	Cat# ab1218, RRID: AB_298911
Mouse monoclonal anti-FLAG (M2)	Sigma-Aldrich	Cat# F1804, RRID: AB_262044
Rabbit polyclonal anti-Myosin Light Chain (phospho S20)	Abcam	Cat# ab2480 RRID: AB_303094
Rabbit polyclonal anti-Myf5 (C20)	Santa Cruz	Cat#SC-320 RRID:AB_2146886
Rabbit polyclonal anti-Phospho-LATS1 (Thr1079)	Cell Signaling Technologies	Cat# 9159S, RRID: AB_10549072
Rabbit monoclonal anti-Phospho-p38 MAPK (Thr180/Tyr182) (D3F9)	Cell Signaling Technologies	Cat#4511,RRID:AB_2139682
Rabbit monoclonal anti-Phospho-p44/42 MAPK (Erk1/2) (Thr202/Tyr204) (D13.14.4E)	Cell Signaling Technologies	Cat# 4370, RRID: AB_2315112
Rabbit monoclonal anti-Phospho-AKT (Thr308) (244F9)	Cell Signaling Technologies	Cat#4056 **RRID:AB_331163**
Mouse monoclonal anti-AKT (40D4)	Cell Signaling Technologies	Cat#2920 **RRID:AB_10694382**
Rabbit monoclonal anti-Phospho-Smad2 (Ser465/467) (138D4)	Cell Signaling Technologies	Cat# 3108, RRID:AB_490941
Rabbit monoclonal anti-Phospho-Smad3 (Ser423/425) (C25A9)	Cell Signaling Technologies	Cat# 9520, RRID:AB_2193207
Rabbit polyclonal anti-Phospho-YAP (Ser127)	Cell Signaling Technologies	Cat# 4911S, RRID:AB_2218913
Rabbit monoclonal anti-Phospho-YAP (Ser397) (D1E7Y)	Cell Signaling Technologies	Cat# 13619, RRID:AB_2650554
Rabbit monoclonal anti-Smad2 (D43B4)	Cell Signaling Technologies	Cat# 5339, RRID:AB_10626777
Rabbit monoclonal anti- Smad3 (C67H9)	Cell Signaling Technologies	Cat# 9523, RRID:AB_2193182

Rabbit polyclonal anti-Smooth Muscle Myosin Heavy Chain (Myh11)	Biomedical Technologies	Cat# BT-562, RRID:AB_10013421
Rabbit polyclonal Anti-Sox9	Millipore Sigma	Cat# AB5535 **RRID:AB_2239761**
Rabbit polyclonal anti-TAZ (V386)	Cell Signaling Technologies	Cat# 4883S, RRID:AB_1904158
Mouse monoclonal anti-Vinculin	Sigma-Aldrich	Cat# V9131, RRID:AB_477629
Mouse monoclonal anti-YAP1	Abcam	Cat# ab56701, RRID:AB_2219140
Rabbit polyclonal anti-YAP (H-125)	Santa Cruz	Cat# sc-15407, RRID:AB_2273277
Goat polyclonal anti-Mouse IgG (H+L), HRP	Jackson ImmunoResearch	Cat#115-035-166, RRID:AB_2338511
Goat polyclonal anti-Rabbit IgG (H+L), HRP	Jackson ImmunoResearch	Cat# 111-035-003, RRID:AB_2313567
Goat polyclonal anti-Mouse IgG1 Secondary Antibody, Alexa Fluor 488 conjugate	Thermo Fisher Scientific	Cat# A-21121, RRID:AB_2535764
Goat polyclonal anti-Mouse IgG2a Cross-Adsorbed Secondary Antibody, Alexa Fluor 488	Thermo Fisher Scientific	Cat# A-21131, RRID:AB_2535771
Goat polyclonal anti-Mouse IgG2a Cross-Adsorbed Secondary Antibody, Alexa Fluor 594	Thermo Fisher Scientific	Cat# A-21135, RRID:AB_2535774
Goat polyclonal anti-Rabbit IgG (H+L) Cross-Adsorbed Secondary Antibody, Alexa Fluor 488	Thermo Fisher Scientific	Cat# A-11008, RRID:AB_143165
Goat polyclonal anti-Rabbit IgG (H+L) Cross-Adsorbed Secondary Antibody, Alexa Fluor 594	Thermo Fisher Scientific	Cat# A-11012, RRID:AB_2534079
IRDye® 680RD Goat anti-Mouse IgG (H+L)	LI-COR Biosciences	Cat# 925-68070, RRID:AB_2651128
IRDye® 800CW Goat anti-Rabbit IgG (H+L)	LI-COR Biosciences	Cat# 925-32211, RRID:AB_2651127
Bacterial and Virus Strains		
pInducer20_Yap1S127A-Flag	Vector Builder (Song et al., 2014)	N/A
pLV[Exp]-Puro-CMV>EGFP	Vector Builder	N/A
Chemicals, Peptides, and Recombinant Proteins		
Dextran, Texas Red®, 70,000 MW	Thermo-Scientific	Cat#D1864
Okadaic acid, *Prorocentrum concavum*	Sigma-Aldrich	Cat# **O7885** **CAS:** 155751-72-7
Phalloidin CF™594	Biotium	Cat#00045
Recombinant Human TGFβ1	R&D Systems	Cat#240-B-002 Accession # P01137
Tautomycetin	Tocris	Cat# 2305 CAS: 119757-73-2
Verteporfin	United States Pharmacopeia	Cat# ***1711461 USP*** ***CAS:*** 129497-78-5
Deposited Data		
Experimental Models: Cell Lines		
*Acomys: A.C*_E_M20	This Study	N/A
Acomys: A.C_E_M20_ hYap-GFP	This Study	N/A

*Acomys: A.C*_E_N=6	This Study	N/A
Mouse: M.M_E_CD1	This Study	N/A
Human: SK5 Dermal	Gift of Elaine Raines (Gronwald et al., 1988)	RRID: CVCL_5H87
C3H/10T1/2	ATCC	CCL-226
Experimental Models: Organisms/Strains		
Acomys cahirinus: Egyptian Spiny Mouse	This Study	N/A
Mus musculus: Crl:CD1(ICR)	Charles River	RRID:IMSR_CRL:22
Recombinant DNA		
pEGFP-C3-hYAP2	Gift of Marius Sudol (Song et al., 2014)	Addgene: #17844
Software and Algorithms		
Fiji (Image J)	http://fiji.sc/	N/A
Imaris	Bitplane	N/A
Image Studio Light V5.2	https://www.licor.com/bio	N/A
VS-Desktop	Olympus	N/A
Prism7.03	Graph Pad	N/A
Other		

CHRIS M. BREWER

Seattle Children's Research Institute
1900 9th Ave
Seattle, WA 98101
+1 (562) 533-8068 (USA Cell)
chrisbr2@uw.edu

I am an experimental pathologist who is interested in understanding what are the cellular and molecular decisions that influence regeneration or scar tissue mediated wound repair in vertebrates. I am currently a graduate student with Dr. Mark Majesky, PhD, and I am scheduled to defend in Spring 2018. My research is currently focused on examining how reactivation of developmental signaling pathways can influence complex tissue regeneration in adult mammalian species.

EDUCATION

2018 Doctor of Philosophy – Pathology: *Molecular Basis of Disease*
University of Washington, Seattle

2010 Bachelor of Science – *Cellular and Development Biology*, Minor in Chemistry
California State University, Fullerton.

RESEARCH EXPERIENCE

2012 – Doctoral Student, University of Washington, Seattle
Mentor: Mark W. Majesky, PhD
Thesis Dissertation: "Evolutionary adaptations in developmental signaling pathways underlie regenerative scar-free wound repair in African Spiny Mouse (Genus *Acomys*) "

Identified homeostatic adaptations in the organogenesis regulatory pathway Hippo-YAP is necessary in mediating adult *Acomys* epimorphic regenerative wound repair in external organs (i.e. skin). Furthermore, I participated in discovering this phenomenon extends into internal organs (e.g. kidney) with *Acomys* demonstrating abrogated fibrotic repair in various injury models.

2011 – 12 First Year Doctoral Student Rotations, University of Washington, Seattle
Mentors: William Parks, PhD and Jean Campbell, PhD

Characterized T-Regulatory cell behavior in *Mus Mmp10*$^{-/-}$ using acute lung Inflammation injury and lung infection model *Pseudomonas aeruginosa* (W. Parks). Investigated the role of PDGF in inhibition of hepatocyte turnover and liver regeneration in partial hepatectomy in *Mus* with liver fibrosis (J. Campbell).

2010-11 Post-Baccalaureate Research Assistant, University of Massachusetts, Amherst
Mentor: Samuel J. Black, PhD; Northeast Alliance for Graduate Education and the Professoriate (NEAGEP)

Characterized murine B-cell antibody isotype switching and clonal exhaustion in response to chronic parasitic protozoa *Trypanosoma brucei* infection.

2009 Research Technician, Chiang Mai University, Thailand
Mentors: Richard Deming, PhD and Prachya Kongtawelert, PhD

Description: Isolated and identified novel small molecules from native plant species that promote osteoblasts deposition of bone matrix components.

2006-08,10 Undergraduate Research Assistant, California State University – Fullerton

Mentor: Katherine Kantardjieff, PhD

Determined the atomic structure of the bacterial heme protein Cytochrome C' by multiple methods of biophysical analysis such as x-ray diffraction, NMR and EPR.

PUBLICATIONS

1. **Brewer, C.M**., and Majesky, M.W. Branch Point Smooth Muscle Cells Highlighted by Novel Lineage Tracking Approach. Circ Res (2018) 122(2):194-196. PMID:29348244
2. **Brewer, C.M**., Nelson, B., Wakenight, P., Mckenna, A., Mahoney, Jr., W.M., Shendure, J., Timms, A., Millen, K., Majesky, M. Evolutionary adaptations in developmental Hippo-Yap pathway underlies regenerative scar-free wound repair in African Spiny Mice (*Acomys cahirinus*). [in review]
3. Okamura, D.M*., **Brewer, C.M***., Nelson, B., Wakenight, P., Piliponsky, A., Bahrami, N., Bernadi, K., Tran, A., Shi, K., Olson, J., Beier, D., Millen, K., Majesky, M.W. Scarless wound repair of acute and chronic kidney injury in African Spiny mice (*Acomys cahirinus*). [in review]

* *denotes equal contribution*

TEACHING EXPERIENCE

Fall 2014 Responsible Conduct of Research, Teaching Assistant
University of Washington, Seattle; Supervisor: Nancy Maizels, PhD

Facilitated discussion for 1st year Molecular Medicine and Mechanisms of Disease (M3D) graduate students. This course was designed to promote open discussion regarding moral and ethical dilemmas potentially faced in research careers. Subjects of discussion included authorship, collaborative research, conflicts of interest, human subjects, and research misconduct.

Spring 2011 Introductory to Flow Cytometry, Teaching Assistant
University of *Massachusetts – Amherst*; Supervisor: Lisa M. Minter PhD

Short course for new users covering the basics of flow cytometry and an introduction to the use of the various flow cytometry instruments and software analysis of data collected.

RESEARCH FUNDING

2015- Revealing the regenerative potential in mammalian genomes
W.M Keck Foundation Medical Research Grant
PI: MW Majesky, Seattle Children's Research Institute

2012-15 Role of Hippo-dependent signaling pathway in maintenance of AdvSca1 progenitor cells
NIH T32-HL007312: Experimental Pathology of Cardiovascular Disease
PIs: SM Schwartz, PhD (University of Washington)
MW Majesky, PhD (Seattle Children's Research Institute)

PRESENTATIONS & ABSTRACTS

INVITED TALKS:

1. *Evolutionary adaptations in organ size control pathways underlie regenerative scar-free wound repair in African Spiny Mice.* Seattle Children's Research Institute Center for Integrative Brain Research (CIBR) monthly trainee talks. (2017) Seattle, WA

2. *Evolutionary adaptations in organ size control pathways underlie regenerative scar-free wound repair in African Spiny Mice.* (2016) University of Washington Molecular Basis of Disease Graduate Student Program Retreat. Seattle, WA.
3. *Alterations in Yap regulation by an adult mammalian regenerative genome* (2015) University of Washington Department of Pathology annual retreat. Seattle, WA.
4. *Regenerative scar free wound repair in adult mammals (Genus Acomys).* (2014-2017) Seattle Children's Research Institute Center for Developmental Biology and Regenerative Medicine (CDBRM) monthly work in progress trainee talks. Seattle, WA

ABSTRACTS:

5. Brewer C.M., Dong X.R., Nelson B. Wakenight P. Mckenna A. Shendure J. Timms A. Millen K. Majesky M. Evolutionary adaptations in organ size control pathway Hippo-Yap underlies regenerative scar free wound repair in African Spiny Mouse (*Acomys cahirinus*). Office for Teaching, Education and Research (OTER) First Annual Postdoc and Grad Student Fall Research Symposium @ Seattle Children's Research Institute (2017) (Poster)
6. Brewer C.M., Dong X.R., Nelson B. Wakenight P. Mckenna A. Shendure J. Timms A. Millen K. Majesky M. Evolutionary adaptations in developmental pathways underlies regenerative scar free wound repair in African Spiny Mouse. American Society for Cell Biology Annual Meeting @ Moscone Convention Center, San Francisco, CA (2016) (Poster)
7. Brewer C.M., Dong X.R., Nelson B. Wakenight P. Mckenna A. Shendure J. Timms A. Millen K. Majesky M. Evolutionary adaptations in organ size control pathways underlies regenerative scar free wound repair in African Spiny Mouse (*Acomys cahirinus*). University of Washington Department of Pathology Retreat @ Sleeping Lady Resort, WA. (2016) (Poster)
8. Brewer C.M., Giannandrea M., Birkland T., Parks B. T-Regulatory Cell Behavior in Mmp10-/- using Acute Lung Inflammation model *Pseudomonas aeruginosa*. Department of Pathology Graduate Student Rotation @ University of Washington, Seattle WA (2012) (Poster)
9. Brewer C.M., Riehle K., Johansson F., Vaquero J., Bauer.R., Fausto N., Campbell J. Inhibition of Liver Regeneration after Partial Hepatectomy in Mice with Liver Fibrosis. Department of Pathology Graduate Student Rotation @ University of Washington, Seattle WA (2011) (Poster)
10. Brewer C.M., Frankel D., and Black,S. Determination of Bone Marrow/Spleen Lymphocyte Populations during parasitic infections of protozoa *Trypanosoma brucei*. Northeast Alliance for Graduate Education and the Professoriate Summer Research Symposium (NEAGAP) @ University of Massachusetts Amherst (2010) (Poster)
11. Brewer C.M., Kongtawelert P., Deming R. LSAMP/ ESRT International Research Experience in Chiang Mai, Thailand. LSAMP Summer Enrichment Program @ California State University Sacramento (2009) (Poster)
12. Brewer C.M., Madain S., Weir J. Purification, Isolation and Characterization of Protein Cytochrome C'. Southeastern Association of Educational Opportunity Program Personnel (SAEOPP) @ McNair Research Conference Meeting Atlanta, Ga. (2009) (Poster)
13. Frankel**,** D., Brewer C.M., Black S.J., B-cell clonal exhaustion and apoptosis in response to chronic *Trypanosoma brucei* infection. @ American Society for Parasitology Meeting Fancy Gap (2012) (Poster)
14. Sennett, R.L., Pawlak E., Brewer C.M., Black S.J., Discerning the roles of ADAM-4 in equine digital laminitis. @ University of Massachusetts Amherst (2011) (Poster)

STUDENTS MENTORED (Students' status during training)

Mikayla Chang (Undergraduate) *Whitman College, Walla Walla, WA* Summer 2017

Jonathan Lee (Undergraduate) *University of Washington Seattle,* Fall 2016 – Fall 2017
Rosa Lee Sennet (Undergraduate) *University of Massachusetts Amherst* – Fall 2010- Summer 2011

ACADEMIC HONORS

2012-15	Cardiovascular Pathology Fellowship – University of Washington, Seattle
2011	GO-MAP Graduate School Fellowship – University of Washington, Seattle
2010	NEAGAP Research Fellowship Summer – University of Massachusetts, Amherst
2009	Environmental Science Research in Thailand Fellowship – Chiang Mai University, Thailand
2009-10	LSAMP Research Scholar– California State University, Fullerton
2008-10	McNair Research Scholar– California State University, Fullerton
2007, 08, 10	Dean's List– California State University, Fullerton

AWARDS

2016	1st Place, Department of Pathology Research Retreat, University of Washington, Seattle (Poster)
2010	1st Place, Veterinary Science Research Symposium, University of Massachusetts, Amherst (Poster)
2010	2nd Place, Southeastern Association of Educational Opportunity Program Personnel (SAEOPP), McNair Research Conference, Georgia State University (Poster)

PROFESSIONAL SOCIETY MEMBERSHIPS

2006 –	American Chemical Society (ACS)
2008 –	American Association for the Advancement of Science (AAAS)
2011 –	American Society for Parasitology (ASP)
2015 –	American Society of Cell Biology (ASCB)

REFERENCES

Mark W. Majesky, Ph.D.
Professor of Pediatrics, Division of Cardiology
Professor of Pathology, Center for Cardiovascular Biology
Member, Institute for Stem Cell & Regenerative Medicine
University of Washington School of Medicine
mwm84@uw.edu
Director, Myocardial Regeneration Initiative
Center for Developmental Biology & Regenerative Medicine
Seattle Children's Research Institute
mark.majesky@seattlechildrens.org

Kathleen J. Millen, Ph.D
Professor of Pediatrics, Division of Genetics
University of Washington School of Medicine
Seattle Children's Research Institute
Center for Integrative Brain Research
kathleen.millen@seattlechildrens.org

David R. Beier, MD, PhD
Professor of Pediatrics, Division of Genetic Medicine
University of Washington School of Medicine
Director, Center for Developmental Biology and Regenerative Medicine
Seattle Children's Research Institute
David.Beier@Seattlechildrens.org

William M. Mahoney, Jr., PhD
Associate Professor, Department of Pathology
University of Washington, School of Medicine
Co-Director, Molecular Medicine & Mechanisms of Disease (M3D) PhD Program
UW Graduate School, Office of Postdoctoral Affairs
UW Medicine, Health Professions Academy
wmahoney@uw.edu